DESIGN AND SYNTHESIS OF THERAPEUTIC AGENTS: FROM SMALL MOLECULES TO POLYMERIC NANOMATERIALS

by

Büşra Cengiz

B.S., Chemistry Education, Marmara University, 2013

M.S., Chemistry, Boğaziçi University, 2016

Submitted to the Institute for Graduate Studies in
Science and Engineering in partial fulfillment of
the requirements for the degree of
Doctor of Philosophy

Graduate Program in Chemistry

Boğaziçi University

2024

DESIGN AND SYNTHESIS OF THERAPEUTIC AGENTS: FROM SMALL MOLECULES TO POLYMERIC NANOMATERIALS

DATE OF APPROVAL: 05.02.24

Dedicated to my beloved, EGE

ACKNOWLEDGEMENTS

Firstly, I would like to thank my thesis supervisor Prof. Amitav SANYAL for his endless scientific guidance and support during my graduate studies.

I would like to thank my thesis jury, Prof. Rana SANYAL, Assist. Prof. Özgül GÖK ÖZATAY, Prof. Emrah ÇAKMAKÇI, and Prof. A. Neren ÖKTE for giving their valuable time and constructive review for the final manuscript of my thesis.

I would like to thank Yavuz for his kindness and patience while helping and answering all my endless questions. I appreciate for your all support during my PhD adventure and of course his valuable friendship. I would like to thank Tuğçe for sharing her optimistic approach to lab life all the time and her worthy friendship. I would like to thank Laura, it was a great pleasure to meet you on some point of life timeline.

I would like to thank all Sanyal Group members for their companion and make such a cheerful lab ambiance.

I would like to thank my sweetie undergrad İdil for all effort and contribution on dual-functionalizable polymer brush coated magnetic nanoparticles project.

I would like to thank my mother and father, they shared my burden all the time whenever I need them. I am proud of being their little daughter.

I would like to thank my dear nuclear family. With you, I feel like the luckiest person in the world. It was a long 10 years adventure to here with my all graduate studies and each day was perfect together. Ege, I owe you this graduation.

Photothermally active hydrogel project was supported by The Scientific and Technological Research Council of Turkey (TÜBİTAK) 2214-A International Research Fellowship Program. Thanks to University of Lille, CNRS for their educational hospitality.

The project related to dual-drug-based prodrug as a novel entity for addressing pancreatic cancer was financially supported by The Scientific and Technological Research Council of Turkey (TÜBİTAK) (Project No: 115S997).

The fabrication of Diels-Alder functionalizable polymer brush-coated iron oxide nanoparticles project was financially supported by Bogazici University Research Fund (Project No: 19795, Project BOUN No: 23BD5).

ABSTRACT

DESIGN AND SYNTHESIS OF THERAPEUTIC AGENTS: FROM SMALL MOLECULES TO POLYMERIC NANOMATERIALS

Novel approaches are needed to address the limitations of traditional therapy methods that are in practice today, for improved treatment of diseases. This thesis evaluates such approaches through the development of new molecular and materials-based systems. The first part of this thesis focuses on the synthesis of a prodrug molecule for pancreatic cancer treatment while the second part includes polymeric nanomaterial-containing delivery systems for biological applications. In the first part, two synthetic pathways were investigated to synthesize a prodrug system comprised of gemcitabine, a chemotherapy agent, and hydroxychloroquine which is known to eradicate pancreatic cancer stem cells. Products linked with acid-sensitive linkages with and without disulfide bonds between them were synthesized, and evaluated for their in vitro cytotoxicity against the Bx-PC3 cell line. Another approach to specifically deliver drugs involves the utilization of localized delivery systems. In this regard, in the second part of this thesis, polymeric nanomaterials were evaluated as drug delivery platforms. As nanomaterials, carbon nanotubes (CNTs), magnetic iron-oxide nanoparticles (IONPs) and reduced graphene oxides (rGOs) were utilized in four distinct projects. CNTs wrapped with a reactive polymer using physical interactions were fabricated, and evaluated for attachment of bioactive molecules using the thiol-maleimide reaction. In another project, rGO-embedded photothermal hydrogels were synthesized using a thiol-ene reaction and were evaluated for on-demand active release using near-infrared (NIR) light to release antibacterial agents inside the hydrogel. In the last two projects, IONPs were coated with two different polymers using reversible addition-fragmentation chain transfer (RAFT) polymerization and these constructs were used to design different drug delivery and release systems. Overall, this thesis puts forth new drug delivery platforms that may find therapeutic applications.

ÖZET

DESIGN AND SYNTHESIS OF THERAPEUTIC AGENTS: FROM SMALL MOLECULES TO POLYMERIC NANOMATERIALS

Günümüzde hastalıkların daha iyi tedavi edilebilmesi için uygulanan geleneksel tedavi yöntemlerinin sınırlılıklarını giderecek yeni yaklaşımlara ihtiyaç vardır. Bu tez, bu tür yaklaşımları yeni moleküler ve malzeme bazlı sistemlerin geliştirilmesi yoluyla değerlendirmektedir. Bu tezin ilk kısmı pankreas kanseri tedavisine yönelik bir ön ilaç molekülünün sentezine odaklanırken, ikinci kısmı biyolojik uygulamalara yönelik polimerik nanomateryal içeren dağıtım sistemlerini içermektedir. İlk bölümde, kemoterapi ajanı gemsitabin ve pankreas kanseri kök hücrelerini yok ettiği bilinen hidroksiklorokin'den oluşan bir ön ilaç sisteminin sentezlenmesi için iki sentetik yol araştırıldı. Aralarında disülfit bağları bulunan ve bulunmayan, asidik ortama duyarlı bağlantılarla bağlanan ürünler sentezlendi ve Bx-PC3 hücre hattına karşı in vitro sitotoksisiteleri değerlendirildi. İlaçların özel olarak dağıtımına yönelik başka bir yaklaşım, bölgesel dağıtım sistemlerinin kullanılmasını içerir. Bu bağlamda tezin ikinci bölümünde polimerik nanomalzemeler ilaç dağıtım platformları olarak kullanılmıştır. Dört farklı projede nanomalzemeler olarak karbon nanotüpler (CNT'ler), manyetik demir oksit nanopartikülleri (IONP'ler) ve indirgenmiş grafen oksitler (rGO'lar) kullanıldı. Fiziksel etkileşimler kullanılarak reaktif bir polimerle sarılmış CNT'ler üretildi ve tiyol-maleimid reaksiyonu kullanılarak biyoaktif moleküllerin bağlanması açısından değerlendirildi. Başka bir projede, rGO gömülü fototermal hidrojeller, bir tiyol-en reaksiyonu kullanılarak sentezlendi ve hidrojel içindeki antibakteriyel maddeleri serbest bırakmak için yakın kızılötesi (NIR) ışık kullanılarak isteğe bağlı aktif salım açısından değerlendirildi. Son iki projede, IONP'ler, tersinir ekleme-parçalanma zincir transferi (RAFT) polimerizasyonu kullanılarak iki farklı polimerle kaplandı ve bu yapılar, farklı ilaç dağıtım ve salım sistemlerinin tasarlanması için kullanıldı. Genel olarak bu tez, terapatik uygulamalar bulabilecek yeni ilaç dağıtım platformlarını ortaya koymaktadır.

TABLE OF CONTENTS

ACKNOWLEDGEMENTS iv
ABSTRACT vi
ÖZET vii
LIST OF FIGURES xiii
LIST OF TABLES xxiii
LIST OF ACRONYMS/ABBREVIATIONS xxiv
1. INTRODUCTION 1
1.1. Drug Delivery Agents for Cancer Treatment 1
1.2. Nanomaterials 3
1.2.1. Hydrogels Containing Nanomaterials 8
2. RESEARCH OVERVIEW 13
3. SYNTHESIS OF GEMCITABINE COMBINED WITH HYDROXYCHLOROQUINE SMALL DRUG MOLECULE FOR ANTITUMOR ACTIVITY IN PANCREATIC CANCER CELLS 14
3.1. Introduction 14
3.1.1. Pancreatic Cancer 14
3.1.2. Gemcitabine (GEM) and Hydroxychloroquine (HCQ) Drugs 15
3.2. Experimental 18
3.2.1. Materials and Characterizations 18
3.2.2. Synthesis of Hydroxyundecanoic Acid 19
3.2.3. Protection of OH Group of Hydroxyundecanoic Acid Linker 19
3.2.4. Synthesis of Hydroxychloroquine (HCQ) 20
3.2.5. Protection of Acid Group of Linker 20
3.2.6. Deprotection of Alcohol Group of Linker 20
3.2.7. NHS Activation of Alcohol Group on Linker 21
3.2.8. TBDMS Protection of Gemcitabine (GEM) 21
3.2.9. Gemcitabine Addition to NHS Activated Linker 21
3.2.10. Deprotection of Acid Group of Linker 22
3.2.11. HCQ Addition to Linker 22
3.2.12. Deprotection of GEM-HCQ Drug Molecule OH groups 22

3.2.13. Modification of HCQ with Aldrithiol 23
3.2.14. NHS activation of Bis(11-hydroxyundecyl) Disulfide 23
3.2.15. GEM Addition to Disulfide Containing Linker 24
3.2.16. Deprotection of Disulfide Containing Bis GEM Molecule 24
3.2.17. Synthesis of GEM-SH 24
3.2.18. Synthesis of Disulfide Containing Drug Molecule (GEM-SS-HCQ)... 24
3.3. Results and Discussion 25
3.3.1. Synthetic Pathway of Small Drug Molecule without Disulfide Bond.. 25
3.3.2. Synthetic Pathway of Small Drug Molecule with Disulfide Bond 32
3.3.3. In Vitro Analysis of the Drug Molecules 35
3.4. Conclusion 36
4. TAILORING AQUEOUS DISPERSIBILITY AND BIOFUNCTIONALIZATION OF CARBON NANOTUBES USING MALEIMIDE CONTAINING CLICKABLE POLYMERS 38
4.1. Introduction 38
4.2. Experimental 41
4.2.1. Materials and Characterizations 41
4.2.2. Instrumentation 41
4.2.3. Synthesis of Pyrene-terminated Furan-Protected Maleimide-containing Copolymers 42
4.2.4. Synthesis of Ethyl α-Bromoisobutyrate Initiated Furan Protected Maleimide Containing Copolymer (P2) 42
4.2.5. Synthesis of Pyrene Initiated PEGMEMA Polymer (P3) 43
4.2.6. Synthesis of Ethyl α-Bromoisobutyrate Initiated Polymer 43
4.2.7. General Procedure for Activation of Maleimide Groups via Retro Diels-Alder Reaction 43
4.2.8. General Procedure for Modification of MWCNTs with copolymers ... 44
4.2.9. Conjugation of Polymer Functionalized MWCNTs with Glutathione via Thiol-ene Reaction 44
4.2.10. Conjugation of Polymer Functionalized MWCNTs with Biotin-PEG-SH via Thiol-ene Reaction 44
4.2.11. Conjugation of FITC-Streptavidin Protein 44
4.2.12. Conjugation of Streptavidin-coated Qdot 45
4.2.13. Conjugation of RGDC Peptide 45

4.2.14. Cell Culture Studies 45
4.2.15. Cytotoxicity Assays 46
4.3. Results and Discussion 46
4.3.1. Synthesis of Maleimide Containing Copolymers 46
4.3.2. Modification of CNTs via Non-Covalent Interaction 48
4.3.3. Functionalization of Copolymer Coated MWCNTs using Thiol-Maleimide Conjugation 51
4.3.4. Functionalization of CNTs with and FITC-Streptavidin and Qdot-Streptavidin 53
4.3.5. Conjugation with cell adhesive peptide RGDC and Cell Culture and Cell Viability Assays 54
4.4. Conclusion 55
5. PHOTOTHERMALLY ACTIVE RGO-EMBEDDED ANTIBACTERIAL HYDROGELS FOR THE TREATMENT OF BACTERIAL INFECTIONS 56
5.1. Introduction 56
5.2. Experimental 59
5.2.1. Materials and Characterizations 59
5.2.2. Synthesis of Modified Dextran 60
5.2.3. Synthesis of Per-6-Thio-Beta Cyclodextrin 60
5.2.4. Fabrication of Hydrogel via Thiol-ene Chemistry 60
5.2.5. Water Uptake Analysis of Hydrogel 61
5.2.6. Antibiotic Loading and Release Experiments 61
5.2.7. Drug Release via NIR light 61
5.2.8. Bacteria Experiments 62
5.3. Results and Discussion 62
5.3.1. Modification of Monomers for Hydrogelation 62
5.3.2. Hydrogel Synthesis and Characterization 63
5.3.3. Water Uptake Analysis 65
5.3.4. Antibiotic Loading Experiments 65
5.3.5. Drug Release with NIR light 67
5.3.6. Bacteria Experiments 69
5.4. Conclusion 72
6. FABRICATION OF DIELS-ALDER FUNCTIONALIZABLE POLYMER BRUSH COATED IRON OXIDE NANOPARTICLES 74

6.1. Introduction 74
6.2. Experimental 75
6.2.1. Materials and Characterizations 75
6.2.2. Synthesis of Iron Oxide Nanoparticles 76
6.2.3. Synthesis of Dopamine Modified 2-(Dodecylthiocarbonothioylthio)-2-Methyl Propionic acid (Dopa-CTA) 77
6.2.4. Synthesis of Azobis-azide Exchange Reagent 77
6.2.5. Synthesis of Alkyne Modified cRGDfK 77
6.2.6. Place Exchange Reaction with Catechol Modified RAFT Agent (Dopa-CTA) 78
6.2.7. General Procedure for Surface-Initiated RAFT Polymerization on IONPs 78
6.2.8. Terminal Group Modification of Polymer Coated IONPs with Azide 79
6.2.9. Terminal Group Functionalization of Azide Bearing IONPs with cRGDfK via Azide-Alkyne Huisgen Cycloaddition 79
6.2.10. Surface Functionalization of Polymer Coated IONPs via Diels-Alder Reaction with N-(5-Fluoresceinyl) Maleimide 79
6.2.11. Diels-Alder Reaction with BODIPY Maleimide 79
6.2.12. Diels-Alder Reaction with N-Ethyl Maleimide 80
6.2.13. Conjugation with Aldoxorubicin via Diels-Alder Reaction 80
6.2.14. Aldoxorubicin Release Experiment from Polymer Coated IONPs 80
6.3. Results and Discussion 80
6.3.1. Fabrication of Furan Containing Polymer Coated IONPs 80
6.3.2. Functionalization of Polymer Coating via Diels-Alder Reaction. 83
6.4. Conclusion 87
7. DUAL-FUNCTIONALIZABLE POLYMER BRUSH COATED MAGNETIC NANOPARTICLES 89
7.1. Introduction 89
7.2. Experimental 91
7.2.1. Materials and Characterizations 91
7.2.2. Synthesis of Iron Oxide Nanoparticles (IONPs) 92
7.2.3. Synthesis of Dopamine-Functionalized Chain Transfer Agent (Dopa-CTA) 92

7.2.4. Place Exchange Reaction with Catechol Modified RAFT Agent (Dopa-CTA) 93
7.2.5. General Procedure for Surface-Initiated RAFT Polymerization on IONPs 93
7.2.6. Retro Diels-Alder Reaction of Copolymer Coated IONPs 93
7.2.7. Surface Functionalization of Polymer Coated IONPs via Thiol-ene Reaction with BODIPY-SH 94
7.2.8. Surface Functionalization of Bodıpy Functionalized Polymer Coated IONPs via Strain Promoted Azide-Alkyne Click Chemistry (SPAAC) Reaction with Cyanine5 Tetrazine Dye 94
7.2.9. Surface Functionalization of Polymer Coated IONPs via Thiol-ene Reaction with DOX-SH 94
7.3. Results and Discussion 94
7.3.1. Fabrication of Functionalizable Polymer Coated IONPs 94
7.4. Conclusion 103
8. CONCLUSION 104
REFERENCES 106
APPENDIX A: SPECTROSCOPY DATA 127
APPENDIX B: COPYRIGHTS 138

LIST OF FIGURES

Figure 1.1.	Types of drug delivery systems [2].	1
Figure 1.2.	Illustration of EPR effect of prodrug in normal and tumor tissue. Adapted from reference [4].	2
Figure 1.3.	Schematic illustration of carbon nanomaterials.	4
Figure 1 4.	Schematic representation of DOX attached BSA-rGO nanosheet and release via NIR application.	5
Figure 1.5.	Functionalization of CNTs via covalent and non-covalent way.	6
Figure 1.6.	Representation of coating SWCNTs with pyrene modified PEG and using for both fluorescence and photothermal effects.....	7
Figure 1.7.	Different polymers coating of IONPs with polymers.....	8
Figure 1.8.	Fabrication of DOX and cisplatin loaded hydrogel and schematic illustration of drug release.	9
Figure 1.9.	DOX containing hydrogel formation.....	10
Figure 1.10.	Schematic illustration of hydrogel formation, loading a nanoparticle cargo and degradation of responsive hydrogel via β-lactamase.	11
Figure 1.11.	Fabrication of drug loaded rGO hydrogel.	11
Figure 3.1.	Schematic illustration of metastasis of PDAC via circulating tumor cell in blood stream. Adapted from ref [21].	15

Figure 3.2. Inhibition of tumor growth in vivo by mix of CQ and GEM. (a) images of tumors surgically removed from xenograft. (b) Tumor volumes of xenograft measured twice a week. (c) Tumor mass of xenograft after 4-week growth in nude mice..... 16

Figure 3.3. (a) HCQ-GEM drug molecule with carbon chain linker. (b) HCQ-GEM drug molecule with disulfide bond including linker..... 17

Figure 3.4. Structure of released gemcitabine and hydroxychloroquine drugs. ... 18

Figure 3.5. Synthetic pathway for drug molecule without disulfide bond on the linker..... 25

Figure 3.6. Protection of OH groups of GEM. 26

Figure 3.7. ^{1}H NMR spectrum of OH groups protected GEM. 26

Figure 3.8. ^{1}H NMR spectrum of first step product..... 27

Figure 3.9. ^{1}H NMR spectrum of acetyl protection of OH group..... 27

Figure 3.10. ^{1}H NMR spectrum of t-butyl alcohol protection of acid group..... 28

Figure 3.11. ^{1}H NMR spectrum of acid protected linker..... 28

Figure 3.12. ^{1}H NMR spectrum of NHS activated linker..... 29

Figure 3. 13. ^{1}H NMR spectrum of GEM attached linker. 29

Figure 3.14. ^{1}H NMR spectrum of GEM attached linker. 30

Figure 3.15. ^{1}H NMR spectrum of GEM and HCQ bearing linker. 31

Figure 3.16. ^{1}H NMR spectrum of synthesized prodrug molecule without disulfide bond on the linker. 31

Figure 3.17. Synthesis of the pyridyl disulfide modified HCQ. 32

Figure 3.18. ^{1}H NMR spectrum of the pyridyl disulfide modified HCQ. 32

Figure 3.19. Synthetic pathway for GEM-SS-HCQ drug molecule. 33

Figure 3.20. ^{1}H NMR spectrum of GEM-SH molecule. 34

Figure 3.21. ^{1}H NMR spectrum of GEM-SS-HCQ drug molecule. 34

Figure 3.22. Stability graphs of free GEM (a and b) and HCQ (c and d) drugs at pH 5.5 and 7.4. 35

Figure 3.23. Cleavage products of GEM-HCQ drug molecule in pH 5.5 and 7.4 buffer solutions. 35

Figure 3.24. (a) Cytotoxicity of free drugs and synthesized prodrugs on BxPC-3 cell line. (b) Statistical analysis of drug molecules, (****= 0.0001, ***= 0.001, **= 0.01, ns= P>0.05), GEM is represented with red, HCQ + GEM is green, GEM-HCQ is black and GEM-SS-HCQ is blue. 36

Figure 4.1. Schematic illustration of the fabrication of functionalizable carbon nanotubes using thiol-reactive maleimide group containing pyrene-terminated hydrophilic copolymers, and their facile interfacing with biomolecules and cells. 40

Figure 4.2. Synthesis of copolymers utilized for CNT solubilization and functionalization. 47

Figure 4.3. Stacked ^{1}H NMR spectra of polymers P1-P4. 47

Figure 4.4. Modification of MWCNTs with polymers P1, P2, P3, and P4. 49

Figure 4.5. (a) FTIR spectra; and TGA analysis of (b) pristine CNTs, P1 polymer and P1-CNTs, and (c) comparison of various polymer (P1-P4) coated CNTs. 50

Figure 4.6. (a) Comparison of aqueous dispersity upon functionalization of P1-CNT and P2-CNT polymer-coated nanotubes with glutathione, and (b) comparison of functionalized polymer coatings on glutathione treated nanotubes. 52

Figure 4.7. (a) Schematic illustration of bioimmobilization with streptavidin conjugated dyes; Fluorescence image of (b) FITC-streptavidin conjugated biotinylated P1-CNTs, and (c) Streptavidin-coated Qdot conjugated biotinylated P1-CNTs (scale bar: 100 μm). 53

Figure 4.8. (a) Comparison of cell viability of fibroblasts treated with pristine CNTs, P1-coated CNTs, and RGD-P1-coated CNTs; fluorescence microscopy images of L929 mouse fibroblast cells stained with Alexafluor-488 phalloidin (green) and DAPI (blue) after incubation for 48 h on (b) pristine CNT coated surfaces, (c) P1-CNT coated surfaces, and (d) RGD-P1-CNT coated surfaces (Scale bar: 100 μm). 54

Figure 5.1. Synthesis of Ag NP containing hydrogel and simultaneous schematic representation of the synergistic effect of photothermal and antibacterial silver under NIR light. Adapted from ref [95]..... 58

Figure 5.2. Modification of dextran using 4-pentenoic anhydride. 62

Figure 5.3. Synthesis of thiol modified beta cyclodextrin. 63

Figure 5.4. Fabrication of rGO embedded hydrogel under UV light..... 63

Figure 5.5. (a) Images of synthesized with and without rGO hydrogels, respectively, (b) SEM images of hydrogel with rGO, (c) Results of rheological analysis of hydrogel with rGO (G' storage modulus and G'' loss modulus) (d) FT-IR spectra of β-CD-SH, modified dextran and hydrogels, (e) swelling ratio of hydrogels. 64

Figure 5.6. Loading and passive release of ampicillin..... 66

Figure 5.7. Loading and passive release for cefepime..... 66

Figure 5.8. Loading and passive release percentage for antibiotic, cip. 67

Figure 5.9. Photo of NIR application to hydrogel. 68

Figure 5.10. Heating curves of rGO loaded hydrogel for 10 and 20 minutes..... 68

Figure 5.11. NIR light activation to amp loaded hydrogel for 1h and the drug amounts at 10, 20, 30 and 60 minutes. 70

Figure 5.12. (a) MIC value graph for ampicillin, (b) and (c) viability graphs of NIR released amp on *E. coli* with two different amount strategy. 70

Figure 5.13. (a) MIC value graphs for cefepime on E. *coli* and S. *aureus*, (b) and (c) viability graphs of NIR released cef on *E. coli* and *S. aureus*. 71

Figure 5.14. MIC values graphs of ciprofloxacin on *E. coli, S. aureus* and *S. epidermidis*. 71

Figure 5.15. Bacteria viability graphs of NIR released cip on *E. coli, S. aureus* and *S. epidermidis.* 72

Figure 6.1. (a) Synthetic route for polymerization on IONPS. (b) Image of aqueous solution of polymer coated IONPs collected via the magnet. 81

Figure 6.2. STEM images of pristine and coated IONPs (scale bar: 200 μm). 81

Figure 6.3. (a) FT-IR spectra of oleic acid, CTA and polymer coated IONPs. (b) TGA graph of oleic acid, CTA and polymer coated IONPs..... 82

Figure 6.4. N-ethylmaleimide attachment to polymer via Diels-Alder reaction. . 83

Figure 6.5. XPS analysis of N-ethylmaleimide attached P1, P2 and P3 polymers coated IONPs. 84

Figure 6.6. (a) BODIPY-maleimide attachment to polymer coating on IONPs. (b) UV-Vis spectra of BODIPY attached polymer coated IONPs. (c) Photos of BODIPY functionalized IONPs under daylight and d) under UV light. 85

Figure 6.7. Modification of polymer coating with cRGDfK targeting group..... 86

Figure 6.8. Modification of targeting group containing polymer coating with dox-mal. 87

Figure 7.1. Representation of grafting to and from approaches. Adapted from ref. [133]. 89

Figure 7.2. Fabrication water soluble polymer coated IONPs and functionalization with different methods [130]. 90

Figure 7.3. Coating IONPs with Dopa-CTA via place exchange reaction. 95

Figure 7.4. Graft from polymerization on IONPs and activation of maleimide groups via retro Diels-Alder reaction, respectively..... 95

Figure 7.5. Polymer coated IONPs in aqueous solution, before and after affected by a magnet..... 96

Figure 7.6. STEM images of CTA and PEG, 10%, 20% and 30% FuMaMA containing polymers coated IONPs. 96

Figure 7.7. FT-IR spectra of including FuMaMA polymers coated IONPs. 97

Figure 7.8. FT-IR spectra of maleimide bearing polymers coated IONPs. 97

Figure 7.9. Thermogravimetric analysis results of pristine IONPs, dopa-CTA coated IONPs and 10% FuMaMA bearing IONPs..... 98

Figure 7.10. TGA results of 10, 20 and 30% FuMaMA bearing polymers coated IONPs. 99

Figure 7.11. XPS analysis of the control group (PEG-IONPs) and 10, 20 and 30% maleimide bearing polymer-IONPs..... 99

Figure 7.12. TGA results comparisons of PEG coated IONPs, 30% maleimide bearing IONPs and half protected and activated maleimide bearing polymers coated IONPs. 100

Figure 7.13. Schematic illustration of dual functionalization of polymer coating on IONPs with BODIPY-maleimide and Cy5-tetrazine dye respectively and UV-vis graph of the attachments..... 101

Figure 7.14. Schematic illustration and UV-vis spectrum of doxorubicin drug attachment on the surface coating of IONPs. 102

Figure 7.15. Addition of DOX-SH and cRGDfK-tetrazine on half activated polymer coating of IONPs. 102

Figure A.1. FT-IR spectrum of oleic acid coated iron oxide nanoparticles. 127

Figure A.2. ^{1}H NMR spectrum of Dopa-CTA. 127

Figure A.3. ^{1}H NMR spectrum of NHS activated alkyne group bearing molecule. 128

Figure A.4. ^{1}H NMR spectrum of per-6-thiolated β cyclodextrin. 128

Figure A.5. HPLC calibration curves in different concentrations for ampicillin, vancomycin, cefepime and ciprofloxacin drugs. 129

Figure A.6. ^{1}H NMR spectrum of vinyl modified dextran polymer. 130

Figure A.7. Calibration curve of BODIPY-maleimide via UV-vis spectroscopy. 130

Figure A.8. ^{1}H NMR spectrum of azide azobis molecule. 131

Figure A.9. Calibration curve of aldoxorubicin via UV vis spectra. 131

Figure A.10. BCA analysis graph of RGD attached polymer coated IONPs. 132

Figure A.11. ^{1}H NMR spectrum of FuMaMA. 132

Figure A.12. Calibration curve of BODIPY-SH via UV-vis spectroscopy. 133

Figure A.13. Calibration curve of Dox-SH via UV-vis spectroscopy. 133

Figure A.14. ^{1}H NMR spectrum of pyrene initiator. 133

Figure A.15. ^{1}H NMR spectrum of pyrene end group furan protected maleimide copolymer (P1) 134

Figure A.16. ^{1}H NMR spectrum of furan protected maleimide bearing P2 copolymer. 134

Figure A.17. SEC plots of copolymers. 135

Figure A.18. TEM micrographs of (a) copolymer P1 coated CNTs, and (b) pristine CNTs..... 135

Figure A.19. Fluorescence spectra of (a) copolymer P1, and (b) P1-CNTs, in water 136

Figure A.20. FTIR spectra of pristine CNT, P2 polymer and P2-polymer coated CNT. 136

Figure A.21. FTIR spectra of pristine CNT, P3 polymer and P3-polymer coated CNT. 137

Figure A.22. FTIR spectra of pristine CNT, P4 polymer and P4-polymer coated CNT. 137

Figure A.23. Streptavidin conjugation to P1-coated CNTs without biotin (scale bar 200 μ). 138

Figure B.1. Permission for Figure 1.1. 140

Figure B.2. Permission for Figure 1.2. 142

Figure B.3. Permission for Figure 1.3. 144

Figure B.4. Permission for Figure 1.4. 145

Figure B.5. Permission for Figure 1.5. 147

Figure B.6. Permission for Figure 1.6. 149

Figure B.7. Permission for Figure 1.7. 151

Figure B.8. Permission for Figure 1.8. 153

Figure B.9. Permission for Figure 1.9. 155

Figure B.10. Permission for Figure 1.10. 157

Figure B.11. Permission for Figure 1.11. 159

Figure B.12. Permission for Figure 3.1. 160

Figure B.13. Permission for Figure 3.2. 162

Figure B.14. Permission for Chapter 4. 163

Figure B.15. Permission for Figure 5.1. 165

Figure B.16. Permission for Figure 7.1. 167

Figure B.17. Permission for Figure 7.2. 168

LIST OF TABLES

Table 4.1. Characteristics of synthesized copolymers..... 48

LIST OF ACRONYMS/ABBREVIATIONS

ACN	Acetonitrile
CDCl3	Deuterated Chloroform
CNTs	Multi Walled Carbon Nanotubes
CSC	Cancer Stem Cells
CTA	Chain Transfer Agent
DCC	N, N'-Dicyclohexylcarbodiimide
DCM	Dichloromethane
DCU	1,3-Dicyclohexylurea
Dex	Dextran
Dex-FITC	Fluorescein Isothiocyanate-Dextran
DMAP	4-Dimethylaminopyridine
DMF	Dimethylformamide
DMPA	2,2-Dimethoxy-2-Phenylacetophenone
DMSO	Dimethyl Sulfoxide
DSC	N'N'-Disuccinimidyl Carbonate
EtOAc	Ethyl Acetate
EtOH	Ethyl Alcohol
FT-IR	Fourier Transform Infrared
GEM	Gemcitabine
HCQ	Hydroxychloroquine
HPLC	High-Performance Liquid Chromatography
IONPs	Iron Oxide Nanoparticles
IPA	Isopropyl Alcohol
KI	Potassium İodide
Na_2SO_4	Sodium Sulfate
NaCl	Sodium Chloride
NHS	N-hydroxysuccinimide
NIR	Near Infrared Light
NMR	Nuclear Magnetic Resonance
Py	Pyrene

Rbf	Round Bottom Flask
rGOs	Reduced Graphene Oxides
SEM	Scanning Electron Microscope
TBAF	Tetra-n-Butylammonium Fluoride
TBDMSCl	Tert-Butyldimethylsilyl Chloride
TEM	Transmission Electron Microscope
TFA	Trifluoroacetic Acid
UV	Ultraviolet Light
UV-Vis	Ultraviolet-Visible Spectroscopy
β -CD-$(SH)_7$	Thiolated Beta Cyclodextrin

1. INTRODUCTION

1.1. Drug Delivery Agents for Cancer Treatment

Conventional drug delivery systems have many limiting issues in the treatment of diseases due to the poor solubility of many of the drugs, accompanied by several side effects, and because of the spreading of the drug all over the body which means that very little drug will reach the disease area [1]. A controlled drug delivery system on the other hand aims to deliver drug molecules to the disease area rather than the entire body. This means lower toxicity to the body, as well as less amount of drug administration. Sending drugs to the required disease site can be achieved in several ways as shown in Figure 1.1, through benefitting from nanosized delivery vehicles such as nanoparticles, nanocapsules, polymeric or dendrimeric structures [2].

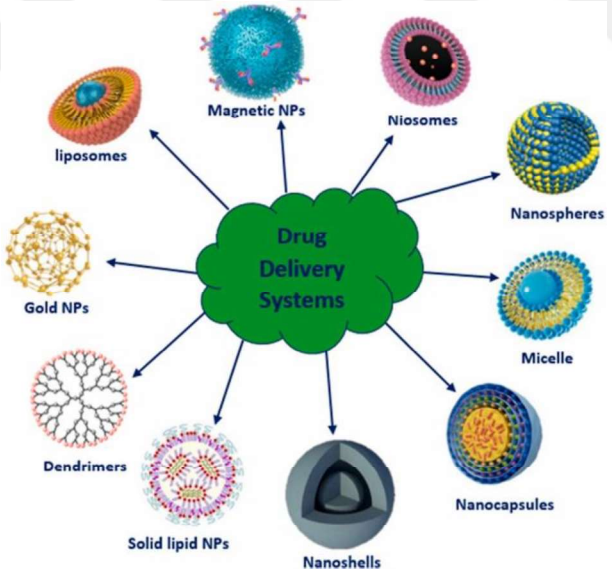

Figure 1.1. Examples of commonly utilized drug delivery systems. Adapted from reference [1].

In addition to these larger drug carrier systems, controlled delivery can be achieved via a prodrug concept. A prodrug is an inactive or less active form of the cytotoxic drug until reaching to cancerous area where it releases the active form of the drug mediated by stimuli such as an enzyme, temperature or pH [3]. While an active chemotherapy drug goes to

healthy and cancerous cells at the same time, since the inactive form of the drug has noticeably less toxicity, it diminishes the side effects of the drug on the patient. While designing the prodrug, drug attachment generally defines how and when the drug will reach the desired area and get released in its active form. The first issue is to deliver prodrug to the cancerous side without activation. This can be generally accomplished using two ways, active targeting via pH, temperature, light etc. and passive targeting which is provided by the enhanced permeability and retention effect. The enhanced permeability and retention (EPR) effect is mainly a concept stating that molecules with certain sizes like nanoparticles or macromolecular drugs go into the tumorous area rather than normal tissue due to disruption of the cell lining in the tumor site and results in an increase in the gap between the cells (Figure 1.2).

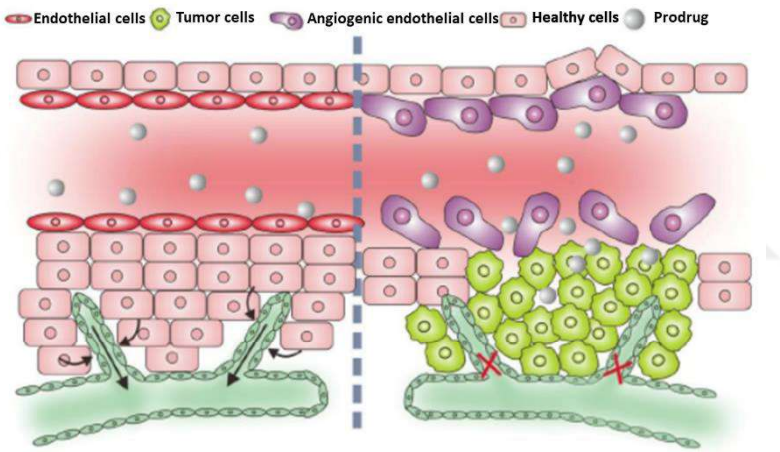

Figure 1.2. Illustration of EPR effect of prodrug in normal and tumor tissue. Adapted from reference [2].

For example, Sun and coworkers fabricated a macromolecular prodrug which benefitted from the EPR effect [3]. They were used gemcitabine (GEM) as a drug and turned it into a prodrug by functionalization with blood circulating albumin through cys34. They synthesized four prodrugs which contains different linkers with and without disulfide bond, as well as different bond types (carbamate and carbonate) between linker and drug. Obtained prodrugs were tested in terms of stability (cleavage of bonds) and accumulation on tumor. Comparing with free GEM, it was found that the prodrug with carbonate bond is 21 times more effective than free GEM in terms of bioavailability and showed 7 times higher tumor accumulation. In another work, a pH-responsive prodrug was synthesized by Zhang and coworkers [4]. They fabricated a prodrug including chemotherapy drug doxorubicin (DOX),

a targeting moiety GRGDS, coumarin as fluorescent dye and used pH-responsive hydrazone bonds. While the GRGD sequence targets $\alpha_v\beta_3$ integrin receptors which are overexpressed in many tumor cells of prostate, pancreas, breast, etc., coumarin provides simultaneous tracking using the change in fluorescence intensity arising due to quenching with DOX. The prodrug was applied on U87 human glioblastoma cell line, and it was demonstrated that the system has a potential for *in vivo* study. In addition to using one drug bearing prodrug systems, by placing two drugs on the same prodrug molecule, synergistic effect can be utilized. Synergistic effect of two drugs refers to more effective activity of the combination of the drugs on cancerous area rather than as achieved through their separate application [5]. For example, Qiu and coworkers showed that chloroquine (CQ) enhances the activity of GEM on the pancreatic tumor cells while using together which provides a very promising approach [6].

1.2. Nanomaterials

As a term nanomaterial means a construct having size between 1 to 100 nm. A nanometer can be defined as 10^{-6} mm which is approximately 100.000 times thinner than of a human hair. Since they are in small size, they have gained attention for using in many fields and they show some unique features such as large surface area, high bioavailability [7,8]. Nanomaterials are classified mainly according to their morphology, component and properties [9]. Carbon-based, polymeric nanomaterials and metal nanoparticles are some common types of nanomaterials [10]. Figure 1.3 shows carbon-based nanomaterials which consisting of carbons, their types and application areas like cellular imaging, drug delivery, in vivo imaging. One of the most feature example of this section is graphene sheets. Graphene sheets consists of sp^2 carbons connected in hexagonal structure. With reduction reaction of graphene sheet, reduced graphene oxides (rGO) are obtained. Comparing to graphene oxide, rGO is more preferable since they have better electrical conductivity [11] and propose higher surface functionalization via not only pi-pi interaction as physically but also hydroxyl and carboxylic acid groups appearing during reduction as covalently. Demirel *et al*. demonstrated and compared graphene sheets via pi-pi interaction solubilization with terminal pyrene group and pyrene pendant groups bearing PEGMA-MMA-PMA copolymer by using different pathways for solubilization [13]. At the same time, they have used different length of PEG chain (mw from 500 to 2000) to compare biocompatibility of the

obtained systems and found solubilized rGOs by longer PEG chain were less cytotoxic to cell lines.

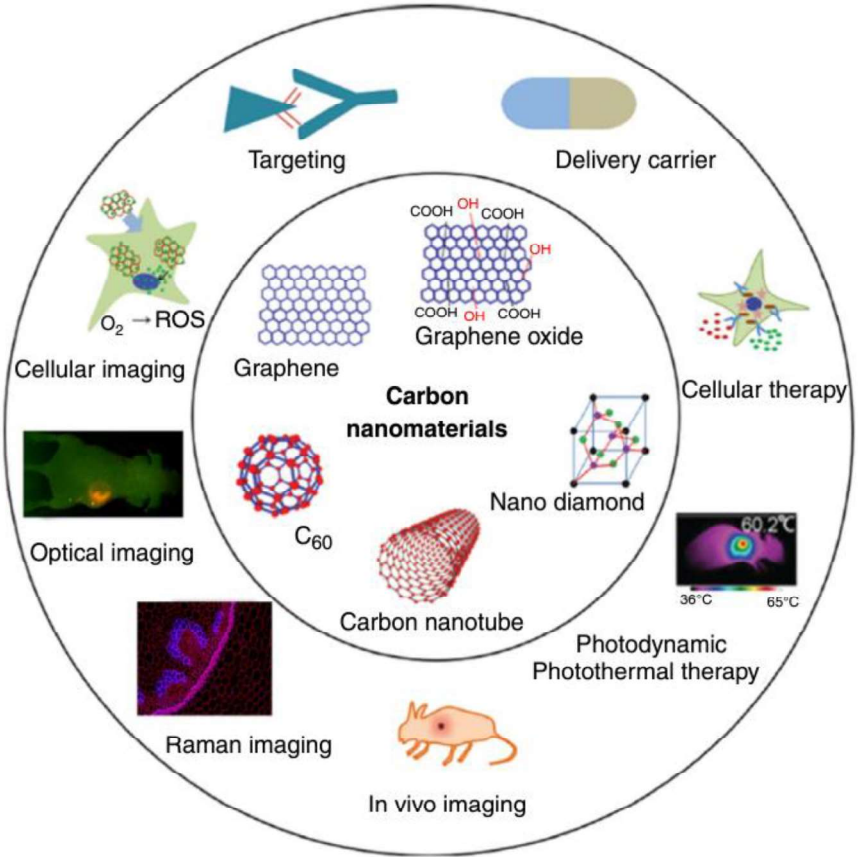

Figure 1.3. Schematic illustration of carbon nanomaterials. Adapted from reference [12].

Addition to biocompatibility of solubilized rGOs which are really good candidate for photothermal therapy (PTT) by absorbing near infrared (NIR) light and turning into heat. Chung and coworkers fabricated a drug carrier system by using BSA functionalized rGO nanosheets as doxorubicin carrier (Figure 1.4) [14]. They applied the system on U87 cell line and they were not cytotoxic till some concentration as demonstrated dose depended cytotoxicity. Then the release experiment of DOX was carried out via NIR light application on the cell line, and showed significant difference in cell viability ratio comparing with and without NIR light application. In addition to sheet form, GOs can be in the form of tubes which is called carbon nanotubes (CNTs). On the contrary of GOs two dimension, CNTs have three dimensions with sp^2 hybridization. These GOs can be turned into tube form as only one or two layers or multi layers. Thus, CNTs are called as single walled, di-walled, or multi walled CNTs (MWCNTs).

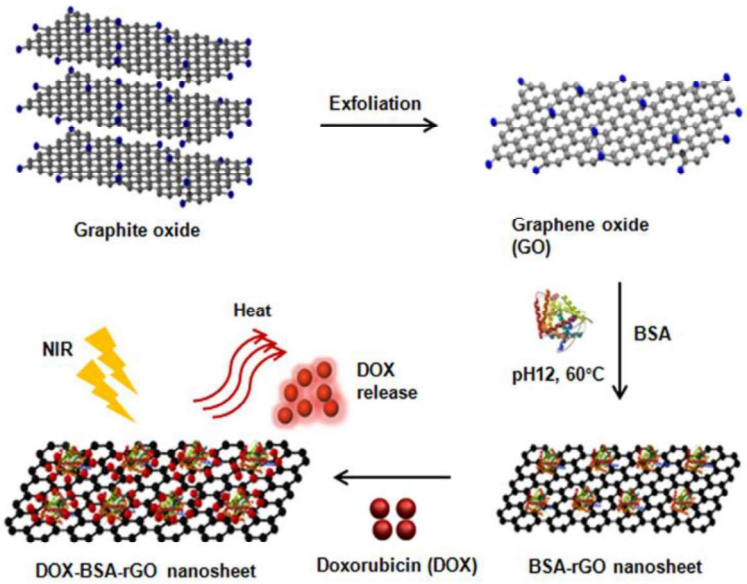

Figure 1.4. Schematic representation of DOX attached BSA-rGO nanosheet and release via NIR application. Adapted from reference [14].

Before CNTs had been discovered by Iijima in 1991 [15], diamonds were known as having good thermal conductivity, but CNTs showed better thermal conductivity much higher than diamonds [16]. CNTs have large surface area to volume ratio with small size, thus with all these features they are useful for lots of area such as an implant in tissue engineering, drug carrier or as an imaging agent [17,18]. Their most important drawback is insolubility in organic and inorganic solvents but this can be achieved via functionalization of them which can be carried out using covalent or non-covalent method with a small molecule or polymer chain (Figure 1.5) [19]. On the way of chemical interaction, Riant and coworkers demonstrated functionalization of graphene, single and multi-walled CNTs with nucleophilic addition of alkynyl moiety as well as alkyne-azide Huisgen click reaction with an azide bearing molecules like coumarin and ferrocene [20]. TGA, raman and XPS analysis were done for characterization and conductivity measurement showed the protection of CNTs electrical property but mostly, covalent interaction with CNTs damages some characteristic features of CNTs since a chemical interaction ruins regular graphene construction [21]. Thus, for CNTs, to utilize from physical interaction for functionalization is more preferable. In another way, physical interaction is preferred by using an aromatic ring bearing molecule such as pyrene unit which allows π-π interaction with CNTs. Holzinger *et al*. fabricated a small molecule which is functionalized SWCNTs via dip coating method [22].

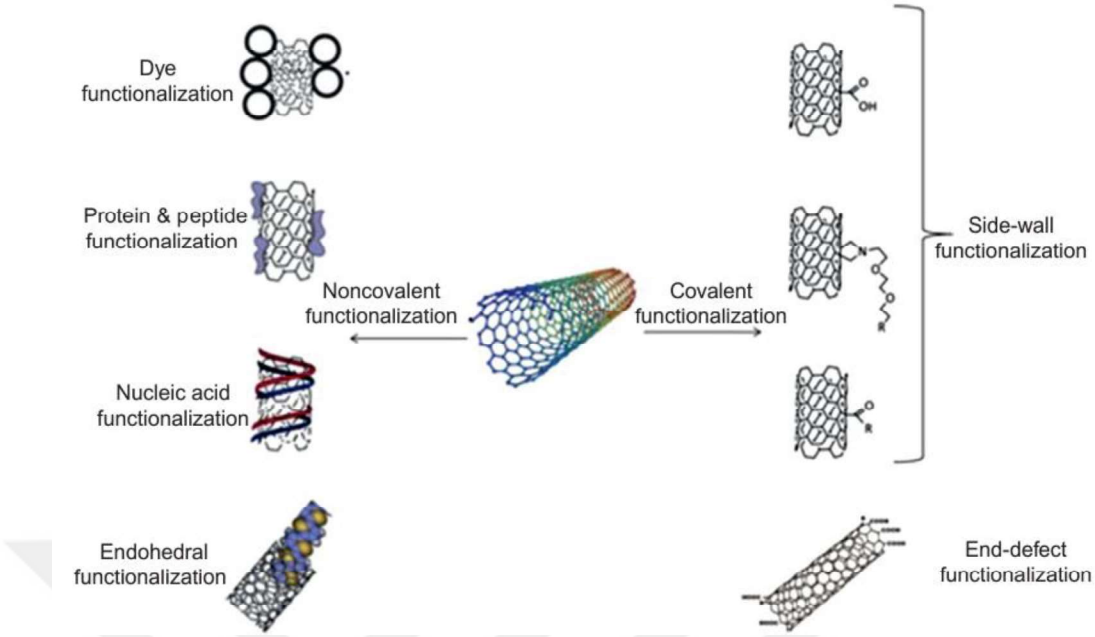

Figure 1.5. Functionalization of CNTs via covalent and non-covalent way. Adapted from reference [19].

For the functionalization they have used three different pyrene unit bearing molecules nitrilotriacetic acid (NTA), biotin and adamantane. Then to obtain polyvalent biosensor. Besides small molecule, PEG chain is really useful for functionalization in terms of providing biocompatibility and water solubility to CNTs. For example Kwon and coworkers showed functionalization with PEG chain of SWCNTs for the purpose of fluorescence imaging and photothermal therapy [23]. First, they have attached a pyrene unit to PEG chain and then it was coated to CNTs surface via π-π interaction (Figure 1.6). While pyrene unit provided fluorescence feature, with the NIR light (808 nm) application system got heated due to photothermal feature of CNTs.

Addition to PEG chain, modification of CNTs with a polymer is frequently preferred since it offers to system more functionalizable parts like chain end or side chains of the polymer and more amount addition of demanded molecule. Oh and coworkers fabricated a block copolymer containing pyrene and furan on pendant groups [24]. While pyrene groups were used for physically interact with CNTs, furan groups provided Diels-Alder (DA) reaction with maleimide bearing linker to form gelation moreover the gelation can go back via retro DA (rDA) reversibly.

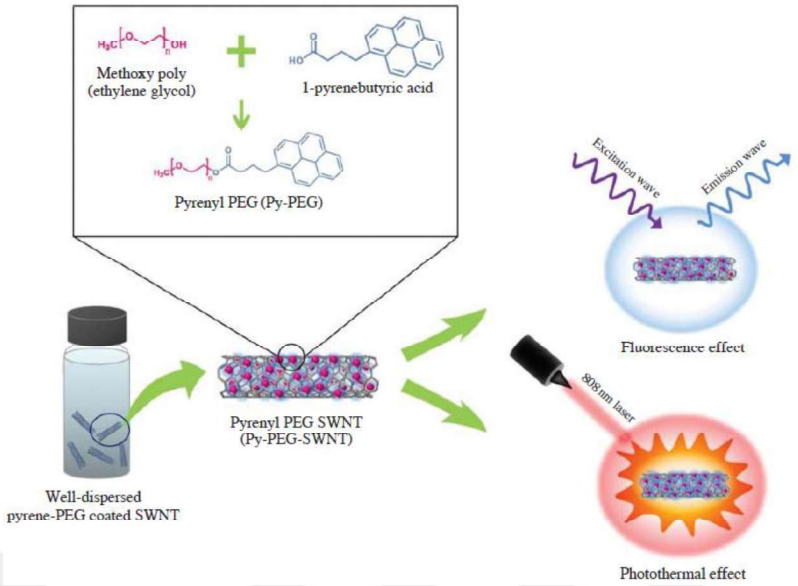

Figure 1.6. Representation of coating SWCNTs with pyrene modified PEG and using for both fluorescence and photothermal effects. Adapted from reference [23].

One of the most utilized metal nanoparticles are iron oxide nanoparticles (IONPs), they have superparamagnetic feature addition to their small size, high biocompatibility and non-toxicity. With all these features, IONPs are really functional for using such as MRI agent, drug delivery systems or sensor applications [25]. Besides good features, because of high surface area to volume ratio IONPs prone to come together and form agglomeration to decrease their surface energy. To overcome this problem, one way is to add some surfactant to IONPs solution. This plays an important role for IONPs application. Among surfactants, oleic acid is generally used for IONPs. Thus, not only prevent precipitation but also provide a way for modification of IONPs. An example of small molecule coating showed by Mathur and coworkers [26]. They have first coated α-Fe_3O_4 with maleimide bearing molecule and γ-Fe_3O_4 with a furan including molecule and then assembled different size of α-Fe_3O_4 and γ-Fe_3O_4 nanoparticles using DA reaction on the surface of NPs. By rDA, detachment of nanoparticles was achieved and showed reversibility of the system. Besides small molecules, polymer coating is the mostly preferred bringing lots of advantages although polymerization type can change depends on the demanded application area (Figure 1.7) [27]. Recently, polymer coated nanomaterials have gained attention due to their great deal of features which provide to nanomaterials after coating or attaching them. One of problems with bare nanomaterials is solubility issues, this can be easily solved with a hydrophilic polymer addition.

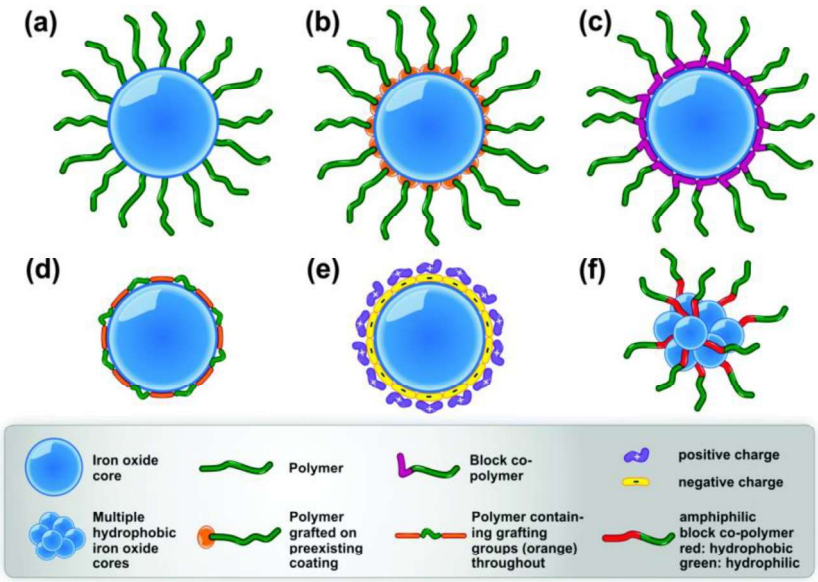

Figure 1.7. Different polymers coating of IONPs with polymers. Adapted from reference [27].

Besides, polymers are more beneficial for functionalization rather than a small molecule, because they give opportunity to add much more numbers of molecules compared to single functionalization and it is easy to adjust number of attached molecules during the synthesis or via post modification. Polymer coating is not the only way for functionalization of nanomaterials, another way is to embed nanoparticles inside a gel.

1.1.1. Hydrogels Containing Nanomaterials

Hydrogels are 3D crosslinked polymeric structures and they are known as water-loving structures due to the pores between their reticulated structures, they can swell by absorbing water without losing their viscoelastic structure and have larger volume. With the usage amount and properties of the monomers for gelation, desired hydrogel can be fabricated with the desired features such as the size of pores inside hydrogel structure. One of the study belong to Sanyal and coworkers showed adjustability of the hydrogel pores [28]. Using with different ratio of thiol modified β-cyclodextrin and diallyl PEG chains including different number of repeating PEG units as molecular weights 2, 4 and 8 KDa hydrogels were obtained by thiol-ene click reaction. Different PEG chains provide different pore sizes and that adjustable pore size opens up to hydrogel a way of carrying cargo which can be a protein, drug or etc. inside hydrogels pores. Steinle et al. showed synthetic mRNA loading to

chitosan-alginate injectable hydrogel to aim desired protein synthesis for some time [29]. Synthetic Gaussia luciferase (hGluc) mRNA loaded hydrogel during fabrication of hydrogel via electrostatic interaction then release rate of hGluc mRNA was monitored for 21 days. Results showed the system can be utilized for continuous transmission mRNA at the intended area. In another study, Zhang and coworkers fabricated an in situ formed hydrogel which loaded with two different chemotherapy drugs doxorubicin (DOX) and cisplatin (Figure 1.8) [30].

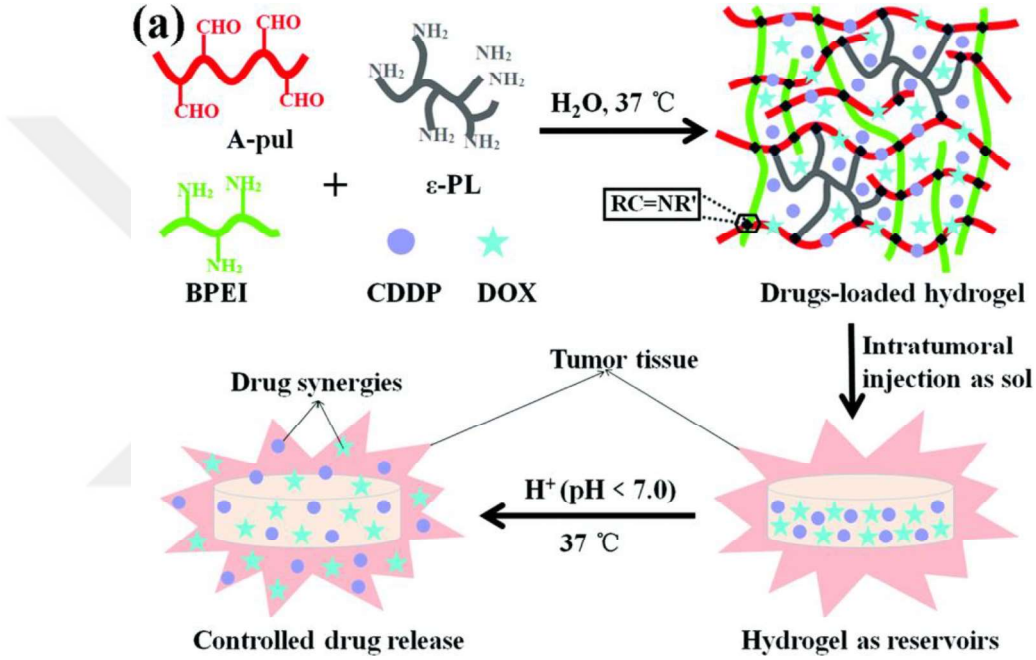

Figure 1.8. Fabrication of DOX and cisplatin loaded hydrogel and schematic illustration of drug release. Adapted from reference [30].

The reason for using cisplatin together with DOX is that while its effect on cancerous cells is around 17%, it is more effective when combined with another drug such as 5-fluouracil and DOX. So, the aim is to benefitting from synergistic effect of DOX and cisplatin. Thus, they have loaded drugs on hydrogel via both physical and chemical ways. The obtained drug carrier gels applied on Huh-7 cell in as in vivo, and also applied on mice bearing H_{22} liver tumor and showed good inhibition effect and also low systemic cytotoxicity. Not only carrying the cargo but also providing longer retention time to it is vital for an effective drug delivery system. For hydrogels-based drug delivery platforms, the gel can be either fabricated as ready for the drug loading which can be done beforehand or after gelation, or formulated as an injectable. The cargo can be integrated inside the hydrogel in

various ways [31]. They can be loaded to the gel via physical interactions such as electrostatic; or through chemical attachment, as well as loading can be achieved via specific host-guest type hydrophobic association. Besides, some additives can be placed within the gel to obtain extended retention time. For example, incorporation of rGOs inside gel can hold the aromatic ring bearing cargo molecule via pi-pi interaction, or cyclodextrins (CDs) can provide a cavity making a complex with a guest molecule for host-guest interaction [32,33]. Giammona and coworkers fabricated an injectable gel via azo-type Michael addition between amine modified hyaluronic acid vinyl sulfone containing β-CDs [34].

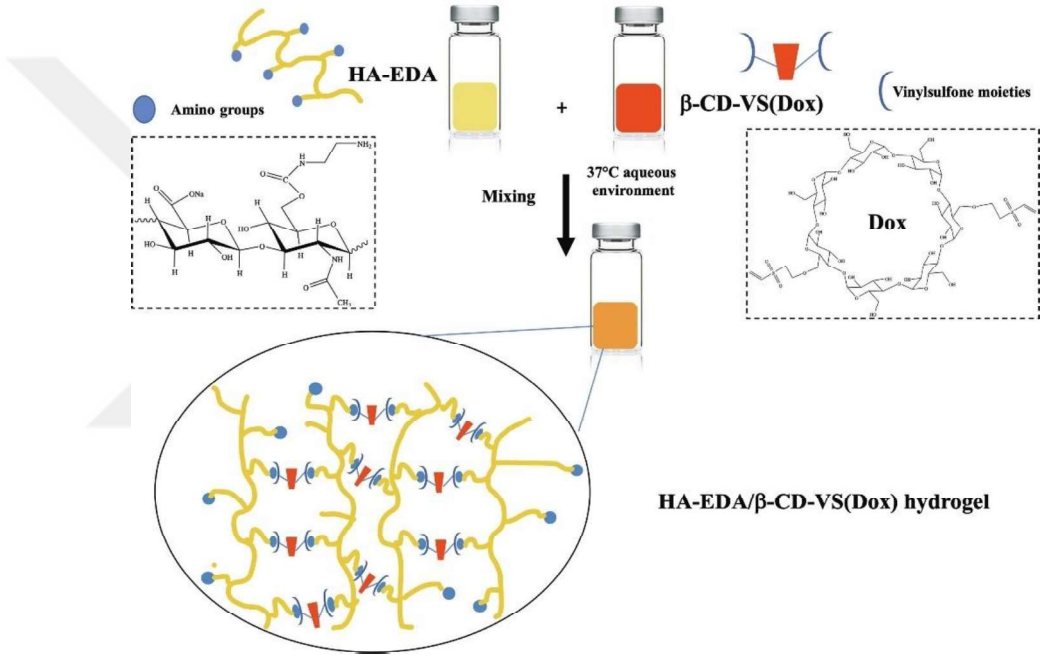

Figure 1.9. DOX containing hydrogel formation. Adapted from reference [34].

Benefitting from complexation of DOX with β-CD (Figure 1.9), they obtained sustained release in vitro study and in vivo experiment results showed considerable shrinkage of human colon carcinoma tumor volume.

On-demand release is another factor which is mainly needed for some hydrogel carrier systems. To release cargo from hydrogel a stimulus such as pH, temperature, enzymatic cleavage, etc. is provided. Shukla and coworkers fabricated a hydrogel using a maleimide modified cephalosporin as a crosslinker and four arms thiol end groups including PEG, through Michael type addition [35]. Two types of hydrogels as responsive and non-responsive were synthesized with β-lactamase cleavable linker and PEG chain between

maleimide units, respectively. This responsive linker makes hydrogel responsive to bacteria since β-lactamase is only produced by bacteria (Figure 1.10). Although other common enzymes were tried, hydrogels did not show any degradation. They showed the responsive hydrogel can act as a carrier for nanoparticles like micelles, liposomes and nanogels with size between 25-100 nm.

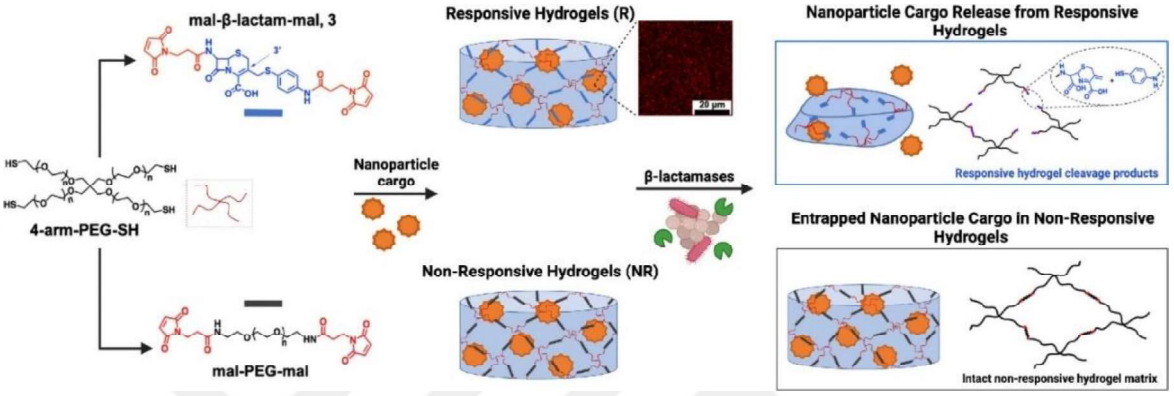

Figure 1.10. Schematic illustration of hydrogel formation, loading a nanoparticle cargo and degradation of responsive hydrogel via β-lactamase. Adapted from reference [35].

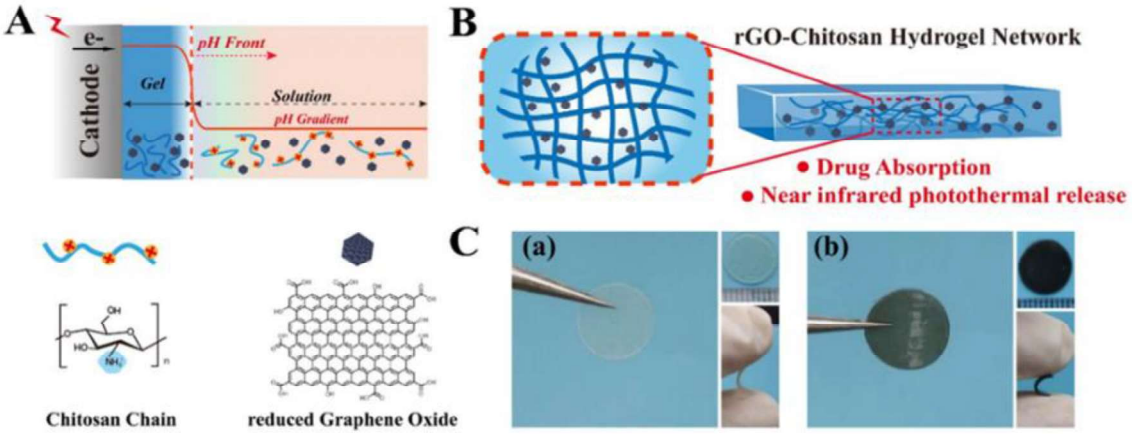

Figure 1.11. Fabrication of drug loaded rGO hydrogel. Adapted from reference [37].

Some of these stimuli can provided through nanoparticles which are embedded into hydrogel [36]. Photothermal therapy is based on temperature increase due to a light absorber nanoparticle which can convert light into heat and provide hyperthermia to NPs containing area. For the hydrogel systems, it is a frequently preferred way for release of cargo. Using NIR light on demand release, a thermoresponsive antibacterial hydrogel was fabricated by Wang *et al*. [37]. A graphene-containing chitosan hydrogel film was synthesized for loading

teriparatide which is a drug for osteoporosis treatment (Figure 1.11). In trial on rats, osteoporotic regeneration was achieved with using the constructed on demand system.

2. RESEARCH OVERVIEW

The first part of the thesis includes a synthesis of small drug molecule for pancreatic cancer treatment utilizing two drug molecules; gemcitabine and hydroxychloroquine. While gemcitabine is a chemotherapy drug using for lots of cancer types, chloroquine is a malaria drug which is recently found that it may have an effect on autophagy mechanism and can enhance the effect of a chemotherapy agent. By this purpose, a synthetic pathway was fabricated and two prodrug molecules on include GEM and HCQ with and without disulfide on the linker between them was synthesized for the treatment of pancreatic cancer.

In the second part of the thesis, three different nanomaterials were utilized for different purposes on next four projects; carbon nanotubes (CNTs), reduced graphene oxide (rGO) and iron oxide nanoparticles (IONPs). In the second project, multi walled CNTs were coated with a polymer which provides water solubility and functionality to CNTs. With successful coating and functionalization, cytotoxicity of CNTs were searched against fibroblast cells and high viability results were demonstrated. In the third project, rGO containing hydrogels were fabricated. Hydrogel was synthesized via crosslinking between thiol modified beta-cyclodextrins (β-CDSH) and vinyl group modified dextrans (dex). After obtained and characterized hydrogels, antibiotics were loaded to hydrogel by absorption method and release experiments were done as using NIR active release and passive release ways. Obtained release antibiotics were applied on different bacteria strains and successful killing of bacteria was achieved. On the fourth part of the thesis, IONPs were coated with polymer via “graft from” method including furan and poly (ethyleneglycol) (PEG) on side chains. Utilizing furan units on polymer coating, by different maleimide bearing molecules functionalization was achieved via Diels-Alder (DA) reaction. On the last part, by using FuMaMA monomer and poly (ethylene glycol) methyl ether methacrylate (PEGMEMA), a polymer was grafted on the CTA-coated IONPs. Retro Diels-Alder (rDA) reaction was achieved for activation of maleimide units. Coating was functionalized using thiol-ene and inverse electron demand Diels-Alder (iedDA) reaction sequentially and orthogonality of the system was demonstrated successfully. It can be anticipated that the system with the magnetic feature, including drug and targeting group, may be a viable candidate for the targeted drug delivery.

3. SYNTHESIS OF GEMCITABINE COMBINED WITH HYDROXYCHLOROQUINE SMALL DRUG MOLECULE FOR ANTITUMOR ACTIVITY IN PANCREATIC CANCER CELLS

3.1. Introduction

3.1.1. Pancreatic Cancer

Cancer stands as one of the most widespread causes of death in the world. The disease involves an abnormality of cells growth in the body. Pancreatic ductal adenocarcinoma (PDAC) is one of the most frequently seen type of pancreatic cancer, ranking fourth in cancer-related deaths. Its overall five years survival rate is only around 5% which is really low compared to other major cancer types [38]. Besides, early detection on first stages of the pancreatic cancer is nearly impossible, it is a really silent disease. When it gets to the level of being diagnosed, it is usually in stage 4 and metastatic, unfortunately [39,40]. With damage on a cell as a result of genetic or other factors, a mutated cell arises and then every individual cancer cell divide, grows and multiplies anomalously at a rapid rate. This creates a tumor on that area and without any diagnosis or treatment, the damaged cancerous cells will travel throughout the body, which is called metastasis [41]. That is the reason for approximately 80% of the patients with PDAC are considered to be inconvenient for a subtraction operation [42]. Even with a successful surgical removal of the tumor, 5-year survival rate is under 25% and after a while it returns back to more than 75% of patients. As a most potential reason for this recurrence, circulating cancer stem cells (CSC) are considered and they can explain why pancreatic cancer is so resistant to chemotherapy. CSC are stem cells coming from cancerous cells that participate in blood stream and are carried through the body (Figure 3.1) [43]. In this sense, it is really crucial to fabricate an effective drug or treatment method for pancreatic cancer. With the diagnosis of pancreatic cancer, firstly chemotherapy is recommended and applied as treatment no matter which phase in it. Efficiency of chemotherapy is important especially for the patients who are not convenient for surgical operation because of metastasis.

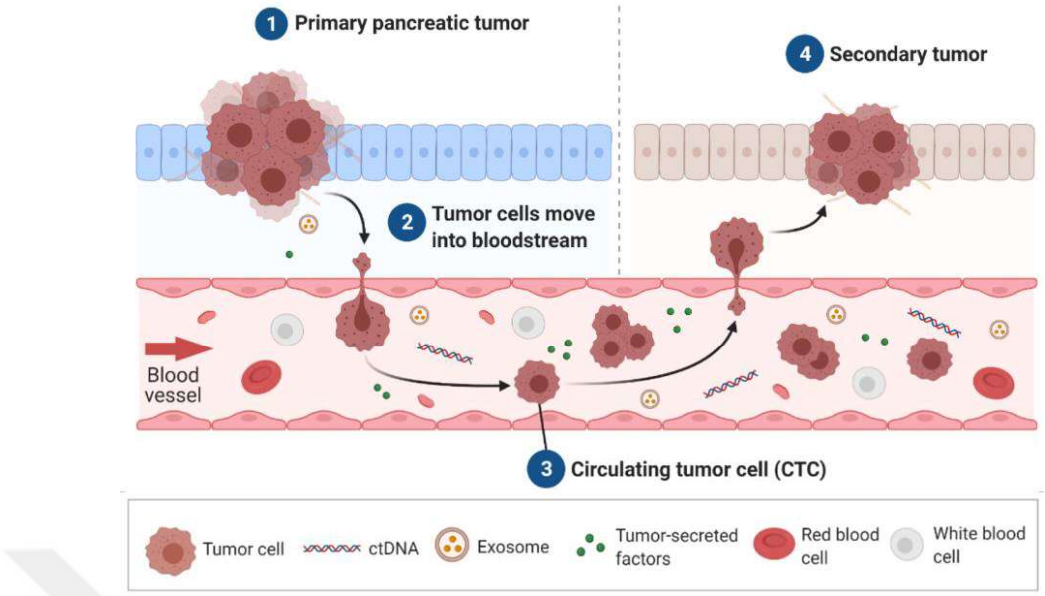

Figure 3.1. Schematic illustration of metastasis of PDAC via circulating tumor cell in blood stream. Adapted from reference [43].

3.1.2 Gemcitabine (GEM) and Hydroxychloroquine (HCQ) Drugs

Gemcitabine (GEM) is one of the most commonly used chemotherapy drug, not only used for pancreatic cancer but also it is used to treat a number of other cancers such as breast, ovarian and bladder cancer [44-46]. For chemotherapy it is applied by slow injection into a vein and it targets cells that are dividing rapidly including cancer cells and healthy cells. When it is used in its free form, lot of drawbacks come together along with the benefits. Firstly; free GEM suffers from lack of tumor specificity, and goes to cancerous and healthy cells at the same time and this leads to high general toxicity to the body. Secondly, approximately 90% of GEM undergoes rapid deactivation exhibiting a short half-life nearly 45 min in blood circulation due to formation of an inactive derivative; dFdU [47]. Third, many pancreatic cancer cells exhibit resistance to GEM treatment and make the treatments ineffective [48]. In order to obtain more effective treatment, several studies were carried by using GEM along with an autophagy inhibitor molecule by taking advantage of synergistic antitumor effect [49,50]. Liang and coworkers showed application of WP1130 which is a partially selective deubiquitinating enzyme, together with GEM increases sensitivity to pancreatic tumor by inhibiting autophagy [51]. In another study, Qiao et al. demonstrated synergistic activity of GEM with triptolide that is a drug derived from a herb called *Tripterygium wilfordii*. In addition to uses for inflammation, autoimmune disease and organ

transplantation, it induces apoptosis. Their combination were tested on Panc-1 and BxPC-3 cell lines and results demonstrated triptolide enhances antitumor activity of GEM on pancreatic cells [52].

Recently, some studies has showed that chloroquine (CQ) or hydroxychloroquine (HCQ) can target stem cells and stop proliferation [53], and also may be an inhibitor of autophagy which is an auto-cleaning process of damaged cells [54,55]. Chloroquine derivatives are known anti-malarial drugs used for malaria treatment [56]. One of that studies revealed that chloroquine can be an effective adjuvant when it is used in combination with a chemotherapy drug for treatment by targeting CSC via inhibition of hedgehog signaling and CXCR4 by triggering apoptosis of cells [53]. In another study, Qiu and coworkers showed that CQ can be a good candidate for treatment of pancreatic cancer together with GEM [6]. They have applied CQ and GEM separately and at the same time on BxPC-3 and Panc-1 cell lines, and compared their antitumor effect, as well as they applied drug mixture on a xenograft model (Figure 3.2).

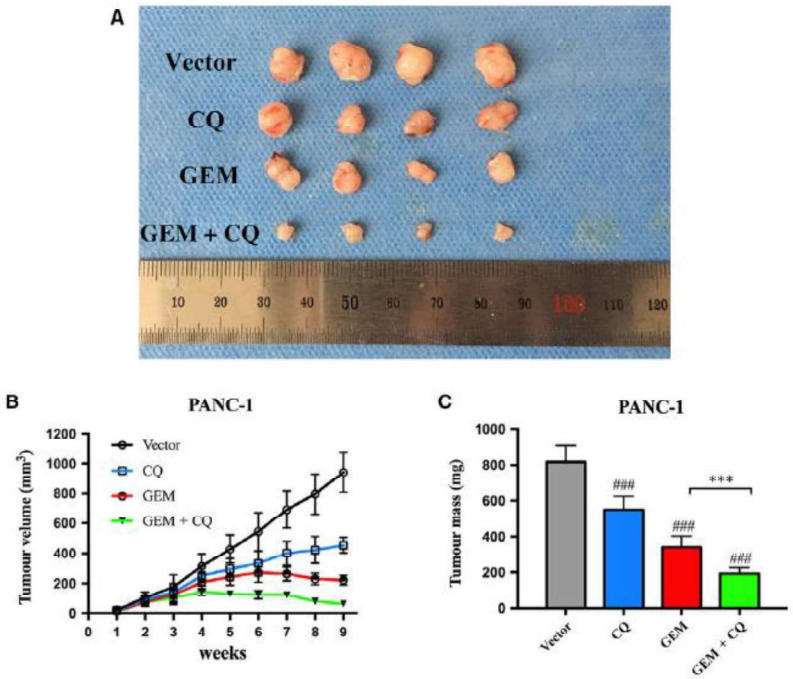

Figure 3.2. Inhibition of tumor growth in vivo by mix of CQ and GEM. (a) images of tumors surgically removed from xenograft. (b) Tumor volumes of xenograft measured twice a week. (c) Tumor mass of xenograft after 4-week growth in nude mice. Adapted from reference [6].

In this project, the aim is to design a prodrug consisting of HCQ and GEM connected via covalent attachment with a linker and evaluate their synergistic effect. A prodrug is a drug that is administered to the body in an inactive form [57,58]. Once administered, the prodrug undergoes metabolism to convert into an active form. This strategy enhances the drug's specificity and selectivity for its intended target. To this end, different release mechanisms can be used such as disulfide, amide or carbamate bonds can be installed between carrier and drug, so it provides release of drug on cancerous side as active form. In this project, it is aimed to obtain lower side effects by fabrication a prodrug GEM while taking advantage of synergistic effect with targeted stems cells via HCQ.

Two different molecules were synthesized; while one possesses a regular carbon chain linker between two drug molecules, the other includes a disulfide bond on the linker which eases the release of drugs since disulfide bond is redox-responsive, and thus gets cleaved rapidly inside cancerous cells (Figure 3.3).

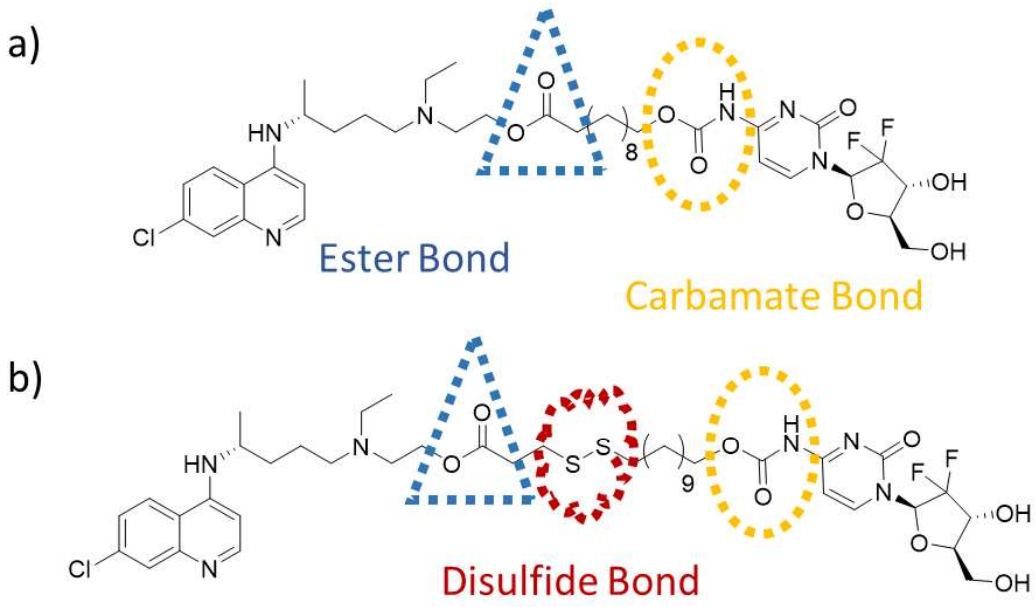

Figure 3.3. a) HCQ-GEM drug molecule with carbon chain linker. b) HCQ-GEM drug molecule with disulfide bond including linker.

HCQ is connected covalently to the linker via an ester bond and GEM is attached to the linker through a carbamate bond. The expectation is controlled release of drugs in their active

(free) forms with cleavage of these bonds inside the cancerous cells due to their acidic nature, as well as their reducing environment (Figure 3.4).

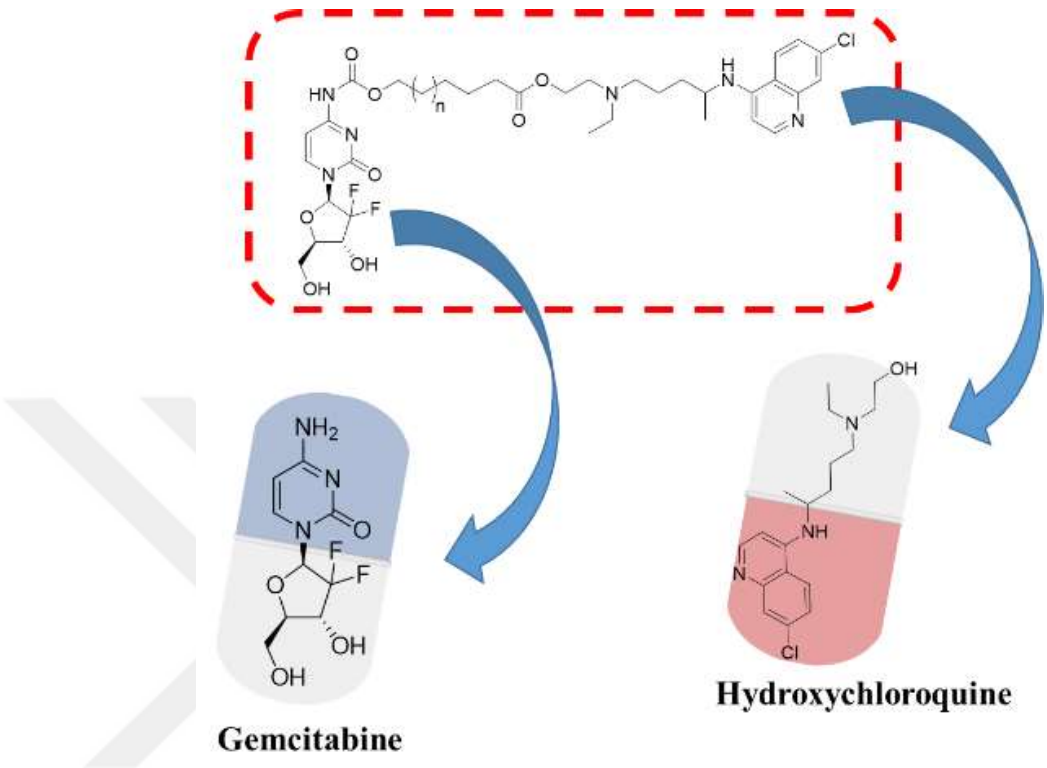

Figure 3.4. General structure of released gemcitabine and hydroxychloroquine drugs.

3.2. Experimental

3.2.1. Materials and Characterizations

All chemicals were obtained from various commercial sources unless otherwise stated. 11-bromoundecanoic acid was obtained from Sigma-Aldrich. Hydroxy undecanoic acid, TBDMSCl protected GEM, disulfide containing bis GEM were synthesized by following the previously published literature, respectively [59-61]. Triethylamine (TEA) and DMAP were obtained from Sigma-Aldrich. 1-(3-(dimethylamino)propyl)-3-ethylcarbodiimide hydrochloride (EDCI) and N-hydroxysuccinimide (NHS) were obtained from Alfa-Aesar. Dichloromethane (DCM), dimethylformamide (DMF), ethanol, chloroform, n-hexane and toluene were purchased from Merck. Anhydrous solvents were dried via molecular sieves except anhydrous solvents; toluene, THF and DCM which were

obtained from ScimatCo Purification System. Thin layer chromatography and column chromatography were performed by using silica gel plates (Kiesel gel 60 F254, 0.2 mm, Merck) and Silicagel-60 (43−60 μm), respectively. NMR spectra were recorded on 400 MHz Bruker spectrometer and measurements were collected in solvent, deuterated chloroform ($CDCl_3$) or dimethyl sulfoxide (DMSO). UV studies were done with Varian Cary 50 Scan UV/vis spectrophotometer. Fluorescent spectra were recorded via Varian Cary Eclipse Fluorescence spectrometer (Varian, Agilent, U.S.A.). Liquid chromatography-mass spectrometry (LC−MS) analysis results were obtained from LCMS 2020-Mass Spectrometer System (Shimadzu, Japan) equipped with a C-18 (5 μm, 150 × 4.6 mm) column.

3.2.2. Synthesis of Hydroxyundecanoic Acid

Hydroxyundecanoic acid was synthesized according to literature [59]. 11-bromoundecanoic acid (1.6 g, 6.08 mmol) was dissolved in a rbf and 70 mL $KOH_{(aq)}$ (2M). Reaction mix was stirred at 100 ºC for 16 h. After reaction, it was cold to room temperature, its pH was adjusted to 1 by using concentrated HCl. White ppt was collected via filtration and dried via freeze-dryer. Product was obtained as white solid with 89% yield and characterized with ^{1}H NMR. ^{1}H NMR (400 MHz, $CDCl_3$) δ (ppm): 3.64 (t, 2H, J=6.8 Hz), 2.34 (t, 2H, J=7.2 Hz), 1.58 (m, 4H), 1.26 (m, 12H); ^{13}C NMR (101 MHz, $CDCl_3$) 24.6, 25.7, 29, 29.2, 29.3, 29.4, 32.7, 33.9, 63.0, 178.7. FTIR (cm^{-1}) 1689, 2848, 2917, 3318, 3408.

3.2.3. Protection of OH Group of Hydroxyundecanoic Acid Linker

Protection was done according to literature [62]. 11-hydroxyundecanoic acid (550 mg, 2.71 mmol) was dissolved in acetic acid (816 mg, 13.58 mmol) at 0 ^{0}C. Addition of acetyl chloride (640 mg, 8.15 mmol) was done dropwise and reaction was stirred at rt for 18h. In the end of reaction, solvent was evaporated under vacuum and solid was dissolved into H_2O and extraction was done with EtOAc (3x). After it was dried via Na_2SO_4, concentrated under vacuum. Yellow viscous pure product (660 mg, 81% yield) was obtained. ^{1}H NMR (400 MHz, $CDCl_3$) δ (ppm): 4.04 (t, 2H, J=6.4 Hz), 2.34 (t, 2H, J=7.2 Hz), 2.04 (s, 3H), 1.60 (m, 4H), 1.28 (m, 12H).

3.2.4. Synthesis of Hydroxychloroquine (HCQ) from Hydroxychloroquine sulphate salt

Hydroxychloroquine sulphate salt (1g, 2.3 mmol) was dissolved in an Erlenmeyer by using 20 mL H_2O and stirred at room temperature. Then 1M NaOH solution was added to Erlenmeyer dropwise and pH was adjusted to 11. By changing pH, HCQ was precipitated as white solid. This water solution was washed with DCM a few times, and organic phase was collected and dried under vacuum. HCQ was obtained as transparent viscous (862 mg, 86% yield). ^{1}H NMR (400 MHz, $CDCl_3$) δ (ppm): 8.52 (d, 1H, J=5.2 Hz), 7.95 (d**,** 1H, J=2 Hz), 7.69 (d, 1H, J=8.8 Hz), 7.37 (dd, 1H, J1=8.8 Hz, J2=2 Hz), 6.40 (d, 1H, J=5.6 Hz), 4.89 (d, 1H, J=7.2 Hz), 3.70 (m, 1H), 3.55 (t, 2H, J=5.2 Hz), 2.55 (m, 6H), 1.63 (m, 4H), 1.32 (d, 3H, J=6.4 Hz), 1.01 (t, 3H, J=7.2 Hz).

3.2.5. Protection of Acid Group of Linker

Acetyl protected linker (663 mg, 2.71 mmol), DMAP (816 mg, 13.58 mmol), tBuOH (442 mg, 5.97 mmol) were put in a rbf and dissolved into DCM. Rbf was put into water-ice bath for 0 ^{0}C. EDCI (675 mg, 3.52 mmol) was added slowly and rxn vas left for 18h at rt. After reaction, solvent was evaporated under vacuum and crude was dissolved into H_2O and by washing with EtOAc product was obtained (330 mg, 43% yield). ^{1}H NMR (400 MHz, $CDCl_3$) δ (ppm): 4.04 (t, 2H, J=6.4 Hz), 2.19 (t, 2H, J=7.2 Hz), 2.04 (s, 3H), 1.59 (4H, m), 1.44 (s, 9H), 1.28 (m, 12H).

3.2.6. Deprotection of Alcohol Group of Linker

Deprotection was carried out according to literature [63]. Alcohol and acid groups protected linker (300 mg, 1 mmol) was dissolved into MeOH in a rbf. K_2CO_3 (414.6 mg, 3 mmol) was dissolved into MeOH - H_2O mix in a vial and added to rbf dropwise in 15 min at 0 ^{0}C. The reaction was mixed at room temperature for 16 h. In the end of reaction, DCM was added to rbf and organic phase was extracted via an extraction funnel. After dried with Na_2SO_4, product was filtered and obtained via under vacuum (175 mg, 67% yield). ^{1}H NMR (400 MHz, $CDCl_3$) δ (ppm): 3.64 (q, 2H, J=6 Hz), 2.19 (t, 2H, J=7.6 Hz), 1.54 (m, 2H), 1.44 (s, 9H), 1.28 (m, 12H).

3.2.7. NHS Activation of Alcohol Group on Linker

Linker with deprotected of alcohol group (280 mg, 1.08 mmol) and DSC (832.55 mg, 3.25 mmol) were taken in a rbf and dissolved into DCM. After TEA (657.53 mg, 6.498 mmol) addition, reaction was carried out at rt for 24 h. In the end of reaction, solvent was evaporated and diluted with sat. $NaHCO_3$. Product was obtained after an extraction with EtOAc (x3), dried with Na_2SO_4 and evaporated under vacuum (260 mg, 65% yield). ^{1}H NMR (400 MHz, $CDCl_3$) δ (ppm): 4.30 (t, 2H, J=6.8 Hz), 2.82 (s, 4H), 2.19 (t, 2H, J=7.2 Hz), 1.72 (m, 2H), 1.55 (m, 2H), 1.43 (s, 9H), 1.28 (m, 12H).

3.2.8. TBDMS Protection of Gemcitabine (GEM)

GEM (100 mg, 0.38 mmol), imidazole (77.61 mg, 1.14 mmol) were taken in a rbf and dissolved in DMF. TBDMSCl (143.18 mg, 0.95 mmol) and TEA (43.87 mg, 0.418 mmol) were added, respectively. The reaction took place at rt for 30 h. Reaction was monitored via TLC and it was stopped when all GEM starting material was spent. Solvent was evaporated under vacuum and product was purified via column chromatography (166 mg, 89% yield). ^{1}H NMR (400 MHz, $CDCl_3$) δ (ppm): 7.66 (d, 1H, J=8 Hz), 6.32 (dd, 1H, J=12, 4 Hz), 5.69 (d, 1H, J=16 Hz), 4.29 (q, 1H, J= 12, 8 Hz), 3.97 (d, 1H, J= 12 Hz), 3.88 (d, 1H, J=8 Hz), 3.78 (d, 1H, J=12 Hz), 1.73 (s, 2H), 0.93 (s, 9H), 0.90 (s, 9H), 0.11 (t, 12H, J=4 Hz).

3.2.9. Gemcitabine Addition to NHS Activated Linker

NHS activated linker (100 mg, 0.25 mmol) and TBDMS protected GEM (615 mg, 1.25 mmol) were taken in a rbf and dissolved into DCM. While reaction was stirred at rt, pyridin (100 mg, 1.27 mmol) was added to rbf. After reaction took place at 45 ^oC for 2 d, solvent was evaporated under vacuum and product purification was achieved via column chromatography (136 mg, 70% yield). ^{1}H NMR (400 MHz, $CDCl_3$) δ (ppm): 8.04 (d, 1H, J=7.6 Hz), 7.22 (d, 1H, J=7.6 Hz), 6.34 (dd, 1H, J1=10 Hz, J2=3.6 Hz), 4.34 (m, 1H), 4.18 (t, 2H, J=6.4 Hz), 4.00 (d, 1H, J=11.6 Hz), 3.94 (d, 1H, J=8 Hz), 3.81 (1H, d, J=12 Hz), 2.19 (t, 2H, J=7.6 Hz), 1.67 (m, 2H), 1.55 (m, 2H), 1.44 (s, 9H), 1.28 (m, 12H), 0.93 (d, 18H, J=18.4 Hz), 0.10 (d, 12H, J= 10Hz).

3.2.10. Deprotection of Acid Group of Linker

GEM attached linker (100 mg, 0.128 mmol) was dissolved into DCM in a rbf. Temperature of the mix was adjusted to 0 ºC. While reaction was stirring TFA (440.7 mg, 3.86 mmol) was added and reaction was done at rt for 2 h. After reaction, solvent was evaporated under vacuum and product was obtained (44 mg, 95% yield). ^{1}H NMR (400 MHz, $CDCl_3$) δ (ppm): 8.02 (d, 1H, J=8 Hz), 7.29 (d, 1H, J=7.2 Hz), 6.31 (dd,1H, J1=9.2 Hz, J2=3.6 Hz), 4.32 (m, 1H), 4.20 (t, 1H, J=8 Hz), 4.00 (d, 1H, J=11.6 Hz), 3.94 (d, 1H, J=7.2 Hz), 3.81 (d, 1H, J=12 Hz), 2.38 (t, 2H, J=6.4 Hz), 1.65 (m, 4H), 1.30 (m, 12H), 0.92 (d, 18H, J=18 Hz), 0.11 (d, 12H, J= 9.2 Hz).

3.2.11. HCQ Addition to Linker

GEM attached linker (200 mg, 0.283 mmol), HCQ (47.26 mg, 0.141 mmol), DCC (61.07 mg, 0.296 mmol) and DMAP (5.13 mg, 0.042 mmol) were taken in a rbf and dissolved into anhydrous DCM. Reaction solution was purged with N_2 for 15 min. Reaction was checked with TLC and took place at rt for 48h. Solvent was evaporated under vacuum. After purified by column chromatography, pure product was obtained (15 mg, 1.5% yield). ^{1}H NMR (400 MHz, $CDCl_3$) δ (ppm): 8.52 (d, 1H, J=4.4 Hz), 8.02 (d, 1H, J=4.8 Hz), 7.95 (s, 1H), 7.71 (d, 1H, J=9.2 Hz), 7.31 (d, 1H, J=8.8), 6.41 (d, 1H, J=5.2 Hz), 6.33 (d, 1H, J=9.2 Hz), 5.24 (d, 1H, J=4), 4.33 (m, 1H), 4.15 (m, 4H), 4.00 (d, 1H, J=11.2 Hz), 3.94 (d, 1H, J=8 Hz), 3.80 (d, 1H, J=11.6 Hz), 3.74 (s, 1H), 2.69 (t, 2H, J=5.2 Hz), 2.51 (m, 4H), 2.25 (t, 2H, J=6.8 Hz), 1.63 (m, 8H), 1.30 (d, 3H, J=5.2 Hz), 1.24 (m, 12H), 0.99 (t, 3H, J=6.4 Hz), 0.96 (s, 9H), 0.90 (d, 18H, J=18.4 Hz), 0.11 (d, 12H, J= 9.2 Hz).

3.2.12. Deprotection of GEM-HCQ Drug Molecule OH groups (GEM-HCQ)

GEM and HCQ bearing linker (15 mg, 0.0145 mmol) were taken in a rbf and dissolved in THF. After TBAF (9.12 mg, 0.029 mmol) addition to rbf, reaction was carried out at rt for 24 h. After reaction done, H_2O was added to rbf and product was extracted via an extraction with DCM. Organic phase was collected and dried with addition of Na_2SO_4. Evaporating of DCM under vacuum, pure product was obtained (3 mg, 25% yield). ^{1}H NMR (400 MHz, $CDCl_3$) δ (ppm): 8.40 (d, 1H, J=4.4 Hz), 8.19 (d, 1H, J=4.8 Hz), 7.92 (s, 1H),

7.86 (t, 1H, J=9.2 Hz), 7.33 (d, 1H, J=8.8), 6.42 (d, 1H, J=5.2 Hz), 6.24 (t, 1H, J=6.8 Hz), 5.11 (d, 2H, J=4 Hz), 4.50 (m, 1H), 4.50 (m, 5H), 4.01 (m, 3H), 3.64 (s, 1H), 2.73 (m, 2H), 2.58 (m, 4H), 2.24 (t, 2H, J=6.8 Hz), 1.56 (m, 4H), 1.32 (d, 3H, J=5.2 Hz), 1.24 (m, 12H), 1.01 (t, 3H, J=6.4 Hz).

3.2.13. Modification of HCQ with Aldrithiol

Aldrithiol modified HCQ was synthesized in two steps reactions. In the first part, aldritiol (500 mg, 2.27 mol) was taken in a rbf and dissolved into EtOH (12 mL) in the presence of AcOH (62 µl). In a different vial 3-mercaptopropionic acid (160.6 mg, 1.51 mol) was dissolved in EtOH (6 mL) and added to rbf dropwise in 30 minutes. The mixture was stirred at rt for 24h. In the end of reaction, product was obtained via column chromatography purification (204 mg, 63% yield). ^{1}H NMR spectrum was compatible with literature. In the second part, first part product (200 mg, 0.929 mol) was put in a rbf and dissolved in DCM (2 mL) together with HCQ (624.3 mg, 1.858 mol), EDCI (231.4 mg, 1.207 mol) and DMAP (34 mg, 0.278 mol). Reaction was carried out at rt for 24h. After column chromatography, pure product was obtained (150 mg, 30% yield). ^{1}H NMR (400 MHz, $CDCl_3$) δ (ppm): 8.50 (d, 2H, J=5.2 Hz), 8.44 (d, 1H, J=5.6 Hz), 7.94 (d, 1H, J=1.6 Hz), 7.66 (m, 3H), 7.34 (dd, 1H, J1=8.8 Hz, J2=2 Hz), 7.10 (m, 1H), 6.41 (d, 1H, J=5.6 Hz), 5.06 (d, 1H, J=6.8 Hz), 4.17 (m, 2H), 3.70 (m, 1H), 3.00 (t, 1H, J=7.2 Hz), 2.73 (m, 4H), 2.66 (m, 4H), 1.71 (m, 4H), 1.30 (d, 3H, J=8 Hz), 1.01 (t, 3H, J=7.2 Hz).

3.2.14. NHS activation of Bis(11-hydroxyundecyl) Disulfide

Bis(11-hydroxyundecyl) disulfide synthesized according to literature procedure, was taken in a rbf and dissolved into 25 mL ACN:DCM mixture (20:5). With the addition of DSC (493.26 mg, 1.8 mmol) and TEA (100 mg, 0.24 mmol), reaction was completed at rt for 5h. After 5h, solvents were evaporated under vacuum. Crude was dissolved in EtOAc (50 mL) and extracted with brine solution (10 mL). It was dried over Na_2SO_4 and product was obtained via concentration under vacuum (150 mg, 91% yield). ^{1}H NMR (400 MHz, $CDCl_3$) δ (ppm):1.26-1.36 (m, 28H); 1.61-1.174 (m, 8H); 2.66 (t, J= 8, 4H); 2.82 (s, 8H); 4.295 (t, J=6, 4H).

3.2.15. GEM Addition to Disulfide Containing Linker

NHS activated disulfide molecule (200 mg, 0.29 mmol) and TBDMS protected GEM (344.84 mg, 0.726 mmol) were dissolved into DCM (2 mL) under N_2 atmosphere. After pyridine addition (91.98 mg, 1.16 mmol), reaction was mixed at rt for 5d. Crude product was washed with brine solution (10 mL) and dried over Na_2SO_4. Pure product was obtained after column chromatography (76.5 mg, 37% yield). ^{1}H NMR (400 MHz, $CDCl_3$) δ (ppm): 0.07-0.12 0.925 (m, 24H); (d, J= 2, 36H); 1.25-1.66 (m, 34H); 2.675 (t, J= 6, 4H); 3.80 (d, J= 12, 2H); 3.94-3.04 (m, 4H); 4.18 (t, J= 8, 4H); 4.29-4.37 (m, 2H); 6.34 (dd, J= 4, J= 12, 1H); 8.23 (d, J=8, 1H); 7.26 (s, 2H); 7.71 (b.s, 2H); 8.05 (d, J=8, 1H).

3.2.16. Deprotection of Disulfide Containing Bis GEM Molecule OH Groups

TBDMS protected disulfide containing bis GEM molecule (76.5 mg, 0.053 mmol) was dissolved into THF (5 mL) and tetra-n-butylammoniumfloride (TBAF) (134.1 mg, 0.425 mmol) was added. The reaction was done at rt for 12h. Reaction solution was diluted with 10 mL water and washed with EtOAc:acetone (50:20) (70 mL). After evaporation of the solvent under vacuum, product was obtained (46.5 mg, 89% yield).

3.2.17. Synthesis of GEM-SH

Disulfide containing bis GEM molecule (93 mg, 0.095 mmol) was taken and dissolved into THF:H_2O mixture (50:50, 4 mL) in the presence of DTT (13.12 mg, 0.085 mmol). Reaction was completed at rt for 12h. After reaction, product was obtained with the evaporation of THF and lyophilization of H_2O.

3.2.18. Synthesis of Disulfide Containing Drug Molecule (GEM-SS-HCQ)

Aldrithiol-modified HCQ (24.3 mg, 0.049 mmol) was dissolved into EtOH (0.4 mL) and added to GEM-SH (1.14 mg, 0.019 mmol) solution in 0.6 mL EtOH. Reaction was carried out at rt for 12h. After evaporation of EtOH, product was washed via diethyl ether and obtained as white solid. ^{1}H NMR (400 MHz, $CDCl_3$) δ (ppm):1.00 (t, J= 8, 3H); 1.13-1.24 (m, 17H); 1.48- 1.58 (m, 8H); 2.525 (t, J= 6, 2H); 2.57- 278 (m, 8H); 3.565 (t, J= 6,

2H); 2.61- 2.75 (m, 3H); 3.77- 3.81 (m, 2H); 3.95 (t, J= 8, 1H); 4.035 (t, J= 6, 2H); 4.09- 4.19 (m, 8H); 5.765 (t, J= 4, NH); 6.07- 6.12 (m, 1H); 7.15- 7.18 (m, 1H); 7.28 (d, J= 8, 1H); 7.65- 7.71 (m, 2H); 8.06 (d, J= 8, 1H); 8.21 (d, J= 8, 1H). ^{13}C NMR (101 MHz, CD_3OD) 11.52, 20.25, 23.96, 25.48, 29.71, 34.32, 48.07, 48.37, 51.43, 53.32, 70.58, 75.46, 99.24, 117.32, 121.35, 125.01, 128.62, 134.80, 149.17, 149.97, 151.93. 171.05.

3.3. Results and Discussion

3.3.1. Synthetic Pathway of Small Drug Molecule without Disulfide Bond

General synthesis steps can be seen on the Figure 3.5, synthesis of the drug molecule was completed after 10 steps reactions. In order to attach the two drug molecules, a linker which is a linear chain includes 10 carbons was used.

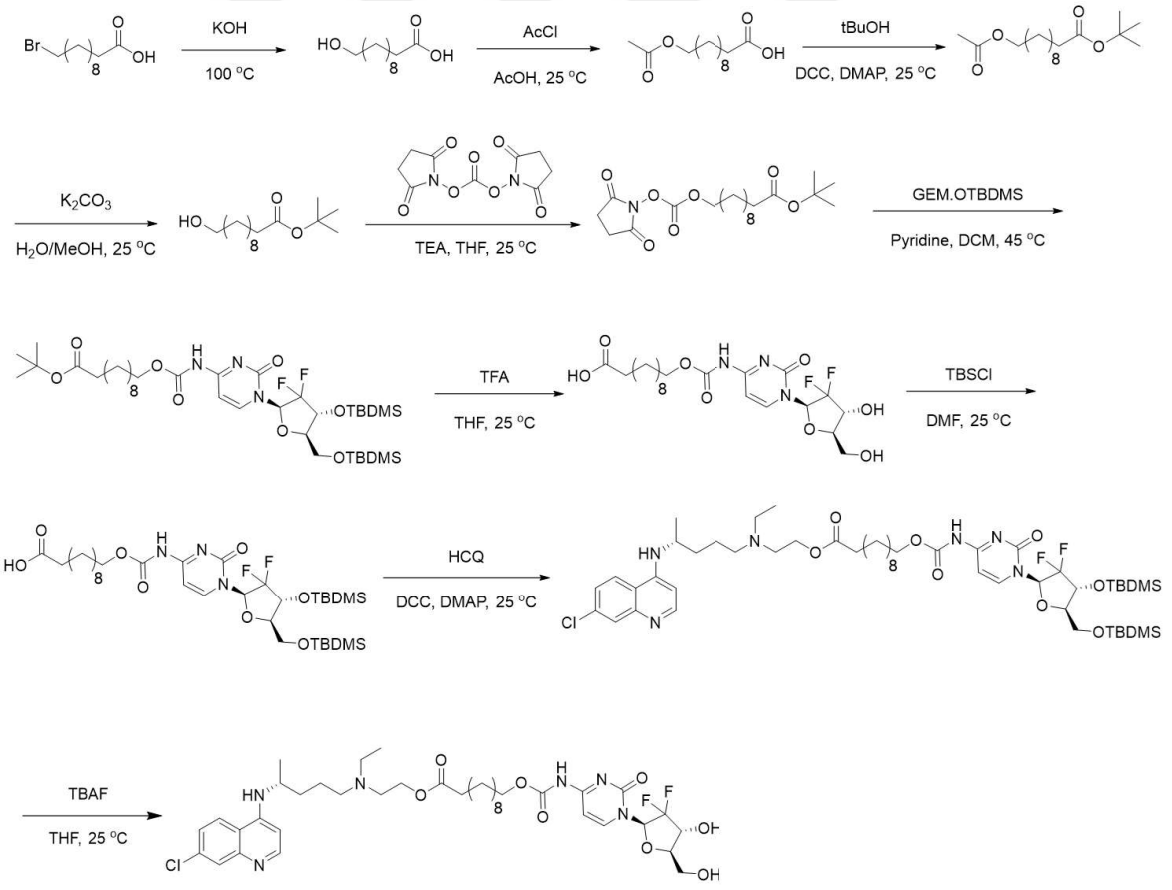

Figure 3.5. Synthetic pathway for dual drug containing prodrug, without disulfide linker.

Drug molecules were attached to the linker in a step-wise manner. First, the addition of GEM to linker via carbamate bond was accomplished. Since the -OH groups of GEM are reactive, they were protected with silyl ether protecting groups using TBDMSCl together with imidazole (Figure 3.6).

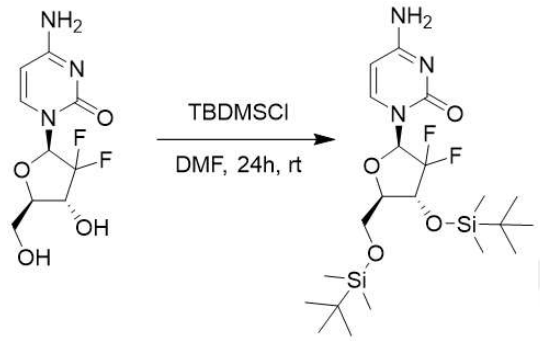

Figure 3.6. Protection of OH groups of GEM.

After purification with column chromatography, pure product was obtained, and its purity was confirmed using ^{1}H NMR (Figure 3.7). Peaks ‘a’ and ‘b’ belonging to the TBDMS protection group can be observed around 0.9 and 0.1 ppm.

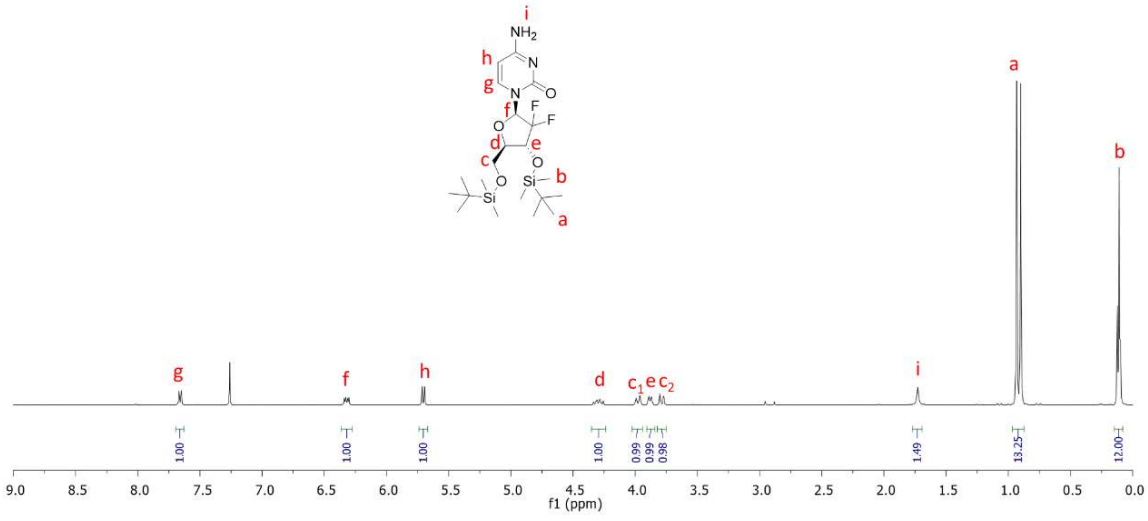

Figure 3.7. ^{1}H NMR spectrum of OH group protected GEM.

In the synthesis of the linker, firstly, 11-bromoundecanoic acid was reacted with KOH at 100 ^{o}C for 16h (Figure 3.8). After reaction, a filtration was carried out as work-up and white solid product was obtained.

After obtained first step product, in order to react OH group with NH_2 group of protected GEM, acid group of the linker had to be protected. For this purpose, OH group of linker was protected first via acetyl group.

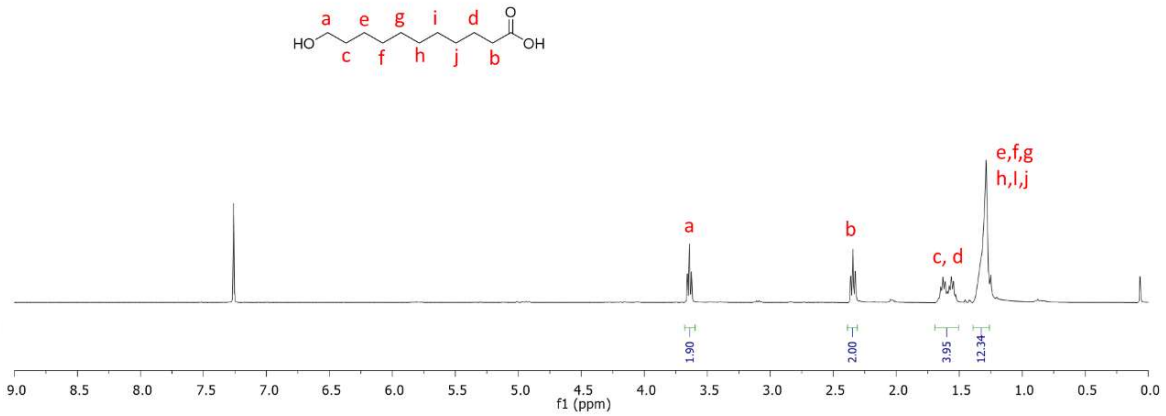

Figure 3.8. ^{1}H NMR spectrum of 11-hydroxyundecanoic acid.

Successful protection was confirmed with protons at 2 ppm belongs to acetyl group of ^{1}H NMR spectrum (Figure 3.9). Thus one side with acid functional group and the other side with acetyl protected group product was obtained.

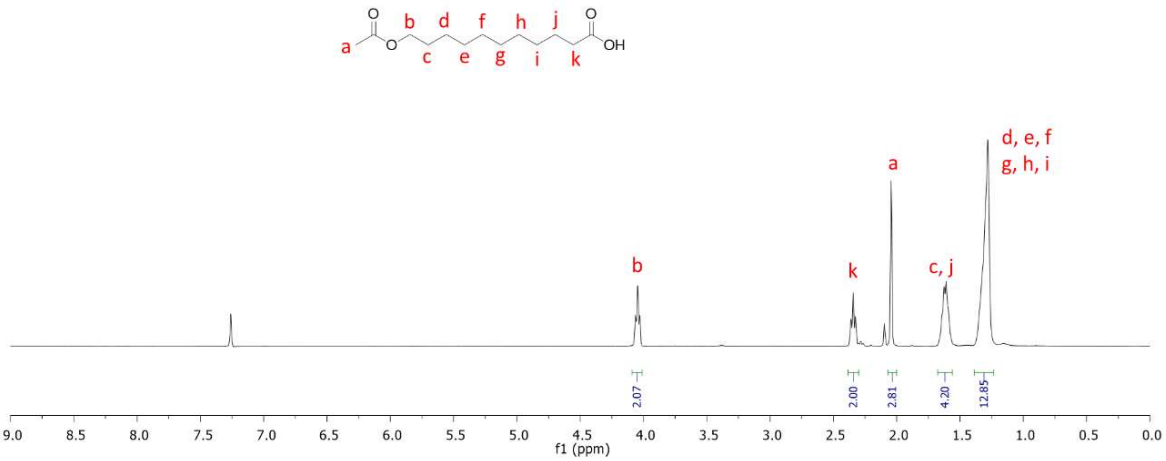

Figure 3.9. ^{1}H NMR spectrum of acetyl protected acid-containing linker.

On the next step, acid group of the linker was protected via reaction with tert-butyl alcohol at room temperature. After purification, pure product with both OH and acid groups in their protected form was obtained and characterized. Tert-butyl protection group peak can be seen around 1.4 ppm on the NMR spectrum (Figure 3.10).

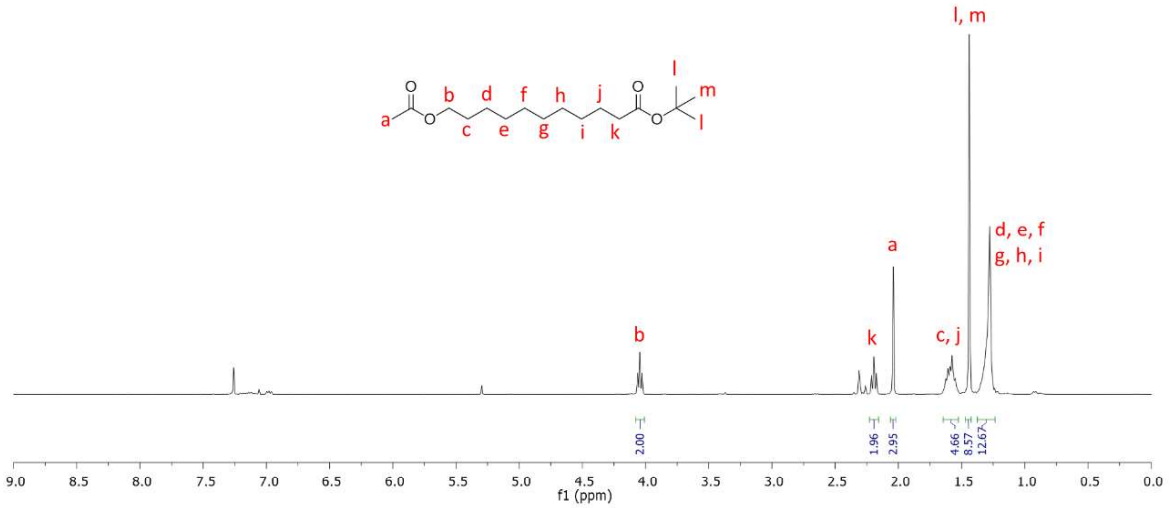

Figure 3.10. ^{1}H NMR spectrum of t-butyl ester and acetyl group containing linker.

In order to react OH group of the linker, protecting group was removed using K_2CO_3 in MeOH/H_2O medium. Obtained ^{1}H NMR spectrum verified the product with disappearance of the acetyl peak at 2.12 ppm (Figure 3.11).

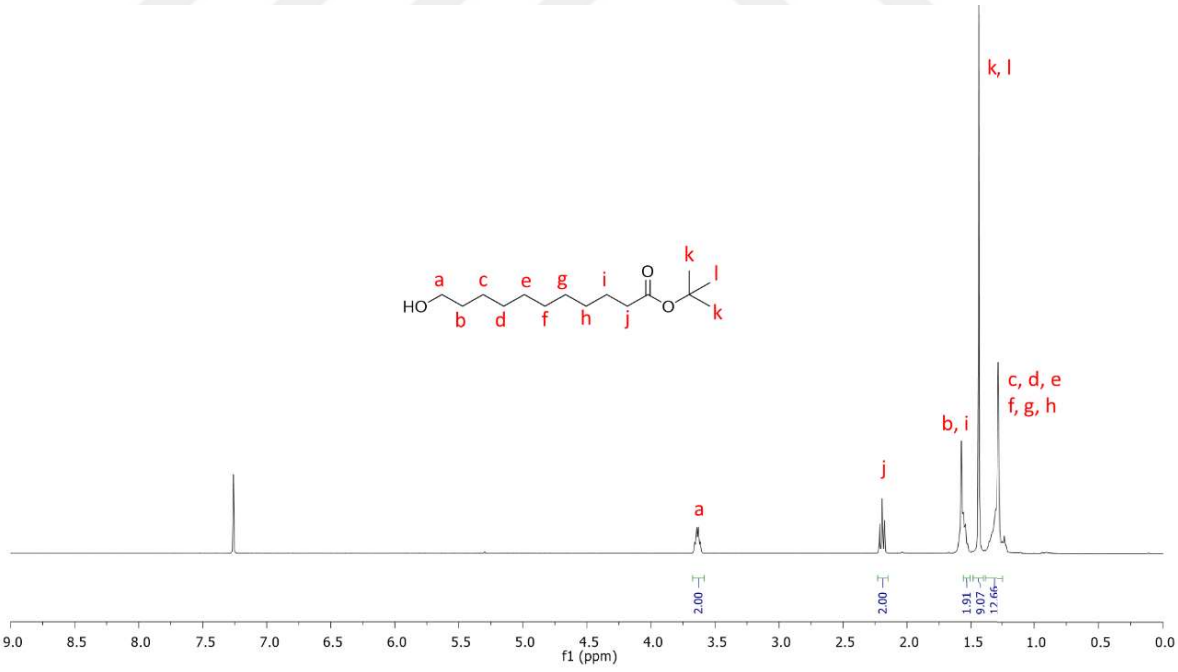

Figure 3.11. ^{1}H NMR spectrum of acid protected hydroxyl group containing linker.

For addition of GEM to linker, OH group of linker was activated via NHS in the presence of DSC and triethylamine (TEA).

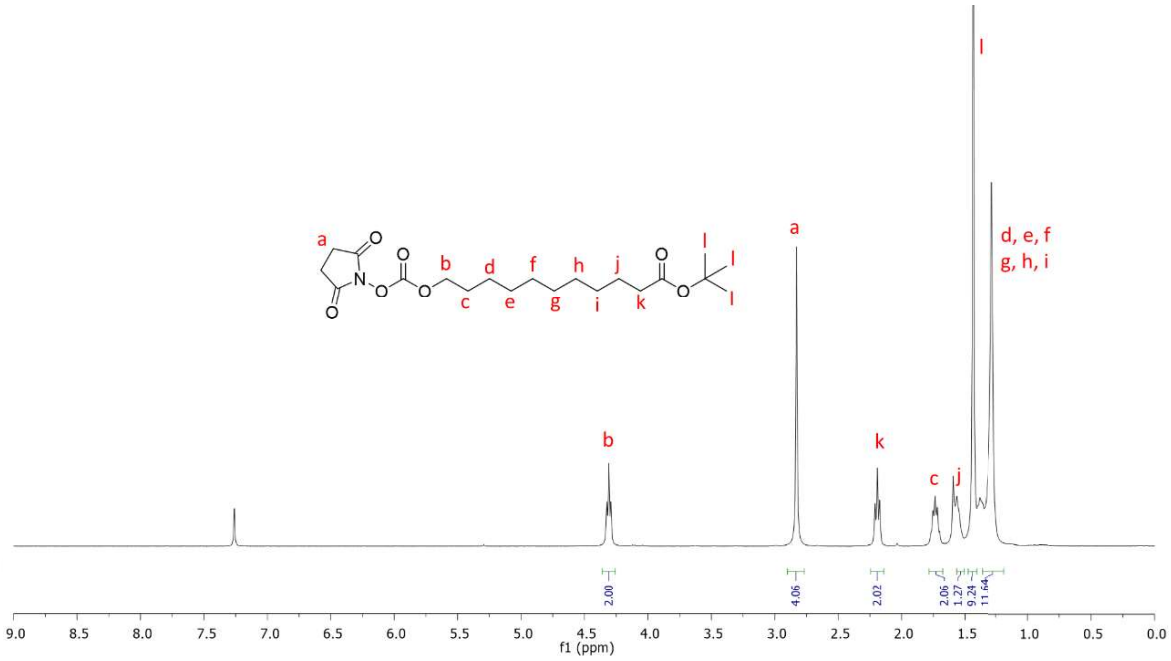

Figure 3.12. ^{1}H NMR spectrum of NHS activated tert-butyl ester containing linker.

Product was purified and characterized via column chromatography and ^{1}H NMR spectrum, respectively (Figure 3.12). Presence of protons belonging to the NHS peak at 2.8 ppm confirmed the product.

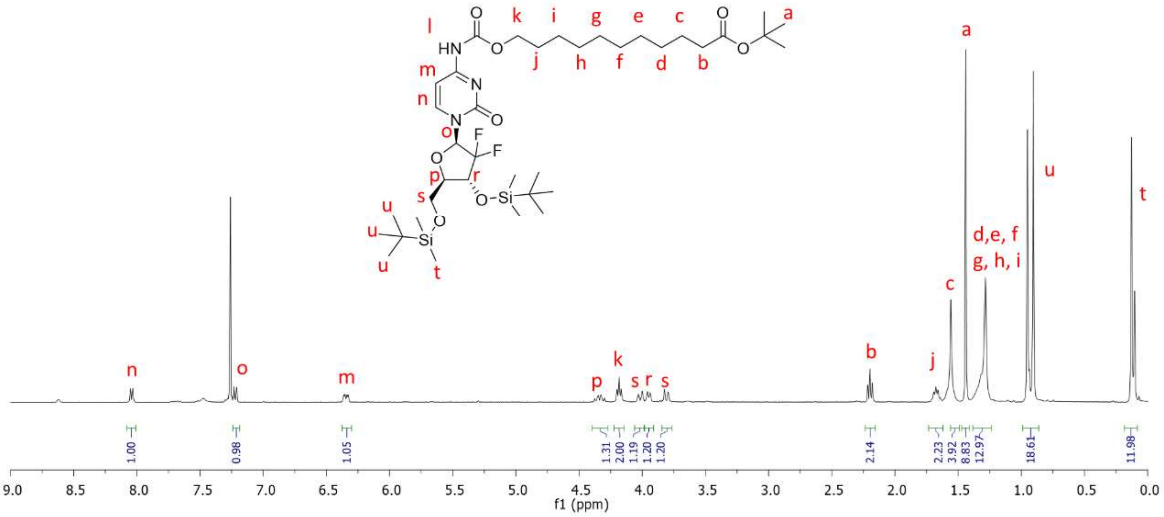

Figure 3.13. ^{1}H NMR spectrum of GEM attached tert-butyl ester containing linker.

With the successful activation of OH group, obtained linker molecule was reacted with TBDMS protected GEM at rt for 48h. After product was collected on a column chromatography, it was characterized with ^{1}H NMR (Figure 3.13) and LC-MS.

Obtained GEM added linker molecule was used for reaction with HCQ on the next step. For this reason, first removal of acid protection is done. Thus, with the aim of removing t-butyl protection of acid group, reaction was carried out with trifluoroacetic acid (TFA) and complete removal was confirmed via ^{1}H NMR and it was seen that also not only acid group protection but also protection of OH groups of GEM was removed. Since on the next step Gem-linker molecule will be reacted with OH group of HCQ, it is really crucial to be under protection for OH groups of GEM. A few different reactions with different concentrations and reaction conditions including TFA, TBAF and K_2CO_3 were tried for removal of only protection on acid group but none of them worked. The easier way was to do protection again, thus, as next step OH groups of GEM was protected again via TBDMSCl using same reaction conditions at the beginning. After reaction and purification step, pure product obtained with desired protection of OH groups and ^{1}H NMR spectrum exhibited peaks coming from TBDMS group together with expected integral of that peaks (Figure 3.14).

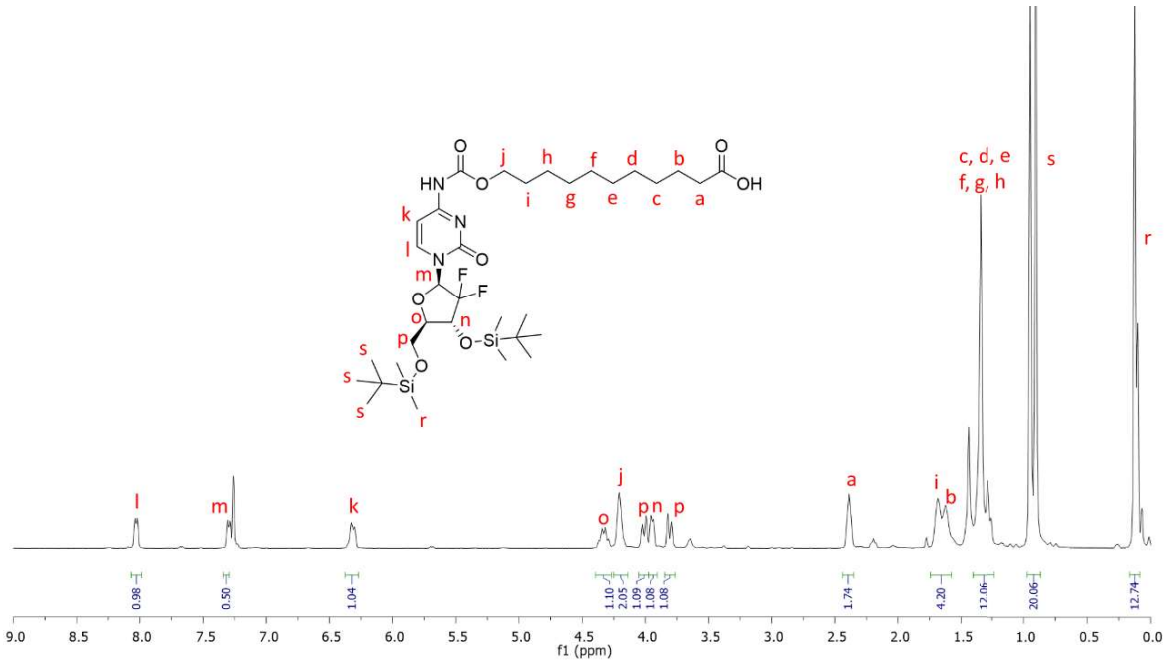

Figure 3.14. ^{1}H NMR spectrum of GEM attached acid-containing linker.

On the next step, in the presence of DCC and DMAP, GEM attached linker and HCQ were reacted through an esterification reaction.

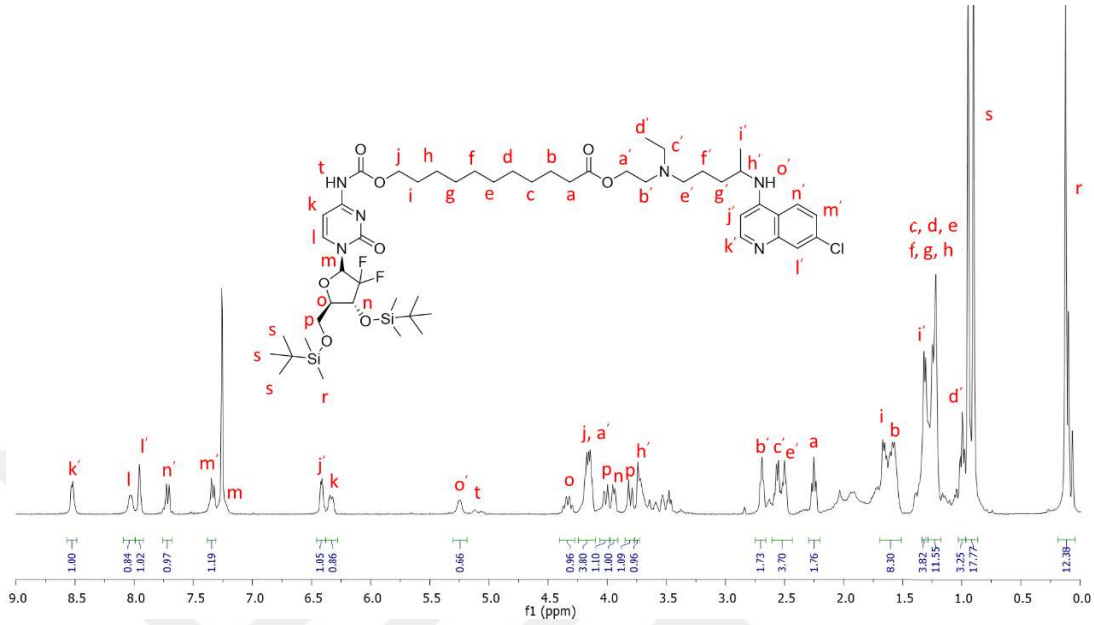

Figure 3.15. ^{1}H NMR spectrum of GEM and HCQ bearing linker.

Purification with column chromatography was difficult since product was so polar and moved on silica hardly and there were lots of side products on the TLC. As a result, reaction yield was really low which was around 25%. Obtained product was characterized via ^{1}H NMR (Figure 3.15) and LC-MS.

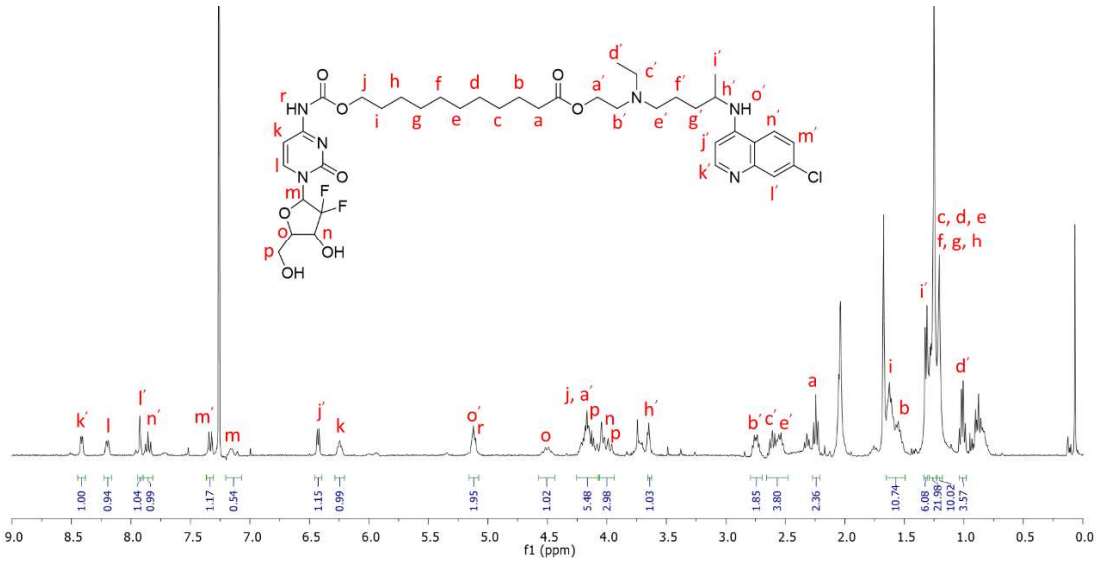

Figure 3.16. ^{1}H NMR spectrum of synthesized prodrug molecule without disulfide bond on the linker.

The last step of the synthesis was removal of OH group protections of GEM on drug molecule. Reaction was carried out at rt with using TBAF and final pure product was obtained with really low yield and confirmed via ^{1}H NMR (Figure 3.16) and LC-MS.

3.3.2. Synthetic Pathway of Small Drug Molecule with Disulfide Bond

For the synthesis of prodrug with disulfide bond, 2 different pathways were carried out and combined.

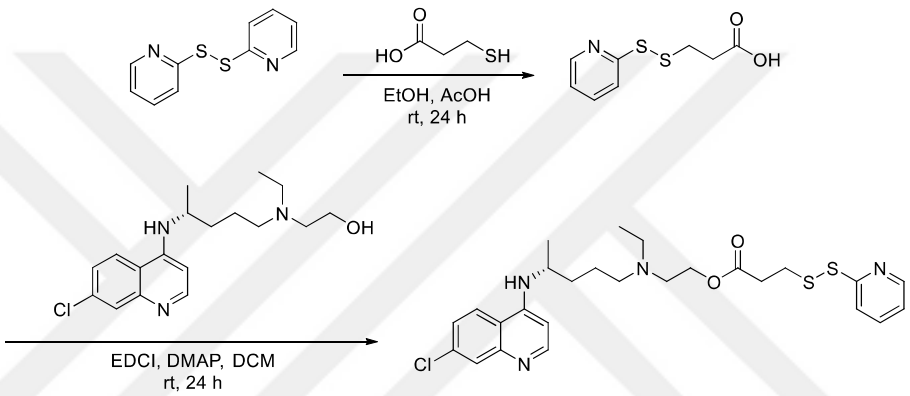

Figure 3.17. Synthesis of the pyridyl disulfide modified HCQ.

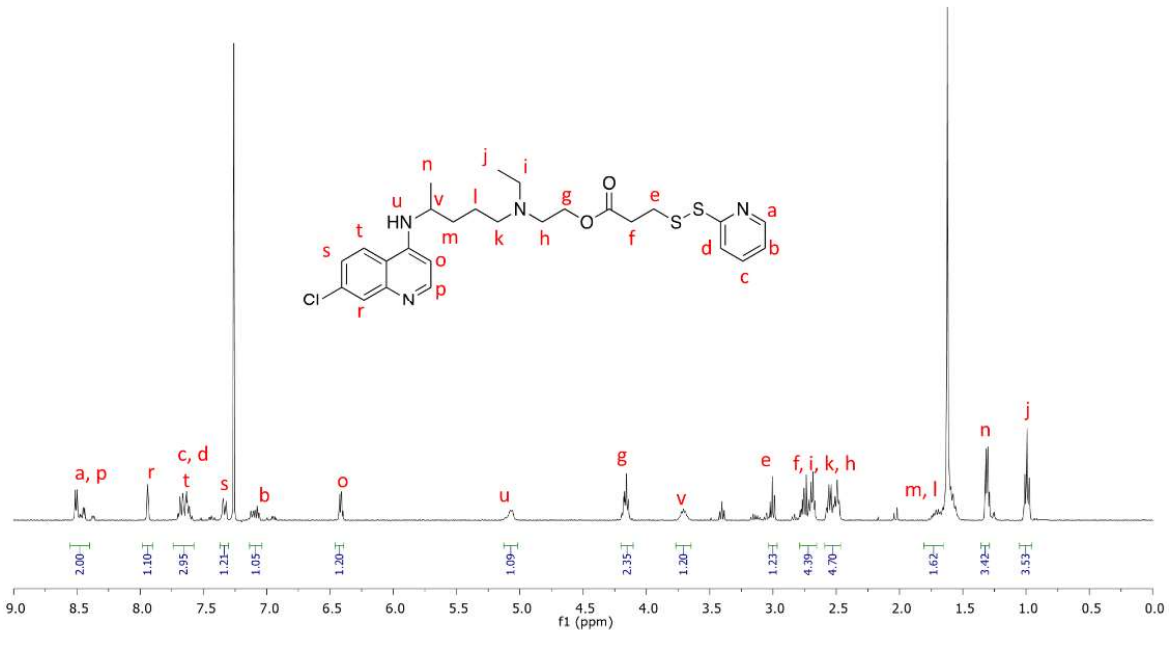

Figure 3.18. ^{1}H NMR spectrum of aldrithiol modified HCQ.

In the first part, aldrithiol was reacted with 3-mercaptopropionic acid at rt for 24h. After purification step, the reaction was done with obtained product and HCQ in the presence of DMAP and EDCI at room temperature (Figure 3.17). With the column chromatography pure modified HCQ product was obtained and characterized by ^{1}H NMR (Figure 3.18). The bond formed between HCQ and pyridyl disulfide named as g on spectrum at 4.1 ppm proves the product.

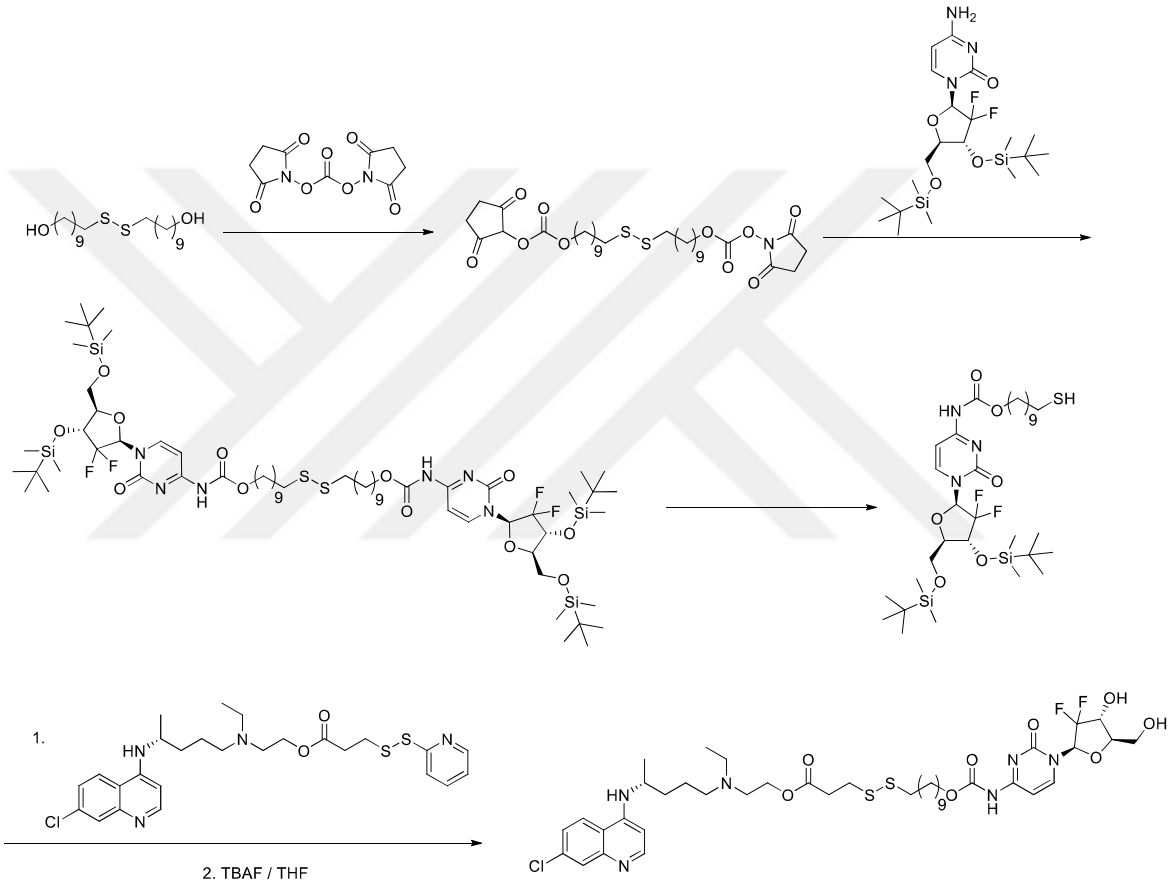

Figure 3.19. Synthesis of GEM-SS-HCQ dual drug containing molecule.

In the second part (Figure 3.19), bis(11-hydroxyundecyl) disulfide was activated via DSC and then reacted with TBDMS protected GEM at rt. The product was obtained after column chromatography purification and characterized by ^{1}H NMR. Peaks coming from both GEM and undecyl disulfide were assigned and integrals of peaks confirmed the product. After successful deprotection was done via TBAF, GEM-SH was obtained through the cleavage of the disulfide bond using DTT. ^{1}H NMR spectrum showed GEM-SH was obtained in pure form (Figure 3.20).

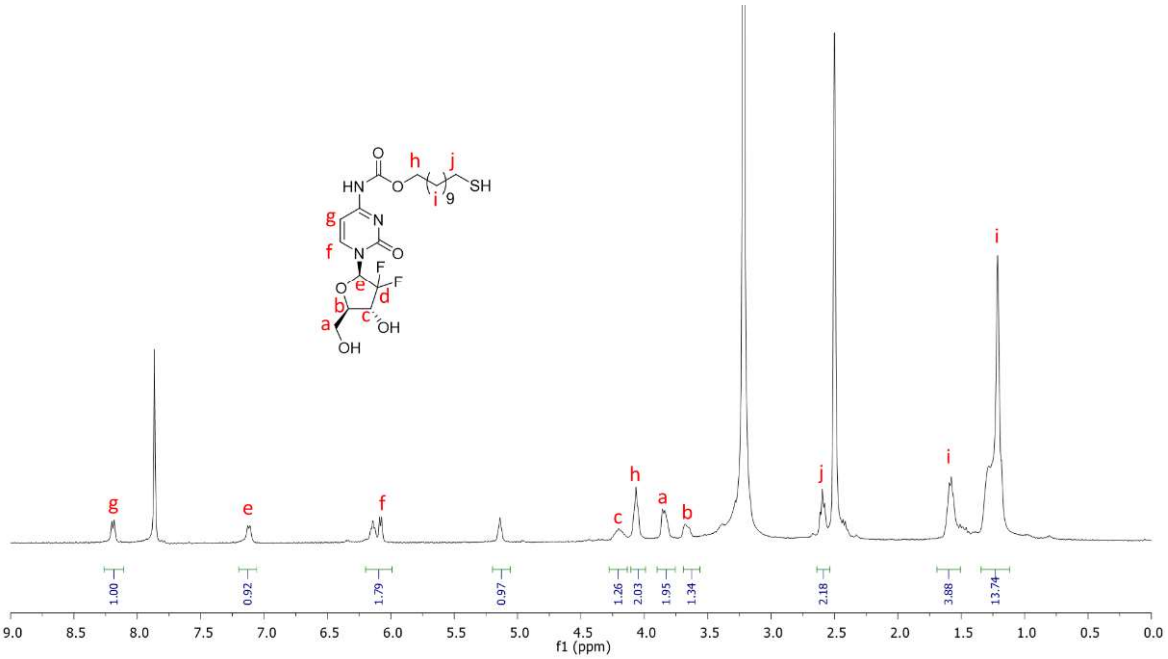

Figure 3.20. ^{1}H NMR spectrum of GEM-SH molecule.

Lastly, GEM-SH was reacted with aldrithiol modified HCQ in EtOH at rt for 12h. Pure product was obtained via washing with ether many times and characterization was done via ^{1}H NMR (Figure 3.21).

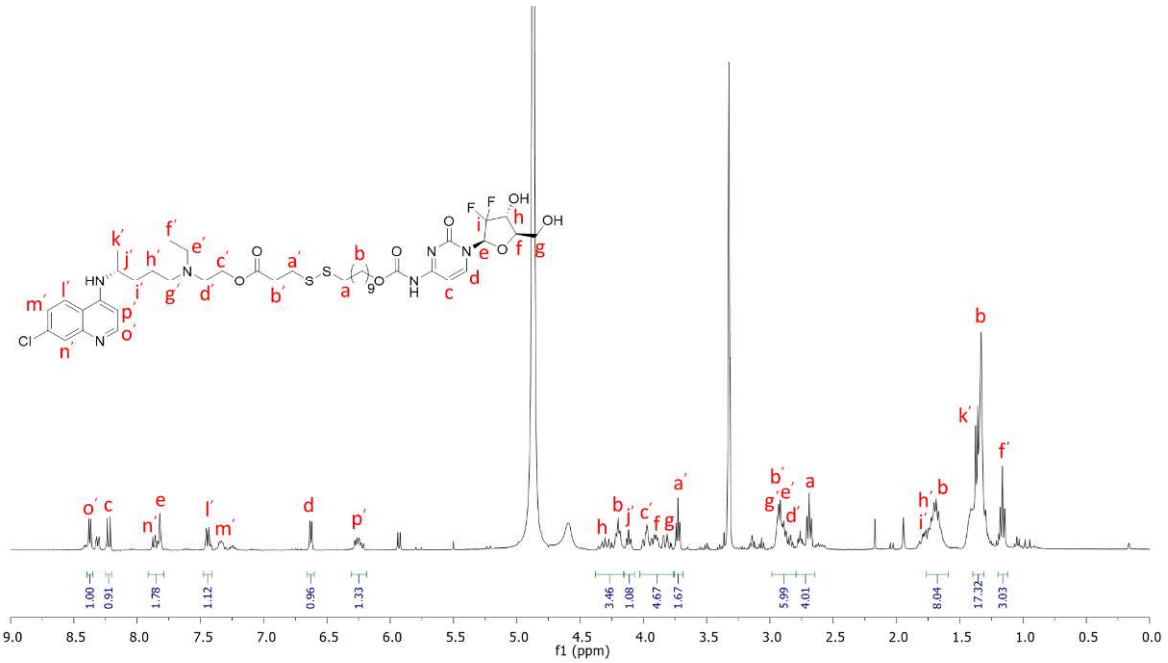

Figure 3.21. ^{1}H NMR spectrum of GEM-SS-HCQ drug molecule.

3.3.3. *In Vitro* Analysis of the Drug Molecules

Firstly, stability studies were carried out for free GEM and HCQ drugs in pH 5.5 acetate and pH 7.4 phosphate buffer solutions (Figure 3.22). They were incubated at 37 ºC and samples were removed at certain time intervals to analysis on LCMS. It was found that both GEM and HCQ molecules were stable in pH 5.5 and 7.4 buffer solutions.

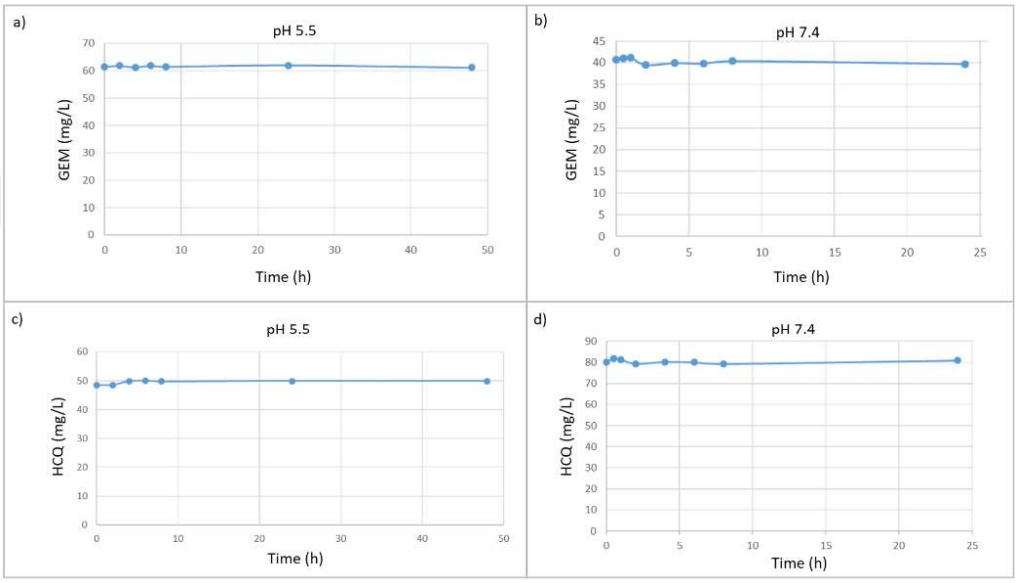

Figure 3.22. Stability graphs of free GEM (a and b) and HCQ (c and d) drugs at pH 5.5 and 7.4.

In the next step, cleavage products of GEM-HCQ drug molecule were investigated (Figure 3.23). Drug molecule (1 mg/mL) was incubated in pH 5.5 and 7.4 buffers at 37 ºC and samples were checked on LCMS.

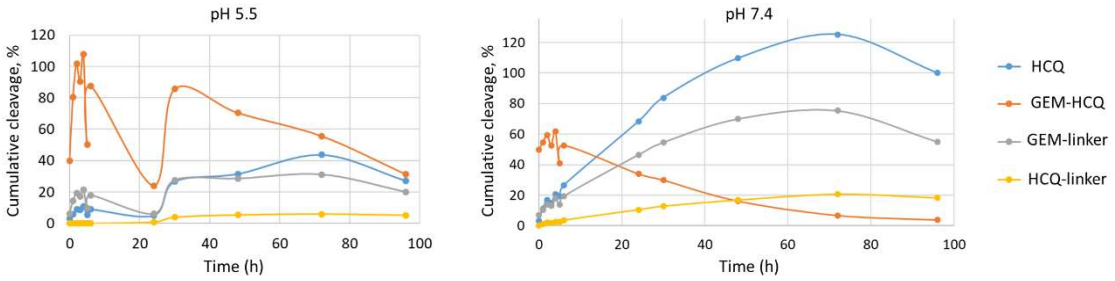

Figure 3.23. Cleavage products of GEM-HCQ drug molecule in pH 5.5 and 7.4 buffer solutions.

Products GEM-linker and HCQ-linker which formed in cleavage of GEM-HCQ drug molecule was tracked via changing in mass. Increasing of GEM-linker, HCQ-linker and HCQ as time dependent were observed.

In vitro experiments, cell viability of GEM-HCQ and Gem-SS-HCQ were investigated, free GEM, GEM and HCQ were used as control groups (Figure 3.24). Comparing two drug molecules according to their EC50 value drug with disulfide bond (EC_{50} = 8.65 x 10^{-8}) was seen as more effective with less concentration than drug without disulfide bond (EC_{50} = 4.44 x 10^{-6}) while EC_{50} value of GEM was 1.82 x 10^{-8} and GEM + HCQ was 1.55x10^{-8}. The difference between EC_{50} values of GEM-HCQ and GEM-SS-HCQ molecules due to release of free drugs via more cleavage of disulfide bond on the environment.

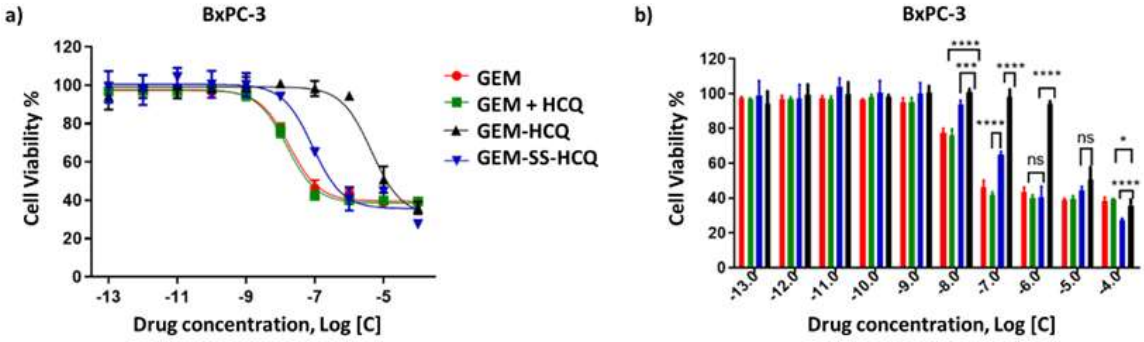

Figure 3.24. (a) Cytotoxicity of free drugs and synthesized prodrugs on BxPC-3 cell line. (b) Statistical analysis of drug molecules, (****= 0.0001, ***= 0.001, **= 0.01, ns= P>0.05), GEM is represented with red, HCQ + GEM is green, GEM-HCQ is black and GEM-SS-HCQ is blue.

3.4. Conclusion

In conclusion, it was aimed to utilize GEM as chemotherapy drug and reduce its side effects on the patient and use HCQ to improve effectivity of GEM. In order to see if the effect of drug molecule may be improved via using disulfide bond which more cleaved in tumor side. By following synthetic pathways each reaction was carried out according to procedures, needed work up steps for purification like extraction, column etc. were done and

two drug molecules bearing GEM and HCQ as with and without disulfide bond were synthesized successfully. Characterizations of each step products were done. In vitro analysis showed molecule with disulfide bond is more effective than molecule without disulfide bond.

4. TAILORING AQUEOUS DISPERSIBILITY AND BIOFUNCTIONALIZATION OF CARBON NANOTUBES USING MALEIMIDE CONTAINING CLICKABLE POLYMERS

The study in this section has been published as [65]: Cengiz, B., R. Sanyal, and A. Sanyal, "Tailoring Aqueous Dispersibility And Biofunctionalization Of Carbon Nanotubes Using Maleimide-Containing Clickable Polymers.", *ACS Aplied Polymer Materials*, Vol 3, 5707-5716, 2021.

4.1. Introduction

Since their discovery by Iijima almost three decades ago [15], carbon nanotubes continue to gain increasing interest due to their potential applications in a wide variety of fields such as nanocomposites, nanoscale electronics, biosensors, neural devices, delivery vectors for biologically active small molecules and biomolecules [64-66]. It is their unique properties like hollow tubular structure, high surface area, and remarkable mechanical, optical and thermal properties which makes them attractive building blocks for fabrication of various functional materials. In native state, CNTs can be perceived as a rolled-up graphene sheet as single or multi walled with sp^2 hybridization. Despite their all excellent features, due to strong intrinsic van der Waals forces, CNTs have poor dispersion in most organic and aqueous solvent. The intrinsic hydrophobicity that stems from the all hydrocarbon structure limits its utilization for many biological applications where intimate interfacing with the aqueous milieu is a basic requirement. While introduction of hydrophilic groups such as hydroxyl and carboxylic acid moieties are possible through chemical modifications [20], [67,68], they often result in introducing defects into the extended conjugation; hence, the approach to impart aqueous dispersibility to such carbon-based materials by anchoring hydrophilic polymeric chains mediated through Van der Waals interactions has been widely employed [69-71]. Such non-covalent interaction mediated solubilization approaches are mostly preferred since the CNTs preserve their structure and original properties, unlike covalent modifications which compromises various properties of the CNTs by ruining the extended sp^2 hybridization [21,72].

Poly(ethylene glycol) (PEG) is a polymer chain with high biocompatibility and hydrophilicity. Surface PEGylation is an important method for coating CNTs which improves their solubility in aqueous medium and thus enlarges their applications range. PEGylation not only render CNTs soluble but also decrease their toxicity compared to pristine CNTs [73]. In terms of the physical modification of various carbon-based materials such as CNTs and graphene derivatives, aromatic moiety (such as pyrene, fluorene and porphyrin) bearing small molecules or polymers are commonly used [67], [74-77]. For modification of CNTs with a polymer, aromatic moieties can be used as an initiator or they can be monomer for a polymerization and thus, pendant groups on polymer. In case of modification via a polymer, aromatic moieties can be used as an initiator or they can be a monomer for polymerization and thus, pendant groups on polymer. In an elegant approach, Oh and coworkers utilized a pyrene-terminated polymer synthesized using ATRP and then solubilized CNTs by using physical interaction [78]. In another recent study, graphene, a flat analog, was solubilized by using π-π interaction with multiple pyrene units on a PEG-based polymer as pendant groups [77].

A quick glance at the literature highlights that most of the efforts in this area has focused on using hydrophilic polymers containing hydrophobic groups like pyrene at chain end or as side chain residues for solubilization of CNTs [79,80]. Besides solubilization of CNTs, polymers can provide a route to surface functionalization of CNTs when copolymers containing reactive functional groups as side chain residues are employed, as demonstrated using polyfluorene conjugated polymers containing clickable azide groups by Adronov and coworkers [81,82]. Along these lines, recently Oh and coworkers reported synthesis of a block copolymer composed of furan and pyrene group as side chain residues, which were used to coat nanotubes and obtain crosslinked materials using the Diels-Alder chemistry [83]. One can envision that decoration of CNTs with hydrophilic PEG-based copolymers containing reactive clickable groups for facile subsequent functionalization with small molecules or bioactive ligands will expand the utility of these carbon-based nanomaterials. Among the various possible clickable groups such as azides, alkynes, and alkenes functional groups have been extensively utilized in post-polymerization functionalization. In particular, the electron deficient maleimide group has been employed as an efficient handle for conjugation of thiol-containing (bio)molecules for the past several decades [84-91]. Although it is not possible to directly incorporate the maleimide group during

polymerization, a Diels-Alder/retro-Diels Alder reaction based manipulation is well-established to provide facile access to maleimide group containing polymeric materials [87], [92-94]. Thus, fabrication of CNTs coated with PEG-based hydrophilic copolymers containing the thiol-reactive maleimide groups as side chains will provide a system amenable for reagent-free functionalization to engineer desired functional interfaces.

Herein, we report an approach that enables simultaneous solubilization and functionalization of carbon nanotubes. A set of thiol-reactive maleimide group containing amphiphilic copolymers are designed using controlled radical polymerization. Apart from the hydrophobic maleimide groups as side chain residues, an aromatic pyrene ring is introduced at chain termini of the polymers. Interestingly, while copolymers devoid of the pyrene group allows significant solubilization in aqueous media (Figure 4.1). Importantly, the role of the pyrene anchor is clear upon subsequent functionalization of these polymeric coatings with a hydrophilic tripeptide through the thiol-maleimide conjugation reaction. Only the nanotubes with the pyrene group at chain end remain dispersible, whereas the other one precipitates after conversion of the hydrophobic maleimide units to hydrophilic residues. Subsequent functionalizations with bioactive ligands are undertaken to demonstrate directed protein attachment, as well as enhanced interaction with fibroblast cells.

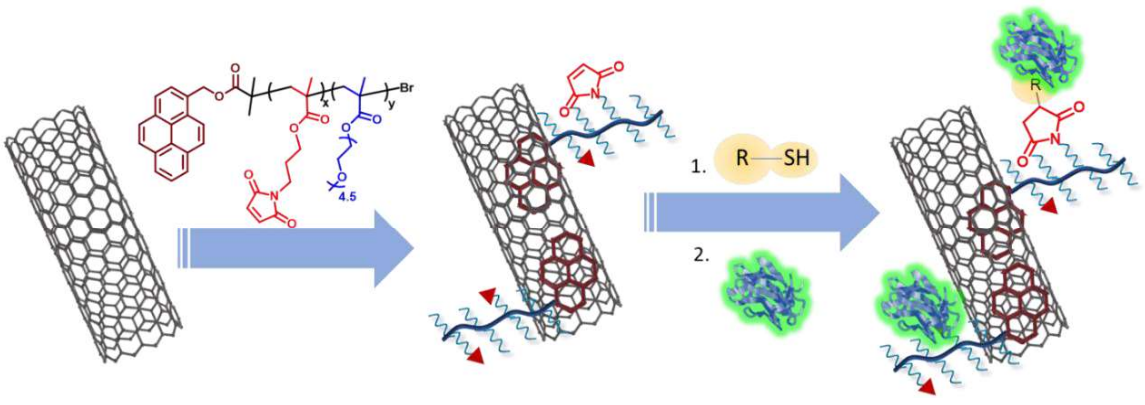

Figure 4.1. Schematic illustration of the fabrication of functionalizable carbon nanotubes using thiol-reactive maleimide group containing pyrene-terminated hydrophilic copolymers, and their facile interfacing with biomolecules and cells.

4.2. Experimental

4.2.1. Materials and Characterizations

All chemicals were obtained from commercial sources unless otherwise stated. PEGMEMA (M_n = 300 g/mol^{-1}) was purchased from Sigma-Aldrich. Before use it was passed through basic alumina column to remove inhibitor. Furan-protected maleimide-containing methacrylate monomer (FuMaMA) was synthesized according to our previous procedure [94]. 1-Pyrenylmethyl 2-bromopropanoate (pyrene initiator, PY-I) was synthesized by following previously reported protocol [95]. 1- Pyrene methanol, ethyl α-bromoisobutyrate (EIBBr), copper(I) bromide (CuBr, 99.9 %), *N*,*N*,*N*',*N*'',*N*''-pentamethyldiethylenetriamine (PMDETA) and L-glutathione reduced (GSH, 98%) were obtained from Sigma-Aldrich. Biotin-PEG-SH (MW: 1000 Da) was purchased from Nanocs (USA). Multi walled carbon nanotubes (MWCNTs) were obtained from Bayer Material Science. Streptavidin-fluorescein isothiocyanate (FITC) conjugate and Qdot 605 streptavidin were obtained from Thermo Scientific Pierce Protein Research Products. TRITC-conjugated extravidin and DAPI were obtained from Sigma. H-Arg-Gly-Asp-Cys-OH (RGDC) was purchased from Carbosynth. BCA assay kit was obtained from ThermoFisher Scientific, USA. Alexa Fluor 488 phalloidin was purchased from Invitrogen. Anhydrous solvents were obtained from ScimatCo Purification System. Thin layer chromatography and column chromatography were performed by using silica gel plates (Kiesel gel 60 F254, 0.2 mm, Merck) and Silicagel-60 (43−60 μm), respectively.

4.2.2. Instrumentation

NMR spectra were recorded on a 400 MHz Bruker spectrometer and measurements were taken in deuterated chloroform ($CDCl_3$). The molecular weights of the copolymers were determined by gel permeation chromatography (GPC) using a PSS-SDV (gram linear, length/ID 8 × 300 mm, 10 μm particle size) column calibrated with poly(methyl methacrylate) standards (1−175 kDa) using a refractive-index detector. Dimethylacetamide (DMAC) with 0.05% lithium bromide (LiBr) was used as eluent at a flow rate of 1.0 mL/min at 30 °C. Fourier transform infrared (FTIR) spectra were obtained using a Thermo Scientific Nicolet 380 FT-IR spectrometer. Microscope images were taken at room temperature with

an inverted fluorescence microscope (Zeiss Observer A1 equipped with AxioCam MRc5). Thermogravimetric analysis results were recorded with TA instrument TGA 55 analyzer.

4.2.3. Synthesis of Pyrene-terminated Furan-Protected Maleimide-containing Copolymers

Furan-protected maleimide-containing monomer (113 mg, 0.380 mmol) and Cu(I)Br (5.5 mg, 0.038 mmol) were taken in a round bottom flask equipped with a magnetic stir bar and dissolved in anisole (0.8 mL). PMDETA (13.17 mg, 0.076 mmol) and PEGMEMA (1.05 g, 3.50 mmol) were added to the stirring mixture. Pyrene initiator PY-I (14.48 mg, 0.038 mmol) was taken in a vial and dissolved in anisole (0.2 mL). After both mixtures were degassed with N_2 for 15 min, mixture in round bottom flask was taken in an oil bath at 80 ^oC and to the stirring mixture was added pyrene initiator solution. The reaction was stirred for 15 min at 80 ^oC. After the reaction, the reaction mixture was precipitated into cold diethyl ether in order to remove unreacted monomers and passed through aluminum oxide to remove residual copper complex. Copolymer P1 was obtained as a colorless viscous solid (Figure S3). Conversion = 34%, $M_{n,theo}$ =16000 g.mol^{-1}, $M_{n,GPC}$ = 17300 g.mol^{-1}, M_w/M_n = 1.41. ^{1}H NMR ($CDCl_3$, δ, ppm) 8.35-8.00 (m, 9H), 6.54 (s, 2H, CH=CH), 5.26 (s, 2H, CH bridgehead protons), 4.08 (s, 2H, OCH_2 ester protons of PEGMEMA), 3.91 (br s, 2H, OCH_2), 3.75-3.50 (m, 4H, OCH_2 of PEGMEMA and NCH_2), 3.38 (s, 3H, OCH_3 of PEGMEMA), 2.88 (s, 2H, CH-CH, bridge protons), 1.90-1.80 (m, 2H), 1.05-0.80 (m, 2H).

4.2.4. Synthesis of Ethyl α-Bromoisobutyrate Initiated Furan Protected Maleimide Containing Copolymer (P2)

Furan protected maleimide containing monomer (113 mg, 0.380 mmol) and Cu(I)Br (5.5mg, 0.038 mmol) were taken in a round bottom flask equipped with a magnetic stir bar and dissolved in anisole (1.8 mL). PMDETA (13.17 mg, 0.076 mmol) and PEGMEMA (1.05 mg, 3.50 mmol) were added to the stirring mixture. EIBBr initiator (7.41 mg, 0.038 mmol) was taken in a vial and dissolved in anisole (0.2 mL). After both mixtures were purged with N_2 for 15 min, mixture was immersed in an oil bath at 80 ^oC, and to the stirring mixture was added initiator-containing solution. The reaction was stirred for 15 min at 80 ^oC. After the

reaction, the reaction mixture was precipitated into cold diethyl ether in order to remove unreacted monomers and passed through aluminum oxide to remove residual copper complex. Copolymer P2 was obtained as a colorless viscous solid (Figure S4). Conversion = 30%, $M_{n,theo}$ =16000 g.mol^{-1}, $M_{n,GPC}$ = 16700 g.mol^{-1}, M_w/M_n = 1.45. ^{1}H NMR ($CDCl_3$, δ, ppm) 6.54 (s, 2H, CH=CH), 5.26 (s, 2H, CH bridgehead protons), 4.08 (s, 2H, OCH_2 ester protons of PEGMEMA), 3.91 (br s, 2H, OCH_2), 3.70-3.50 (m, 4H, OCH_2 of PEGMEMA and NCH_2), 3.38 (s, 3H, OCH_3 of PEGMEMA), 2.88 (s, 2H, CH-CH, bridge protons), 1.90-1.75 (m, 2H), 1.05-0.80 (m, 2H).

4.2.5. Synthesis of Pyrene Initiated PEGMEMA Polymer (P3)

Copolymer P3 was synthesized using the procedure used for obtaining copolymer P1, without the addition of FuMaMA monomer. $M_{n,theo}$ =15000 g.mol^{-1}, $M_{n,GPC}$ = 15100 g.mol^{-1}, M_w/M_n = 1.18. ^{1}H NMR ($CDCl_3$, δ, ppm) 8.35-8.00 (m, 9H), 4.08 (s, 2H, OCH_2 ester protons of PEGMEMA), 3.82 (br s, 2H, OCH_2), 3.75-3.50 (m, 4H, OCH_2 of PEGMEMA), 3.38 (s, 3H, OCH_3 of PEGMEMA), 1.90-1.80 (m, 2H), 1.05-0.80 (m, 2H).

4.2.6. Synthesis of Ethyl α-Bromoisobutyrate Initiated PEGMEMA Polymer (P4)

Copolymer P4 was synthesized using the procedure used for obtaining copolymer P2, without the addition of FuMaMA monomer. $M_{n,theo}$ =15000 g.mol^{-1}, $M_{n,GPC}$ = 12200 g.mol^{-1}, M_w/M_n = 1.10. ^{1}H NMR ($CDCl_3$, δ, ppm) 4.08 (s, 2H, OCH_2 ester protons of PEGMEMA), 3.82 (br s, 2H, OCH_2), 3.70-3.50 (m, 4H, OCH_2 of PEGMEMA), 3.38 (s, 3H, OCH_3 of PEGMEMA), 1.90-1.75 (m, 2H), 1.05-0.80 (m, 2H).

4.2.7. General Procedure for Activation of Maleimide Groups via Retro Diels-Alder Reaction

The furan-protected maleimide-containing copolymer was dissolved in anhydrous toluene and stirred under reflux at 110 ^{o}C for 8 h. After the completion of the reaction, solvent was evaporated under reduced pressure, and obtain polymer was dried under vacuum.

4.2.8. General Procedure for Modification of MWCNTs with copolymers

Copolymer (10 mg) was dissolved in H_2O (5 mL) and MWCNT (1 mg) was added to solution. After sonication for 1 h at 25 ^oC, suspension was stirred at room temperature for 48 h. Thereafter, suspension was filtered through a filter paper for removal of unbound polymer. The polymer coated CNTs on filter paper was obtained with rinsing the filter paper with tetrahydrofuran (THF). After evaporation of THF, polymer coated CNTs were obtained as black solid.

4.2.9. Conjugation of Polymer Functionalized MWCNTs with Glutathione via Thiol-ene Reaction

L-reduced glutathione (2 mg) was added to the polymer functionalized MWCNT solution (2.0 mg in 5 mL H_2O) and reacted with maleimide groups on copolymer for 24 h at room temperature. After reaction, unreacted glutathione was removed by centrifugation at 9000 rpm for 20 min. The GSH functionalized CNTs were obtained as a black solid.

4.2.10. Conjugation of Polymer Functionalized MWCNTs with Biotin-PEG-SH via Thiol-ene Reaction

A stock solution was prepared with biotin-PEG-SH (0.1 mg/mL H_2O) and 20 μL of it was added to polymer functionalized MWCNT solution (2.0 mg in 5 mL H_2O). Mixture was stirred for 24 h at room temperature. GSH Modified CNTs were obtained via centrifugation (9000 rpm, 20 min).

4.2.11. Conjugation of FITC-Streptavidin Protein

FITC-streptavidin containing solution (20 μL) from the stock solution (0.1 mg/mL in H_2O) was added to biotin conjugated CNT solution (0.4 mg/ mL H_2O), and the reaction was incubated at room temperature for 12 h. Unbound FITC-streptavidin was removed by centrifugation (9000 rpm, 20 min), precipitate was washed with water, followed by centrifugation to obtain the protein conjugated nanotubes.

4.2.12. Conjugation of Streptavidin-coated Qdot

Qdot streptavidin solution (20 μL) from the stock solution (2 μL of 1 μM Qdot streptavidin solution in H_2O) was added to biotin conjugated CNT solution (0.4 mg/mL H_2O) and the reaction was shaken at room temperature for 12 h. Unbound Qdot streptavidin was removed by centrifugation (9000 rpm, 20 min), followed by washing the precipitate with water, and centrifugation to obtain QDot-conjugated nanotubes.

4.2.13. Conjugation of RGDC Peptide

RGDC (0.6 mg) was added to copolymer P1 modified CNTs aqueous solution (0.4 mg/mL H_2O), and the reaction was stirred overnight at room temperature. Thereafter, unreacted RGDC was removed by centrifugation. The peptide (RGDC) amount conjugated onto polymer coated CNT was quantified using a bicinchoninic acid (BCA) kit. All measurements were done as three replicates.

4.2.14. Cell Culture Studies

Firstly, pristine CNTs, copolymer P1 coated CNTs, and RGDC-conjugated CNTs were coated on glass slides. L929 mouse fibroblasts were seeded onto this surface with density of $5x10^4$ cells/m^2. After addition of the cell suspension onto coated slides, incubation at 37 ºC in 5% CO_2 containing atmosphere was done for 3h. At the end of 3h, cell media (1 mL) was added into each well containing CNT samples coated slides. After 24 h incubation and removal of cell media, slides were washed with 1X PBS and cell fixation was done with 3.7% formaldehyde solution at room temperature. For the determination of intracellular action distribution, firstly cells were incubated in 0.1% Triton X 100 in PBS, then they were washed with 1X PBS and incubated in Alexa Fluor 488 phalloidin solution (5 units/mL conc. containing 1% bovine serum albumin (BSA) in 1X PBS). Finally, cell nuclei were stained with DAPI and images of cell attached CNTs coated slides were taken and processed via Zeiss AxioVision software.

4.2.15. Cytotoxicity Assays

For cytotoxicity experiment, L929 mouse fibroblast cells were used which were allowed to grow in 5% CO_2 containing atmosphere at 37 ºC Cells were cultures in Dulbecco's Modified Eagle's Medium (DMEM) low supplemented with 10% fetal bovine serum (FBS) (PAN Biotech). For all experiments, cells in their exponential growth phase were seeded. For cytotoxicity assay, cells were seeded onto 96 well plates as $8x10^3$ cells/cm^2 in triplicates. Then different CNTs sample solutions as pristine CNTs, P1 polymer attached CNTs and RGDC attached CNTs with same CNTs percentage were prepared with addition of DMEM. Dilutions were made to obtain final CNTs solutions in different concentrations. Then cells were treated with these various concentrations and incubated for 48 h. To determine cell viability, CCK-8 assay was carried out according to manufacturer's recommendations. Viability values were calculated by using GraphPad Prism software.

4.3. Results and Discussion

4.3.1. Synthesis of Maleimide Containing Copolymers

For this study, a set of four polymers were synthesized to understand the role of the building blocks toward nanotube solubilization. Using a pyrene-based initiator PY-I (Figure S1 and S2) prepared according to a previous report, furan-protected maleimide-containing methacrylate monomer (FuMaMA) and poly(ethylene glycol) methyl ether methacrylate monomer (PEGMEMA) were polymerized in the presence of PMDETA and CuBr using atom transfer radical polymerization (ATRP) at 80 ºC (Figure 4.2). The choice of using ATRP was dictated by the ability to obtain well-defined polymers with FuMaMA as a comonomers from a previous study [96]. Addition to copolymer P1; copolymers P2, P3 and P4 were also synthesized using the same approach. The copolymer P2 was synthesized using ethyl α-bromoisobutyrate, a widely used commercially available initiator, which does not contain a pyrene unit. It is anticipated that a comparison between copolymers P1 and P2 will shed light on the importance of the pyrene group in stacking of the polymers with the CNTs. Additionally, copolymers P3 and P4 that are similar to copolymers P1 and P2, but devoid of the FuMaMA monomer were also synthesized to understand if the hydrophobic FuMaMA monomer plays any role in CNT solubilization.

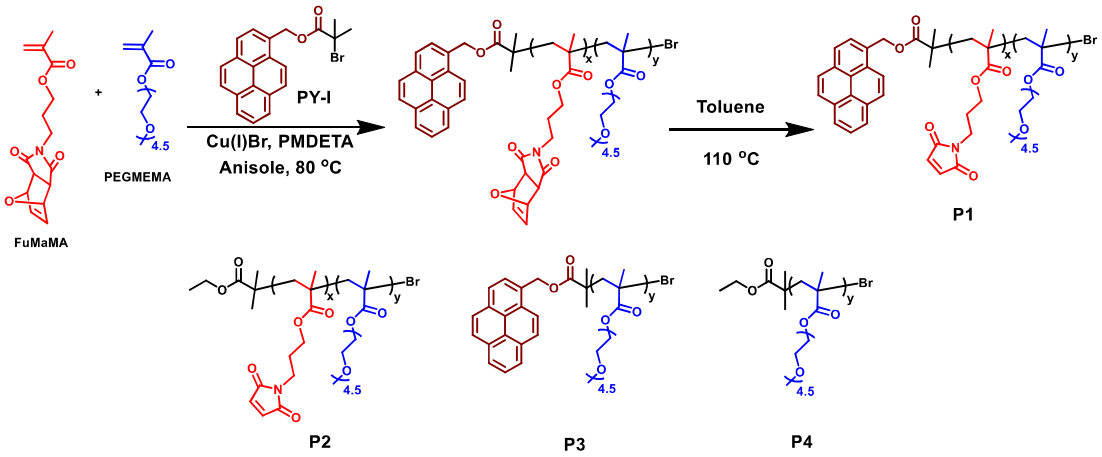

Figure 4.2. Synthesis of copolymers utilized for CNT solubilization and functionalization.

The furan-protected maleimide containing copolymers were activated to unmask the thiol-reactive maleimide groups through a retro Diels-Alder reaction, which was carried out at 110 °C under reflux in toluene.

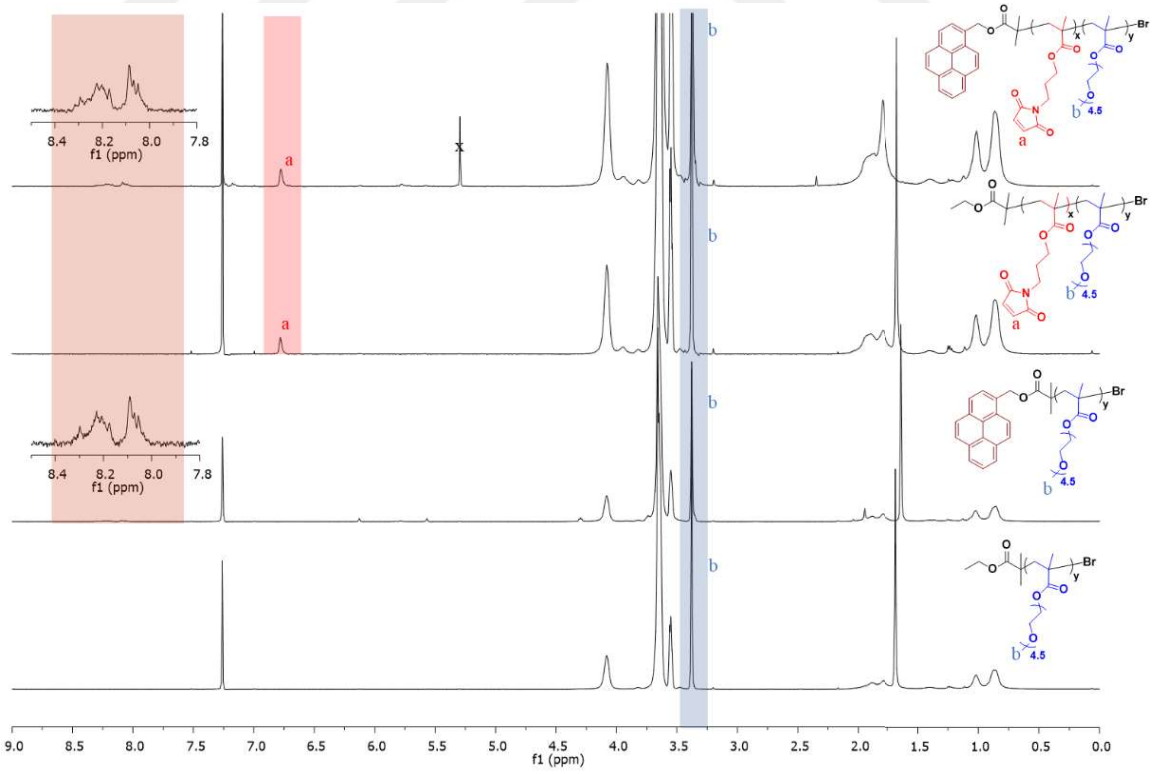

Figure 4.3. Stacked ^{1}H NMR spectra of polymers P1-P4.

A quantitative removal of the furan protecting group was completed within 8 h, as confirmed through lack of any proton resonances belonging to the bicyclic adduct using ^{1}H NMR spectroscopy. While peaks belonging to the pyrene unit appeared between 8.0-8.5 ppm, characteristic peak of the vinylic protons in the maleimide ring appeared at 6.75 ppm. Integrals of proton peaks in ^{1}H NMR spectra indicated that the polymerizations performed with a 10% maleimide feed for copolymers P1 and P2 yielded polymers with a maleimide content around 8.5% (Figure 4.3).

Analysis using SEC measurements indicated that polymers with similar molecular weights and narrow distribution were obtained (Table 1).

Table 4.1. Characteristics of synthesized copolymers.

NO	POLYMER	FEED RATIO [M1]:[M2]^a	OBTAINED RATIO [M1]:[M2]^b	M_n^{c} (g/mol)	M_w/M_n^{c}
1	P1	90:10	91.6:8.4	17300	1.41
2	P2	90:10	91.2:8.8	16700	1.45
3	P3	100:0	100:0	15100	1.18
4	P4	100:0	100:0	12200	1.10

^{a}M1: PEGMEMA, M2: FuMaMA, $[I]_0:[M_{total}]_0$:[CuBr]:[PMDETA]=1:100:1:2. ^{b}Calculated using ^{1}H NMR spectra. ^{c}Estimated by SEC eluted with DMAC, relative to linear PMMA standards.

4.3.2. Modification of CNTs via Non-Covalent Interaction

CNTs were treated with the copolymers P1-P4 to assess their effectiveness in enhancing dispersibility in aqueous media. An aqueous dispersion containing the polymer (10 mg) and CNT (1 mg) in H_2O (5 mL) was sonicated at room temperature for 1 h, followed by stirring for 48 h. Thereafter, copolymer-modified CNTs were obtained using filtration, followed by drying under vacuum. In order to assess the effect of different copolymers in enhancing the dispersibility of thus modified CNTs in aqueous media, obtained dispersions were monitored periodically for a total of 48 h (Figure 4.4).

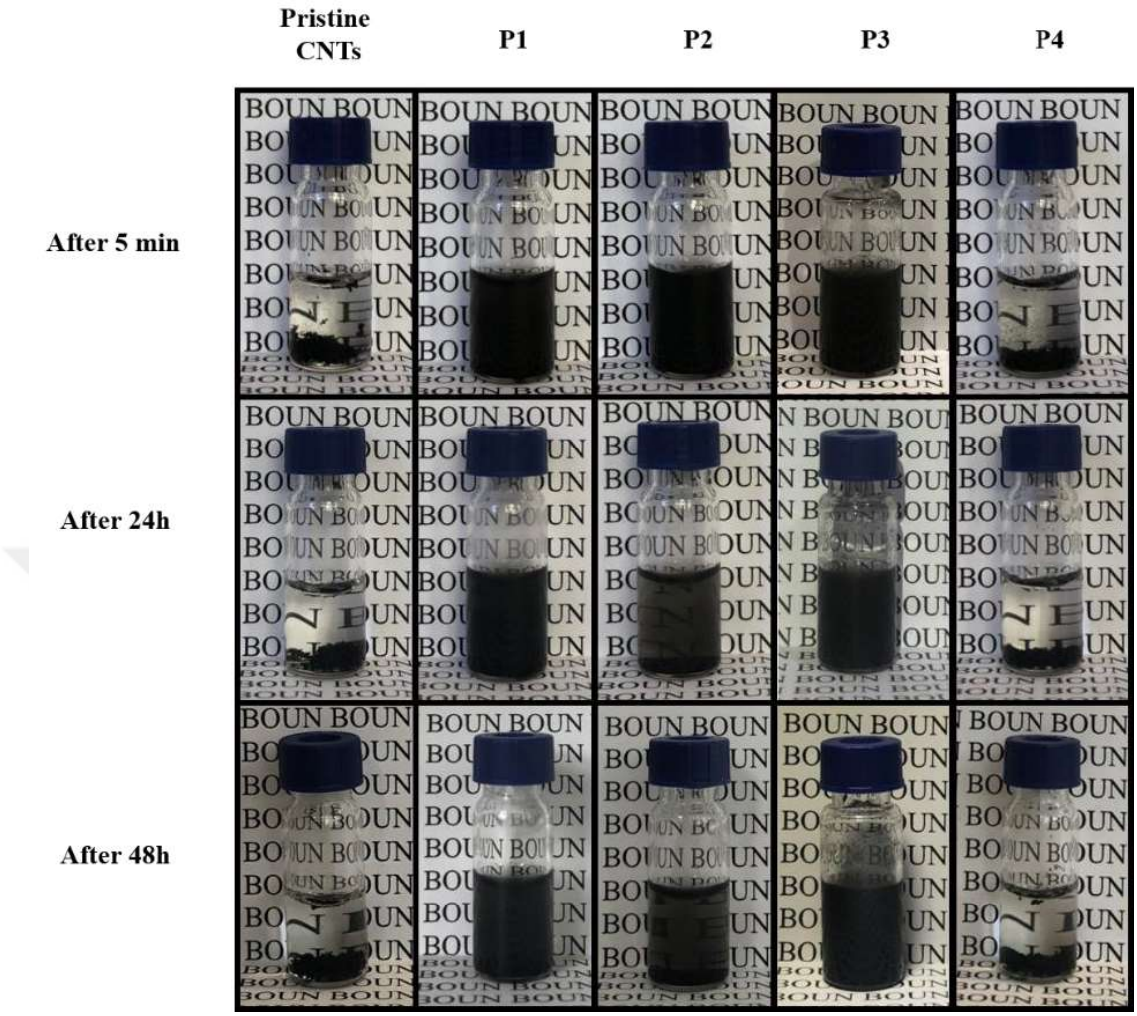

Figure 4.4. Modification of MWCNTs with polymers P1, P2, P3, and P4.

Within 5 min after sonication, pristine CNTs (CNTs) and P4 polymer coated CNTs (P4-CNTs) started to precipitate, and had completely precipitated over the next 24 h. Interestingly, while polymers P1 and P3 enabled dispersion of the CNTs; copolymer P2, which was devoid of the pyrene-based anchoring group also solubilized the CNTs to some extent. As seen in Figure 3, even at the end of 48 h, some of the CNTs treated with copolymer P2 remained dispersed, in contrast to the dispersion obtained with copolymer P4. These observations suggest that the hydrophobic maleimide groups as side chain residues in the copolymers also undergo hydrophobic interaction with the CNTs to provide some level of anchoring. To determine the presence of the polymeric coating, FT-IR spectrum of dry samples of polymer coated CNTs was recorded, and compared with spectra obtained for CNTs and copolymer P1 (Figure 4.5a).

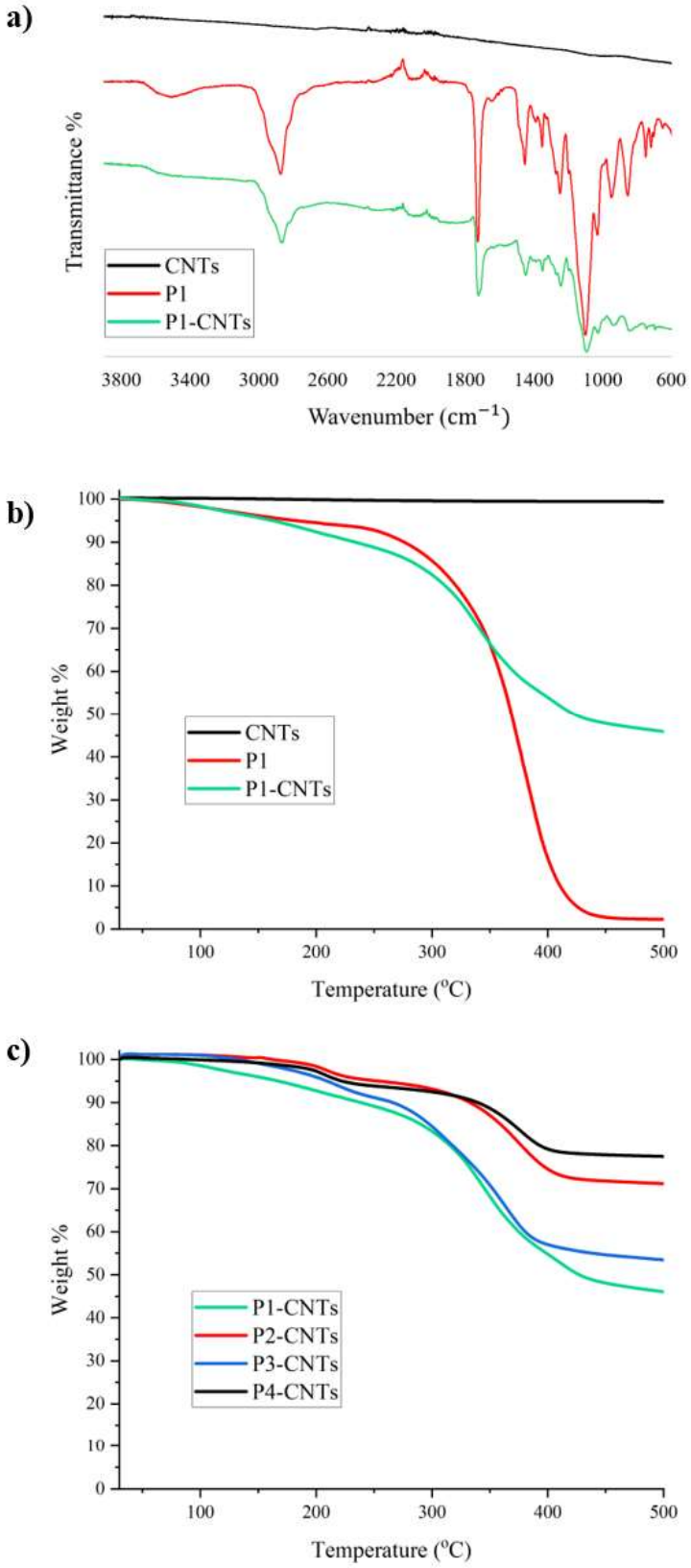

Figure 4.5. (a) FTIR spectra; and TGA analysis of (b) pristine CNTs, P1 polymer and P1-CNTs, and (c) comparison of various polymer (P1-P4) coated CNTs.

While the spectrum for CNTs was nearly linear; for the copolymer P1, peaks belonging to the maleimide carbonyl group can be seen at 1702.47 cm^{-1}, adjacent to peak from C=O stretching band at 1724.85 cm^{-1} belonging to the ester carbonyl group, along with the C-H stretching band around 2870 cm^{-1}. The FT-IR spectrum of P1-CNTs were completely in accordance with the P1 copolymer spectra, with C=O stretching band at 1720.58 cm^{-1} and C-H stretching band at 2865.46 cm^{-1}. After characterization of polymer coated CNTs using FT-IR, thermo gravimetric analysis (TGA) was carried out to understand the effectiveness of polymer grafting on CNTs (Figure 4.5b). As expected, copolymer P1 polymer completely decomposed before 450 ºC, whereas the weight loss of pristine CNTs stayed constant at that temperature. On the other hand, TGA analysis of copolymer P1 modified CNTs showed a 50% weight loss at 450 ºC. As can be seen in Figure 4.5c, all TGA spectra of polymers attached CNTs exhibited consistent behavior, where P1-CNTs had the highest amount of polymer, while the least amount of polymer was observed for P4-CNTs. Interestingly, even though the P2-CNTs had slightly more copolymer stacked onto the nanotube surface, it provided them with appreciable water dispersibility to remain suspended in aqueous media after a prolonged period of 48 h.

4.3.3. Functionalization of Copolymer Coated MWCNTs using Thiol-Maleimide Conjugation

After solubilization of CNTs with maleimide group containing copolymers P1 and P2, it was seen that there was an unexpected difference between them, which was more than expected solubilization of P2-CNTs in spite of the lack of the pyrene group. Since both have maleimide unit on polymer chain, in order to check whether P2-CNTs solubility is coming from interaction between maleimide groups and CNTs, a nucleophilic thiol-ene reaction was performed in the presence of L-reduced glutathione (GSH) (Figure 4.6). This experiment will also shed light upon any modulation of interaction of these polymers with CNT surfaces upon functionalization. Aqueous dispersions of nanotubes coated with copolymers P1 and P2 were treated with GSH. The reaction was stirred at 25 ºC, and both solutions were visualized for 24 h (Figure 4.6a). It was observed that most of the P2-CNTs precipitated, whereas P1-CNTs remained as stable suspension. After the reaction, the CNT composites were purified by washing water to remove residual non-conjugated GSH.

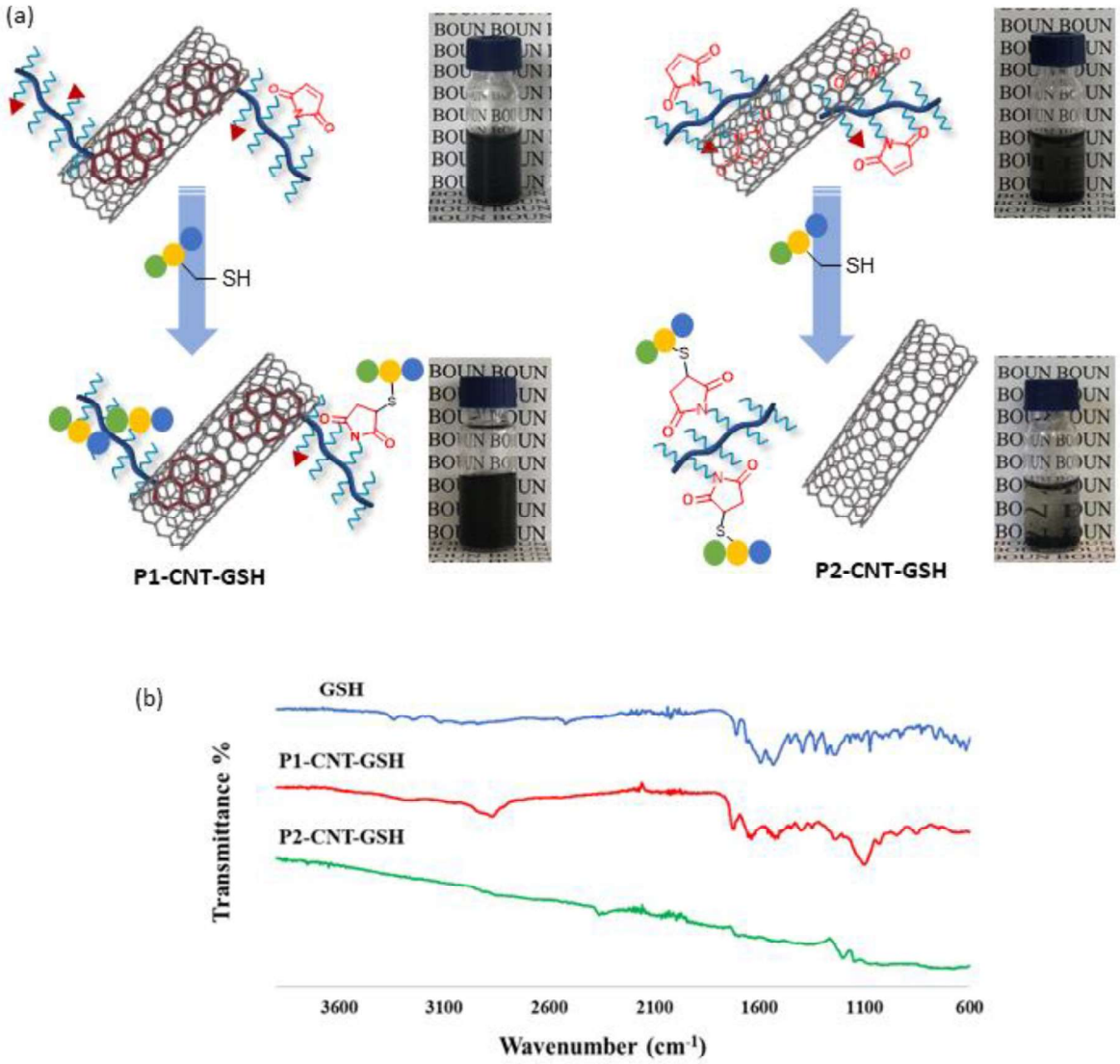

Figure 4.6. (a) Comparison of aqueous dispersity upon functionalization of P1-CNT and P2-CNT polymer-coated nanotubes with glutathione, and (b) comparison of functionalized polymer coatings on glutathione treated nanotubes.

Samples were freeze-dried, and their FT-IR spectra were recorded. While P1-CNTs spectrum exhibited peaks belonging to copolymer P1 polymer GSH, P2-CNTs did not have even peaks belonging to the polymer (Figure 4.6b). This suggests that interaction between P2 polymer and CNTs was considerably diminished upon conjugation with the hydrophilic peptide GSH. These experiments underscore the important role played by the pyrene anchoring group to not only obtain stable polymer coated dispersions, but also keep them anchored upon subsequent functionalization with hydrophilic moieties.

4.3.4. Functionalization of CNTs with and FITC-Streptavidin and Qdot-Streptavidin

In order to show facile functionalization of polymer attached CNTs, reaction with Biotin-PEG-SH, a bioactive ligand known for its high affinity to streptavidin was undertaken. Residual Biotin-PEG-SH was removed from medium via centrifugation, and the obtained solid pellet of biotinylated CNTs were redispersed in aqueous media. Thereafter, FITC-streptavidin was added to the solution to conjugate onto P1-CNTs (Figure 4.7).

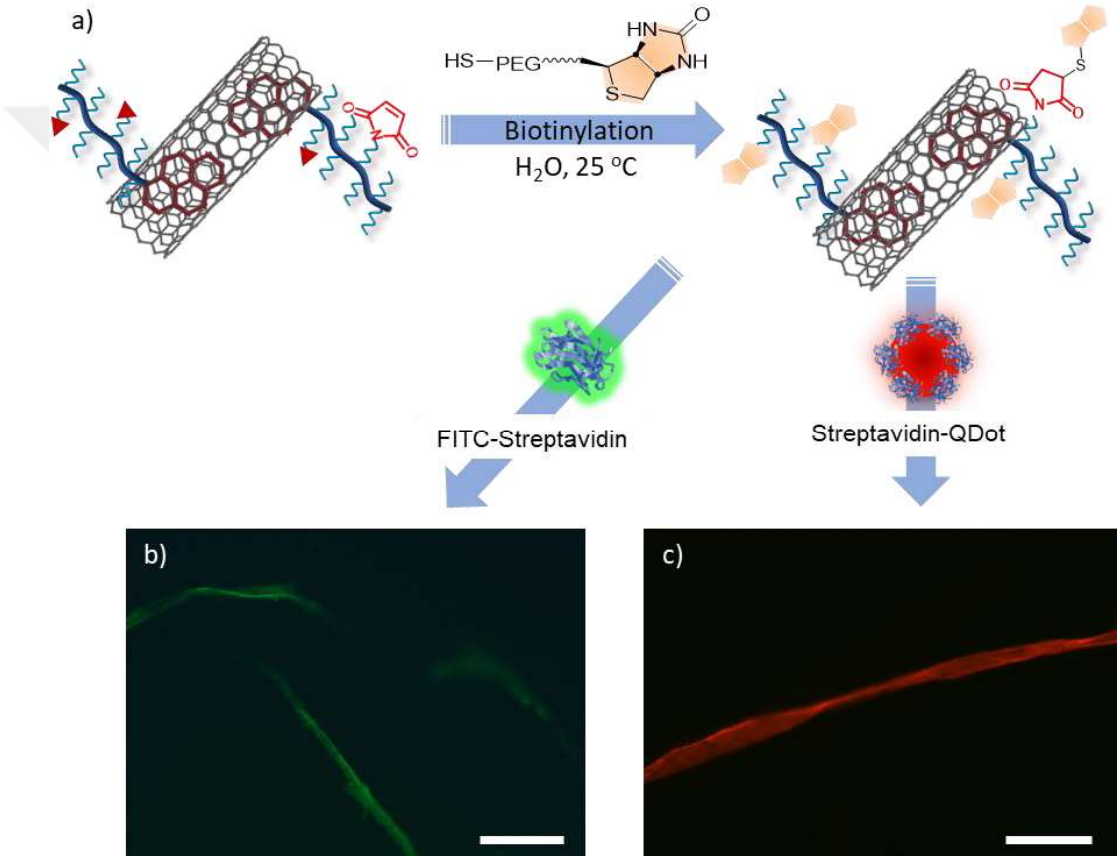

Figure 4.7. (a) Schematic illustration of bioimmobilization with streptavidin conjugated dyes; Fluorescence image of (b) FITC-streptavidin conjugated biotinylated P1-CNTs, and (c) Streptavidin-coated Qdot conjugated biotinylated P1-CNTs (scale bar: 100 μm).

Another biotinylated sample of nanotubes was incubated with streptavidin-coated QDots, and thus modified nanotubes were obtained using centrifugation. Analysis of thus modified CNTs using fluorescence microscopy indicated successful conjugation of FITC-streptavidin and streptavidin-coated QDots onto the biotinylated CNTs samples from the characteristic green and red fluorescence, respectively. In parallel, conjugations with FITC-

streptavidin and streptavidin-coated Qdots were carried out by using P1-CNTs directly without prior Biotin-PEG-SH conjugation. As expected, conjugation with streptavidin could not be achieved in the absence of the biotin ligand, as no fluorescence was observed (Figure A.23).

4.3.5. Conjugation with cell adhesive peptide RGDC and Cell Culture and Cell Viability Assays

By using same conditions with the former functionalization reaction, RGDC attachment to CNTs was achieved via maleimide groups on polymer. After reaction, residual peptide was removed via centrifugation and BCA assay was done to check total amount of conjugated RGDC. The P1-CNT and RGDC-P1-CNT samples were incubated in BCA working reagent at 60 ºC for 30 min. After incubation, absorbance was measured via UV spectroscopy at 562 nm, and the amount of RGDC conjugated onto the polymer coated CNTs was calculated using calibration curve of BSA standard.

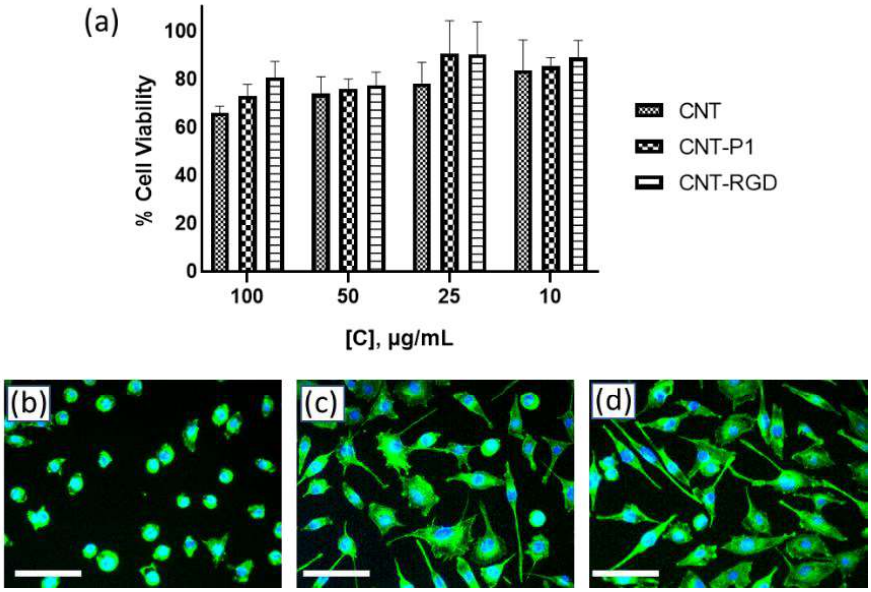

Figure 4.8. (a) Comparison of cell viability of fibroblasts treated with pristine CNTs, P1-coated CNTs, and RGD-P1-coated CNTs; fluorescence microscopy images of L929 mouse fibroblast cells stained with Alexafluor-488 phalloidin (green) and DAPI (blue) after incubation for 48 h on (b) pristine CNT coated surfaces, (c) P1-CNT coated surfaces, and (d) RGD-P1-CNT coated surfaces (Scale bar: 100 µm).

For the cell culture experiment, L929 mouse fibroblast cells were seeded onto CNTs samples coated slides. Different CNT samples were used for surface coating, pristine CNTs, P1 polymer attached CNTs and RGD conjugated CNTs. After seeded cells, they were incubated for 24h at 37 ^{o}C. Then fluorescence microscopy images of cell adhered surfaces were taken to investigate filamentous actin morphology right after cells were stained with Alexa Flour Phalloidin 488 and DAPI. As a crucial part of cytoskeleton, filamentous actins (F-actin) have an important role on cell stability and morphogenesis [97]. It can be seen on Figure 4.8b, while cells on CNT coated slide were in spherical shape as usual for L929, F-actins of cells on CNT-P and CNT-RGD coated slides were prone to undergo stretching. CCK-8 assay revealed that even though pristine CNTs have some cytotoxicity on L929 cells, cells have shown less cytotoxic effect when they functionalized with polymer and RGD (Figure 4.8).

4.4. Conclusion

In conclusion, a facile approach to obtain functionalizable polymeric coatings on carbon nanotubes using hydrophilic polymers containing thiol-reactive maleimide groups as side chain residues and a pyrene unit at chain end is reported. While the oligoethylene glycol chains render the carbon nanotubes dispersible in aqueous media, the maleimide groups enable surface modification using a metal-free click reaction. Interestingly, while polymers without the pyrene unit are able to impart aqueous dispersibility to some extent, they do not provide a stable coating upon functionalization of the maleimide groups with peptide units. Functionalization of biotinylated polymer-coated nanotubes is demonstrated by attachment of fluorescent dye-labelled streptavidin and quantum dots. Additionally, we demonstrate that the functionalization of polymer-coated with cell-adhesive peptides not only improves their biocompatibility through reduced cytotoxicity, but also promotes the proliferation and spreading of fibroblast, as opposed to their resistance to spread on unmodified nanotubes. One can envision that the approach disclosed here can be applied for coating of carbon-based materials to fabricate materials and devices with improved interfacing with the biological materials.

5. PHOTOTHERMALLY ACTIVE RGO-EMBEDDED ANTIBACTERIAL HYDROGELS FOR THE TREATMENT OF BACTERIAL INFECTIONS

5.1. Introduction

Bacterial infections, particularly in open wounds, have become common health problems, potentially leading to death without proper treatment [98,99]. Especially the misuse of antibiotics in managing these infections causes bacterial resistance toward drugs, diminishing their effects and rendering the treatment ineffective. Hence, it's crucial to administer antibiotics accurately and in appropriate doses [100-102].

Hydrogels are known as 3D crosslinked polymeric networks in general. Their linked structures possess pores that allow them to swell by absorbing water without losing their viscoelastic structure. They exhibit soft and flexible properties based on the crosslink ratio in their composition show a high degree of biocompatibility with their similarity to swollen body tissues by absorbing water [103]. Hydrogel structures can be designed by changing monomers properties or amount, and they can gain desired characteristics and pore sizes [28]. Given these attributes, hydrogels take part in versatile applications for drug delivery systems, implants, and in tissue engineering, etc. which has become a frequently used option [104-106]. The pores within hydrogels act as reservoirs for molecules such as drugs and proteins and provide their transport and release. At the same time, the physicochemical properties of hydrogels reduce the toxicity of the carried molecule together with prolonging its release time. Besides extendable release time, cargo inside hydrogel can be released as controlled via such as pH and temperature [107,108].

Hydrogels can be acquired through two general methods: physical crosslinking (involving hydrophobic, ionic or electrostatic interactions between the polymeric structures) and chemical crosslinking (established through covalent bonds between these structures). Compared to the physical method, chemical crosslinking offers more advantages: it allows more precise control over crosslinking density and controlled release of carried cargo by breaking down via the breakable bonds. It provides longer stability over an extended period.

Within chemical crosslinking methods, click reactions like Diels-Alder, azide-alkyne cycloaddition reactions, and thiol-ene reactions are frequently preferred since they possess the advantage of facile occurrence, unaffected by the presence of air, water, or other cargo molecules [109,110].

Cyclodextrins (CD) can be utilized as macromolecules to keep cargo inside and enhance controlled drug release. CDs possess a hydrophilic outer part and a hydrophobic inner part, and can be categorized into three types: alpha, beta, and gamma. Their differences lie in the sizes of their internal spaces. While α and γ CDs have 6 and 8 glucopyranose groups on their structure, β-CD, composed of 7 glucopyranose groups, is predominantly employed in such drug delivery systems due to its interior space compatibility with desired drug molecules. β-CDs form complexes with hydrophobic molecules through their internal cavities, providing solubility, stability, and biocompatibility. Sanyal and coworkers showed the drug release from hydrogels obtained via the thiol-ene click reaction. In this study, besides using highly biocompatible poly(ethylene glycol) (PEG) in the hydrogel, β-CD was integrated within the hydrogel. The investigation focused on the release of a slightly water-soluble drug, puerarin from hydrogels upon varying lengths of PEG chains and diverse equivalent amounts of β-CD [28].

In addition to enhancing drug stability in the hydrogel via β-CDs, there are many advantages of being able to release the drug on demand. Primarily, it ensures precise administration for the necessary duration and dosage, preventing the intake of more or less medication. Moreover, extending drug release over a certain time period reduces the frequency of re-administration of the drug. One prevalent method for controlled drug release from hydrogels involves photosensitivity, often referred to as photothermal therapy. This approach utilizes a photosensitizer (graphene, gold nanoparticles, or carbon nanotubes etc.) [111]. As a result of laser application on a hydrogel system, light is absorbed and converted to heat by photosensitizer, and the cargo (drug or etc.) is released due to the change in the pore volume of hydrogel with the heating. In this way, while the drug is released on the desired area, adjusting the power of the applied light enables control over the amount of drug released.

On traditional drug treatment via oral or intravenous administration, not only more drug doses but also more time is needed since it goes all over the body until it reaches the

infected area, and it may bring some side effects together. On the other hand, on photothermal application, light-triggered release directly to the infected area of the skin provides more efficient and faster treatment with less drug dosage by minimizing side effects. In a study by Liu et al., using gallic acid functionalized silver nanoparticles and biocompatible polysaccharides, a hydrogel was synthesized that benefits from synergistic effect of silver nanoparticles (Ag NPs) as a photothermal agent as well as an antibacterial agent.

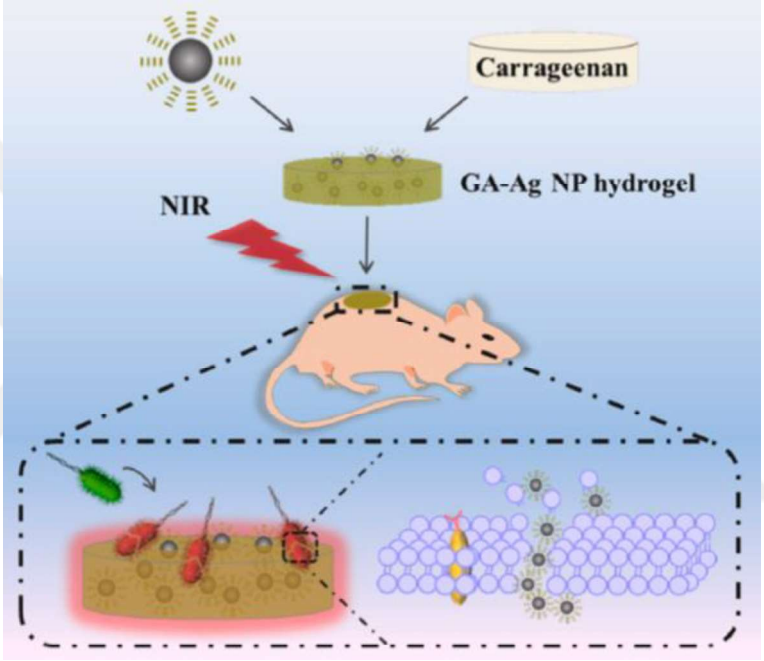

Figure 5.1. Synthesis of Ag NP containing hydrogel and simultaneous schematic representation of the synergistic effect of photothermal and antibacterial silver under NIR light. Adapted from ref [112].

The effects of the obtained hydrogel on bacteria under NIR light were investigated by in vitro and in vivo experiments (Figure 5.1) [112]. In the bacteria experiments on gram-positive *E. coli* and gram-negative *S. aureus,* it was found that Ag NPs embedded hydrogel killed almost all bacteria together with NIR application.

In this project, reduced graphene oxides (rGOs) including hydrogel was fabricated by using thiol-ene reaction between vinyl groups on modified dextran polymer and thiol groups on β-CD. Dextran is a polymer consisting of a branched polysaccharide chain. High water

solubility and biocompatibility make dextran very suitable for a hydrogel. While β-CDs provide cavity for antibacterial drugs used in this project (ampicillin, cefepime, vancomycin, and ciprofloxacin), reduced graphene oxides (rGOs) serve as photosensitizers within the hydrogel. GOs were used as reduced due to superior electrical conductivity exhibition and easier to form bonds with other molecules than graphene oxide (GO) [113]. Beyond their efficient absorption of NIR light, the aromatic ring on rGOs enhances the retention of antibiotics containing aromatic rings within the hydrogel through pi-pi interactions with rGOs. In addition to rGOs, four different antibiotics that are commonly employed in treating bacterial infections; ampicillin, vancomycin, cefepime and ciprofloxacin, have been loaded into the hydrogel. With the loading of drugs onto the hydrogel it is aimed at treating the infection by effectively stopping the proliferation of bacteria, the antibacterial effect of the NIR-triggered released drug was assessed across three distinct bacterial strains. Findings indicated that the released drug successfully killed more than 95% of the bacteria.

5.2. Experimental

5.2.1. Materials and Characterizations

All chemicals were obtained from commercial sources unless otherwise stated. Ciprofloxacin and ampicillin were obtained from Fischer Scientific. Vancomycin and cefepime were purchased from Sigma-Aldrich. β-cyclodextrin was obtained from Sigma-Aldrich. 4-(dimethylamino) pyridine (DMAP), iodine, 4-pentenoic anhydride were obtained from Sigma-Aldrich. NaOH was obtained from merck. Dextran from leuconostoc mesenteroides (average mw 9000-11000) was purchased from Sigma-Aldrich. Vinyl group modified dextran and thiolated β-CD were synthesized by following previously reported protocol, respectively [114,115]. rGO in powder form was purchased from Graphenea (Spain). Dichloromethane (DCM), chloroform, ethanol, dimethylformamide (DMF), isopropanol (IPA), and dimethylsulfoxide (DMSO) were purchased from Merck. Anhydrous solvents were obtained from ScimatCo Purification System. NMR spectra were recorded on a 400 MHz Bruker spectrometer, and measurements were taken in deuterated chloroform ($CDCl_3$). Fourier transform infrared (FTIR) spectra were obtained using a Thermo Scientific Nicolet 380 FT-IR spectrometer.

5.2.2. Synthesis of Modified Dextran

Synthesis of vinyl-modified dextran was done according to literature [114]. Dextran (0.1 mmol, 1g) was reacted with 4-pentenoic anhydride (3 mmol, 546 mg) in the presence of DMAP (0.12 mmol, 14.6 mg) and pyridine (0.02 mmol, 1.58 mg) in 6 mL DMS0 at 40 ^{o}C for two days. In the end of the reaction, dextran was precipitated into cold IPA and washed several times via centrifuge (85% yield).

5.2.3. Synthesis of Per-6-Thio-Beta Cyclodextrin

Per-6-thio-beta cyclodextrin was synthesized according to the literature [116]. It includes two steps of reaction. In the first step, Ph_3P (6.92 g, 26.4 mmol), I_2 (6.98 g, 27.6 mmol), and β-CD (2 g, 1.76 mmol) were dissolved in anhydrous DMF (10 mL) in three different vials. Ph_3P solution was put in rbf and, I_2 solution was added dropwise over 15 min. To obtain dark brown solution, β-CD solution was added and put at 70 ^{o}C for 18h. After reaction, the solution was concentrated under vacuum till evaporation of 2/3 DMF (approximately 20 mL). Then NaOMe in MeOH solution (3 M, 10.3 mL) was added to rbf and stirred for 30 min at 0 ^{o}C. At the end of the reaction, the mixture was poured into MeOH to precipitate and washed with MeOH a few times via centrifugation. After dried under vacuum (3.1 g, 92% yield), iodinated β-CD was obtained with off-white color. On the second step, iodinated β-CD (3.1 g, 1.62 mmol) and thiourea (2 g, 27.37 mmol) were dissolved in anhydrous DMF (30 mL). The reaction mixture was stirred at 70 ^{o}C for 15 h. After the reaction was done, DMF was removed under reduced pressure. The remaining solid was dissolved into 20 mL water and it was stirred with the addition of NaOH under reflux for 1 h. Reaction continued by acidifying with aqueous potassium bisulfate and precipitation of the product. After filtration and washing with water, off-white color product was obtained (1.5 g, 75% yield). The final product was characterized via ^{1}H NMR, Ellman's assay and It was compatible with the literature.

5.2.4. Fabrication of Hydrogel via Thiol-ene Chemistry

Modified dextran (100 mg, 0.01 mmol), β-CD-$(SH)_7$ (53 mg, 0.02 mmol), DMPA (0.2 eq for SH) as well as rGO (1%, w/w) for gel with rGO were dissolved into H2O-DMF (1:4)

with a concentration of 0.3 M in an eppendorf. After complete dissolution, the mixture was put in a mold, and it was followed with UV light irradiation for 1 h. The fabricated gel was removed from the mold and washed with first DMF and then H_2O during 24 h. With freeze-drying, the dried gel was obtained with 91% yield.

5.2.5. Water Uptake Analysis of Hydrogel

Dried gels with and without rGOs were put into water. They were weighted for predetermined time intervals. When the weight of the gel stayed stable, data collection was finished, and a graph was drawn showing the swelling percentage over time. Swelling ratio was calculated via the formula; swelling % = $(W_{wet} - W_{dry}) / W_{dry}$ X 100. W_{dry} and W_{wet} refer to weights of hydrogels wetted into water and dried, respectively.

5.2.6. Antibiotic Loading and Release Experiments

Loading of antibiotics into hydrogel was carried out by adsorption method. In general procedure, gel sample (~50 mg) was incubated into the drug solution in desirable amount and the solution was kept onto shaker (250 rpm) for 24 h at room temperature. After loading, solution was analyzed via HPLC and the amount of loaded was calculated according to the calibration curve on HPLC. After loading, hydrogel was washed gently with water to remove the surface-bound drug. The drug amount in washing solution was checked via HPLC, and it was considered for drug release calculations. For passive release, the gel sample was put into PBS solution and shaked for 24 h at 37 C and HPLC samples were taken from PBS solutions at defined time intervals and they were analyzed for released drug amount calculations.

5.2.7. Drug Release via NIR light

The demand release of the drug was provided using near-infrared (NIR) light (980 nm). Three different laser powers, 1.0, 1.5 and 2 W/cm^2 were applied. In order to optimize release, different irradiation time spans were tried.

5.2.8. Bacteria Experiments

For bacteria experiments *E. coli* (K12 MG1655), *S. epidermidis,* and *S. aureus* (ATCC 43300) were utilized. Firstly, colonies were transferred to a sterile culture tube in broth media and incubated overnight at 37 ^{o}C. After overnight, the optical density value was adjusted to 0.1 via OD600 measurement, and they were allowed to grow a mid-log phase. 1 x 10^8 CFU/mL bacteria concentration was used for all experiments.

Minimal inhibitory concentration (MIC) experiments were defined for *E. coli, S. epidermidis,* and *S. aureus* with serial dilutions assay. Antibiotics were dissolved into sterile broth medium with a starting concentration, and serial dilution was done as three replicates. After bacteria solution (1 x 10^8 CFU/mL) was added to each well, incubated at 37 ^{o}C was done for 24 h. Sterile broth medium and bacteria solution were used as control groups. MIC value was calculated via graphpad prism.

The antibacterial effect of NIR-released antibiotics from gels was carried out by bacteria viability measurements based on optical density value at 600 nm for defined time intervals up to 24 h. Experiments were carried out at 37 ^{o}C and done in triplicate.

5.3. Results and Discussion

5.3.1. Modification of Monomers for Hydrogelation

Dextran was reacted with pentenoic anhydride in the presence of DMAP and pyridine at 40 ^{o}C for 2 days (Figure 5.2). After the reaction was completed, modified dextran was precipitated into cold IPA and collected via centrifuge. With freeze-drying, gray-white solid was obtained and characterized via ^{1}H NMR in D_2O.

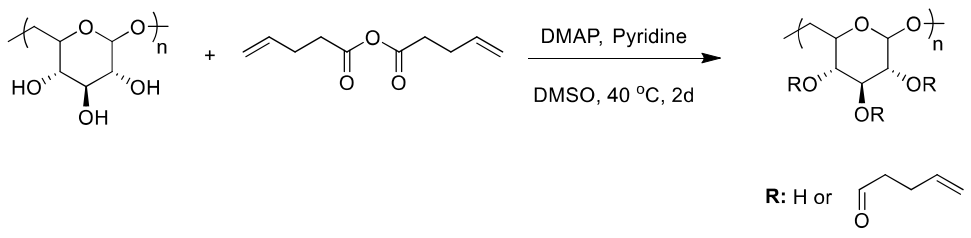

Figure 5.2. Modification of dextran using 4-pentenoic anhydride.

For the synthesis thiol modified beta cyclodextrin, 2 step reactions were carried out according to literature procedure (Figure 5.3) [115]. ^{1}H NMR spectrum of the obtained product was compatible with the literature [115].

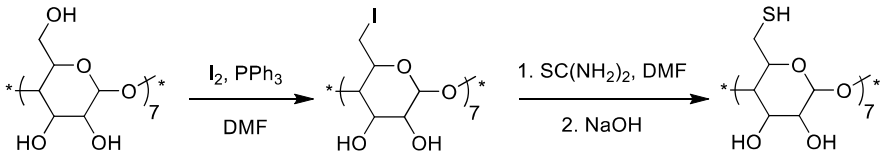

Figure 5.3. Synthesis of thiol modified beta cyclodextrin.

5.3.2. Hydrogel Synthesis and Characterization

After the synthesis of thiol-modified β-CD and vinyl group modified dextran, gelation was carried out under UV light.

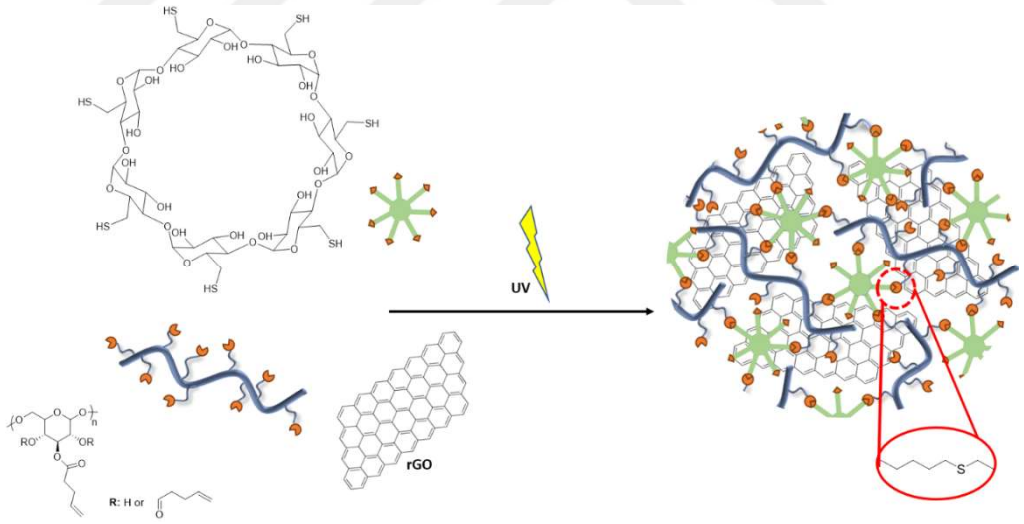

Figure 5.4. Fabrication of rGO embedded hydrogel under UV light.

A thiol-ene click reaction between vinyl groups on dextran and thiol groups on β-CDs was used fir hydrogelation in the presence of the radical photo initiator DMPA (Figure 5.4). Hydrogels were obtained with 1% rGO and characterized via scanning electron microscope (SEM). At the same time gel without rGO and without β-CD-$(SH)_7$ were fabricated as control. Photos of fabricated hydrogels with and without rGO can be seen at Figure 5.5a.

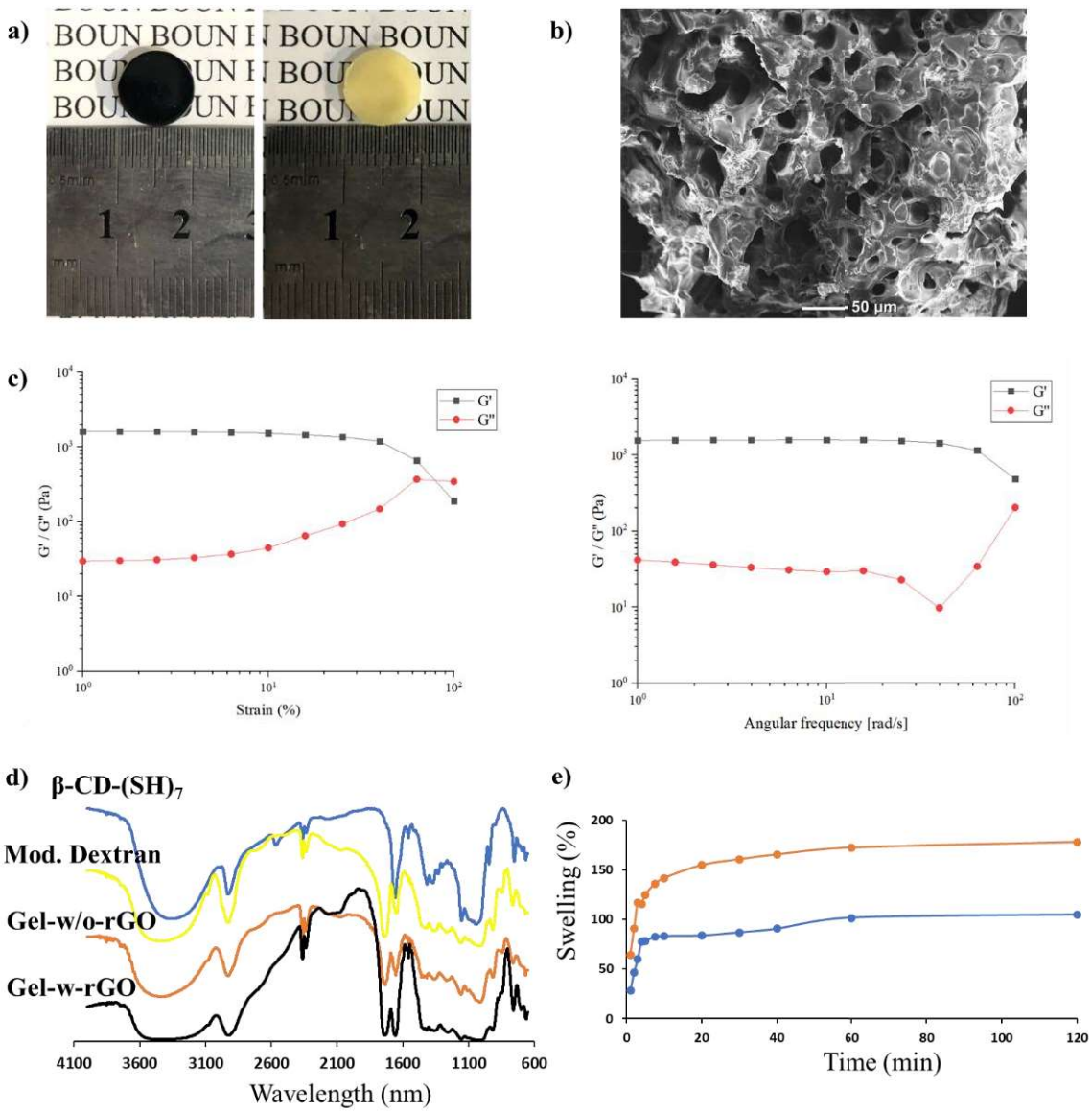

Figure 5.5. (a) Images of synthesized with and without rGO hydrogels, respectively, (b) SEM images of hydrogel with rGO, (c) Results of rheological analysis of hydrogel with rGO (G' storage modulus and G'' loss modulus) (d) FT-IR spectra of β -CD-SH, modified dextran and hydrogels, (e) swelling ratio of hydrogels.

FT-IR spectra for gels and all components were checked (Figure 5.5d). Cyclodextrin vibration coming from SH group can be seen at around 2600 nm^{-1} while double bond on dextran was coming around 1700 nm^{-1}. The swelling profile was also determined for both gels with and without rGO by absorbing water percentage calculation at certain time intervals (Figure 5.5e).

5.3.3. Water Uptake Analysis

The swelling ratio of hydrogels was checked. Generally, hydrogels were put into water and weighted at a time period till gels reached constant weight. Swelling ratio (%) was calculated according to the equation;

$$\boldsymbol{Swelling}\ \% = \frac{\boldsymbol{Wwet - Wdry}}{\boldsymbol{Wdry}}\boldsymbol{x100} \quad (5.1)$$

as W_{wet} and W_{dry} refer weights of wet and dry gel, respectively. At the end of the analysis, gel without rGO was found to be almost 2 times higher compared to gel with rGO, and they reached a stable weight around 1 hour. The experiment was repeated 3 times using different gels (Figure 5.5c).

5.3.4. Antibiotic Loading Experiments

For drug loading experiments, four different antibiotics were utilized: ampicillin, vancomycin, cefepime, and ciprofloxacin. Hydrogel (~50 mg) was put in an aqueous solution (1 mL) containing an antibacterial drug and mixed in the shaker at rt. After 24 hours, the gel was removed, and a sample was taken from aqueous drug solution. Unloaded drug amount was checked via high-performance liquid chromatography (HPLC), and the amount of drug was calculated according to calibration curves which were prepared via HPLC for each drug separately beforehand.

After the loading and washing step, drug loaded gel was put inside phosphate-bufferred saline (PBS) solution at 37 ^{o}C for 24 h. Drug amounts released and stayed inside the hydrogel were calculated by using calibration curves on LC-MS. For antibacterial drug loading, ampicillin solution was used first. While for 400 ug/mL ampicillin loading solution, 45% (182.14 μg) ampicillin was loaded onto rGO gel, it was found only 10% (40 μg) for gel without rGO. On the other hand, for the passive release step, results were really close and relatively high compared to loading (Figure 5.6). Since loading was less and passive release was higher than expected. As a second antibiotic, vancomycin was loaded onto the gel using (200 μg /mL) vancomycin solution for loading. Compared to ampicillin, loading was lower, with 26.5% (53.07 μg) for rGO gel and it was 39% (78.8 μg) for gel without rGO and with checking passive release, almost 100% of drugs were released. Thus, another experiment with vancomycin has not been done.

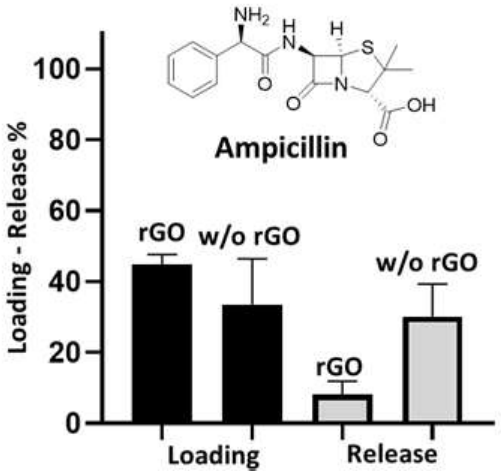

Figure 5.6. Loading and passive release of ampicillin.

Besides two other antibiotics, in order to obtain better loading and release results cefepime (cef) was tried. As the result of the experiment; rGO gel was loaded with 43% (172 μg) of cef, while gel without rGO was loaded with 18.6% (74.4 μg) of it. Although cef loading was nearly the same as ampicillin, passively released drug amount was less than ampicillin, which was 4% (7 μg) for rGO gel and 21.2% (15.8 μg) for gel without rGO (Figure 5.7). Although cef was looked useful for hydrogel in terms of loading and passive release, with NIR light application, the release ratio was really low. Thus, the last drug ciprofloxacin (cip) was loaded onto hydrogel.

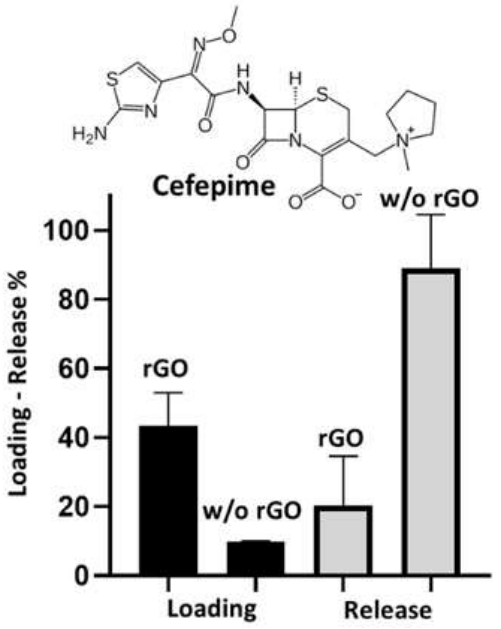

Figure 5.7. Loading and passive release for cefepime.

Firstly 200 µg / mL cip solution was used for loading. It was 49.7% (99.4 µg) for rGO gel and 14% (56 µg) for gel without rGO. Passive release was carried out at 37 ºC for 24h as others. The release ratio was 24.5% (62.8 µg) for rGO gel and 67.8% (38 µg) for gel without rGO. Since cip showed better complexation with β-CD compared to amp, loading with 400 ug/mL solution was done and the best loading percentage was obtained with 63.9% (255.82 µg) for rGO gel (Figure 5.8).

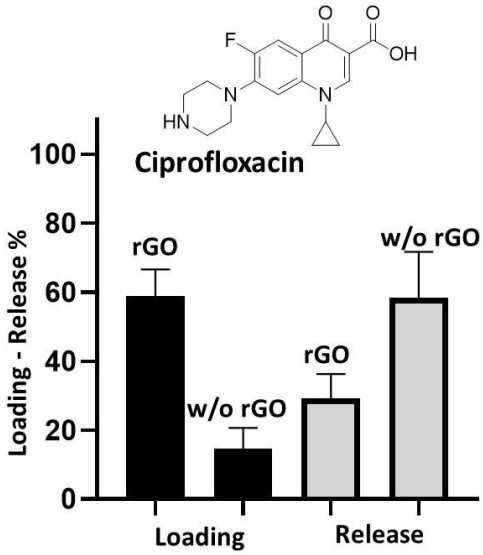

Figure 5.8. Loading and passive release percentage for antibiotic, cip.

5.3.5. Drug Release with NIR light

After the antibiotic loaded hydrogels were prepared, demanded active release of the drug was provided using near-infrared (NIR) light (Figure 5.9). To optimize release, different irradiation time spans and laser power (0.5, 1.0, 1.5, and 2 W/cm^2) were applied to hydrogel with rGO.

As a feature of rGO, during NIR laser application, the temperature increasing was followed via a thermal camera. The temperature rises fast for the first minutes, but after reaching a maximum temperature, it starts to stay nearly stable regardless of the time. Thus, the main adjustment point on active release was to set the maximum temperature that hydrogel could reach (since too high temperature may cause skin burns). Using set variables

for obtained antibiotic loaded hydrogel maximum temperature was around 60 ºC for 10 and 20 min, which is acceptable for an application to the skin (Figure 5.10) [117].

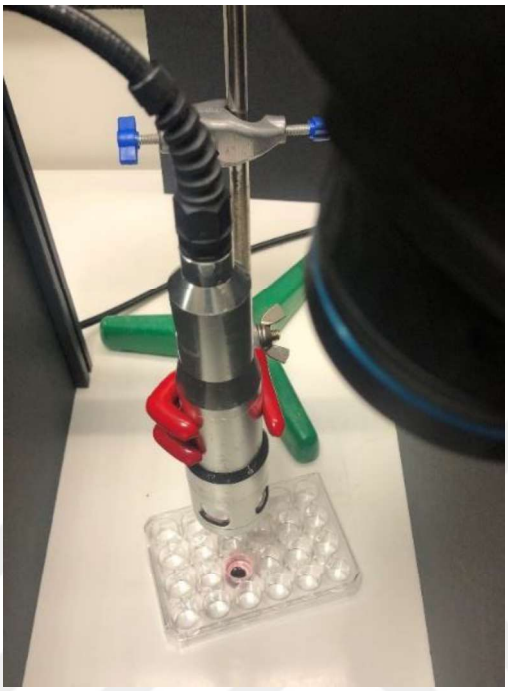

Figure 5.9. Photo of NIR application to hydrogel.

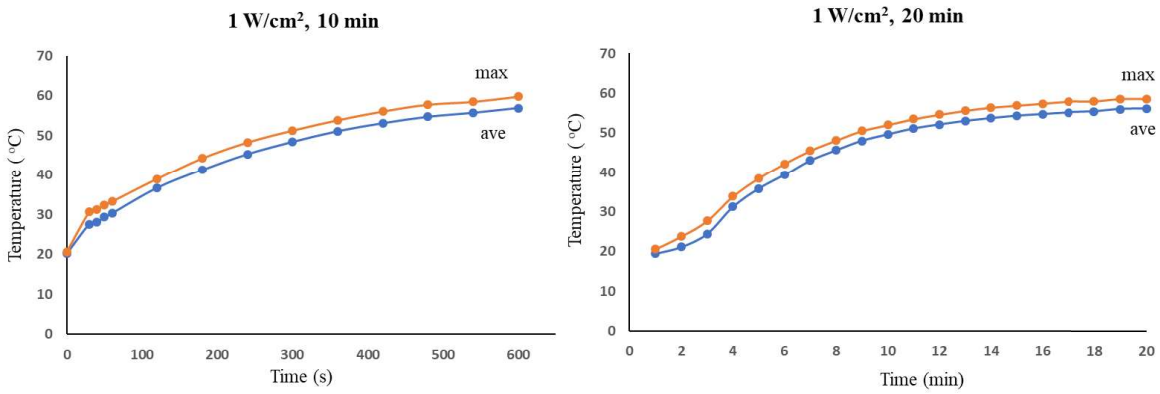

Figure 5.10. Heating curves of rGO loaded hydrogel for 10 and 20 minutes.

While for amp loaded gel, release was around 9.5%, with cef loaded gel, it was only 10.8%. Even with the NIR application for 1h, which was maximum activation time which have been applied, released amount of drug did not increase. For both amp and cef drugs release amounts seems lower than expected compared to literature examples, they were more

than enough to kill bacteria [117,118] On the other hand, with NIR application to cip loaded hydrogel, around 30% drug release was obtained.

5.3.6. Bacteria Experiments

The antibiotic loaded hydrogel was exposed to NIR light and collected supernatants from 3 different antibiotic solutions (amp, cef and cip), and they were applied to different bacteria strains, a range of gram-positive and gram-negative bacteria, including *S. aureus*, *E. coli* and *S. epidermidis*. Viability of bacteria was determined via optical density (OD_{600}) measurement at 600 nm.

Firstly, minimal inhibitory concentrations (MIC) were discovered for each drug molecule as free before loading on different strains of bacteria. Bacteria concentration was set at $1x10^{8,}$ and Mueller Hinton Broth (MHB) medium was used in each experiment. Serially diluted concentrations of drugs were added to the same number of bacteria, including wells in the medium. After 24 h incubation at 37 ºC, OD_{600} values were collected.

Then NIR released antibiotics were applied to bacteria at three different concentrations, which were set according to MIC values as half, same, and double amount of MIC. A kinetic experiment was carried out for the released drug application. Both free antibiotics and released from gel were added to wells in triplicate and results were taken via $OD_{600.}$ The viability of bacteria was monitored for every hour for 24 h with incubation at 37 ºC.

As a result of MIC value experiments, amp, cef and cip were applied as free drugs. Firstly, MIC value for amp on *E. coli* was found as 3.698 μg/mL (Figure 5.12a). In the second step, NIR released amp was obtained and used for the kinetic study to investigate the effect on bacteria. It was achieved by using two different approaches.

In the first method, released amp concentrations were adjusted as MIC/2 (1.849 μg /mL), MIC (3.698 μg /mL), and MIC x2 (7.396 μg /mL) (Figure 5.12b) while other method included directly adding the released amp at certain times (Figure 5.12c) as correlating with NIR activated release time graph (Figure 5.11).

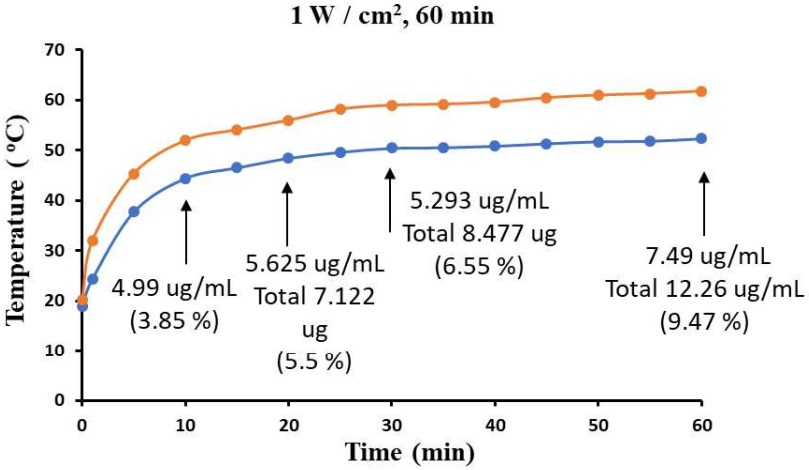

Figure 5.11. NIR light activation to amp loaded hydrogel for 1h and the drug amounts at 10, 20, 30 and 60 minutes.

With 24h kinetic study, bacterial viability was monitored for every hour via OD_{600} measurement and it was seen that released antibiotic with NIR activation from hydrogel MICx2 concentration was able to kill all *E.coli* strain on first application. In the other way, while NIR released antibiotic at 20 min was not enough, released antibiotic at 60 min showed same effect with first concentration (MICx2) application and killed all bacteria.

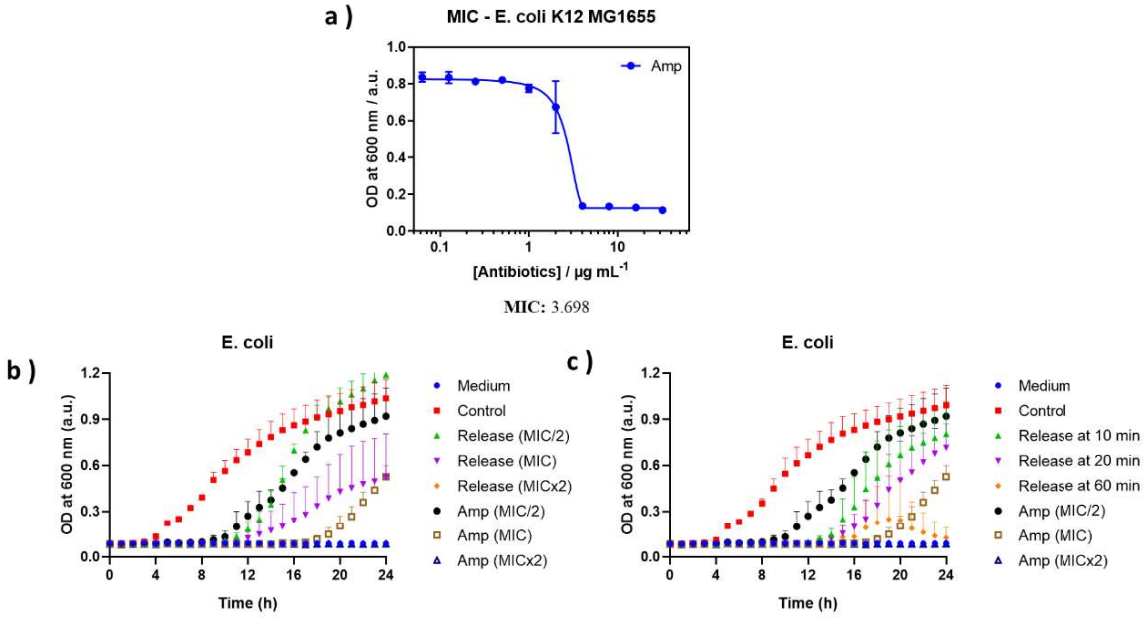

Figure 5.12. (a) MIC value graph for ampicillin, (b) and (c) viability graphs of NIR released amp on *E. coli* with two different amount strategy.

For cefepime, MIC values were found 0.01986 and 2.9596 µg /mL on *E. coli* and *S. aureus*, respectively (Figure 5.13a), and released cef was applied via the same first procedure with amp as the set concentration in terms of MIC values.

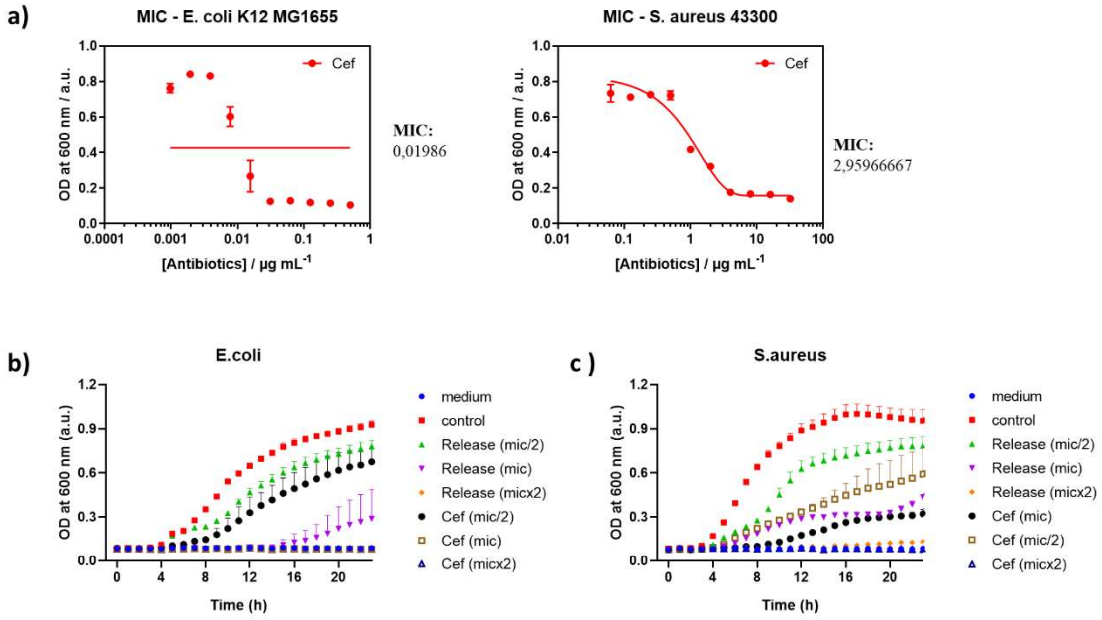

Figure 5.13. (a) MIC value graphs for cefepime on E. *coli* and S. *aureus*, (b) and (c) viability graphs of NIR released cef on *E. coli* and *S. aureus*.

At the end of experiments, it was found out that released cef killed all *E. coli* strain and there was still a small amount *S. aureus* after 24 h even for concentration MICx2 (Figure 5.13b).

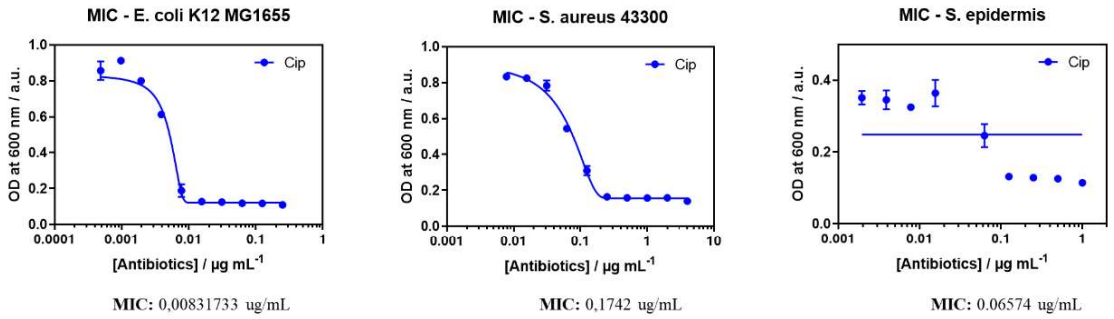

Figure 5.14. MIC values graphs of ciprofloxacin on *E. coli, S. aureus* and *S. epidermidis*.

Lastly, MIC value experiment and viability study were carried out with loaded and released ciprofloxacin. MIC values were found 0.00831, 0.1741, and 0.06574 µg /mL on *E. coli, S. aureus,* and *S.epidermidis*, respectively (Figure 5.14). Then, released cip was applied via the same procedure as set concentrations to around MIC values. After experiment, it was seen that released cip killed successfully all *E. coli* and *S. epidermidis* strains, and there was a tiny amount *S. aureus* after 24 h even with concentration MICx2 (Figure 5.15).

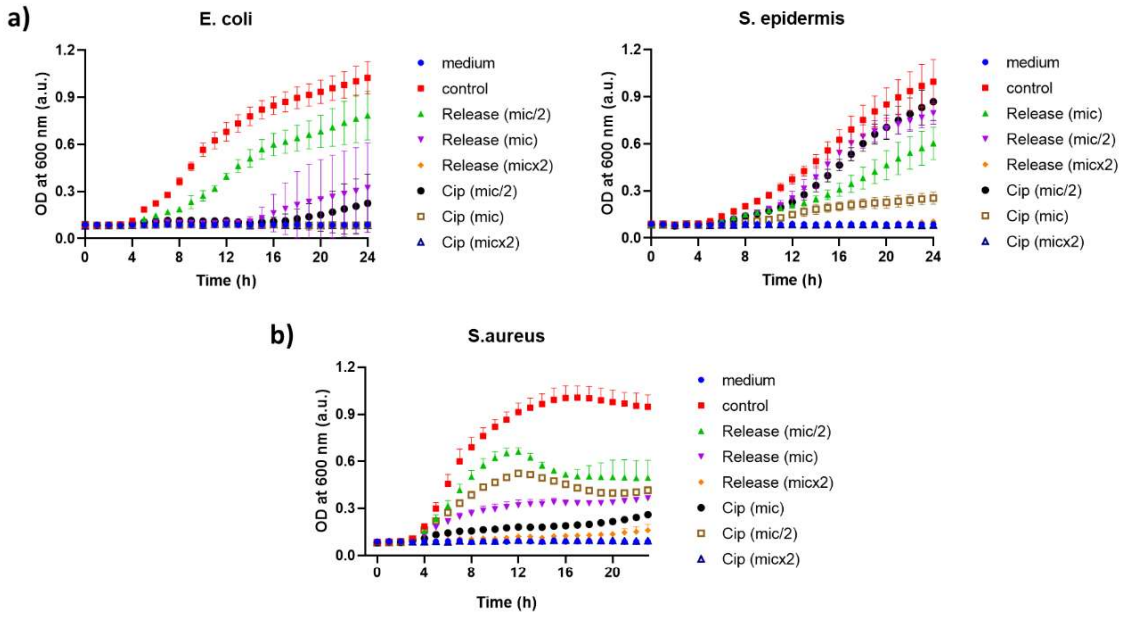

Figure 5.15. Bacteria viability graphs of NIR released cip on *E. coli, S. aureus* and *S. epidermidis*.

5.4. Conclusion

As conclusion, β-CD and rGO included hydrogels were successfully obtained via thiol-ene reaction for the treatment of bacterial infections. Between four different antibiotics, while amp and cef had only 10% NIR release of antibiotic although good loading percentage. Cip showed the best loading and NIR release amount results compared to other drugs. While drug loading to hydrogel was around 60%, NIR release drug amount stayed about 30% for cip. But importantly, this amount is more than enough for the eradication of all bacteria. Since the amount of released drug was higher than MIC values for three drugs (amp, cef and cip), they all were applied to three strains of bacteria. All NIR released drugs achieved to

kill all bacteria, which means the constructed hydrogel system can be a suitable candidate for the treatment of bacterial infections on the skin.

6. FABRICATION OF DIELS-ALDER FUNCTIONALIZABLE POLYMER BRUSH COATED IRON OXIDE NANOPARTICLES

6.1. Introduction

Due to their small size, super-paramagnetic manner, non-toxicity, and high biocompatibility, magnetic nanoparticles are highly desirable in various fields, functioning as drug delivery agents, in hyperthermia treatments, serving as contrast agents in MR imaging, enabling magnetic labeling of cells, and playing an important role in sensor technology [119-121]. There are different types of magnetic iron oxide nanoparticles (IONPs); magnetite (Fe_3O_4), maghemite (γ-Fe_3O_4), and hematite (α-Fe_3O_4). Since IONPs have a large surface area relative to volume ratio, they have a tendency to agglomerate reducing their surface energy [122]. Thus, IONPs must be coated with a surfactant to decrease their surface energy. Surface coating significantly influences both their properties and their potential applications [123]. As a surfactant, oleic acid is the most preferred one to modify the surface of IONPs since oleic acid has a higher affinity towards the surface of IONPs compared to other surfactants [124,125]. In the last decades, many methods have been developed for the synthesis of iron oxide NPs with control over their stability, biocompatibility, shape, and monodispersity. As conventional approaches, co-precipitation, thermal decomposition, hydrothermal synthesis, micro-emulsion, and sonochemical synthesis can be employed [126-129]. Although all methods can be used to fabricate high-quality nanoparticles, the thermal decomposition method is utilized especially because of providing narrow size distribution [130].

In addition to being used as a surfactant, the polymer coating can provide desired characteristics to IONPs, as well as it may decrease or completely remove unwanted features such as solubility problems and thus expand their application areas. Two main methods are utilized for coating IONPs; “grafting to” and “grafting from”. In the ‘grafting to’ approach, the polymer is synthesized first and then it is attached on the surface of IONPs via physical or covalent interactions. In the ‘grafting from’ approach on the other hand, the polymer is directly grown from the surface of IONPs, using an initiator or chain transfer agent that is immobilized on the nanoparticle surface. As one would expect, the steric hindrance is quite

dominant in the ‘grafting to’ approach, and thus causes less dense coating compared to the ‘grafting from’ method. As a result of this, the ‘grafting from’ method is preferable to obtain a more efficient dense surface coating.

For the attachment on the IONPs surface, there are some commonly used anchoring groups that provides strong surface bonding, such as carboxylic acid, trimethoxysilane, phosphonic acid, and the catechol group [131-133]. Among them the catechol group has been extensively utilized for magnetic IONPs because of its strong affinity for the iron-based inorganic surface. With including catechol group on its structure, dopamine is widely used as end group of CTA and thus for attachment on IONPs surface, providing graft from polymerization in the next step [134-136].

In this project, furfuryl-containing peg copolymers with three different ratios of furfuryl groups are fabricated on magnetic IONPs via graft from approach and RAFT polymerization. For this purpose, dopamine containing CTA is coated on IONPs surface by using a place exchange reaction. After obtaining CTA coated magnetic NPs, polymerization is carried out and a copolymer containing furfuryl pendant groups is obtained. Since furfuryl groups can give Diels-Alder (DA) reaction at room temperature with a maleimide group, not only they make the polymer brush on IONPs functionalizable but also make enable loading a cargo with DA reaction and release with retro DA reaction by heating.

6.2. Experimental

6.2.1. Materials and Characterizations

All chemicals were obtained from various commercial sources unless otherwise specified. Poly(ethylene glycol) methyl ether methacrylate (M_n = 500 g/mol) (PEGMEMA, 99%) was purchased from Sigma-Aldrich. Before use, inhibitor was removed using basic alumina column. Furfuryl methacrylate monomer (FuMA) was obtained from Sigma-Aldrich. 2-(dodecylthiocarbonothioylthio)-2-methyl propionic acid (DDMAT, chain transfer agent (CTA)), dopamine functionalized CTA and 6-azido-1-hexanol were synthesized by following the previously published literature, respectively.[137-139] Iron(III) chloride hexahydrate ($FeCl_3 \cdot 6H_2O$), TEA, DMAP, oleic acid, dopamine

hydrochloride, 4,4′-azobis(4-cyanovaleric acid) (V-501), 1-dodecanethiol and 2,2′-Azobis(2-methylpropionitrile) (AIBN) were purchased from Sigma-Aldrich. 1-Octadecene, EDCI, and NHS were obtained from Alfa-Aesar. Sodium oleate was obtained from TCI. Iron oxide nanoparticles were fabricated according to literature via thermal decomposition method [140]. Carbon disulfide (CS_2) was purchased from Fluka. Aldoxorubicin (Dox-mal) was purchased from MedChem. 4,4-difluoro-1,3,5,7-tetramethyl-8-4-bora-3a,4a-diaza-s-indacene (BODIPY) maleimide, was synthesized according to reported literature [141] by Dr. Aysun Degirmenci. DCM, n-hexane, chloroform, toluene, dimethylformamide (DMF), and 1,4-dioxane were obtained from Merck. Thin layer chromatography and column chromatography were performed by using silica gel plates (Kiesel gel 60 F254, 0.2 mm, Merck) and Silicagel-60 (43−60 μm), respectively. Anhydrous solvents (toluene, THF, DCM) were obtained from ScimatCo Purification System, other anhydrous solvents were dried via molecular sieves.

NMR spectra were taken on 400 MHz Bruker spectrometer and measurements were collected in deuterated chloroform ($CDCl_3$) or dimethyl sulfoxide (DMSO). Fourier transform infrared (FTIR) spectra were obtained via a Thermo Scientific Nicolet 380 FT-IR spectrometer. STEM images were obtained from Thermo Scientific Quattro S. Microscope images were taken at room temperature with an inverted fluorescence microscope (Zeiss Observer A1 equipped with AxioCam MRc5). Thermogravimetric analysis was recorded on TA instrument TGA 55 analyzer. XPS analysis was done on Thermo Scientific K-alpha X-ray photoelectron spectrometer. Dynamic light scattering (DLS) measurements were obtained using Malvern Zetasizer Nano ZS analyzer. UV studies were done with Varian Cary 50 Scan UV/vis spectrophotometer. Fluorescent spectra were collected via Varian Cary Eclipse Fluorescence spectrometer (Varian, Agilent, U.S.A.). The dialysis bags (Spectra/Por Cellulose Dialysis Membranes) were obtained from Spectrum Laboratories.

6.2.2. Synthesis of Iron Oxide Nanoparticles

Synthesis of magnetic iron oxide nanoparticles were carried out according to the high temperature thermal decomposition procedure reported in the literature [140].

6.2.3. Synthesis of Dopamine Modified 2-(Dodecylthiocarbonothioylthio)-2-Methyl Propionic acid (Dopa-CTA)

The synthesis of CTA and dopamine-modified CTA were done according to the literature, respectively [137,138]. Firstly 2-(dodecylthiocarbonothioylthio)-2-methyl propionic acid was synthesized in two steps. After the product was activated with N-hydroxy succinimide (NHS), it was reacted with dopamine hydrochloride. Basically, Dopamine·HCl (0.41 g, 2.16 mmol) and TEA (0.22 g, 2.16 mmol) in DMF (15 mL) were taken in a round bottom flask and stirred for 15 min at room temperature. NHS activated CTA (0.95 g, 2.06 mmol) was added to reaction and it was left for 24h at room temperature. Product was purified by column chromatography using hexane/ethyl acetate (1:1) as eluent. ^{1}H NMR (400 MHz, $CDCl_3$) δ (ppm): 6.80 (d, 1H, CH-CH=C-OH), 6.71 (d, 1H, C-CH=C-OH), 6.60 (dd, 1H, C=CH-CH), 5.74 (s, 1H, NH), 3.48 (q, 2H, NH-CH_2-CH_2), 3.32 (t, 2H, S=C-S-CH_2), 2.70 (t, 2H, NH-CH_2-CH_2-C), 1.86-1.68 (m, 8H, S-C-(CH_3)2-C=O, S-CH_2-CH_2-$(CH_2)_9$-CH_3), 1.38-1.26 (m, 18H, CH_2-$(CH_2)_9$-CH_3), 0.86 (t, 3H, CH_2-$(CH_2)_9$-CH_3).

6.2.4. Synthesis of Azobis-azide Exchange Reagent

4,4'-Azobis (4-cyanovaleric acid) (V-501) (0.751 g, 2.6 mmol), 6-azido-1-hexanol (1 g, 6.9 mmol), DMAP (0.13 mg, 1.07 mmol), and EDCI (0.91 g, 5.9 mmol) were taken in a round bottom flask and dissolved in 10 mL anhydrous DCM. Reaction was stirred for 24 h at room temperature. After reaction, the mixture was washed with $NaHCO_3$ and dried over sodium sulfate (Na_2SO_4). Then, the product 4,4'-azobis (azidohexanoyl 4-cyanopentanoate) was obtained after purified via column chromatography using ethyl acetate/hexane mixture (1:4). ^{1}H NMR (CDCl3) δ (ppm): 4.01 (m, 4H, $COOCH_2$), 3.19 (t, 4H, N_3CH_2), 2.40-2.24 (m, 8H, CO−CH_2CH_2−C), 1.64 (s, 3H, CH_3), 1.59-1.53 (m, 11H, C-CH_2CH_2-C, CH_3), 1.31 (m, 8H, C-CH_2CH_2-C).

6.2.5. Synthesis of Alkyne Modified cRGDfK

NHS-activated pentynoic acid was synthesized according to literature.[142] Briefly, NHS (235 mg, 2.0 mmol) and 4-pentynoic acid (200 mg, 2.0 mmol) were taken in a round bottom flask and dissolved in anhydrous THF (7 mL). The mixture was put in an ice bath

and a DCC (421 mg, 2.0 mmol) solution in THF (2 mL) was added dropwise at 0 ºC. After 45 min stirring, mixture was warmed up to room temperature and stirred for 2 h. When the reaction was done, white precipitation (DCU) was filtered off and solvent evaporation was done. Remaining solid was dissolved in ethyl acetate (EtOAc), filtered again and extracted with sat. $NaHCO_3$ solution and brine, respectively. Finally, it was dried over Na_2SO_4 and product was obtained as white solid. Obtained NHS activated pentynoic acid (6.44 mg, 0.033 mmol) and peptide (10 mg, 0.016 mmol) were dissolved in DMF (100 μL) and DIPEA (21.4 mg, 0.16 mmol) was added. Reaction was stirred for 18 h at room temperature. With the completion of reaction, product was obtained as white solid via precipitation in diethyl ether and washing several times for removing unreacted pentynoic acid and DIPEA by using centrifuge.

6.2.6. Place Exchange Reaction with Catechol Modified RAFT Agent (Dopa-CTA)

Oleic acid coated NPs (10 mg) and Dopa-CTA (50 mg) were dissolved in 1 mL chloroform and the solution was stirred at 40 ºC for 48 h under nitrogen atmosphere. After 48 h, solvent was evaporated and methanol was added to reaction mixture and precipitated via centrifuge. Then the mixture was dispersed in THF. This process was repeated, TLC was checked and it was continued until all unattached Dopa-CTA was removed completely.

6.2.7. General Procedure for Surface-Initiated RAFT Polymerization on IONPs

Typically for a polymer including 10% furfuryl methacrylate (FUMA) feeding ratio, Dopa-cta coated IONPs (5 mg), PEGMEMA (0.25 g, 0.46 mmol), FUMA (8.51 mg, 0.05 mmol), and AIBN (0.3 mg, 2.05 μmol) were dissolved in 3 mL of DMF followed by 20 min nitrogen purging, and mixture was put in oil bath at 70 ºC. After polymerization done, solvent was removed via vacuum evaporation. Polymer coated IONPs were precipitated in diethyl ether and precipitated by centrifugation at 9000 rpm. The precipitation process was repeated a few times to complete remove of monomers and all free polymers. For polymers without FUMA, with 20 and 40 % FUMA feeding ratio, desired equivalents were used by following same procedure for polymerization.

6.2.8. Terminal Group Modification of Polymer Coated IONPs with Azide (N_3)

Polymer coated IONPs (10 mg) were dissolved in 0.3 mL anhydrous toluene and azobis-N_3 (19.1 mg, 0.036 mmol) was added to solution and purged with nitrogen for 20 min. The solution was stirred at 65 ^oC for 18 h. After solvent evaporation, azide modified IONPs were precipitated in cold diethyl ether to remove unreacted azobis-N_3.

6.2.9. Terminal Group Functionalization of Azide Bearing IONPs with cRGDfK via Azide-Alkyne Huisgen Cycloaddition

Azide modified polymer coated IONPs (10 mg) were dissolved in 200 µL DMF/H_2O (3:1), and alkyne-cRGDfK (1.23 mg, 1.8 µmol), $CuSO_4 \cdot 5H_2O$ (90 µg, 0.36 µmol) and sodium ascorbate (0.22mg, 1.08 µmol) were added to solution. The reaction was stirred for 24 h at 37 ^oC under nitrogen atmosphere. RGD conjugated IONPs were collected via precipitation and washing with cold diethyl ether. The quantification of peptide conjugated onto IONPs surface was done via a bicinchoninic acid (BCA) kit as following manufacturer's instructions. All measurements were done as three replicates.

6.2.10. Surface Functionalization of Polymer Coated IONPs via Diels-Alder Reaction with N-(5-Fluoresceinyl) Maleimide

Polymer coated IONPs (25 mg) and N-(5-Fluoresceinyl) maleimide (10 µL, from 1 µg/mL stock solution in PBS) were dissolved in 1 mL PBS and the mixture was stirred for 24 h at room temperature. To remove unbounded dye, dialysis in MeOH was done for 3 d.

6.2.11. Diels-Alder Reaction with BODIPY Maleimide

Polymer coated IONPs (10 mg) and BODIPY maleimide (0.1 mg, 0.18 mmol) were dissolved in 100 µL DMF and the mixture was stirred for 24 h at room temperature. In order to remove unbounded dye, BODIPY modified IONPs were precipitated in cold diethyl ether and washed many times.

6.2.12. Diels-Alder Reaction with N-Ethyl Maleimide

Polymer coated IONPs (10 mg) and N-ethyl maleimide (1 mg, 7.99 mmol) were dissolved in 500 μL DMF and the mixture was stirred for 24 h at room temperature. In order to remove unbounded ethyl maleimide, ethyl modified IONPs were precipitated and washed with cold diethyl ether several times.

6.2.13. Conjugation with Aldoxorubicin via Diels-Alder Reaction

Polymer coated IONPs (10 mg) and Dox-mal (aldoxorubicin) (0.1 mg, 0.13 mmol) were dissolved in 100 μL DMF and the mixture was stirred for 96 h at room temperature. In order to remove unbounded dox-mal, dox-mal attached IONPs were precipitated and washed with cold diethyl ether several times.

6.2.14. Aldoxorubicin Release Experiment from Polymer Coated IONPs

Dox-mal attached IONPs (10 mg) were dissolved in 1 mL H_2O and the solution was transferred inside a dialysis bag and put in RBF. After 20 mL H_2O was added to RBF, it was heated to 42 ^oC for 24 h. Samples were removed from RBF at certain time intervals and added equal volume of H_2O. These samples were then analyzed via UV spectrometer to obtain release graph.

6.3. Results and Discussion

6.3.1. Fabrication of Furan Containing Polymer Coated IONPs

Firstly, magnetic iron oxide nanoparticles (IONPs) were obtained via thermal decomposition method with oleic acid coating to prevent aggregation. Characterization was done by FT-IR spectroscopy, TGA and STEM. Spherical nanoparticles were observed on STEM with 9 nm average diameter. Using oleic acid coated NPs, catechol group bearing CTA was attached onto the surface of NPs via place exchange reaction thanks to high irreversible affinity of catechol group to surface of NPs [135]. Catechol bearing CTA was synthesized in four steps, first two steps involve synthesis of a trithiocarbonate group-based

CTA.[137] Other two steps include activation of carboxylic acid group with NHS and then dopamine addition to CTA [143]. The product was characterized using NMR spectroscopy.

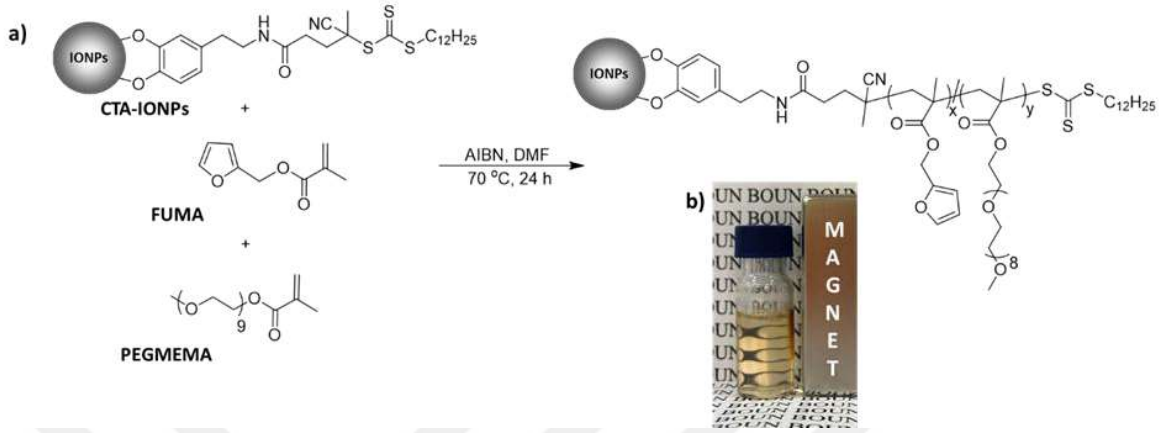

Figure 6.1. (a) Synthetic route for polymerization on IONPS. (b) Image of aqueous solution of polymer coated IONPs collected via the magnet.

With the obtaining CTA-NPs, polymers were grown onto surface of CTA-NPs using reversible addition fragmentation chain transfer (RAFT) polymerization. Simply PEGMEMA, FUMA, AIBN and CTA-NPs were taken in a round bottom flask, dissolved in DMF, after purged with N_2 for 15 min, the mixture was heated to 70 ^oC for 24 h (Figure 6.1).

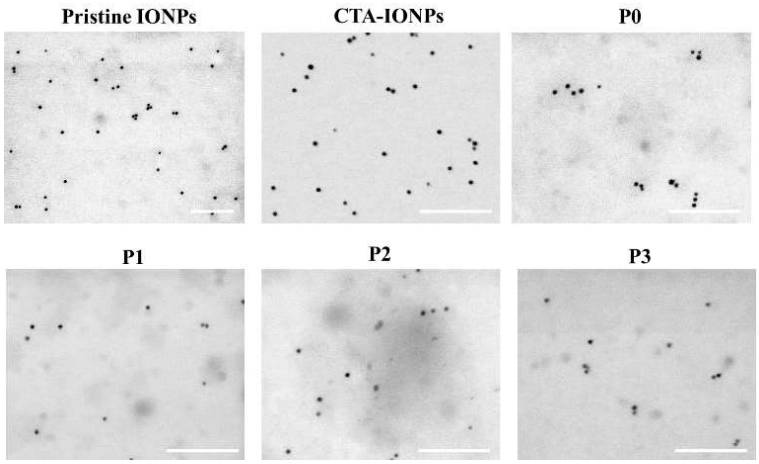

Figure 6.2. STEM images of pristine and coated IONPs (scale bar: 200 μm).

Four different PEG-based copolymers with varying amounts of FUMA were synthesized as 0, 10, 20 and 40% of FUMA. For the characterization of polymers FT-IR spectroscopy, TGA and STEM were carried out. From the STEM images of oleic acid, CTA

and polymer-coated IONPs were (Figure 6.2), it was found that nanoparticles remained as spherical non-aggregated form during all of the reactions.

In the FT-IR spectrum, peak around 1730 cm^{-1} belonging to the ester carbonyl group of PEGMEMA confirmed successful polymer coating. An increasing of furfuryl group ratio on the polymer coating for P1, P2 and P3 was followed with peaks at around 910 and 850 cm^{-1} (Figure 6.3a). From the TGA analysis (Figure 6.3b) while oleic acid coated IONPs had 20% weight change between 190 ºC to 400 ºC, CTA-IONPs had 36% decrease in weight. On the order hand, polymer coated IONPs, P0, P1, P2 and P3 showed 96% loss of weight, implying that polymer coated IONPs consist of mostly polymers by weight.

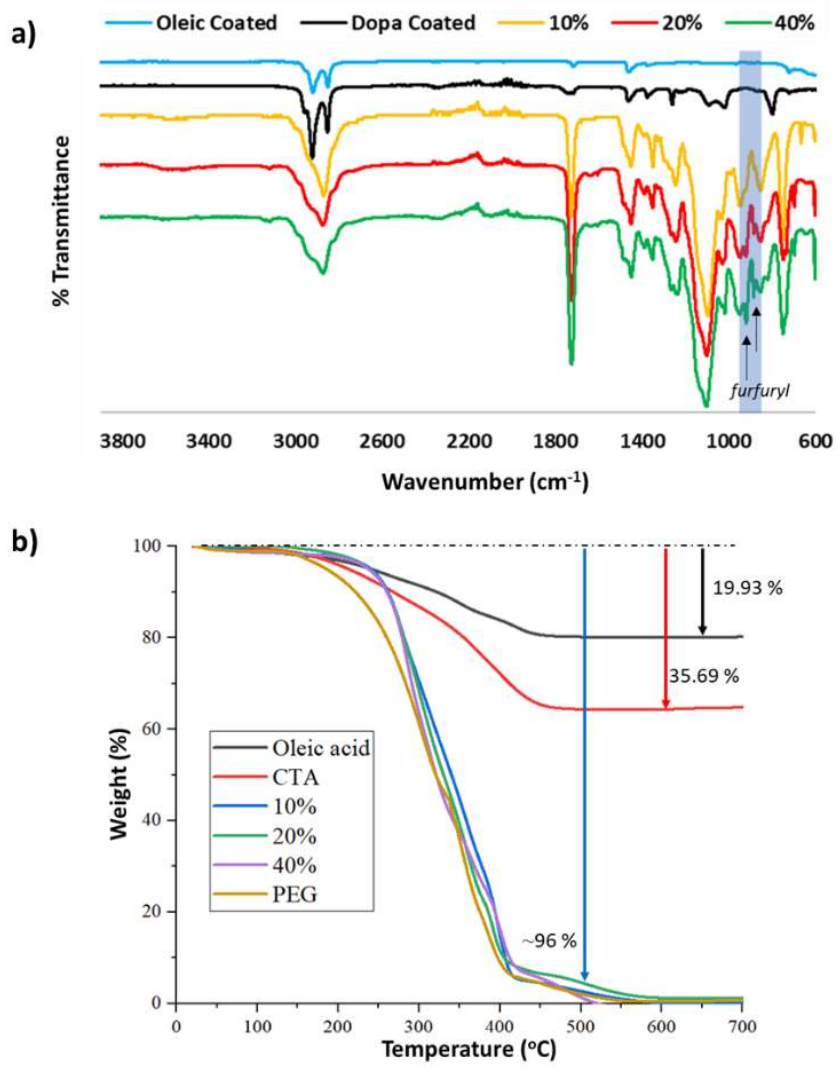

Figure 6.3. (a) FT-IR spectra of oleic acid, CTA and polymer coated IONPs. (b) TGA graph of oleic acid, CTA and polymer coated IONPs.

6.3.2. Functionalization of Polymer Coating via Diels-Alder Reaction.

In order to show functionalization of the polymer coating, firstly, electron deficient N-ethylmaleimide was chosen for addition to electron rich furan groups on polymer side chain via Diels-Alder reaction (Figure 6.4).

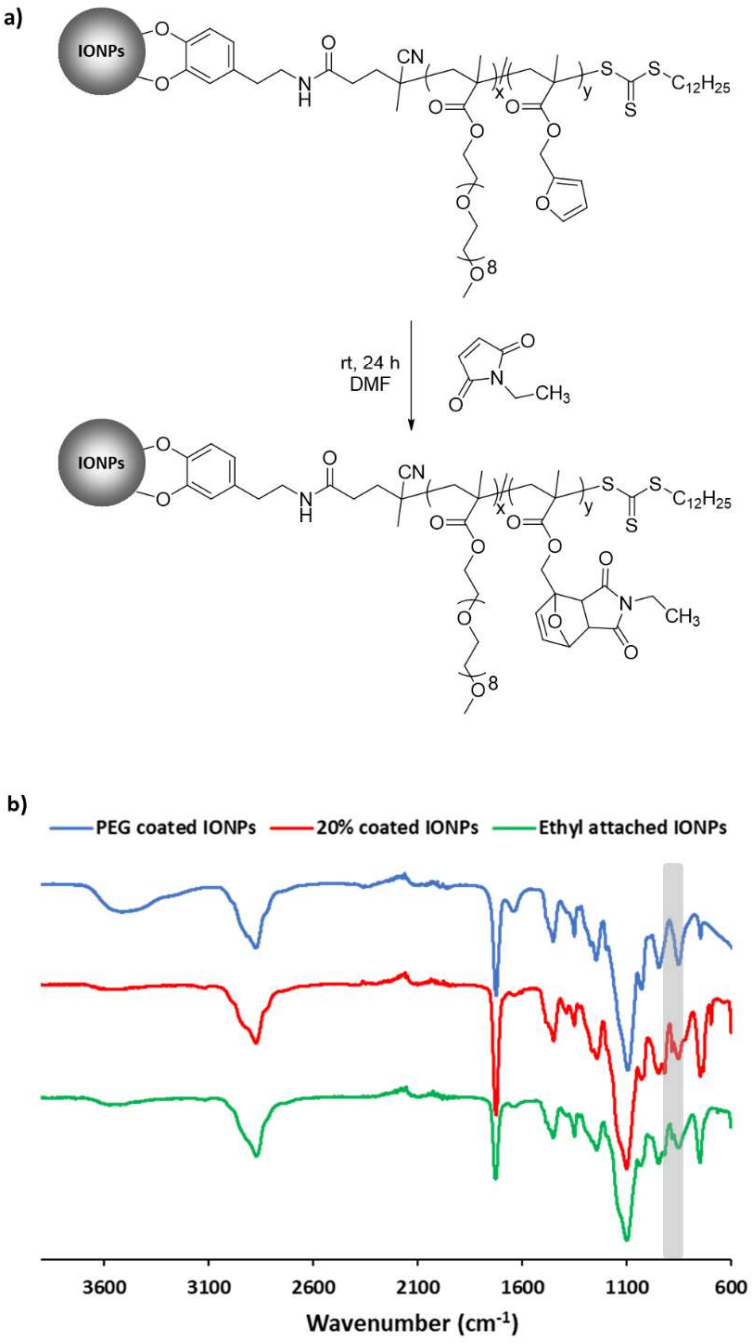

Figure 6.4. (a) N-ethylmaleimide attachment to polymer via Diels-Alder reaction. (b) FTIR spectra of N-ethyl maleimide attached polymer coated IONPs.

For this purpose, polymer-coated nanoparticle P2 was reacted with N-ethylmaleimide at room temperature for 24h. After unattached N-ethylmaleimide was removed by washing with ether a few times, FT-IR was checked and compared with P0 and P2. Since P0 has only PEG chain on the coating, it does not have furfuryl groups, thus there is no peak around 910 and 850 cm^{-1}, and P2 has 20% furfuryl groups on coating. Compared to maleimide attached P2, a sharp decrease in furfuryl peaks was observed which proves occurrence of the Diels-Alder reaction.

Not only FT-IR but also x-ray photoelectron spectroscopy (XPS) analysis was carried out for N-ethylmaleimide attached polymers. Firstly, polymers P1, P2 and P3 were reacted with N-ethylmaleimide with the same procedure as used for addition to P2.

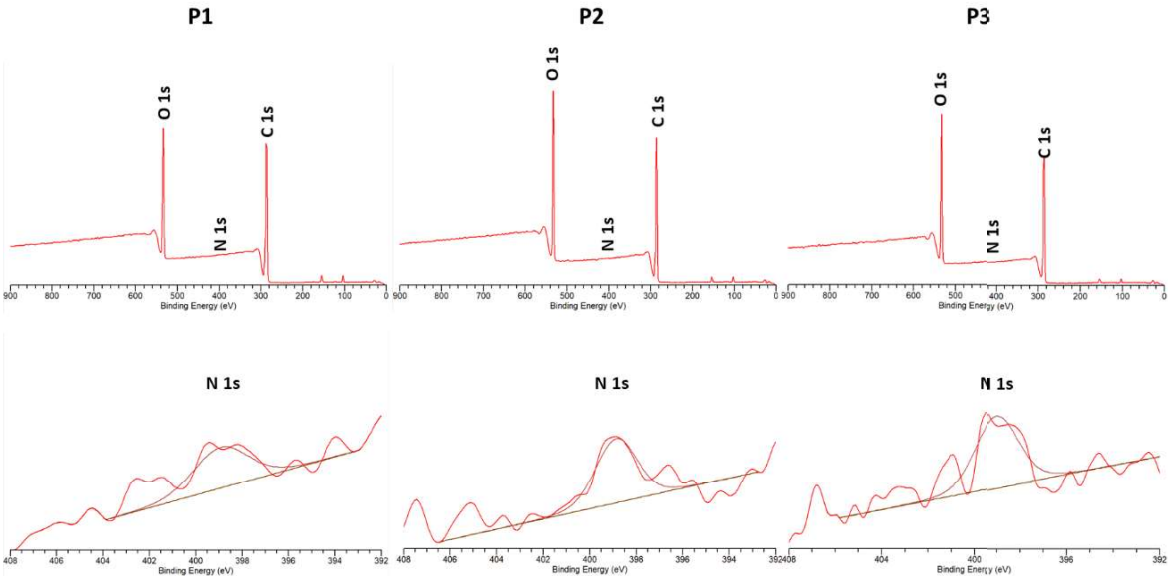

Figure 6.5. XPS analysis of N-ethylmaleimide attached P1, P2 and P3 polymers coated IONPs.

N-ethylmaleimide was chosen for XPS analysis since it has nitrogen atom on its structure which is absent on the polymer coating on IONPs. Thus, XPS analysis can help to determine presence of functionalization. As expected, as the amount of furan group increases in the polymer coating, an increase in the nitrogen peak can be seen in Figure 6.5.

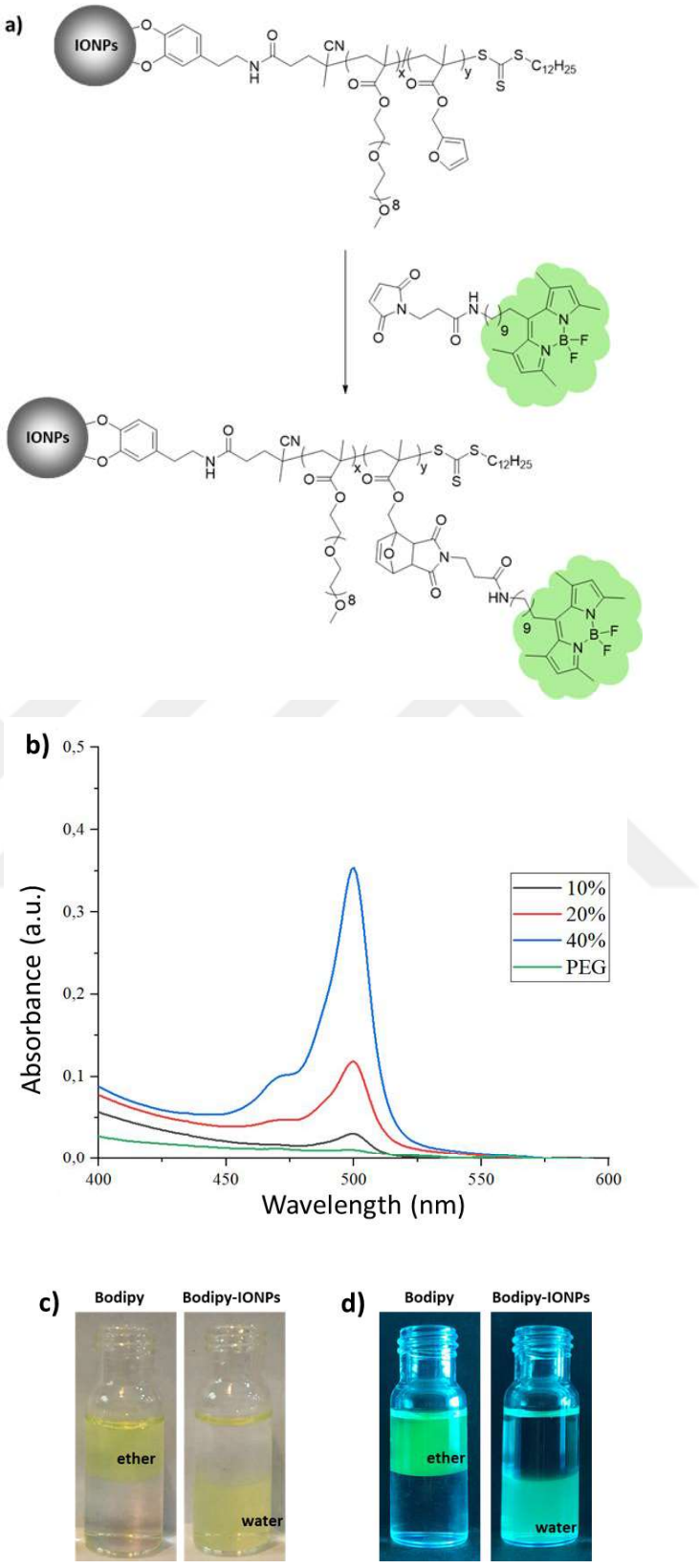

Figure 6.6. (a) BODIPY-maleimide attachment to polymer coating on IONPs. (b) UV-Vis spectra of BODIPY dye attached polymer on IONPs. (c) Photos of BODIPY functionalized IONPs under daylight and (d) under UV light.

Another functionalization with Diels-Alder reaction was carried out using BODIPY-maleimide which is a hydrophobic fluorescent dye molecule (Figure 6.6a). Each polymer (P0, P1, P2 and P3) was reacted BODIPY dye in DMF at room temperature for 24h. In the UV spectrum of P0, which does not contain FuMA, there was no BODIPY attached as expected, and the P1, P2 and P3 nanoparticles gave peaks increasing as proportional to increasing FuMA amounts in the polymer brush (Figure 6.6b). As a small molecule BODIPY maleimide dye is not soluble in water, while it is soluble in diethyl ether. But after attachment to polymer-coated nanoparticles, it is soluble in water since the polymer-coated nanoparticles are water dispersible. Since diethyl ether and water are not miscible, they were put in a vial as equal volume and BODIPY maleimide was added one, and BODIPY attached polymer coated IONPs was added to other one and their photos were collected both under daylight and UV light (Figure 6.6c, d). As expected, while the free BODIPY maleimide was in the ether phase, after attachment to the nanoparticles, it can be seen in the aqueous phase.

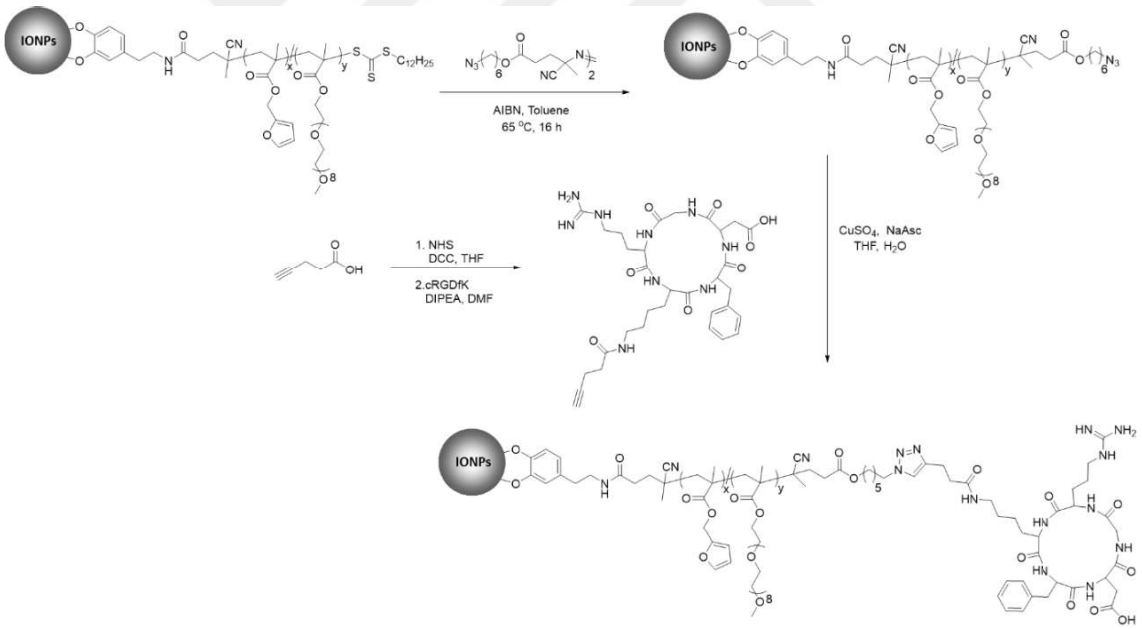

Figure 6.7. Modification of polymer coating with cRGDfK targeting group.

Addition to BODIPY dye, polymer coating was functionalized via maleimide unit bearing doxorubicin drug, aldoxorubicin (Dox-mal) which is a chemotherapy drug. Before dox-mal addition, a targeting group, cRGDfK was placed onto the chain end of polymer. For this purpose, 6-chloro 1-hexanol was reacted with NaN_3 and 6-azido hexanol was obtained according to literature [139]. In the next step it was reacted with V501 and 4,4'-azobis-(azidohexanoyl 4-cyanopentanoate) was obtained [144]. As polymer coated IONPs, P3 was

used due to including 40% of FUMA groups on surface and modification of the polymer chain ends was carried out at 65 ºC using synthesized azobis molecule as well as AIBN since large amount of cRGDfK may have toxicity toward cells during *in vitro* experiments [145]. Terminal azide functionalized polymer coating was later reacted with alkyne modified cRGDfK molecule which synthesized in two steps reactions. Cu(I) catalyzed alkyne azide Huisgen cycloaddition reaction yielded the cRGDfK modified polymer coated IONPs (Figure 6.7). The amount of attached of cRGDfK was calculated as 24 ng/mg of nanoparticles, using the BCA analysis.

Dox-mal was added to the chain end targeting group bearing P3 via Diels-Alder reaction in DMF at room temperature for 4d (Figure 6.8). Reaction was done at room temperature since the endo product was aimed from Diels-Alder reaction, endo product has lower stability and can go back easily through retro Diels-Alder reaction [146].

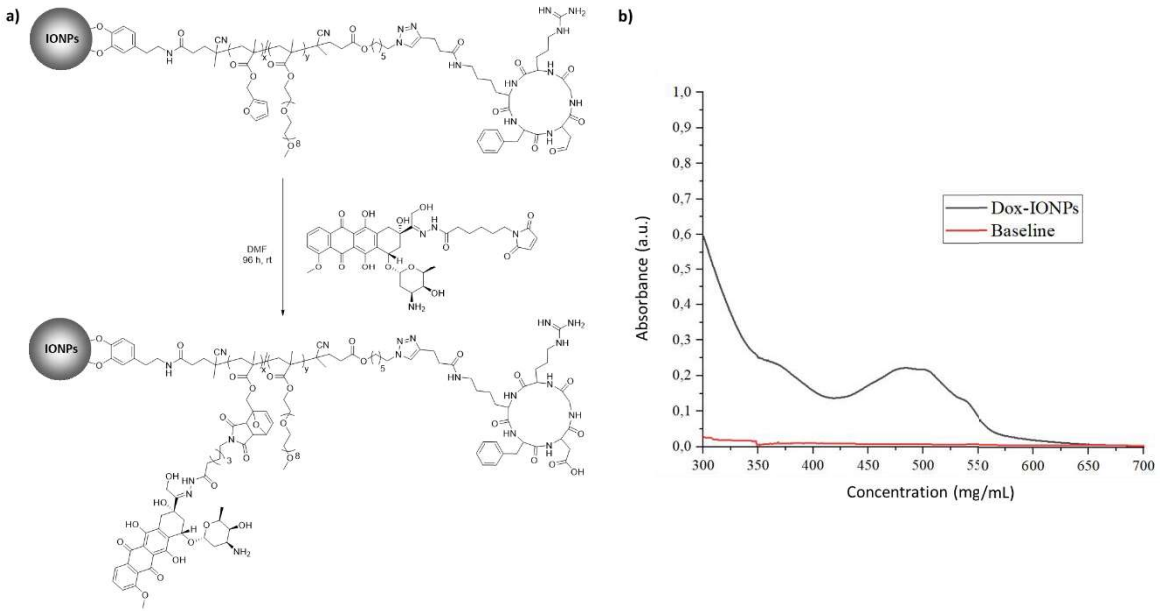

Figure 6.8. Modification of targeting group containing polymer coating with Dox-mal.

6.4. Conclusion

As a conclusion, coating of IONPs with FUMA- PEG copolymer was successfully achieved. Four different polymer brush coated nanoparticles were fabricated using different FUMA feed ratio as 0, 10%, 20% and 40%. First, successful functionalization of the polymer brush coating was demonstrated with conjugation of N-ethylmaleimide; followed by a

hydrophobic fluorescent dye, BODIPY via the Diels-Alder reaction. Finally, maleimide-containing doxorubicin was attached onto the coating to use the fabricated system as a therapeutic agent. Together with doxorubicin, targeting group cRGDfK was attached to coating in order to improve cellular internalization. Overall, fabrication of a polymer-coated magnetic nanoparticle that can be used for targeted drug delivery was established.

7. DUAL-FUNCTIONALIZABLE POLYMER BRUSH COATED MAGNETIC NANOPARTICLES

7.1. Introduction

As an alternative to utilizing a surfactant, IONPs can be turned into aqueous dispersible form by using a hydrophilic coating. For the coating, not only small molecules but also polymer coating is frequently used [147,148]. Beside solubility, polymer coating can give desired features to IONPs as well as eliminate unwanted ones and thus widen the application area [149]. For the surface modification of IONPs with polymerization mainly from two methods; "grafting to" and "grafting from" are benefitted [150]. In "grafting to" approach, polymer is fabricated first and then its attached on the surface of IONPs which can be done as physically or covalently. In grafting from approach on the other hand, polymerization is started and grown on the surface of IONPs directly owing to an initiator previously coated on the surface (Figure 7.1). Sanyal and coworkers synthesized a polymer bearing furan protected maleimide units on the side chain via RAFT polymerization initiated with dopa modified CTA [84]. After obtained polymer with unmasking maleimide groups, IONPs were coated via graft-to approach. Attachment of a dye was achieved in two different methods; photoinitiated thiol-ene reaction and nucleophilic Michael addition reaction and a fluorescent hydrophilic nanoparticle were obtained successfully. In the grafting-to method, steric hindrance is quite dominant compared to the grafting-from approach. As a result, to obtain a dense polymer coating, graft-from method is a preferable approach.

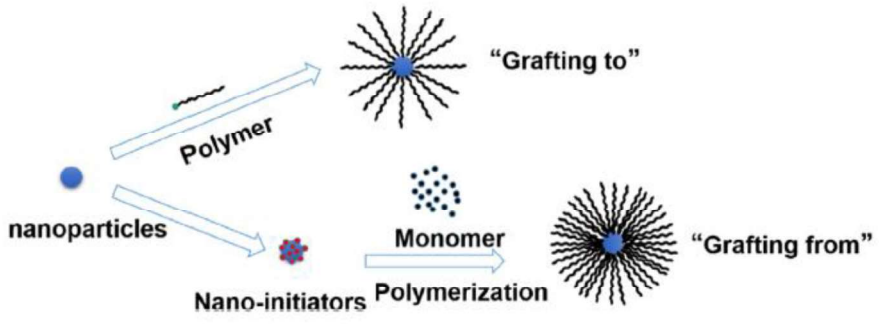

Figure 7.1. Representation of grafting to and from approaches. Adapted from reference [150].

For the polymer coating via graft from approach, RAFT polymerization is a way to achieve coating that needs a chain transfer agent (CTA) to initiation. For the CTA attachment on IONPs surface, there are some anchoring groups that is commonly used and forms strong bonding between IONPs, such as trimethoxy silane, carboxylic acid, catechol group, and phosphonic acid [131-133]. Among them catechol group is mostly utilized for magnetic IONPs since it has more preferable and stable geometry when it is attached to the surface of IONPs. With including catechol group on its structure, dopamine is widely used on modification of CTA and thus for attachment on IONPs surface, provides graft from polymerization in the next step [134-136]. Wang *et al.* have synthesized a copolymer of isobutylene and maleic anhydride, and then functionalize it via nucleophilic addition of dopamine and PEG chain. Using lots of dopamine on the side chain of copolymer, IONPs were coated with the copolymer and changed their solubility property as hydrophilic. Addition with the cy3 dye on the terminal group of PEG chain, in vitro experiment of the coated particles were done on HeLa cell line and demonstrated coated particles were not cytotoxic [151]. Addition to solving solubility issue, polymer coating can allow functionalizability via some post modifications. One of the numerous methods is thiol-ene reaction between a thiol group and maleimide unit. It is mostly preferred since the reaction can be carried out easily and in mild condition [152].

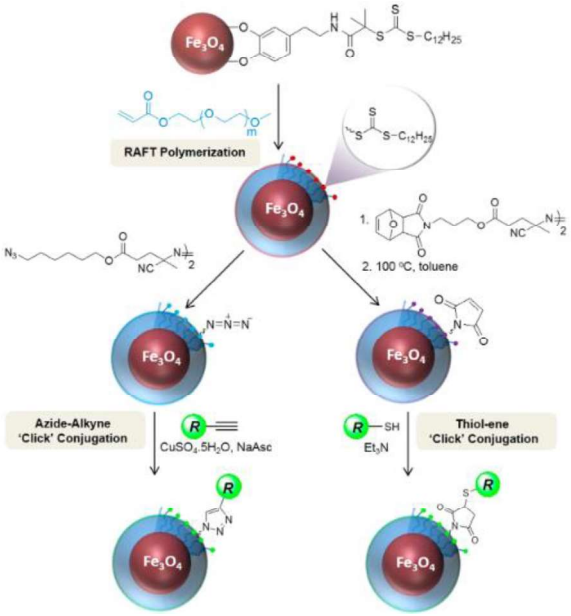

Figure 7.2. Fabrication water soluble polymer coated IONPs and functionalization with different methods. Adapted from reference [147].

In another example, Öz *et al.* fabricated a coated IONPs via graft from method using poly (ethylene glycol) methyl ether acrylate (PEGMEA) [147]. Furan protected maleimide group and azide unit were attached to terminal group of polymer coating with cross coupling reaction, separately. After the rDA reaction, maleimide group was activated and functionalization was achieved via thiol-ene reaction as well as azide-alkyne Huisgen click reaction was carried out for the functionalization via the azide terminal group (Figure 7.2).

Herein, furan protected maleimide (FuMaMA) containing peg co-polymers with four different ratios (0, 10, 20 and 30%) of maleimide groups were growth on magnetic IONPs surface via RAFT polymerization by using CTA coated IONPs. With the obtaining furan protected maleimide bearing polymers coated IONPs, a retro Diels-Alder reaction was utilized for removing furan protection and thus obtained functionalizable maleimide units on polymer coated magnetic IONPs. By using thiol-ene reaction, a thiol group including dye (BODIPY-SH) as well as a chemotherapy drug (dox-SH) was attached to maleimide unit on IONPs coating. Thus, the fabrication of water-dispersible polymer-coated IONPs was achieved, followed by functionalization of the polymeric coating via thiol-maleimide conjugation to use as a drug delivery system.

7.2. Experimental

7.2.1. Materials and Characterizations

All chemicals were obtained from commercial sources unless otherwise stated. PEGMEMA (M_n = 500 g/mol) was purchased from Sigma-Aldrich. Before use, it was filtered through using basic alumina column to remove inhibitor. FuMaMA, DDMAT, chain transfer agent (CTA), dopamine functionalized CTA were synthesized by following the previously published literature, respectively [137,138]. 1-dodecanethiol, iron (III) chloride hexahydrate ($FeCl_3 \cdot 6H_2O$), oleic acid, TEA, DMAP, dopamine hydrochloride, V-501 and AIBN were obtained from Sigma-Aldrich. 1-Octadecene, NHS, and EDCI were purchased from Alfa-Aesar. Sodium oleate was obtained from TCI. Iron oxide nanoparticles were fabricated according to literature by using thermal decomposition method [140]. Carbon disulfide (CS2) was purchased from Fluka. Doxurubicin hydrochloride was purchased from MedChem. Cy5-tetrazine dye was obtained from lumiprobe. 4,4-difluoro-1,3,5,7-

tetramethyl-8-4-bora-3a,4a-diaza-s-indacene (BODIPY) thiol, was synthesized according to reported literature [141] by Dr. Aysun Degirmenci. Doxorubicin thiol was synthesized by following previously published literature [153]. DCM, DMF, ethanol, n-hexane, chloroform, toluene, and 1,4-dioxane were purchased from Merck. Anhydrous solvents (toluene, THF, DCM) were obtained from ScimatCo Purification System, other anhydrous solvents were dried via molecular sieves. Thin layer chromatography and column chromatography were performed by using silica gel plates (Kiesel gel 60 F254, 0.2 mm, Merck) and Silicagel-60 (43−60 μm), respectively. The dialysis bags (Spectra/Por Cellulose Dialysis Membranes) were purchased from Spectrum Laboratories.

NMR spectra were recorded on 400 MHz Bruker spectrometer and measurements were done using deuterated chloroform ($CDCl_3$) or dimethyl sulfoxide (DMSO) as solvent. FTIR spectra were taken using a Thermo Scientific Nicolet 380 FT-IR spectrometer. STEM images were taken from Thermo Scientific Quattro S. Thermogravimetric analysis (TGA) results were recorded with TA instrument TGA 55 analyzer. XPS analysis was carried out Thermo Scientific K-alpha X-ray photoelectron spectrometer. Dynamic light scattering (DLS) measurements were obtained using Malvern Zetasizer Nano ZS analyzer. UV-vis spectroscopy studies were carried out with Varian Cary 50 Scan UV/vis spectrophotometer. Fluorescent spectra were taken via Varian Cary Eclipse Fluorescence spectrometer (Varian, Agilent, U.S.A.).

7.2.2. Synthesis of Iron Oxide Nanoparticles (IONPs)

Magnetic iron oxide nanoparticles were synthesized according to the procedure in literature [140] by Nora Ejderyan.

7.2.3. Synthesis of Dopamine-Functionalized Chain Transfer Agent (Dopa-CTA)

The synthesis of CTA and dopamine-modified CTA were carried out according to the previously published literature, respectively [137,138]. Firstly, DDMAT was synthesized in two steps. After the product was activated with N-hydroxy succinimide (NHS), it was reacted with dopamine hydrochloride. Basically, Dopamine·HCl (0.41 g, 2.16 mmol) was dissolved in DMF (14 mL) in a round bottom flask and TEA (0.22 g, 2.16 mmol) was added

to solution. The solution mix was stirred for 15 min at room temperature. After that NHS activated CTA (0.95 g, 2.06 mmol) was added and reaction was left for 24h at room temperature. Product was purified by column chromatography with hexane/ethyl acetate (1:1) solvent mixture. Characterization was done via ^{1}H NMR in $CDCl_3$.

7.2.4. Place Exchange Reaction with Catechol Modified RAFT Agent (Dopa-CTA)

Oleic acid coated NPs (10 mg) and Dopa-CTA (50 mg) were dissolved in 1 mL chloroform and the solution was stirred at 40 ^{o}C for 48 h under nitrogen atmosphere. After 48 h, solvent was evaporated and methanol was added to reaction mixture and precipitated via centrifuge. Then the mixture was dispersed in THF. This process was repeated, TLC was checked and it was continued until all unattached Dopa-CTA was removed completely.

7.2.5. General Procedure for Surface-Initiated RAFT Polymerization on IONPs

As general procedure, dopa-CTA coated nanoparticles (5 mg), PEGMEMA (0.432 g, 0.864 mmol), and AIBN (6.3 mg, 0.0384 mmol) were dissolved in 4 mL toluene and purged with nitrogen for 20 min. The reaction mixture was placed in a preheated oil bath at 70 °C. After 4 hours, the solvent was evaporated, and polymer-coated nanoparticles were precipitated from a mixture of DCM/diethyl ether (1:50). The resulting polymer-grafted nanoparticles were meticulously collected. Subsequent RAFT co polymerizations of PEGMEMA and FuMaMA with varying percentages (10%, 20%, 30%) were conducted using the procedure.

7.2.6. Retro Diels-Alder Reaction of Copolymer Coated IONPs

Simply, 20 mg of fabricated polymer-grafted IONPs dissolved into 20 mL of anhydrous toluene and stirred under reflux for 8h at 110°C. After the reaction, solvent was evaporated under vacuum and maleimide bearing copolymer coated IONPs were obtained. They were kept in THF for further use.

7.2.7. Surface Functionalization of Polymer Coated IONPs via Thiol-ene Reaction with BODIPY-SH

Side chain maleimide bearing polymer coated IONPs (10 mg) was dissolved into 3 mL THF together with bodipy-SH (0.1 mg, 1.8 μmol) and catalytic amount of TEA. Reaction was completed at room temperature after 6h. Unreacted bodipy dye was removed via dialysis (3.5 KDa) in MeOH for 3d.

7.2.8. Surface Functionalization of Bodıpy Functionalized Polymer Coated IONPs via Strain Promoted Azide-Alkyne Click Chemistry (SPAAC) Reaction with Cyanine5 Tetrazine Dye

BODIPY attached polymer coated IONPs (10 mg) was dissolved into 200 μL MeOH and cy5-tetrazine solution 10 μL from a stock solution (1 mg/mL). Reaction was completed at room temperature after 6h. Unreacted cy5-tetrazine dye was removed via dialysis (3.5 KDa) in MeOH for 24h.

7.2.9. Surface Functionalization of Polymer Coated IONPs via Thiol-ene Reaction with DOX-SH

Side chain maleimide bearing polymer coated IONPs (50 mg) was dissolved into 3 mL H_2O together with dox-SH (0.5 mg, 0.77 mmol) and catalytic amount of TEA. Reaction was completed at 37 ºC for 24h. Unattached dox drug molecule was removed via dialysis (3.5 KDa) in MeOH for 3d.

7.3. Results and Discussion

7.3.1. Fabrication of Functionalizable Polymer Coated IONPs

Firstly, synthesized dopa-CTA was coated IONPs using catechol groups on dopa via place exchange reaction at 40 ºC for 2d (Figure 7.3). Obtained CTA coated particles were washed via centrifuge to remove unbounded CTA, and continued to washing till there is no

spot on TLC of the supernatant. At the same time, FuMaMA monomer was synthesized in two steps according to literature.

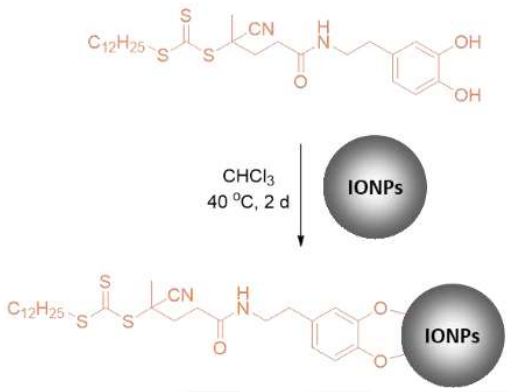

Figure 7.3. Coating IONPs with Dopa-CTA via place exchange reaction.

RAFT polymerization was carried out at 70 ºC for 6h using dopa-CTA coated IONPs in the presence of FuMaMA and PEGMEMA monomers. By using the same procedure, four different polymers were synthesized with different feeding ratio of FuMaMA as 0 (including PEGMEMA only), 10, 20 and 30% (Figure 7.4). Obtained polymers were precipitated into cold ether.

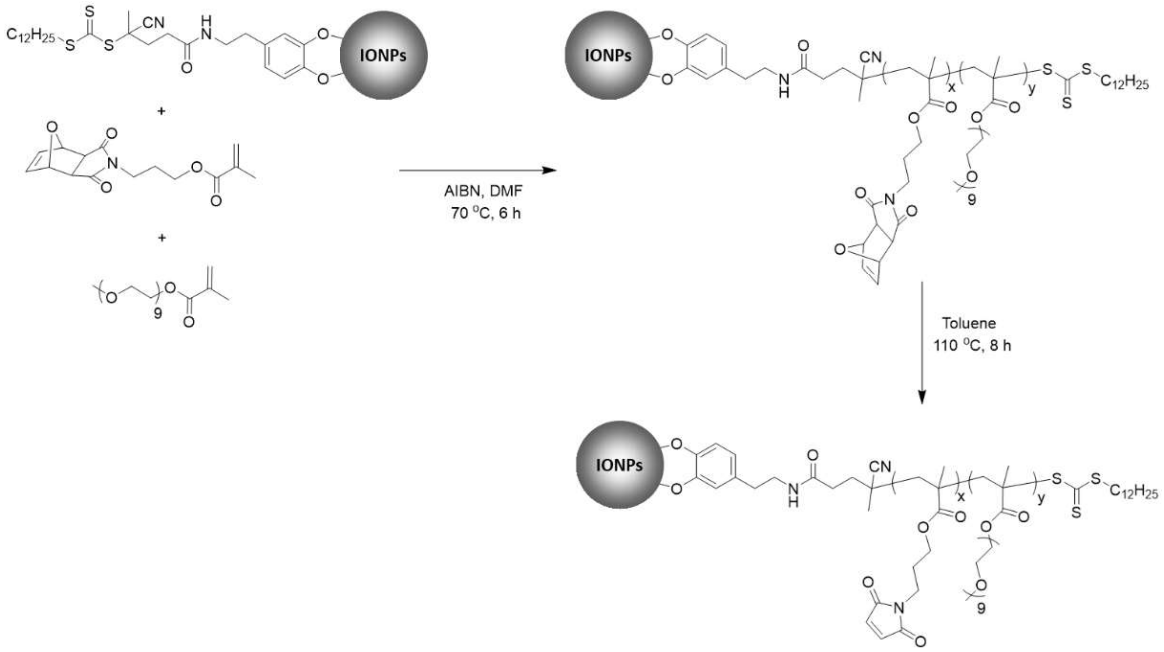

Figure 7.4. Graft from polymerization on IONPs and activation of maleimide groups via retro Diels-Alder reaction, respectively.

Since for the functionalization of polymer coating maleimide units are needed, furan protection groups were removed via rDA reaction at 110 ºC for 8h and after evaporation of toluene, activated maleimide groups bearing polymer coated IONPs were obtained. In order to show their magnetic feature, one of synthesized polymer coated IONPs (10%) were dissolved into H_2O and a photo of it was taken (left photo is in Figure 7.5), then the solution was put near the magnet and waited overnight to collect polymer coated IONPs, the magnetic feature of them can be seen in the right photo in the Figure 7.5.

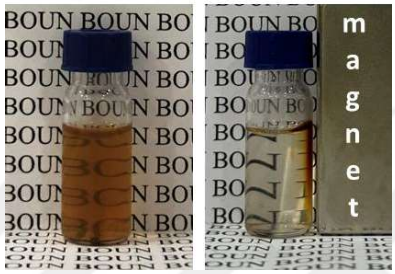

Figure 7.5. Polymer coated IONPs in aqueous solution, before and after affected by a magnet.

After the fabrication of polymer coated NPs, characterization was done via STEM. In the STEM, CTA coated IONPs, PEG-IONPs (as control group), 10, 20 and 30% FuMaMA including polymer coated IONPs were monitored.

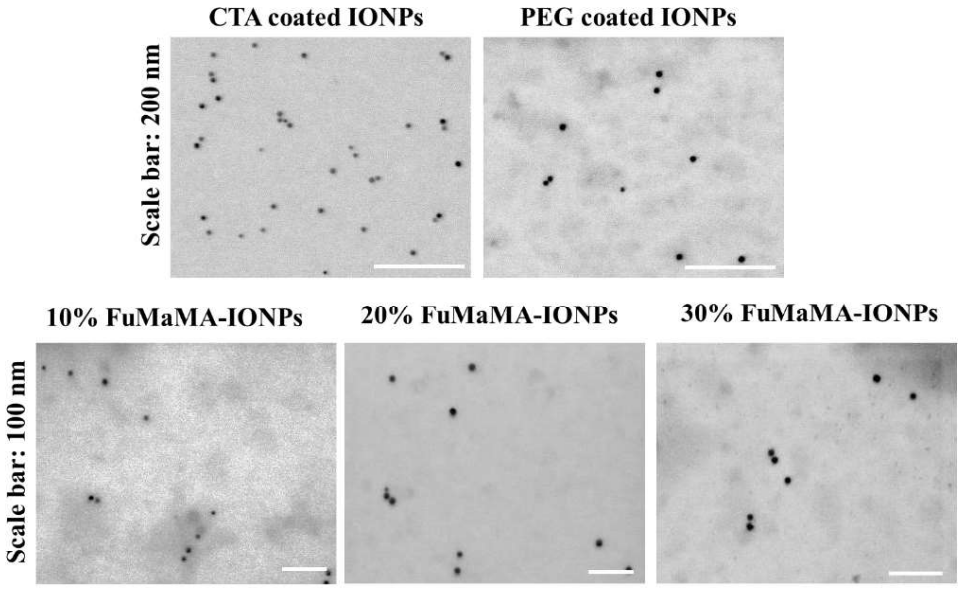

Figure 7.6. STEM images of CTA and PEG, 10%, 20% and 30% FuMaMA containing polymers coated IONPs.

According to results, all coated particles were seeming resemble, dispersed and their sizes were consistent with the each other (Figure 7.6). While before the graft from polymerization, the average size of CTA-IONPs was around 9 nm, after the polymerization on the surface the average size was around 13 nm.

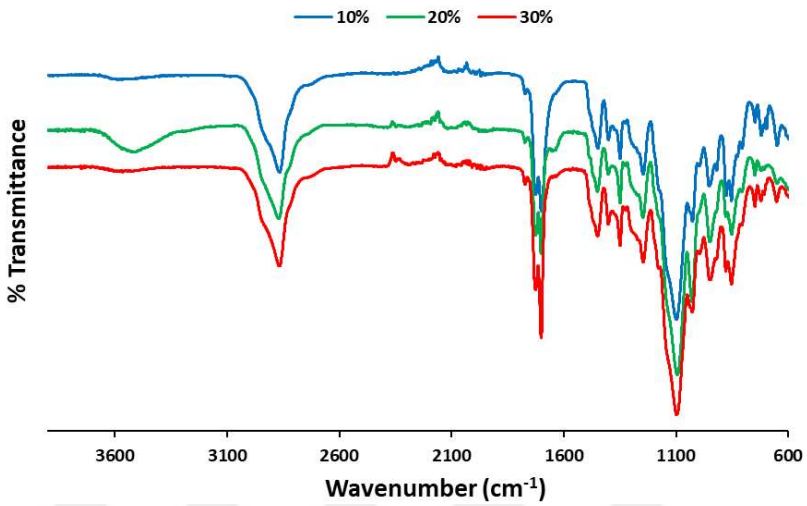

Figure 7.7. FT-IR spectra of including FuMaMA polymers coated IONPs.

Another characterization of the polymer coated system was FT-IR spectroscopy (Figure 7.7). The characteristic peak of protected maleimide carbonyl group was observed at around 1700 cm-1 and comparing of 10, 20 and 30% FuMaMA coated IONPs, it can be seen that peak increased with the increasing ratio of FuMaMA.

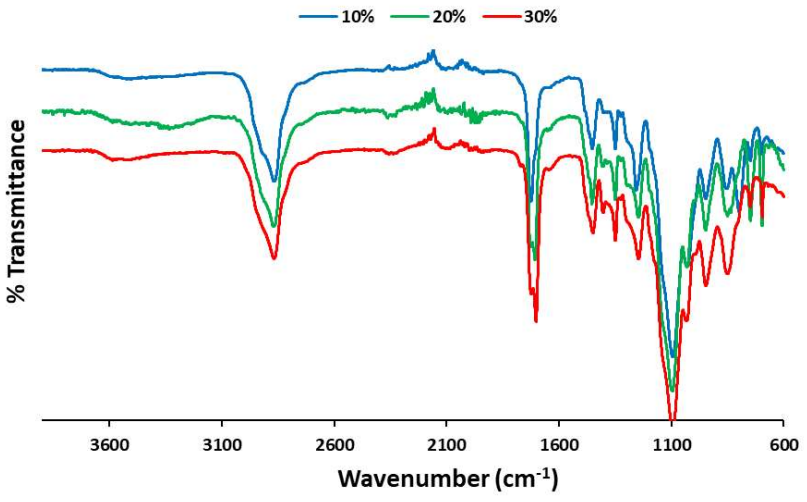

Figure 7.8. FT-IR spectra of maleimide bearing polymers coated IONPs.

After activation of polymers with retro Diels-Alder reaction at 110 °C, FT-IR spectra of the polymers were checked again (Figure 7.8). A slight shift in the carbonyl peaks was observed as expected, and no undesirable new peaks appeared, which conforms that the retro-Diels-Alder reaction proceeded in a clean fashion.

For determination of the weight percentage of polymer coating on the IONPs surface, thermogravimetric analysis (TGA) were carried out (Figure 7.9). While the weight change for oleic acid coated IONPs in the beginning was around 18%, after place exchange reaction with dopa-CTA, the decrease in weight % was around 35. On the other hand, with the polymerization on the surface of IONPs, result showed around 90% of the construct was consisting polymer coating.

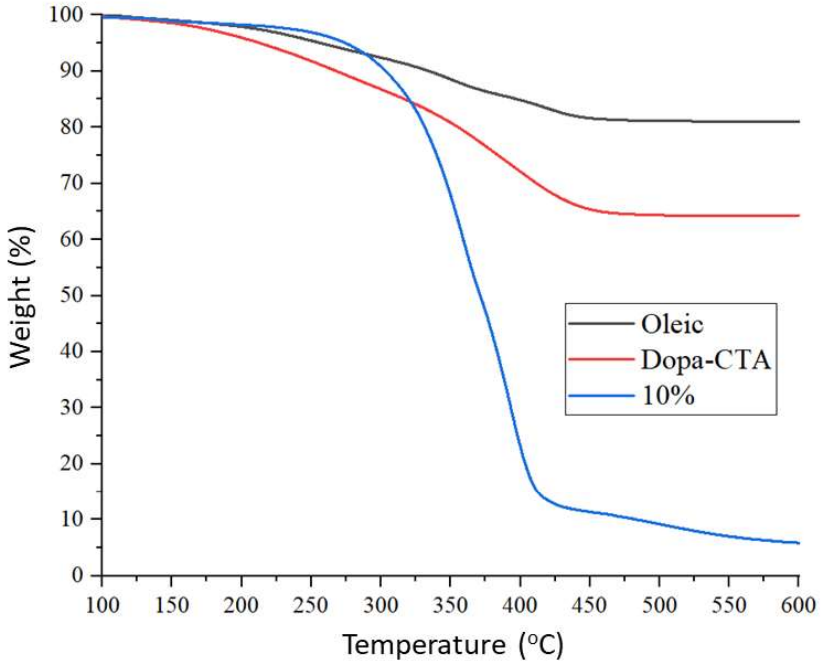

Figure 7.9. TGA results of pristine IONPs, dopa-CTA coated IONPs and 10% FuMaMA bearing IONPs.

For the different amount of FuMaMA containing polymers coating IONPs, on TGA (Figure 7.10) it was seen that, activation of maleimide group was started at around 110 °C, and the decrease continued to around 200 °C. It can be followed that PEG part of the coating was gone around 350 °C and in the end bare IONPs were remined which was around only 10%.

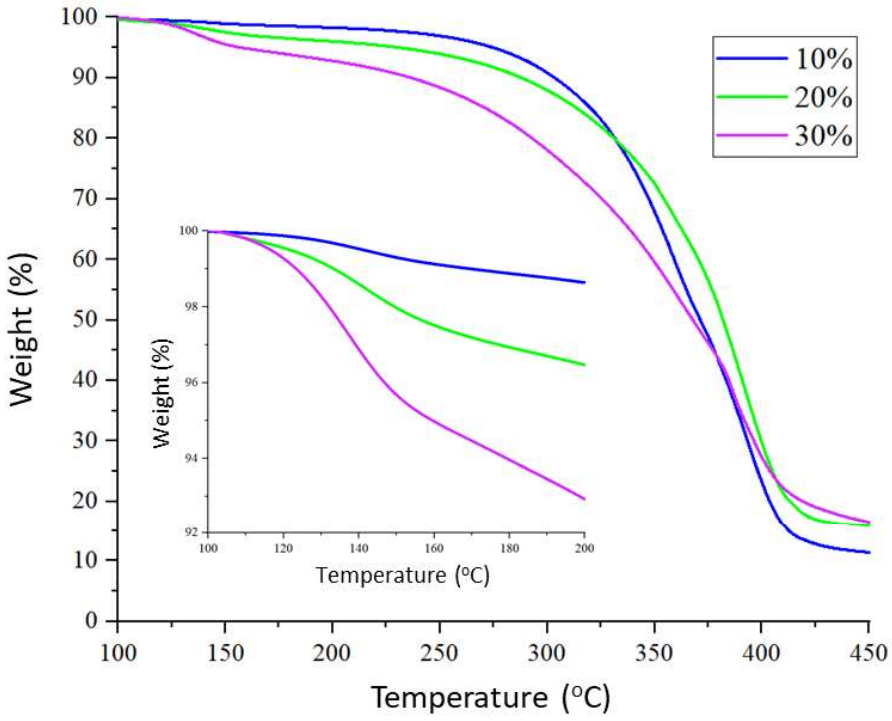

Figure 7.10. TGA results of 10, 20 and 30% FuMaMA bearing polymers coated IONPs.

In the next step, XPS analysis of the four-polymer coated IONPs were achieved (Figure 7.11). Using this way, maleimide ratio on the coating as well as surface coating compositions were analyzed. In the wide scan spectrum, in terms of binding energies, the photoelectron lines of C 1s, N 1s and O 1s were seen at 286 eV, 400 eV and 535 eV, respectively. For the maleimide scan, increase in peaks intensity were clearly seen with increase of maleimide ratio.

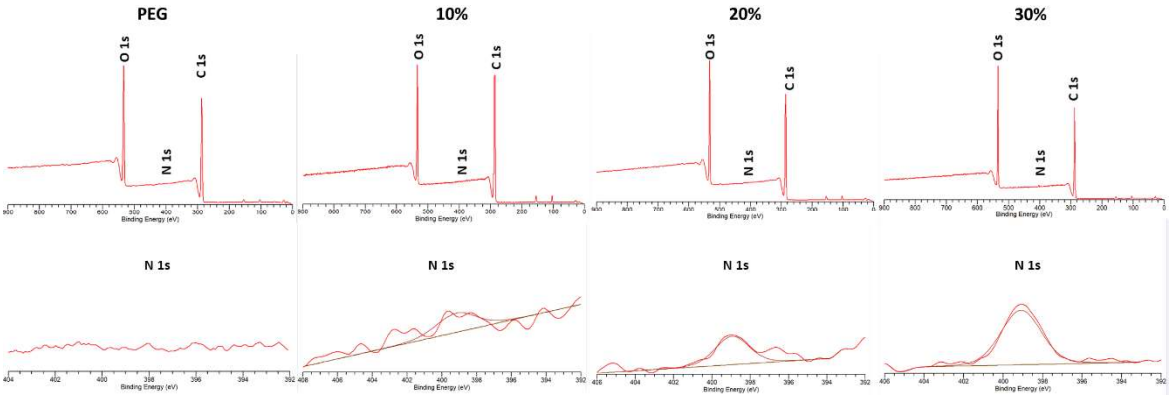

Figure 7.11. XPS analysis of the control group (PEG-IONPs) and 10, 20 and 30% maleimide bearing polymer-IONPs.

With the successful characterization of polymer coated IONPs, to demonstrate dual functionalization of surface coating, rDA reaction was carried out with less timing (6h) in order to obtain half-activation of the maleimide units. Thus, both furan protected maleimide and activated maleimide groups on the same polymer coating was obtained as readily for post functionalization. To verify if the coating has both protected and activated maleimide groups, TGA was done (Figure 7.12). With the comparison of PEG-IONPs, and completely activated 30%-IONPs, the decrease in furan protection was nearly half which proves obtaining half activated polymer coating.

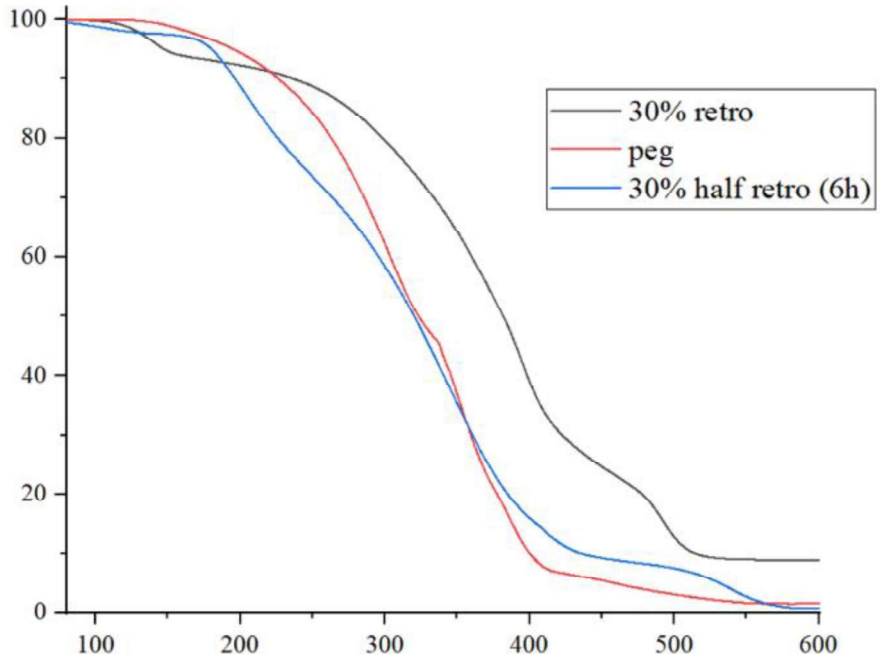

Figure 7.12. TGA results comparisons of PEG coated IONPs, 30% maleimide bearing IONPs and half protected and activated maleimide bearing polymers coated IONPs.

Firstly, synthesized BODIPY-SH which is a fluorescent dye, was attached to obtained half activated polymer coated IONPs using activated maleimide units via thiol-ene reaction, at room temperature during 6h. After reaction precipitation in cold ether was done and washed many times to complete removal of unattached BODIPY dye. Attachment was followed via UV-vis spectroscopy, 1 mg/mL solution of BODIPY-IONPs was and specific peak coming from BODIPY at 500 nm was seen. After BODIPY attachment, polymer coating was functionalized with cy5-tetrazine dye via inverse electron demand Diels-Alder reaction between furan protected maleimide groups and tetrazine unit. Reaction was carried

out at room temperature, in MeOH for 24h and removing unreacted dye was removed via dialysis (3.5 KDa) in MeOH. Functionalized polymer coating with two dye was visualized via UV-vis spectroscopy. Cy5 dye peak was followed around 650 nm. Both peaks belong to BODIPY and CY5 dyes were seen and that means coating has the same dye on it.

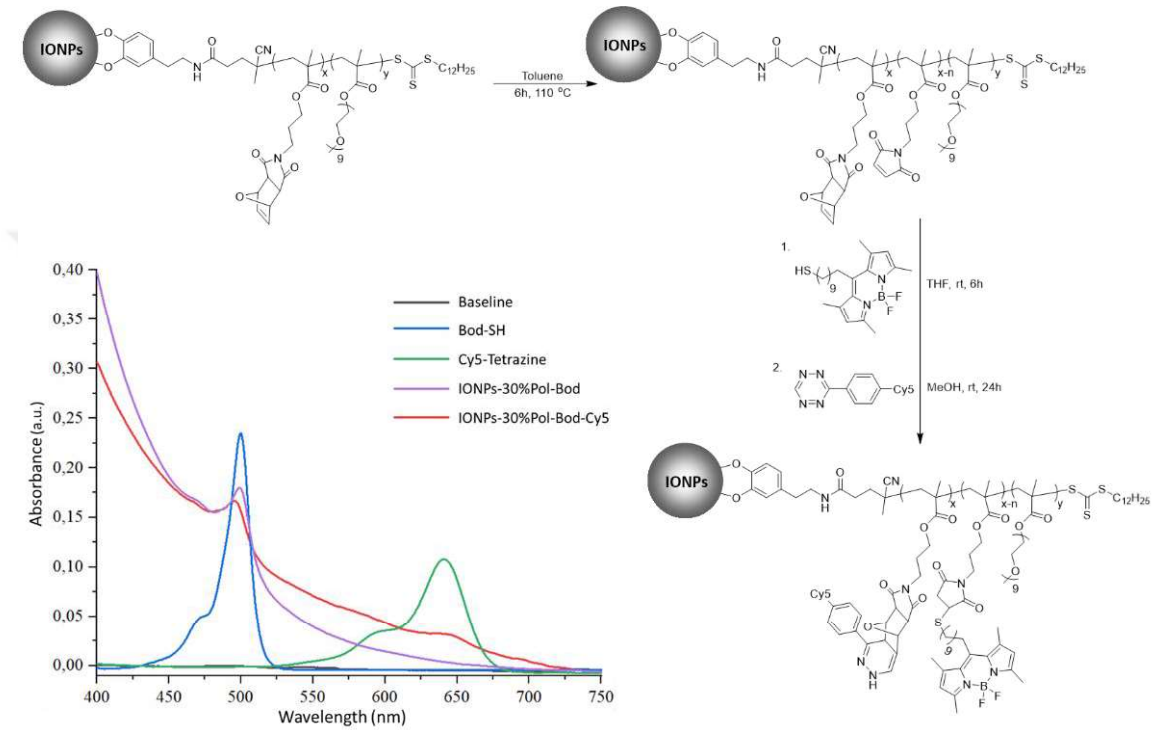

Figure 7.13. Schematic illustration of dual functionalization of polymer coating on IONPs with BODIPY-maleimide and Cy5-tetrazine dye respectively and UV-vis graph of the attachments.

After functionalization of coating with fluorescent dyes, by using 30% activated maleimide including polymer coated IONPs, a thiol containing drug was attached on the surface via thiol-ene reaction. As drug, a chemotherapy drug doxorubicin (DOX) was modified with thiol group according to literature [153]. Reaction was carried out in H_2O for 24h and purification was done via dialysis. Doxorubicin peak was appeared at 485 nm on the UV-vis spectrum (Figure 7.14). By using calibration curve of thiol modified DOX, the attached amount of drug was calculated as 71 µg/mL in 1 mg/mL DOX-IONPs solution.

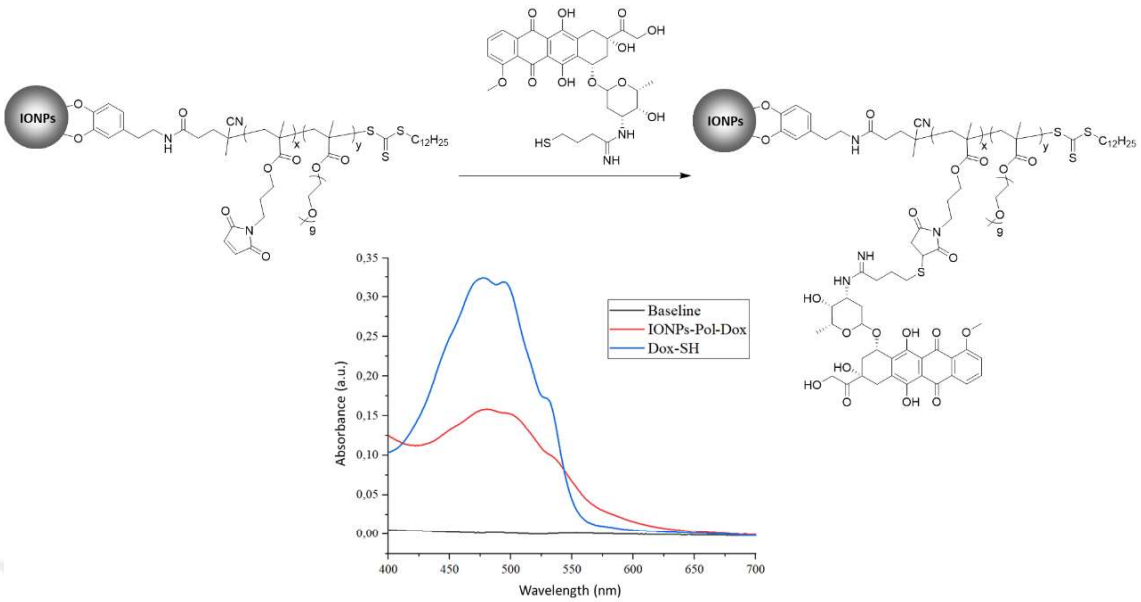

Figure 7.14. Schematic illustration and UV-vis spectrum of doxorubicin drug attachment on the surface coating of IONPs.

To evaluate drug conjugated IONPs in vitro experiments, besides DOX-IONPs, a targeting group cRGDfK was placed onto polymer by using half activated coating. For this purpose, first DOX-SH was attached via thiol-ene reaction, and then cRGDfK modified with tetrazine was added via iedDA reaction (Figure 7.15).

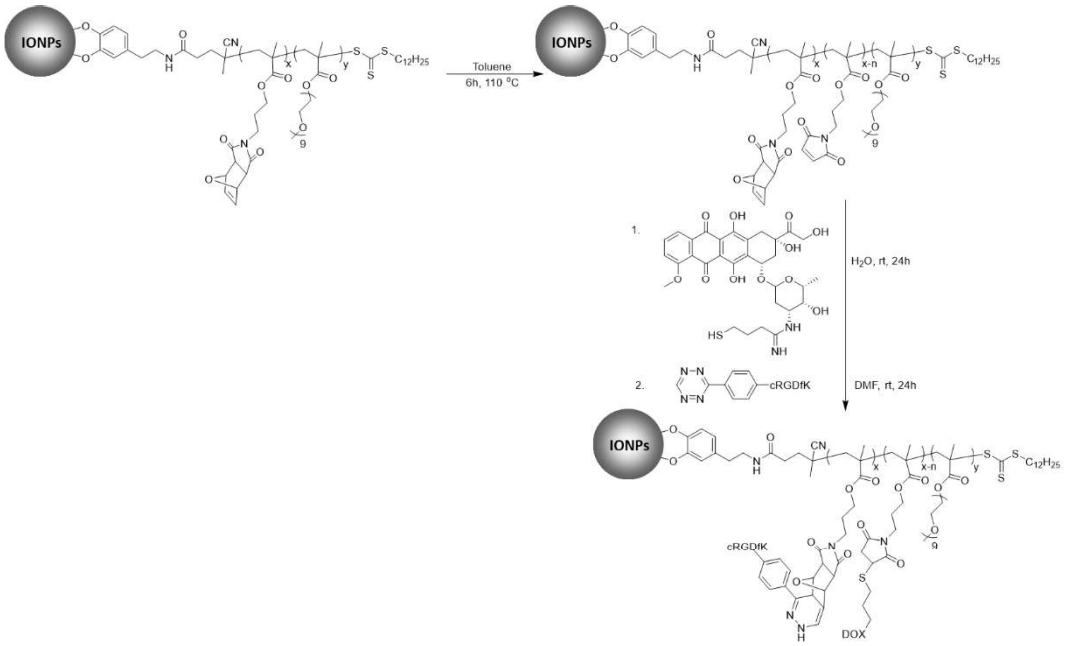

Figure 7.15. Addition of DOX-SH and cRGDfK-tetrazine on half activated polymer coating of IONPs.

While attached DOX was calculated via calibration curve on UV-vis spectroscopy, amount of targeting group was calculated via BCA analysis since amount is important due to toxicity of high amount RGD and also for competitive experiment with addition of same amount free RGD on the targeted coating in vitro analysis.

7.4. Conclusion

In conclusion, IONPs were coated successfully with different feeding ratio of furan protected maleimide monomer as 0, 10, 20 and 30%. rDA reaction provided activated maleimide groups on coating and thus functionalization. For the dual orthogonal functionalization, half activation with less timing rDA reaction was done and TGA was showed there were both protected and activated maleimide on the polymer coating. To this half-activated coating, BODIPY-SH and cy5-tetrazine dyes were attached as sequentially via thiol-ene and iedDA reactions, respectively. UV-vis spectra were proved the successful attachment. Using same half activated polymer brush coating, DOX-SH which is a chemotherapy drug and as targeting group cRGDfK-tetrazine were added. At the same time, completely maleimide bearing IONPs were modified with DOX as non-targeted system to comparison with targeted one in vitro experiment.

8. CONCLUSION

The first part of the thesis includes a synthesis of small drug molecule for pancreatic cancer treatment. Two different drug molecules were utilized; gemcitabine and hydroxychloroquine. While gemcitabine is already employed for chemotherapy as free drug for lots of cancer types, chloroquine is a drug used for malaria treatment. But recently it was found that it may have an effect on the autophagy mechanism and when used as an adjuvant it can enhance the effect of chemotherapy agent. By this approach, obtaining synergistic effect of two drugs on pancreatic cancer cells was aimed and thus two different prodrug molecules include GEM and HCQ with and without disulfide on the linker between them was synthesized and their cytotoxic effect were evaluated on Bx-PC3 cell line.

In the second part, three different nanomaterials were utilized for different purposes on next four projects; carbon nanotubes (CNTs), reduced graphene oxide (rGO) and iron oxide nanoparticles (IONPs). In the second project, multi walled CNTs were coated with a polymer which provides water solubility and functionality to CNTs. In order to fabricate coated CNTs, physical interaction was used between CNTs and pyrene (Py) group on polymer chain. After wrapping the CNTs by polymers, it was functionalized via thiol-ene reaction. With successful coating and functionalization, cytotoxicity of CNTs were probed against fibroblast cells, and high viability results were observed.

In the third project of the thesis, rGO-containing hydrogels were fabricated. Hydrogel was synthesized via crosslinking between thiol-modified beta-cyclodextrins (β-CDSH) and vinyl group modified dextrans (dex). After obtaining and characterizing the hydrogels, three different antibiotics were loaded into hydrogels by absorption method and release experiments were done using active and passive ways. Active release was conducted via NIR light. With application of NIR, rGO inside the gel reaches high temperature and thus eases the release of the antibiotic. Finally, released antibiotics were applied on different bacteria strains (*E. coli*, *S. aureus*, *S. epidermidis*), and successful killing of bacteria was achieved.

On the fourth part of the thesis, IONPs were coated with polymers via the “graft from” method and reversible addition fragmentation chain transfer (RAFT) polymerization. First a catechol group containing chain transfer agent (CTA) was synthesized and coated onto IONPs surfaces. In the next step, a polymer bearing furan and poly (ethyleneglycol) (PEG) on side chains was grown on the IONPs surface. Utilizing furan units on the polymer coating as reactive handles, functionalization with different maleimide bearing molecules was achieved to attach various dyes and drugs onto the surface of IONPs via the Diels-Alder (DA) reaction.

On the last part, by using a masked maleimide containing monomer FuMaMA and PEGMEMA, a polymer coating was fabricated on IONPs via RAFT polymerization. Retro Diels-Alder (rDA) reaction was achieved for removing furan protection and thus activation maleimide units on the polymer coating. Thanks to maleimide groups, coating was functionalized using nucleophilic thiol-ene reaction, e.g. with a thiol bearing dye (BODIPY-SH), and a chemotherapy drug doxorubicin (DOX-SH). Besides, in order to show orthogonality of the system, rDA reaction was carried out for less time to obtain the mixture of maleimide and furan-protected maleimide units on the coating. To this mixed surface coating while BODIPY-SH was added via thiol-ene reaction, cy5-tetrazine dye was added using the inverse electron demand Diels-Alder (iedDA) reaction onto the IONPs surface successfully. Afterward, using the rDA half activation, DOX-SH as a drug was attached by thiol-ene reaction and as targeting unit cRGDfK-tetrazine was attached via iedDA to IONPs. Thus a system possessing magnetic features, as well as carrying a drug and targeting group was obtained. This type of multifunctional construct could be a viable candidate for theranostic applications.

Overall, the thesis puts forth a variety of novel drug delivery platforms for the delivery of therapeutic agents in a targeted manner, as well as reports a small molecule prodrug system which is specifically designed for addressing challenges in pancreatic cancer. A combination of synthetic transformations and polymer chemistry is utilized as a tool for fabrication of these functional constructs. In subsequent investigations, more biological studies on these platforms will be conducted to assess there viability in clinical use.

REFERENCES

1. Aslam, H., S. Shukrullah, M. Y. Naz, H. Fatima, H. Hussain, S. Ullah, and M.A. Assiri, "Current and Future Perspectives of Multifunctional Magnetic Nanoparticles Based Controlled Drug Delivery Systems.", *Journal of Drug Delivery Science and Technology*, Vol. 67, p. 102946, 2022.

2. Xie, X., Y. Zhang, F. Li, T. Lv, Z. Li, H. Chen, L. Jia, and Y. Gao, "Challenges and Opportunities from Basic Cancer Biology for Nanomedicine for Targeted Drug Delivery.", *Current Cancer Drug Targets*, Vol. 19, pp. 257–276, 2018.

3. Zhang, H., K. Wang, K. Na, D. Li, Z. Li, D. Zhao, L. Zhong, M. Wang, L. Kou, C. Luo, Haotian Zhang, Q. Kan, H. Ding, Z. He, and J. Sun, "Striking A Balance Between Carbonate/Carbamate Linkage Bond and Reduction Sensitive Disulfide Bond-Bearing Linker for Tailored Controlled Release: In Situ Covalent Albumin Binding Gemcitabine Prodrugs Promote Bioavailability and Tumor Accumulation.", *Journal of Medicinal Chemistry*, Vol. 61, pp. 4904–4917, 2018.

4. Li, S. Y., L. H. Liu, H. Z. Jia, W. X. Qiu, L. Rong, H. Cheng, and X. Z. Zhang, "A pH-Responsive Prodrug for Real-Time Drug Release Monitoring and Targeted Cancer Therapy.", *Chemical Communications*, Vol. 50, pp. 11852–11855, 2014.

5. Tallarida, R. J., "Quantitative Methods for Assessing Drug Synergism.", *Genes and Cancer*, Vol. 2, pp. 1003–1008, 2011.

6. Fu, Z., X. Cheng, J. Kuang, H. Feng, L. Chen, J. Liang, X. Shen, S. Yuen, C. Peng, B. Shen, Z. Jin, and W. Qiu, "CQ Sensitizes Human Pancreatic Cancer Cells to Gemcitabine Through the Lysosomal Apoptotic Pathway via Reactive Oxygen Species.", *Molecular Oncology*, Vol. 12, pp. 529–544, 2018.

7. Li, J., R. Cha, H. Luo, W. Hao, Y. Zhang, and X. Jiang, "Nanomaterials for the Theranostics of Obesity.", *Biomaterials*, Vol. 223, pp. 119474, 2019.

8. Chen, T., and L. Dai, “Carbon Nanomaterials for High-Performance Supercapacitors.”, *Materials Today*, Vol. 16, pp. 272–280, 2013.

9. Shahryari, Z., M. Yeganeh, K. Gheisari, and B. Ramezanzadeh, “A Brief Review of the Graphene Oxide-Based Polymer Nanocomposite Coatings: Preparation, Characterization, and Properties.”, *Journal of Coatings Technology and Research*, Vol. 18, pp. 945–969, 2021.

10. Kolahalam, L. A., I. V. Kasi Viswanath, B. S. Diwakar, B. Govindh, V. Reddy, and Y. L. N. Murthy, “Review on Nanomaterials: Synthesis and Applications.”, *Materials Today: Proceedings*, Vol. 18, pp. 2182–2190, 2019.

11. Gupta, J., A. Prakash, M. K. Jaiswal, A. Agarrwal, and D. Bahadur, “Superparamagnetic Iron Oxide-Reduced Graphene Oxide Nanohybrid - A Vehicle for Targeted Drug Delivery and Hyperthermia Treatment of Cancer.”, *Journal of Magnetism and Magnetic Materials*, Vol. 448, pp. 332–338, 2018.

12. Patel, K. D., R. K. Singh, and H. W. Kim, “Carbon-Based Nanomaterials as an Emerging Platform for Theranostics.”, *Materials Horizons*, Vol. 6, pp. 434–469, 2019.

13. Demirel, E., E. Karaca, and Y. Yuksel Durmaz, “Effective PEGylation Method to Improve Biocompatibility of Graphene Derivatives.”, *European Polymer Journal*, Vol. 124, p. 109504, 2020.

14. Cheon, Y. A., J. H. Bae, and B. G. Chung, “Reduced Graphene Oxide Nanosheet for Chemo-Photothermal Therapy.”, *Langmuir*, Vol. 32, pp. 2731–2736, 2016.

15. lijima, S, “Helical Microtubules of Graphitic Carbon.”, *Nature*, Vol. 354, pp. 56–58, 1991.

16. Han, Z., and A. Fina, “Thermal Conductivity of Carbon Nanotubes and Their Polymer Nanocomposites: A Review.”, *Progress in Polymer Science (Oxford)*, Vol. 36, pp. 914–

944, 2011.

17. Gong, H., R. Peng, and Z. Liu, “Carbon Nanotubes for Biomedical Imaging: the Recent Advances.”, *Advanced Drug Delivery Reviews*, Vol. 65, pp. 1951–1963, 2013.

18. Gupta, S., C. N. Murthy, and C. R. Prabha, “Recent Advances in Carbon Nanotube Based Electrochemical Biosensors.”, *International Journal of Biological Macromolecules*, Vol. 108, pp. 687–703, 2018.

19. Singh, B., S. Lohan, P. S. Sandhu, A. Jain, and S. K. Mehta, “Functionalized Carbon Nanotubes and Their Promising Applications in Therapeutics and Diagnostics.”, *Nanobiomaterials in Medical Imaging: Applications of Nanobiomaterials,* pp. 455-478, 2016.

20. Desmecht, A., S. Hermans, and O. Riant, “Versatile Two-Step Functionalization of Nanocarbons: Grafting of Propargylic Groups and Click Post-Functionalization.”, *ChemistryOpen*, Vol. 6, pp. 231–235, 2017.

21. Bilalis, P., D. Katsigiannopoulos, A. Avgeropoulos, and G. Sakellariou, “Non-Covalent Functionalization of Carbon Nanotubes with Polymers.”, *RSC Advances*, Vol. 4, pp. 2911–2934, 2014.

22. Holzinger, M., J. Baur, R. Haddad, X. Wang, and S. Cosnier, “Multiple Functionalization of Single-Walled Carbon Nanotubes By Dip Coating.”, *Chemical Communications*, Vol. 47, pp. 2450–2452, 2011.

23. Jang, K., K. Eom, G. Lee, J. H. Han, S. Haam, J. Yang, E. Kim, W. J. Kim, and T. Kwon, “Water-Stable Single-Walled Carbon Nanotubes Coated by Pyrenyl Polyethylene Glycol for Fluorescence Imaging and Photothermal Therapy.”, *Biochip Journal*, Vol. 6, pp. 396–403, 2012.

24. Zhang, G., and J. K. Oh, “Reactive Multidentate Block Copolymer Stabilization to Carbon Nanotubes for Thermoreversible Cross-Linked Network Gels.”, *ACS Applied*

Polymer Materials, Vol. 2, pp. 2319–2326, 2020.

25. Sulistyaningsih, T., S. J. Santosa, D. Siswanta, and B. Rusdiarso, "Synthesis and Characterization of Magnetites Obtained from Mechanically and Sonochemically Assissted Co-Precipitation and Reverse Co-Precipitation Methods.", *International Journal of Materials, Mechanics and Manufacturing*, Vol. 5, pp. 16–19, 2017.

26. Schütz, M. B., K. Lê, S. Ilyas, and S. Mathur, "Reversible Covalent Assembly of Nanoparticles Through on-Surface Diels-Alder Reaction.", *Langmuir*, Vol. 36, pp. 1552–1558, 2020.

27. Barrow, M., A. Taylor, P. Murray, M. J. Rosseinsky, and D. J. Adams, "Design Considerations for The Synthesis of Polymer Coated Iron Oxide Nanoparticles for Stem Cell Labelling And Tracking Using MRI.", *Chemical Society Reviews*, Vol. 44, pp. 6733–6748, 2015.

28. Arslan, M., T. N. Gevrek, R. Sanyal, and A. Sanyal, "Fabrication of Poly(Ethylene Glycol)-Based Cyclodextrin Containing Hydrogels via Thiol-Ene Click Reaction.", *European Polymer Journal*, Vol. 62, pp. 426–434, 2015.

29. Steinle, H., T. M. Ionescu, S. Schenk, S. Golombek, S. J. Kunnakattu, M. T. Özbek, C. Schlensak, H. P. Wende, and M. Avci-Adali, "Incorporation of Synthetic MRNA in Injectable Chitosan-Alginate Hybrid Hydrogels for Local and Sustained Expression of Exogenous Proteins in Cells.", *International Journal of Molecular Sciences*, Vol. 19, p. 1313, 2018.

30. Cheng, C., X. Zhang, Y. Meng, L. Chen, and Q. Zhang, "Development of a Dual Drug-Loaded Hydrogel Delivery System for Enhanced Cancer Therapy: In Situ Formation, Degradation and Synergistic Antitumor Efficiency.", *Journal of Materials Chemistry B*, Vol. 5, pp. 8487–8497, 2017.

31. Cui, R., Q. Wu, J. Wang, X. Zheng, R. Ou, Y. Xu, S. Qu, and D. Li, "Hydrogel-by-Design: Smart Delivery System for Cancer Immunotherapy.", *Frontiers in*

Bioengineering and Biotechnology, Vol. 9, pp. 1–11, 2021.

32. Liu, J., B. Tian, Y. Liu, and J.B. Wan, "Cyclodextrin-Containing Hydrogels: A Review Of Preparation Method, Drug Delivery, And Degradation Behavior.", *International Journal of Molecular Sciences*, Vol. 22, p. 13516, 2021.

33. Yi, J., G. Choe, J. Park, and J. Y. Lee, "Graphene Oxide-Incorporated Hydrogels for Biomedical Applications.", *Polymer Journal*, Vol. 52, pp. 823–837, 2020.

34. Fiorica, C., F. S. Palumbo, G. Pitarresi, R. Puleio, L. Condorelli, G. Collura, and G. Giammona, "A Hyaluronic Acid/Cyclodextrin Based Injectable Hydrogel for Local Doxorubicin Delivery to Solid Tumors.", *International Journal of Pharmaceutics*, Vol. 589, p. 119879, 2020.

35. Alkekhia, D., C. Larose, and A. Shukla, "β-Lactamase-Responsive Hydrogel Drug Delivery Platform for Bacteria-Triggered Cargo Release.", *ACS Applied Materials and Interfaces*, Vol. 14, pp. 27538–27550, 2022.

36. Dannert, C., B. T. Stokke, and R. S. Dias, "Nanoparticle-Hydrogel Composites: from Molecular Interactions to Macroscopic Behavior.", *Polymers*, Vol. 11, p. 275, 2019.

37. Wang, X., W. Guo, L. Li, F. Yu, J. Li, L. Liu, B. Fang, and L. Xia, "Photothermally Triggered Biomimetic Drug Delivery of Teriparatide via Reduced Graphene Oxide Loaded Chitosan Hydrogel for Osteoporotic Bone Regeneration.", *Chemical Engineering Journal*, Vol. 413, p. 127413, 2021.

38. World Health Organization, Cancer Today, "Estimated Age-Standardized Incidence Rates (World) In 2020 , All Cancers, Both Sexes, All Ages.", https://gco.iarc.fr/en, 2022, accessed on December 20, 2023.

39. Muñoz Martín, A. J., J. Adeva, J. Martínez-Galán, J. J. Reina, and M. Hidalgo, "Pancreatic Ductal Adenocarcinoma: Metastatic Disease.", *Clinical and Translational Oncology*, Vol. 19, pp. 1423–1429, 2017.

40. Oberstein, P. E., and K. P. Olive, “Pancreatic Cancer: Why Is It So Hard to Treat?”, *Therapeutic Advances in Gastroenterology*, Vol. 6, pp. 321–337, 2013.

41. Keleg, S., P. Büchler, R. Ludwig, M. W. Büchler, and H. Friess, “Invasion and Metastasis in Pancreatic Cancer.”, *Molecular Cancer*, Vol. 2, pp. 1–7, 2003.

42. Ishiwata, T., “Pancreatic Ductal Adenocarcinoma: Basic and Clinical Challenges for Better Prognosis.”, *Journal of Carcinogenesis & Mutagenesis*, Vol. 01, pp. 9–10, 2013.

43. Yeo, D., A. Bastian, H. Strauss, P. Saxena, P. Grimison, and J. E. J. Rasko, “Exploring the Clinical Utility of Pancreatic Cancer Circulating Tumor Cells.”, *International Journal of Molecular Sciences*, Vol. 23, p. 1671, 2022.

44. Park, J. Y., Y. L. Cho, J. R. Chae, S. H. Moon, W. G. Cho, Y. J. Choi, S. J. Lee, and W. J. Kang, “Gemcitabine-Incorporated G-Quadruplex Aptamer for Targeted Drug Delivery into Pancreas Cancer.”, *Molecular Therapy - Nucleic Acids*, Vol. 12, pp. 543–553, 2018.

45. Silvestris, N., S. Cinieri, I. La Torre, G. Pezzella, G. Numico, L. Orlando, and V. Lorusso, “Role of Gemcitabinein Metastatic Breast Cancer Patients: A Short Review.”, *Breast*, Vol. 17, pp. 220–226, 2008.

46. Shelley, M. D., A. Cleves, T. J. Wilt, and M. D. Mason, “Gemcitabine Chemotherapy for the Treatment of Metastatic Bladder Carcinoma.”, *BJU International*, Vol. 108, pp. 168–179, 2011.

47. Dora, C. P., V. Kushwah, S. S. Katiyar, P. Kumar, V. Pillay, S. Suresh, and S. Jain, “Improved Metabolic Stability and Therapeutic Efficacy of a Novel Molecular Gemcitabine Phospholipid Complex.”, *International Journal of Pharmaceutics*, Vol. 530, pp. 113–127, 2017.

48. De Sousa Cavalcante, L., and G. Monteiro, “Gemcitabine: Metabolism and Molecular Mechanisms of Action, Sensitivity and Chemoresistance in Pancreatic Cancer.”,

European Journal of Pharmacology, Vol. 741, pp. 8–16, 2014.

49. Donohue, E., A. Thomas, N. Maurer, I. Manisali, M. Zeisser-Labouebe, N. Zisman, H. J. Anderson, S. S. W. Ng, M. Webb, M. Bally, and M. Roberge, "The Autophagy Inhibitor Verteporfin Moderately Enhances the Antitumor Activity of Gemcitabine in a Pancreatic Ductal Adenocarcinoma Model.", *Journal of Cancer*, Vol. 4, pp. 585–596, 2013.

50. Kim, M., Y. W. Chin, and E. J. Lee, "A, Γ-Mangostins Induce Autophagy and Show Synergistic Effect with Gemcitabine in Pancreatic Cancer Cell Lines.", *Biomolecules and Therapeutics*, Vol. 25, pp. 609–617, 2017.

51. Ma, T., W. Chen, X. Zhi, H. Liu, Y. Zhou, B. Wei, L. Hu, J. Shen, X. Zheng, S. Zhang, B. Zhang, H. Li, and T. Liang, "USP9X Inhibition Improves Gemcitabine Sensitivity in Pancreatic Cancer By Inhibiting Autophagy.", *Cancer Letters*, Vol. 436, pp. 129–138, 2018.

52. Qiao, Z., M. I. N. He, M. U. He, W. Li, X. Wang, Y. Wang, Q. Kuai, C. Li, S. Ren, and Q. U. N. Yu, "Synergistic Antitumor Activity of Gemcitabine Combined with Triptolide in Pancreatic Cancer Cells.", *Oncology Letters*, Vol. 11, pp. 3527–3533, 2016.

53. Balic, A., M. D. Sørensen, S. M. Trabulo, B. Sainz, M. Cioffi, C. R. Vieira, I. Miranda-Lorenzo, M. Hidalgo, J. Kleeff, M. Erkan, and C. Heeschen, "Chloroquine Targets Pancreatic Cancer Stem Cells via Inhibition of CXCR4 and Hedgehog Signaling.", *Molecular Cancer Therapeutics*, Vol. 13, pp. 1758–1771, 2014.

54. Kim, J., M. L. R. Yip, X. Shen, H. Li, L. Y. C. Hsin, S. Labarge, E. L. Heinrich, W. Lee, J. Lu, and N. Vaidehi, "Identification of Anti-Malarial Compounds as Novel Antagonists to Chemokine Receptor CXCR4 in Pancreatic Cancer Cells.", *PLoS One*, Vol. 7, p. 31004, 2012.

55. Xu, R., Z. Ji, C. Xu, and J. Zhu, "The Clinical Value of Using Chloroquine or

Hydroxychloroquine as Autophagy Inhibitors in the Treatment of Cancers a Systematic Review and Meta-Analysis.", *Medicine (United States)*, Vol. 97, pp. 8–9, 2018.

56. Al-Bari, A. A., "Chloroquine Analogues in Drug Discovery: New Directions of Uses, Mechanisms of Actions and Toxic Manifestations from Malaria to Multifarious Diseases.", *Journal of Antimicrobial Chemotherapy*, Vol. 70, pp. 1608–1621, 2014.

57. Weiss, J. T., J. C. Dawson, C. Fraser, W. Rybski, C. Torres-Sánchez, M. Bradley, E. E. Patton, N. O. Carragher, and A. Unciti-Broceta, "Development and Bioorthogonal Activation of Palladium-Labile Prodrugs of Gemcitabine.", *Journal of Medicinal Chemistry*, Vol. 57, pp. 5395–5404, 2014.

58. Zhang, H., Z. Sun, K. Wang, N. Li, H. Chen, X. Tan, L. Li, Z. He, and J. Sun, "Multifunctional Tumor-Targeting Cathepsin B-Sensitive Gemcitabine Prodrug Covalently Targets Albumin in Situ and Improves Cancer Therapy.", *Bioconjugate Chemistry*, Vol. 29, pp. 1852–1858, 2018.

59. Duveau, D. Y., P. M. Arce, R. A. Schoenfeld, N. Raghav, G. A. Cortopassi, and S. M. Hecht, "Synthesis and Characterization of MitoQ and Idebenone Analogues as Mediators of Oxygen Consumption in Mitochondria.", *Bioorganic and Medicinal Chemistry*, Vol. 18, pp. 6429–6441, 2010.

60. Li, X., X. Wang, C. Xu, J. Huang, C. Wang, Xinyang Wang, L. He, and Y. Ling, "Synthesis and Biological Evaluation of Nitric Oxide-Releasing Hybrids from Gemcitabine and Phenylsulfonyl Furoxans as Anti-Tumor Agents.", *MedChemComm*, Vol. 6, pp. 1130–1136, 2015.

61. Levy, D. E., B. Frederick, B. Luo, and S. Zalipsky, "Heterobifunctional PEGs: Efficient Synthetic Strategies and Useful Conjugation Methodologies.", *Bioorganic and Medicinal Chemistry Letters*, Vol. 20, pp. 6823–6826, 2010.

62. Chojnacka, M. W., and R. A. Batey, "Total Synthesis of (+)-Prunustatin A: Utility of Organotrifluoroborate-Mediated Prenylation and Shiina MNBA Esterification and

Macrolactonization to Avoid a Competing Thorpe-Ingold Effect Accelerated Transesterification.", *Organic Letters*, Vol. 20, pp. 5671–5675, 2018.

63. Schmidt, T., and A. Kirschning, "Total Synthesis of Carolacton, a Highly Potent Biofilm Inhibitor.", *Angewandte Chemie - International Edition*, Vol. 51, pp. 1063–1066, 2012.

64. Cengiz, B., R. Sanyal, and A. Sanyal, "Tailoring Aqueous Dispersibility and Biofunctionalization of Carbon Nanotubes Using Maleimide-Containing Clickable Polymers.", *ACS Apl. Polym. Mater.*, Vol 3, 5707-5716, 2021.

65. Gillen, A. J., and A. A. Boghossian, "Non-Covalent Methods of Engineering Optical Sensors Based on Single-Walled Carbon Nanotubes.", *Frontiers in Chemistry*, Vol. 7, pp. 1–13, 2019.

66. Sun, X., J. Sun, T. Li, S. Zheng, C. Wang, W. Tan, J. Zhang, C. Liu, T. Ma, Z. Qi, Chunxiu Liu, and N. Xue, "Flexible Tactile Electronic Skin Sensor with 3D Force Detection Based on Porous CNTs/PDMS Nanocomposites.", *Nano-Micro Letters*, Vol. 11, pp. 1–14, 2019.

67. Behnam, B., W. T. Shier, A. H. Nia, K. Abnous, and M. Ramezani, "Non-Covalent Functionalization of Single-Walled Carbon Nanotubes with Modified Polyethyleneimines for Efficient Gene Delivery.", *International Journal of Pharmaceutics*, Vol. 454, pp. 204–215, 2013.

68. Zhou, D., Y. Zhang, J. Zhu, J. Yu, Y. Wang, and Z. Hu, "Tailoring the Architecture of Aromatic Polymer for Highly Efficient Dispersion of Carbon Nanomaterial and Their High-Performance Composites.", *Carbon*, Vol. 148, pp. 297–306, 2019.

69. Nunes, A., N. Amsharov, C. Guo, J. Van Den Bossche, P. Santhosh, T. K. Karachalios, S. F. Nitodas, M. Burghard, K. Kostarelos, and K. T. Al-Jamal, "Hybrid Polymer-Grafted Multiwalled Carbon Nanotubes for in Vitro Gene Delivery.", *Small*, Vol. 6, pp. 2281–2291, 2010.

70. Eom, T., V. Barát, A. Khan, and M. C. Stuparu, “Aggregation-Free and High Stability Core–Shell Polymer Nanoparticles with High Fullerene Loading Capacity, Variable Fullerene Type, and Compatibility towards Biological Conditions.”, *Chem. Sci.*, Vol. 12, pp. 4949-4957, 2021.

71. Zhou, H., X. Li, C. Gao, F. Yang, X. Ye, Y. Liu, and L. Wang, “The Ameliorative Thermoelectric Performance Induced by Heteroatom for Dithiophene Cyclopentadiene-Based Polymers and Carbon Nanotubes Composite Films.”, *Composites Science and Technology*, Vol. 201, p. 108518, 2021.

72. Bilgi, M., D. Karaca Balta, B. A. Temel, and G. Temel, “Single-Chain Folding Nanoparticles as Carbon Nanotube Catchers.”, *Journal of Polymer Science, Part A: Polymer Chemistry*, Vol. 56, pp. 2709–2714, 2018.

73. Morishita, T., M. Matsushita, Y. Katagiri, and K. Fukumori, “Noncovalent Functionalization of Carbon Nanotubes with Maleimide Polymers Applicable to High-Melting Polymer-Based Composites.”, *Carbon*, Vol. 48, pp. 2308–2316, 2010.

74. Meran, M., P. D. Akkus, O. Kurkcuoglu, E. Baysak, G. Hizal, E. Haciosmanoglu, A. Unlu, N. Karatepe, and F. S. Güner, “Noncovalent Pyrene-Polyethylene Glycol Coatings of Carbon Nanotubes Achieve in Vitro Biocompatibility.”, *Langmuir*, Vol. 34, pp. 12071–12082, 2018.

75. Fong, D., J. Yeung, E. Meichsner, and A. Adronov, “Reactive, Aqueous-Dispersible Polyfluorene-Wrapped Carbon Nanotubes Modulated with an Acidochromic Switch via Azide–Alkyne Cycloaddition.”, *ACS Applied Polymer Materials*, Vol. 1, pp. 797–803, 2019.

76. Fong, D., Z. Hua, T. R. Wilks, R. K. O’Reilly, and A. Adronov, “Dispersion of Single-Walled Carbon Nanotubes Using Nucleobase-Containing Poly(Acrylamide) Polymers.”, *Journal of Polymer Science, Part A: Polymer Chemistry*, Vol. 55, pp. 2611–2617, 2017.

77. Zhang, N., D. Zhou, N. Zhou, Z. Zhang, and X. Zhu, “Dispersion of Single-Walled Carbon Nanotubes in an Aqueous Medium by Using a Cyclic Copolymer.”, *Reactive and Functional Polymers*, Vol. 113, pp. 85–92, 2017.

78. Demirel, E., E. Karaca, and Y. Yuksel Durmaz, “Effective PEGylation Method to Improve Biocompatibility of Graphene Derivatives.”, *European Polymer Journal*, Vol. 124, p. 109504, 2020.

79. An, S. Y., S. Sun, and J. K. Oh, “Reduction-Responsive Sheddable Carbon Nanotubes Dispersed in Aqueous Solution.”, *Macromolecular Rapid Communications*, Vol. 37, pp. 705–710, 2016.

80. Morishita, T., M. Matsushita, Y. Katagiri, and K. Fukumori, “Synthesis and Properties of Macromer-Grafted Polymers for Noncovalent Functionalization of Multiwalled Carbon Nanotubes.”, *Carbon*, Vol. 47, pp. 2716–2726, 2009.

81. Chen, Q., Y. Li, D. Xiang, Y. Zheng, W. Zhu, C. Zhao, H. Li, H. Han, and Y. Shen, “Enhanced Strain Sensing Performance of Polymer/Carbon Nanotube-Coated Spandex Fibers via Noncovalent Interactions.”, *Macromolecular Materials and Engineering*, Vol. 305, pp. 1–10, 2020.

82. Fong, D., J. Yeung, S. A. McNelles, and A. Adronov, “Decoration of Polyfluorene-Wrapped Carbon Nanotubes via Strain-Promoted Azide-Alkyne Cycloaddition.”, *Macromolecules*, Vol. 51, pp. 755–762, 2018.

83. Fong, D., G. M. Andrews, and A. Adronov, “Functionalization of Polyfluorene-Wrapped Carbon Nanotubes: via Copper-Mediated Azide-Alkyne Cycloaddition.”, *Polymer Chemistry*, Vol. 9, pp. 2873–2879, 2018.

84. Zhang, G., and J. K. Oh, “Reactive Multidentate Block Copolymer Stabilization to Carbon Nanotubes for Thermoreversible Cross-Linked Network Gels.”, *ACS Applied Polymer Materials*, Vol. 2, pp. 2319–2326, 2020.

85. Arslan, M., T. N. Gevrek, J. Lyskawa, S. Szunerits, R. Boukherroub, R. Sanyal, P. Woisel, and A. Sanyal, “Bioinspired Anchorable Thiol-Reactive Polymers: Synthesis and Applications Toward Surface Functionalization of Magnetic Nanoparticles.”, *Macromolecules*, Vol. 47, pp. 5124–5134, 2014.

86. Fenoli, C. R., and C. N. Bowman, “The Thiol-Michael Addition Click Reaction: A Powerful and Widely Used Tool in Materials Chemistry.”, *Chem. Mater.*, Vol. 26, pp. 724-744, 2014.

87. Cengiz, N., T. N. Gevrek, R. Sanyal, and A. Sanyal, “Fabrication of Patterned Hydrogel Interfaces: Exploiting the Maleimide Group as a Dual Purpose Handle for Cross-Linking and Bioconjugation.”, *Bioconjugate Chem.*, Vol. 32, pp. 1382-1391, 2020.

88. Mantovani, G., L. Tao, and D. M. Haddleton, “Design and Synthesis of N-Maleimido-Functionalized Hydrophilic Polymers via Copper-Mediated Living Radical Polymerization : A Suitable Alternative to PEGylation Chemistry.”, *J. Am. Chem. Soc.,* Vol. 127, pp. 2966–2973, 2005.

89. Chambre, L., H. Maouati, Y. Oz, R. Sanyal, and A. Sanyal, “Thiol-Reactive Clickable Cryogels : Importance of Macroporosity and Linkers on Biomolecular Immobilization.”, Bioconjugate Chem., Vol. 31, pp. 2116-2124, 2020.

90. Bays, E., L. Tao, C. Chang, and H. D. Maynard, “Synthesis of Semitelechelic Maleimide Poly (PEGA) for Protein Conjugation by RAFT Polymerization.”, *Biomacromolecules*, Vol. 10, pp. 1777–1781, 2009.

91. Oz, Y., A. Barras, R. Sanyal, R. Boukherroub, S. Szunerits, and A. Sanyal, “Functionalization of Reduced Graphene Oxide via Thiol-Maleimide ‘Click’ Chemistry : Facile Fabrication of Targeted Drug Delivery Vehicles.”, *ACS Appl. Mater. Interfaces*, Vol. 9, pp. 34194-34203, 2017.

92. Gevrek, T. N., K. Yu, J. N. Kizhakkedathu, and A. Sanyal, “Thiol-Reactive Polymers for Titanium Interfaces: Fabrication of Antimicrobial Coatings.”, *ACS Appl. Polym.*

Mater., Vol. 1, pp. 1308-1306, 2019.

93. Sanyal, A., "Diels-Alder Cycloaddition-Cycloreversion: A Powerful Combo in Materials Design.", *Macromolecular Chemistry and Physics*, Vol. 211, pp. 1417–1425, 2010.

94. Oz, Y., and A. Sanyal, "The Taming of the Maleimide: Fabrication of Maleimide-Containing 'Clickable' Polymeric Materials.", *Chemical Record*, Vol. 18, pp. 570–586, 2018.

95. Dispinar, T., R. Sanyal, and A. Sanyal, "A Diels-Alder/Retro Diels-Alder Strategy to Synthesize Polymers Bearing Maleimide Side Chains.", *Journal of Polymer Science, Part A: Polymer Chemistry*, Vol. 45, pp. 4545–4551, 2007.

96. Babin, J., M. Lepage, and Y. Zhao, "'Decoration of Shell Cross-Linked Reverse Polymer Micelles Using ATRP: A New Route to Stimuli-Responsive Nanoparticles.", *Macromolecules*, Vol. 41, pp. 1246–1253, 2008.

97. Gok, O., I. Kosif, T. Dispinar, T. N. Gevrek, R. Sanyal, and A. Sanyal, "Design and Synthesis of Water-Soluble Multifunctionalizable Thiol-Reactive Polymeric Supports for Cellular Targeting.", *Bioconjugate Chemistry*, Vol. 26, pp. 1550–1560, 2015.

98. Liu, Y., K. Mollaeian, M. H. Shamim, and J. Ren, "Effect of F-Actin and Microtubules on Cellular Mechanical Behavior Studied Using Atomic Force Microscope and an Image Recognition-Based Cytoskeleton Quantification Approach.", *International Journal of Molecular Sciences*, Vol. 21, p. 392, 2020.

99. Doernberg, S. B., T. P. Lodise, J. T. Thaden, J. M. Munita, S. E. Cosgrove, C. A. Arias, H. W. Boucher, G. R. Corey, F. D. Lowy, B. Murray, L. G. Miller, and T. L. Holland, "Gram-Positive Bacterial Infections: Research Priorities, Accomplishments, and Future Directions of the Antibacterial Resistance Leadership Group.", *Clinical Infectious Diseases*, Vol. 64, pp. 24–29, 2017.

100. Ferri, M., E. Ranucci, P. Romagnoli, and V. Giaccone, “Antimicrobial Resistance: A Global Emerging Threat to Public Health Systems.”, *Critical Reviews in Food Science and Nutrition*, Vol. 57, pp. 2857–2876, 2017.

101. Cohen, M. L., “Changing Pattern of Infectious Disease.”, *Nature*, Vol. 406, pp. 762-767, 2000.

102. Jones, K. E., N. G. Patel, M. A. Levy, A. Storeygard, D. Balk, J. L. Gittleman, and P. Daszak, “Global Trends in Emerging Infectious Diseases.”, *Nature*, Vol. 451, pp. 990–993, 2008.

103. Zhao, Z., R. Yan, X. Yi, J. Li, J. Rao, Z. Guo, Y. Yang, W. Li, Y.Q. Li, and C. Chen, “Bacteria-Activated Theranostic Nanoprobes against Methicillin-Resistant Staphylococcus Aureus Infection.”, *ACS Nano*, Vol. 11, pp. 4428–4438, 2017.

104. Chen, J., Q. Peng, X. Peng, L. Han, X. Wang, J. Wang, and H. Zeng, “Recent Advances in Mechano-Responsive Hydrogels for Biomedical Applications.”, *ACS Applied Polymer Materials*, Vol. 2, pp. 1092–1107, 2020.

105. Leach, J. B., and C. E. Schmidt, “Characterization of Protein Release from Photocrosslinkable Hyaluronic Acid-Polyethylene Glycol Hydrogel Tissue Engineering Scaffolds.”, *Biomaterials*, Vol. 26, pp. 125–135, 2005.

106. Xu, Q., A. Sigen, Y. Gao, L. Guo, J. Creagh-Flynn, D. Zhou, U. Greiser, Y. Dong, F. Wang, H. Tai, W. Liu, W. Wang, and Wenxin Wang, “A Hybrid Injectable Hydrogel from Hyperbranched PEG Macromer as a Stem Cell Delivery and Retention Platform for Diabetic Wound Healing.”, *Acta Biomaterialia*, Vol. 75, pp. 63–74, 2018.

107. Zhang, W., X. Jin, H. Li, R. run Zhang, and C. wei Wu, “Injectable and Body Temperature Sensitive Hydrogels Based on Chitosan and Hyaluronic Acid for PH Sensitive Drug Release.”, *Carbohydrate Polymers*, Vol. 186, pp. 82–90, 2018.

108. Haidari, H., Z. Kopecki, A. T. Sutton, S. Garg, A. J. Cowin, and K. Vasilev, “Ph-

Responsive ‘Smart’ Hydrogel for Controlled Delivery of Silver Nanoparticles to Infected Wounds.”, *Antibiotics*, Vol. 10, pp. 1–15, 2021.

109. Darge, H. F., A. T. Andrgie, H. C. Tsai, and J. Y. Lai, “Polysaccharide and Polypeptide Based Injectable Thermo-Sensitive Hydrogels for Local Biomedical Applications.”, *International Journal of Biological Macromolecules*, Vol. 133, pp. 545–563, 2019.

110. Alge, D. L., M. A. Azagarsamy, D. F. Donohue, and K. S. Anseth, “Synthetically Tractable Click Hydrogels for Three-Dimensional Cell Culture Formed Using Tetrazine-Norbornene Chemistry.”, *Biomacromolecules*, Vol. 14, pp. 949–953, 2013.

111. Kade, M. J., Burke, D. J., Hawker, C. J., “The Power of Thiol-Ene Chemistry.”, *Journal of Polymer Science: Part A: Polymer Chemistry*, Vol. 48, pp. 743–750, 2010.

112. Xu, X., Z. Huang, Zeqian Huang, X. Zhang, S. He, X. Sun, Y. Shen, M. Yan, and C. Zhao, “Injectable, NIR/pH-Responsive Nanocomposite Hydrogel as Long-Acting Implant for Chemophotothermal Synergistic Cancer Therapy.”, *ACS Applied Materials and Interfaces*, Vol. 9, pp. 20361–20375, 2017.

113. Liu, Y., F. Li, Z. Guo, Y. Xiao, Y. Zhang, X. Sun, T. Zhe, Y. Cao, L. Wang, Q. Lu, and J. Wang, “Silver Nanoparticle-Embedded Hydrogel as a Photothermal Platform for Combating Bacterial Infections.”, *Chemical Engineering Journal*, Vol. 382, p. 122990, 2020.

114. Hidayah, N. M. S., W. W. Liu, C. W. Lai, N. Z. Noriman, C. S. Khe, U. Hashim, and H. C. Lee, “Comparison on Graphite, Graphene Oxide and Reduced Graphene Oxide: Synthesis and Characterization.”, *AIP Conference Proceedings*, Vol. 1892, pp. 1-8, 2017.

115. Mergy, J., A. Fournier, E. Hachet, and R. Auzély-Velty, “Modification of Polysaccharides via Thiol-Ene Chemistry: A Versatile Route to Functional Biomaterials.”, *Journal of Polymer Science, Part A: Polymer Chemistry*, Vol. 50, pp. 4019–4028, 2012.

116. Dernaika, H., S. V. Chong, C. G. Artur, and J. L. Tallon, “Spectroscopic Identification of Neurotoxin Tetramethylenedisulfotetramine (TETS) Captured by Supramolecular Receptor β -Cyclodextrin Immobilized on Nanostructured Gold Surfaces.”, *Journal of Nanomaterials*, Vol. 2014, pp. 1-11, 2014.

117. Zhang, M., X. Wei, X. Xu, Z. Jin, and J. Wang, “Synthesis and Characterization of Water-Soluble β-Cyclodextrin Polymers via Thiol-Maleimide ‘Click’ Chemistry.”, *European Polymer Journal*, Vol. 128, p. 109603, 2020.

118. Altinbasak, I., R. Jijie, A. Barras, B. Golba, R. Sanyal, J. Bouckaert, D. Drider, R. Bilyy, T. Dumych, S. Paryzhak, V. Vovk, R. Boukherroub, A. Sanyal, and S. Szunerits, “Reduced Graphene-Oxide-Embedded Polymeric Nanofiber Mats: an ‘On-Demand’ Photothermally Triggered Antibiotic Release Platform.”, *ACS Applied Materials and Interfaces*, Vol. 10, pp. 41098–41106, 2018.

119. Rosselle, L., A. R. Cantelmo, A. Barras, N. Skandrani, M. Pastore, D. Aydin, L. Chambre, R. Sanyal, A. Sanyal, R. Boukherroub, and S. Szunerits, “An ‘On-Demand’ Photothermal Antibiotic Release Cryogel Patch: Evaluation of Efficacy on an Ex Vivo Model for Skin Wound Infection.”, *Biomaterials Science*, Vol. 21, pp. 5911-5919, 2020.

120. Dadfar, S. M., K. Roemhild, N. I. Drude, S. von Stillfried, R. Knüchel, F. Kiessling, and T. Lammers, “Iron Oxide Nanoparticles: Diagnostic, Therapeutic and Theranostic Applications.”, *Advanced Drug Delivery Reviews*, Vol. 138, pp. 302–325, 2019.

121. Ali, A., H. Zafar, M. Zia, I. ul Haq, A. R. Phull, J. S. Ali, and A. Hussain, “Synthesis, Characterization, Applications, and Challenges oof Iron Oxide Nanoparticles.”, *Nanotechnology, Science and Applications*, Vol. 9, pp. 49–67, 2016.

122. Liu, G., J. Gao, H. Ai, and X. Chen, “Applications and Potential Toxicity of Magnetic Iron Oxide Nanoparticles.”, *Small*, Vol. 9, pp. 1533–1545, 2013.

123. Vayssières, L., C. Chanéac, E. Tronc, and J. Jolivet, “Size Tailoring of Magnetite

Particles Formed by Aqueous Precipitation: An Example of Thermodynamic Stability of Nanometric Oxide Particles.", *Journal of colloid and interface science*, Vol. 205, pp. 205–212, 1998.

124. Kim, D. K., M. Mikhaylova, Y. Zhang, and M. Muhammed, "Protective Coating of Superparamagnetic Iron Oxide Nanoparticles.", *Chemistry of Materials*, Vol. 15, pp. 1617–1627, 2003.

125. Wu, N., L. Fu, M. Su, M. Aslam, K. C. Wong, and V. P. Dravid, "Interaction of Fatty Acid Monolayers with Cobalt Nanoparticles.", *Nano Letters*, Vol. 4, pp. 383–386, 2004.

126. Kataby, G., M. Cojocaru, R. Prozorov, and A. Gedanken, "Coating Carboxylic Acids on Amorphous Iron Nanoparticles.", *Langmuir*, Vol. 15, pp. 1703–1708, 1999.

127. Chen, F., Q. Gao, G. Hong, and J. Ni, "Synthesis and Characterization of Magnetite Dodecahedron Nanostructure by Hydrothermal Method.", *Journal of Magnetism and Magnetic Materials*, Vol. 320, pp. 1775–1780, 2008.

128. Pahwa, M., P. Jain, N. Das Saha, C. Narayana, and S. S. Agasti, "Interfacial Tetrazine Click Chemistry Mediated Assembly of Multifunctional Colloidosomes.", *Chemical Communications*, Vol. 57, pp. 9534–9537, 2021.

129. Hyeon, T., Su Seong Lee, J. Park, Y. Chung, and Hyon Bin Na, "Synthesis of Highly Crystalline and Monodisperse Maghemite Nanocrystallites without a Size-Selection Process.", *Journal of the American Chemical Society*, Vol. 123, pp. 12798–12801, 2001.

130. Lopez Perez, J. A., M. A. Lopez Quintela, J. Mira, J. Rivas, and S. W. Charles, "Advances in the Preparation of Magnetic Nanoparticles by The Microemulsion Method.", *Journal of Physical Chemistry B*, Vol. 101, pp. 8045–8047, 1997.

131. Jana, N. R., Y. Chen, and X. Peng, "Size- and Shape-Controlled Magnetic (Cr, Mn, Fe,

Co, Ni) Oxide Nanocrystals via a Simple and General Approach.", *Chemistry of Materials*, Vol. 16, pp. 3931–3935, 2004.

132. Mohapatra, S., and P. Pramanik, "Synthesis and Stability of Functionalized Iron Oxide Nanoparticles Using Organophosphorus Coupling Agents.", *Colloids and Surfaces A: Physicochemical and Engineering Aspects*, Vol. 339, pp. 35–42, 2009.

133. Bloemen, M., W. Brullot, T. T. Luong, N. Geukens, A. Gils, and T. Verbiest, "Improved Functionalization of Oleic Acid-Coated Iron Oxide Nanoparticles for Biomedical Applications.", *Journal of Nanoparticle Research*, Vol. 14, pp. 1-10, 2012.

134. Javidparvar, A. A., B. Ramezanzadeh, and E. Ghasemi, "The Effect of Surface Morphology and Treatment of Fe3O4 Nanoparticles on The Corrosion Resistance of Epoxy Coating.", *Journal of the Taiwan Institute of Chemical Engineers*, Vol. 61, pp. 356–366, 2016.

135. Amstad, E., T. Gillich, I. Bilecka, M. Textor, and E. Reimhult, "Ultrastable Iron Oxide Nanoparticle Colloidal Suspensions Using Dispersants with Catechol-Derived Anchor Groups.", *Nano Letters*, Vol. 9, pp. 4042–4048, 2009.

136. Guénin, E., Y. Lalatonne, J. Bolley, I. Milosevic, C. Platas-Iglesias, and L. Motte, "Catechol Versus Bisphosphonate Ligand Exchange at the Surface of Iron Oxide Nanoparticles: Towards Multi-Functionalization.", *Journal of Nanoparticle Research*, Vol. 16, p. 2596, 2014.

137. Chen, L. X., T. Liu, M. C. Thurnauer, R. Csencsits, and T. Rajh, "Fe_2O_3 Nanoparticle Structures Investigated by X-Ray Absorption Near-Edge Structure, Surface Modifications, and Model Calculations.", *Journal of Physical Chemistry B*, Vol. 106, pp. 8539–8546, 2002.

138. Ruan, Z., P. Yuan, T. Li, Y. Tian, Q. Cheng, and L. Yan, "Glutathione Triggered Near Infrared Fluorescence Imaging-Guided Chemotherapy by Cyanine Conjugated Polypeptide.", *ACS Biomaterials Science and Engineering*, Vol. 4, pp. 4208–4218,

2018.

139. Oyeneye, O. O., W. Z. Xu, and P. A. Charpentier, “Adhesive RAFT Agents for Controlled Polymerization of Acrylamide: Effect of Catechol-End R Groups.”, *RSC Advances*, Vol. 5, pp. 76919–76926, 2015.

140. Santi, D. V., E. L. Schneider, R. Reid, L. Robinson, and G. W. Ashley, “Predictable and Tunable Half-Life Extension of Therapeutic Agents by Controlled Chemical Release from Macromolecular Conjugates.”, *Proceedings of the National Academy of Sciences of the United States of America*, Vol. 109, pp. 6211–6216, 2012.

141. Park, J., K. An, Y. Hwang, J. E. G. Park, H. J. Noh, J. Y. Kim, J. H. Park, N. M. Hwang, and T. Hyeon, “Ultra-Large-Scale Syntheses of Monodisperse Nanocrystals.”, *Nature Materials*, Vol. 3, pp. 891–895, 2004.

142. Shepherd, J. L., A. Kell, E. Chung, C. W. Sinclar, M. S. Workentin, and D. Bizzotto, “Selective Reductive Desorption of A SAM-Coated Gold Electrode Revealed Using Fluorescence Microscopy.”, *Journal of the American Chemical Society*, Vol. 126, pp. 8329–8335, 2004.

143. Neirynck, P., J. Brinkmann, Q. An, D. W. J. van der Schaft, L. G. Milroy, P. Jonkheijm, and L. Brunsveld, “Supramolecular Control of Cell Adhesion via Ferrocene-Cucurbit[7]Uril Host-Guest Binding on Gold Surfaces.”, *Chemical Communications*, Vol. 49, pp. 3679–3681, 2013.

144. Oyeneye, O. O., W. Z. Xu, and P. A. Charpentier, “Adhesive RAFT Agents for Controlled Polymerization of Acrylamide: Effect of Catechol-End R Groups.”, *RSC Advances*, Vol. 5, pp. 76919–76926, 2015.

145. Heredia, K. L., G. N. Grover, L. Tao, and H. D. Maynard, “Synthesis of Heterotelechelic Polymers for Conjugation of Two Different Proteins.”, *Macromolecules*, Vol. 42, pp. 2360–2367, 2009.

146. Notni, J., T. G. Kapp, and H. Kessler, “Benefits of NOPO as Chelator in Gallium-68 Peptides, Exemplified by Preclinical Characterization of 68 Ga-NOPO-C(RGDfK).”, *Mol. Pharmauceitics*, Vol. 11, pp. 1687-1695, 2014.

147. Discekici, E. H., A. H. St. Amant, S. N. Nguyen, I. H. Lee, C. J. Hawker, and J. Read De Alaniz, “Endo and Exo Diels-Alder Adducts: Temperature-Tunable Building Blocks for Selective Chemical Functionalization.”, *Journal of the American Chemical Society*, Vol. 140, pp. 5009–5013, 2018.

148. Oz, Y., M. Arslan, T. N. Gevrek, R. Sanyal, and A. Sanyal, “Modular Fabrication of Polymer Brush Coated Magnetic Nanoparticles: Engineering the Interface for Targeted Cellular Imaging.”, *ACS Applied Materials and Interfaces*, Vol. 8, pp. 19813–19826, 2016.

149. Amstad, E., M. Textor, and E. Reimhult, “Stabilization and Functionalization of Iron Oxide Nanoparticles for Biomedical Applications.”, *Nanoscale*, Vol. 3, pp. 2819–2843, 2011.

150. Hou, Z., Y. Liu, J. Xu, and J. Zhu, “Surface Engineering of Magnetic Iron Oxide Nanoparticles by Polymer Grafting: Synthesis Progress and Biomedical Applications.”, *Nanoscale*, Vol. 12, pp. 14957–14975, 2020.

151. Zhang, Z., G. Sèbe, Y. Hou, J. Wang, J. Huang, and G. Zhou, “Grafting Polymers from Cellulose Nanocrystals via Surface-Initiated Atom Transfer Radical Polymerization.”, *Journal of Applied Polymer Science*, Vol. 138, pp. 1–29, 2021.

152. Wang, W., X. Ji, H. Bin Na, M. Safi, A. Smith, G. Palui, J. M. Perez, and H. Mattoussi, “Design of a Multi-Dopamine-Modified Polymer Ligand Optimally Suited for Interfacing Magnetic Nanoparticles with Biological Systems.”, *Langmuir*, Vol. 30, pp. 6197–6208, 2014.

153. Cengiz, B., N. Ejderyan, and A. Sanyal, “Functional Polymeric Coatings: Thiol-Maleimide ‘Click’ Chemistry as a Powerful Surface Functionalization Tool.”, *Journal*

of Macromolecular Science, Part A: Pure and Applied Chemistry, Vol. 59, pp. 443–455, 2022.

154. Darwish, S., N. Sadeghiani, S. Fong, S. Mozaffari, P. Hamidi, T. Withana, S. Yang, R.K. Tiwari, and K. Parang, "Synthesis and Antiproliferative Activities of Doxorubicin Thiol Conjugates and Doxorubicin-SS-Cyclic Peptide.", *European Journal of Medicinal Chemistry*, Vol. 161, pp. 594–606, 2019.

APPENDIX A: SPECTROSCOPY DATA

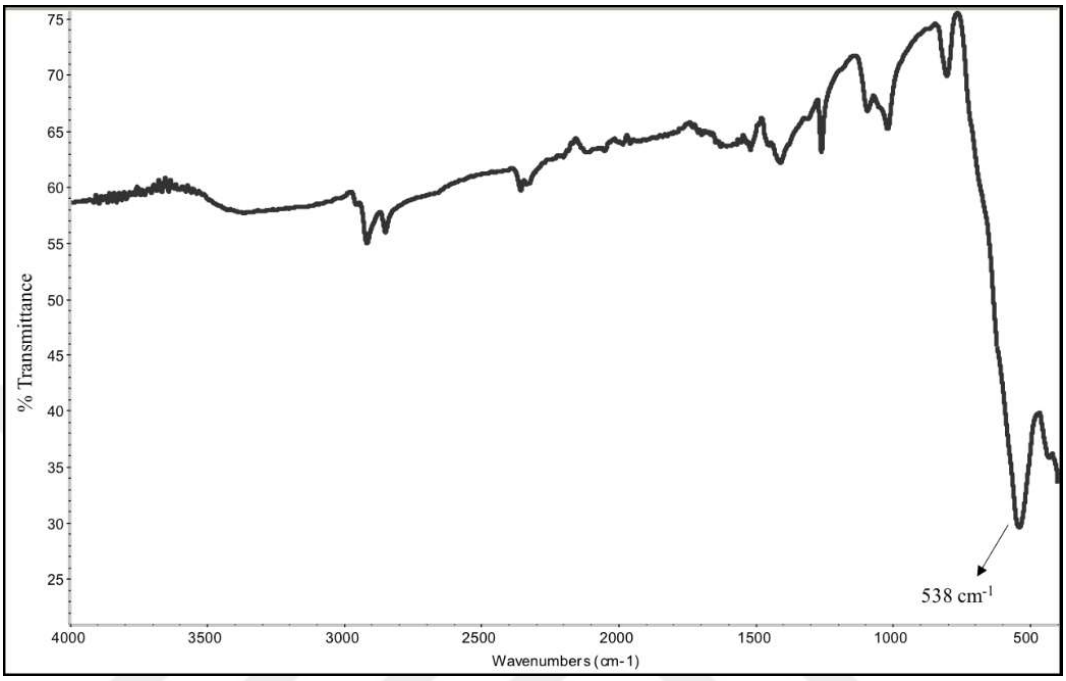

Figure A.1. FT-IR spectrum of oleic acid coated iron oxide nanoparticles.

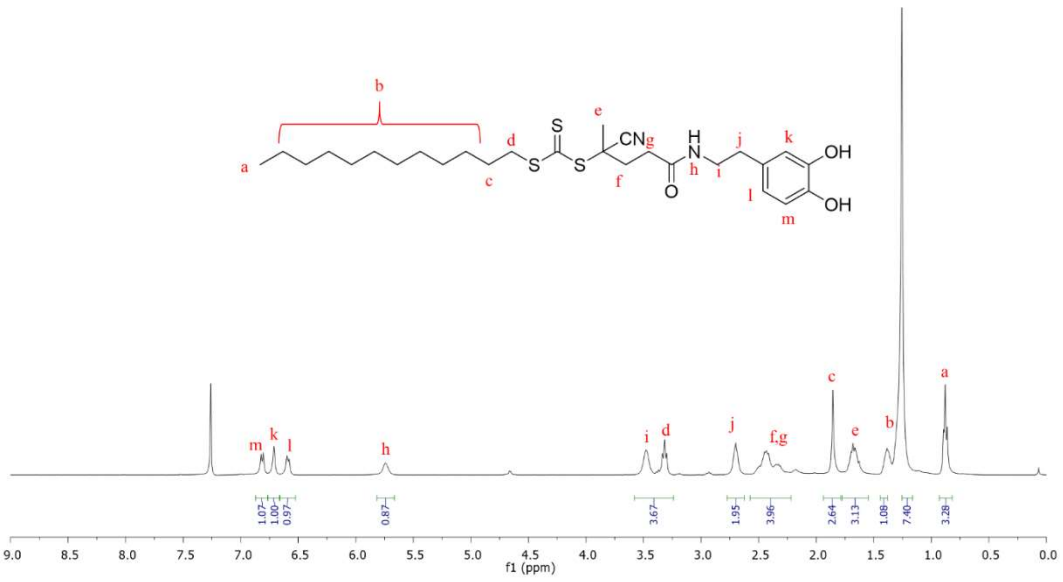

Figure A.2. ^{1}H NMR spectrum of Dopa-CTA.

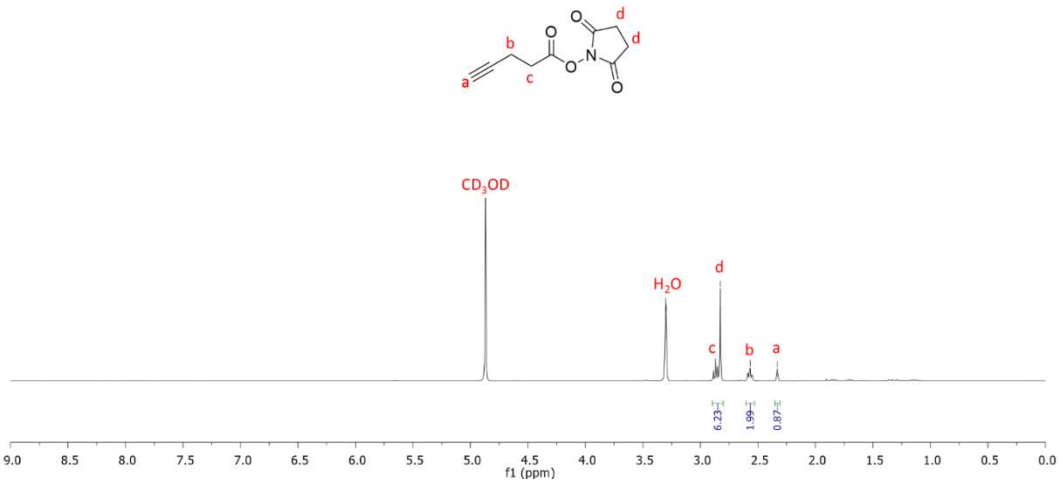

Figure A.3. ^{1}H NMR spectrum of NHS activated alkyne group bearing molecule.

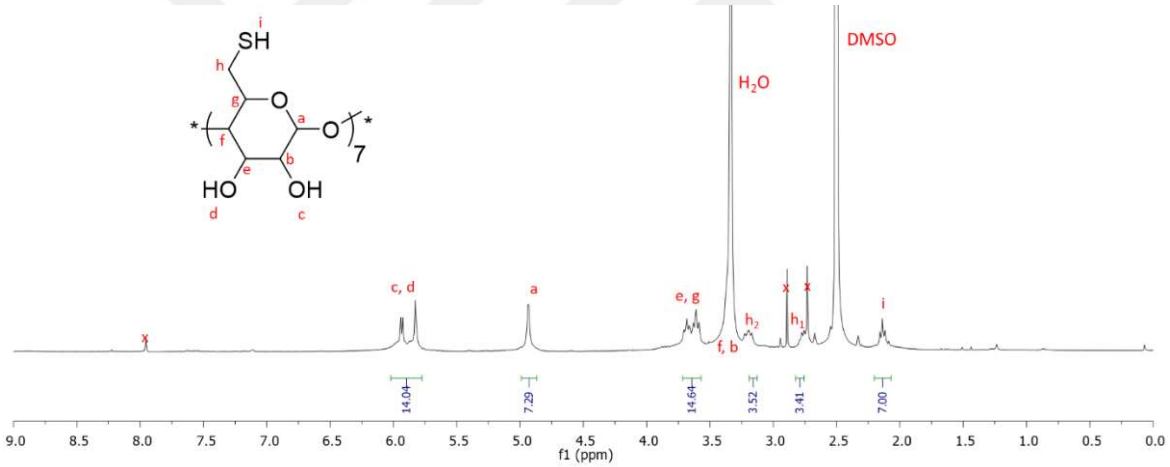

Figure A.4. ^{1}H NMR spectrum of per-6-thiolated β cyclodextrin.

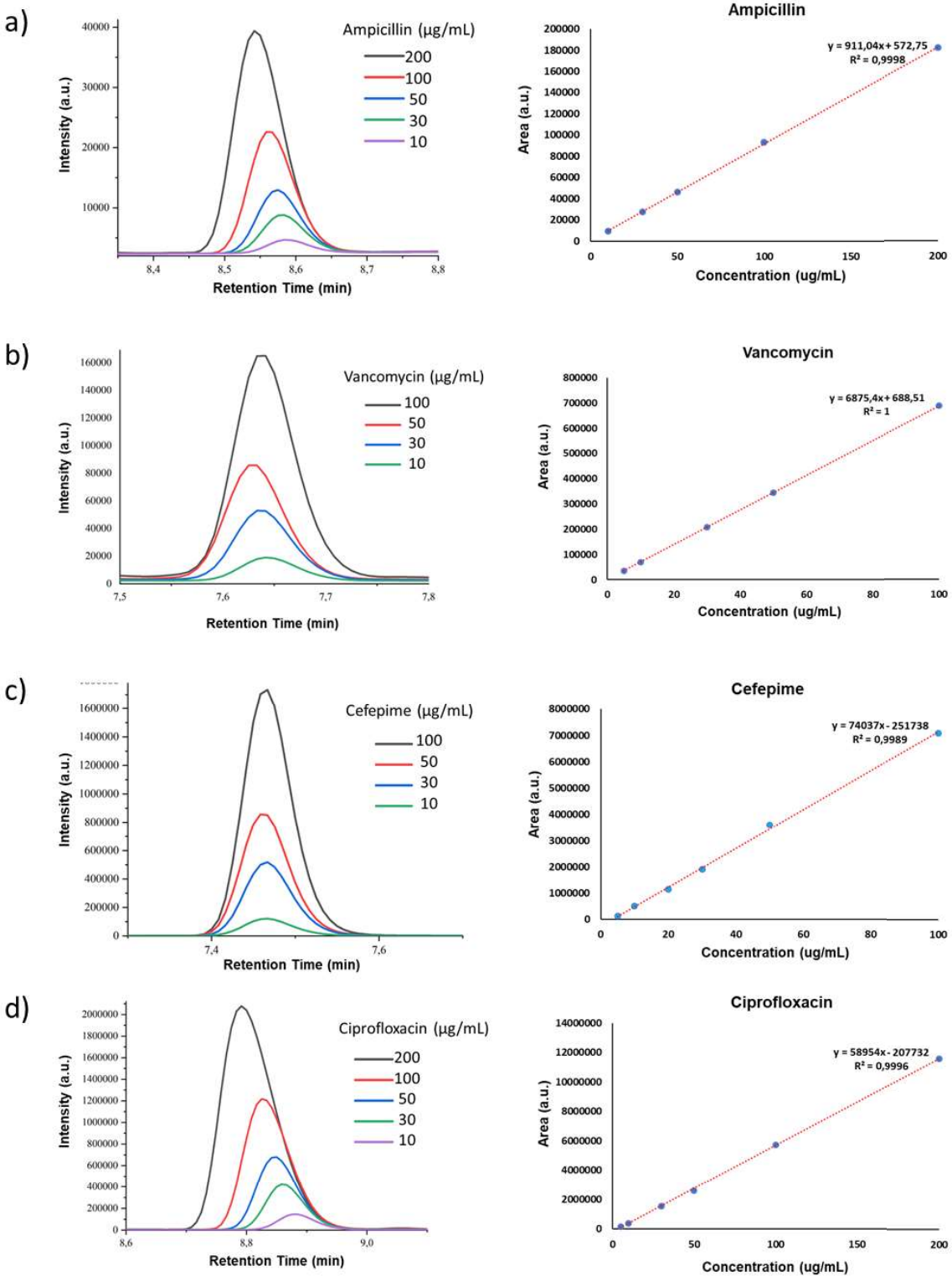

Figure A.5. HPLC calibration curves in different concentrations for ampicillin, vancomycin, cefepime and ciprofloxacin drugs.

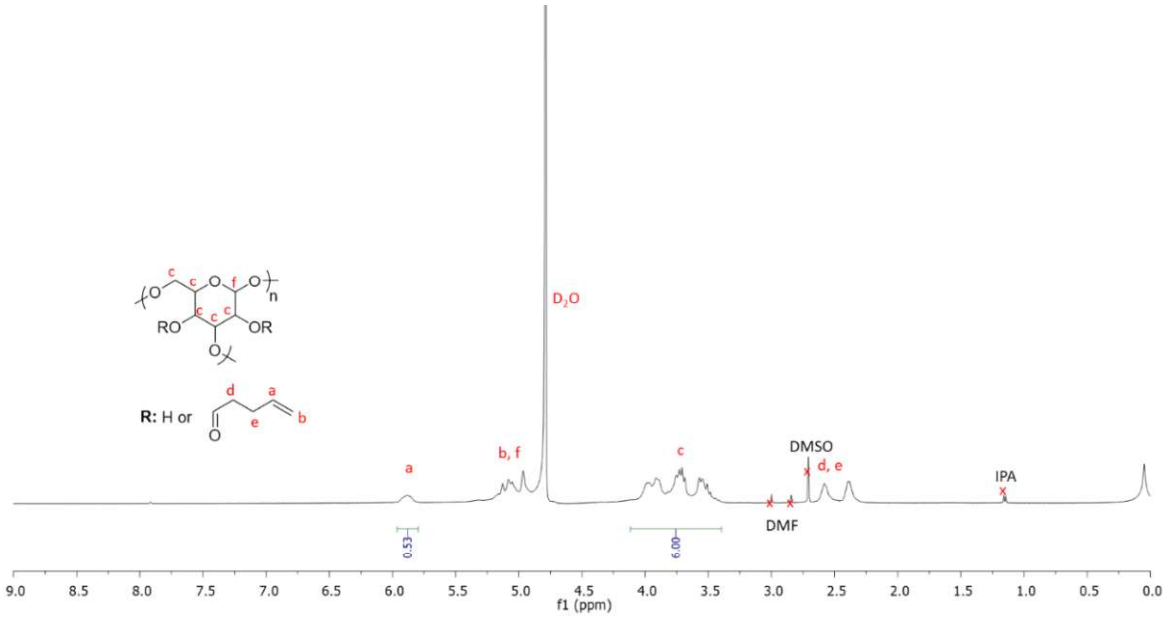

Figure A.6. ^{1}H NMR spectrum of vinyl modified dextran polymer.

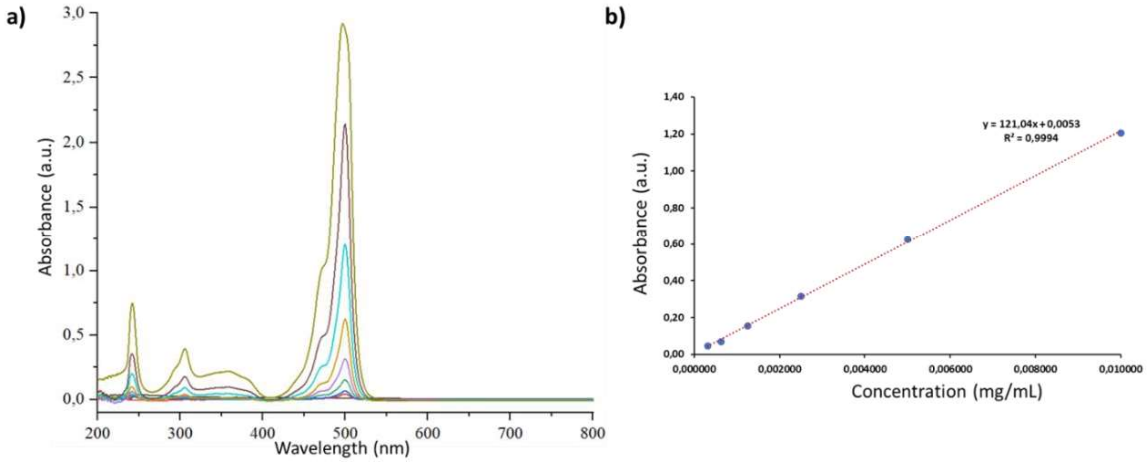

Figure A.7. Calibration curve of BODIPY-maleimide via UV-vis spectroscopy.

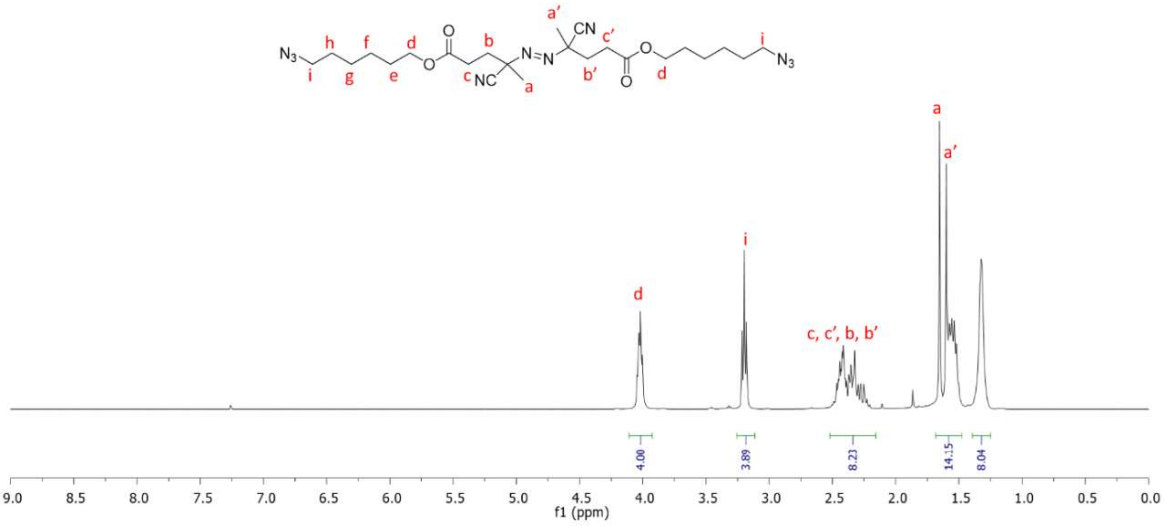

Figure A.8. ^{1}H NMR spectrum of azide azobis molecule.

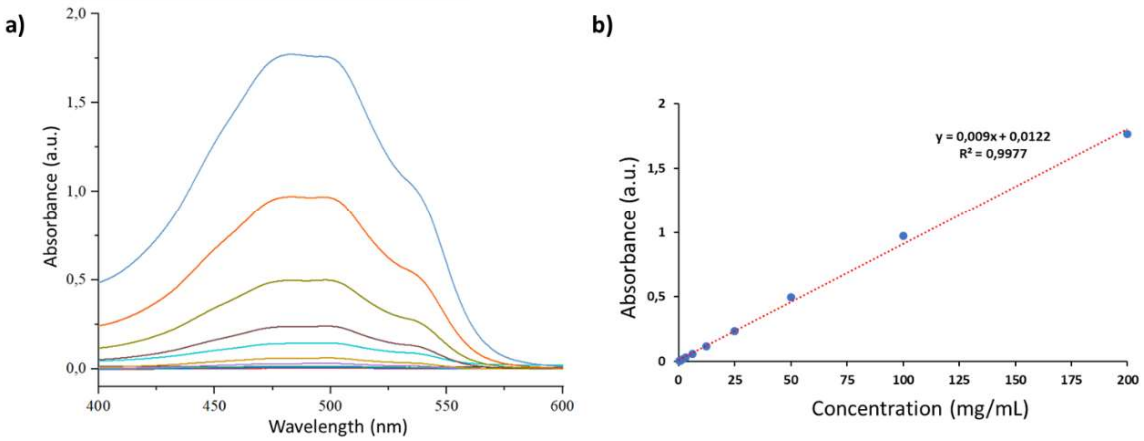

Figure A.9. Calibration curve of aldoxorubicin via UV vis spectra.

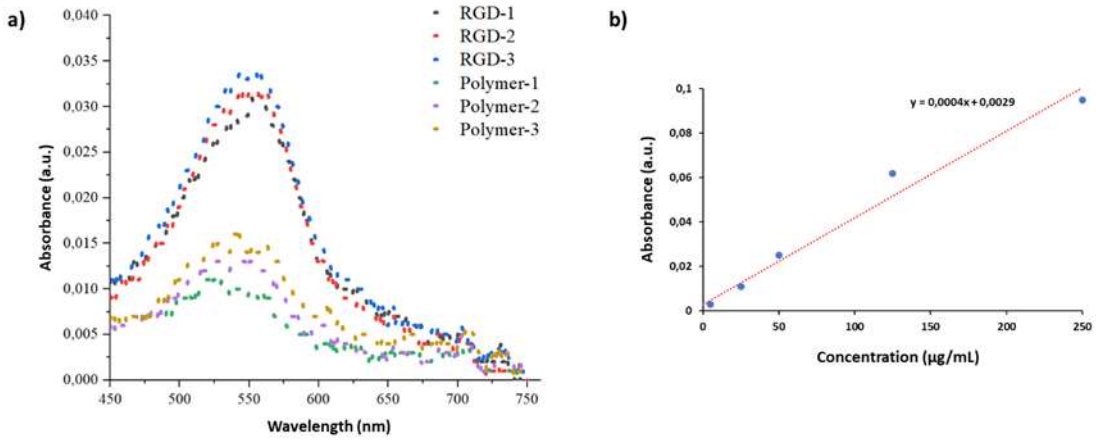

Figure A.10. BCA analysis graph of RGD attached polymer coated IONPs.

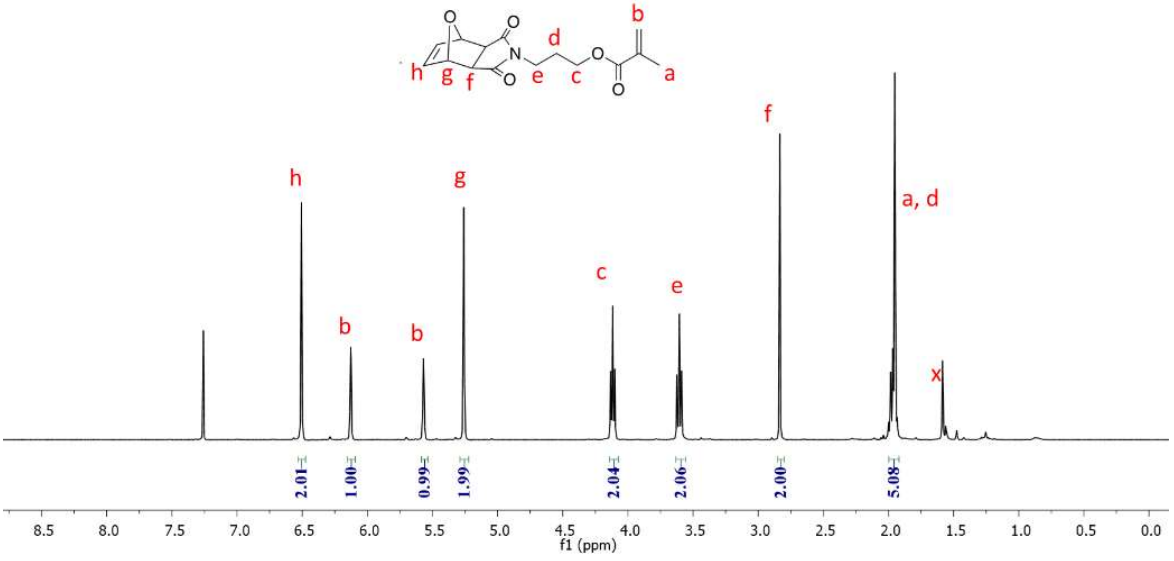

Figure A.11. ^{1}H NMR spectrum of FuMaMA.

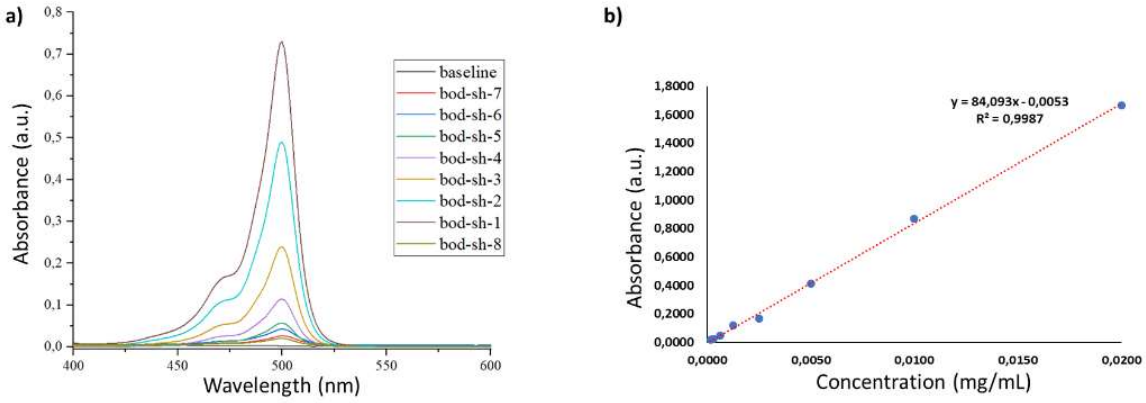

Figure A.12. Calibration curve of BODIPY-SH via UV-vis spectroscopy.

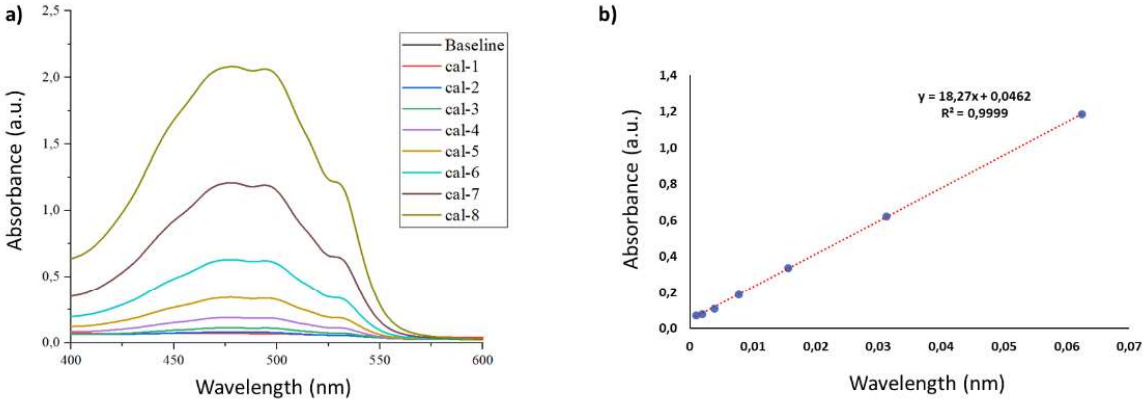

Figure A.13. Calibration curve of Dox-SH via UV-vis spectroscopy.

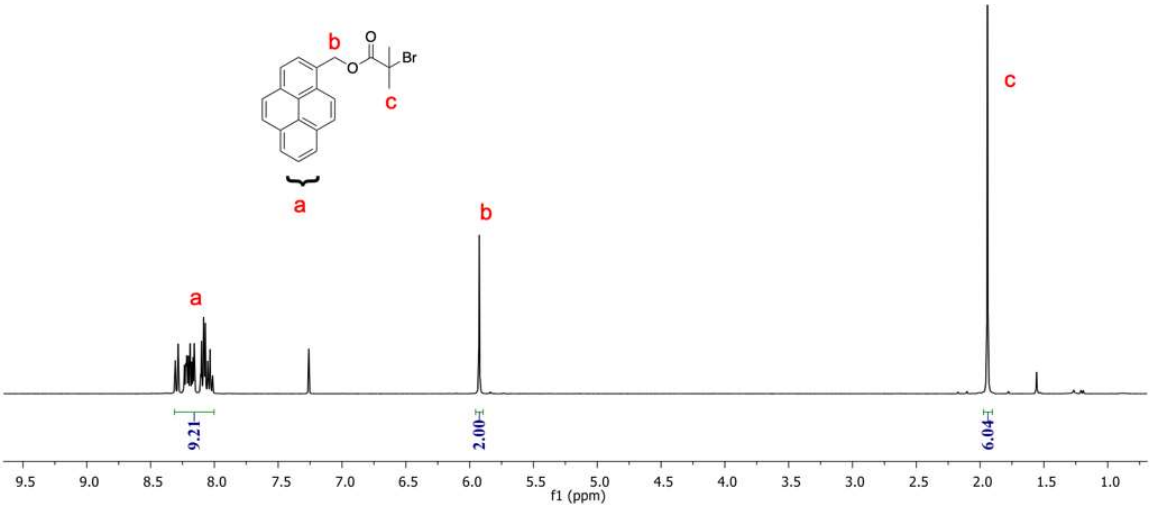

Figure A.14. ^{1}H NMR spectrum of pyrene initiator.

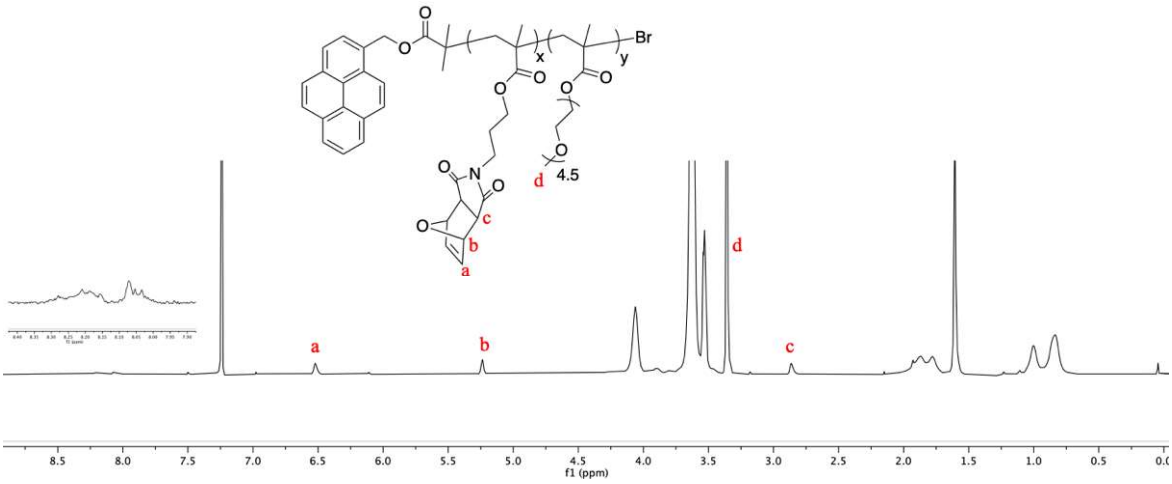

Figure A.15. ^{1}H NMR spectrum of pyrene end group furan protected maleimide copolymer (P1)

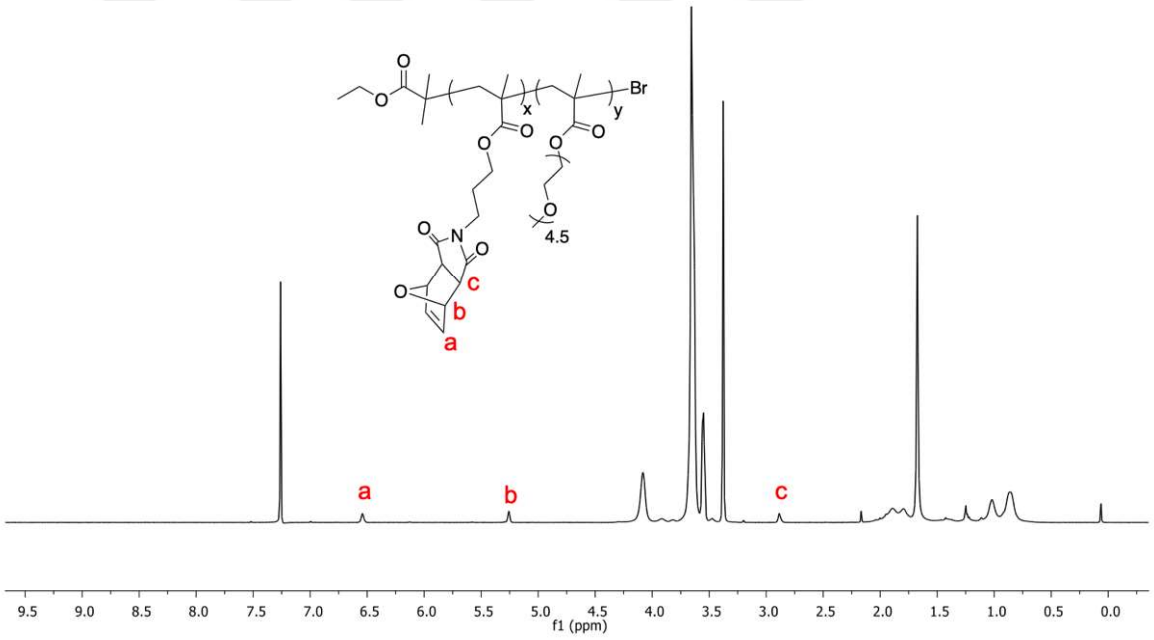

Figure A.16. 1H NMR spectrum of furan protected maleimide bearing P2 copolymer.

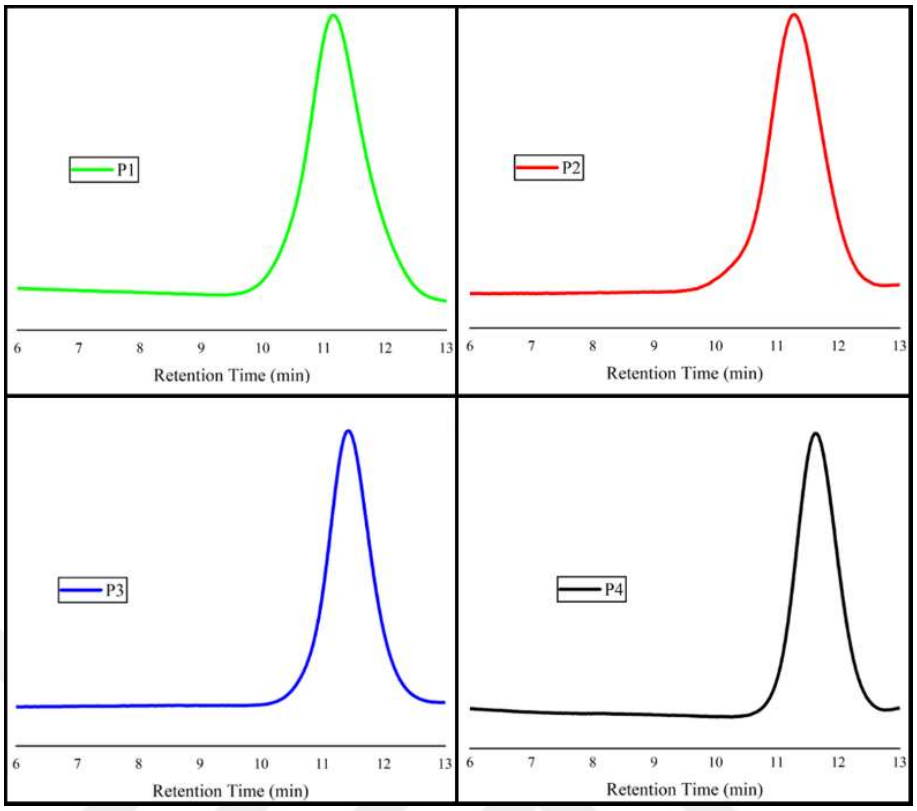

Figure A.17. SEC plots of copolymers.

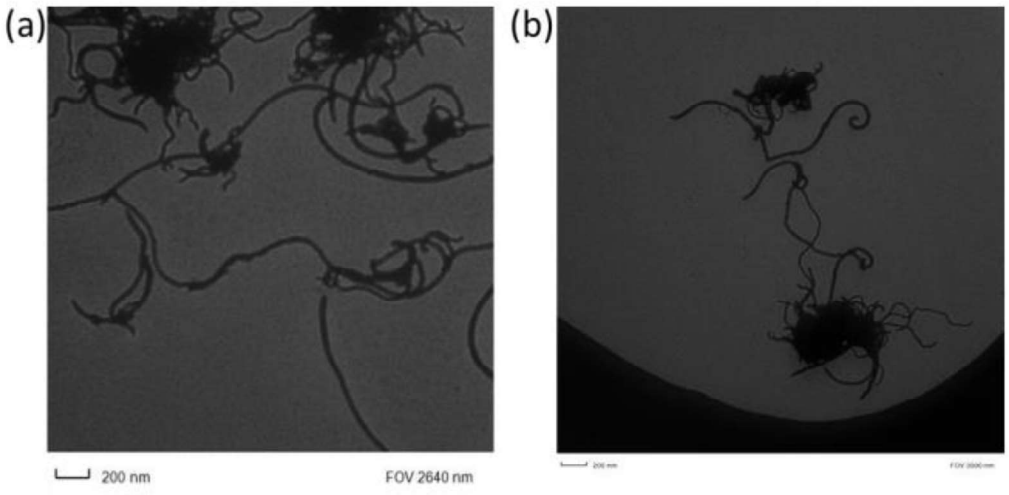

Figure A.18. TEM micrographs of (a) copolymer P1 coated CNTs, and (b) pristine CNTs.

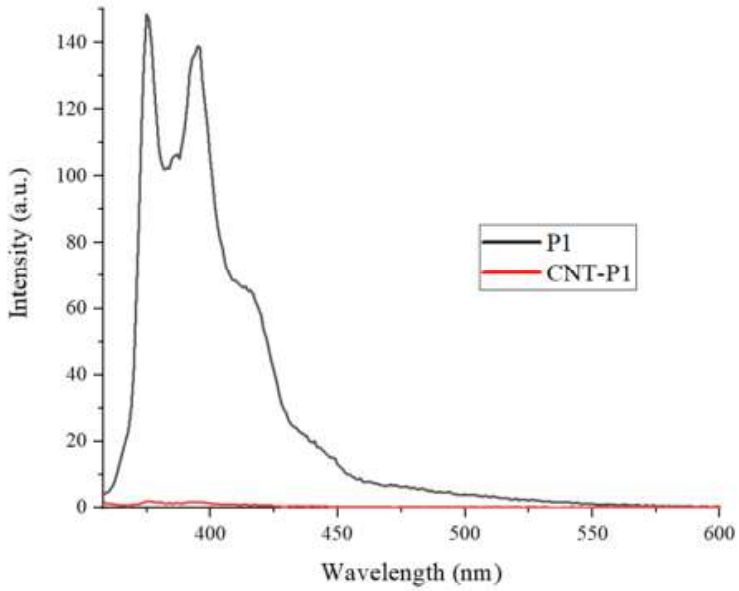

Figure A.19. Fluorescence spectra of (a) copolymer P1, and (b) P1-CNTs, in water

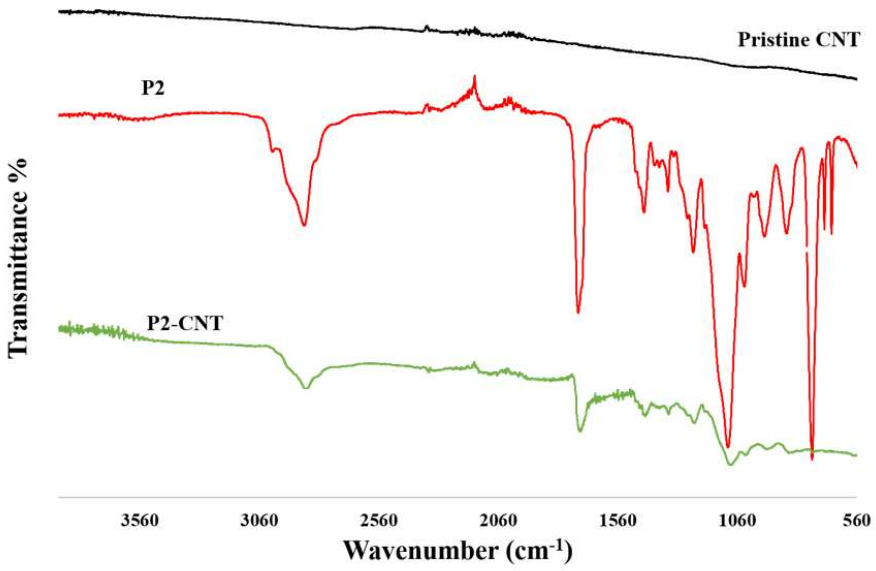

Figure A.20. FTIR spectra of pristine CNT, P2 polymer and P2-polymer coated CNT.

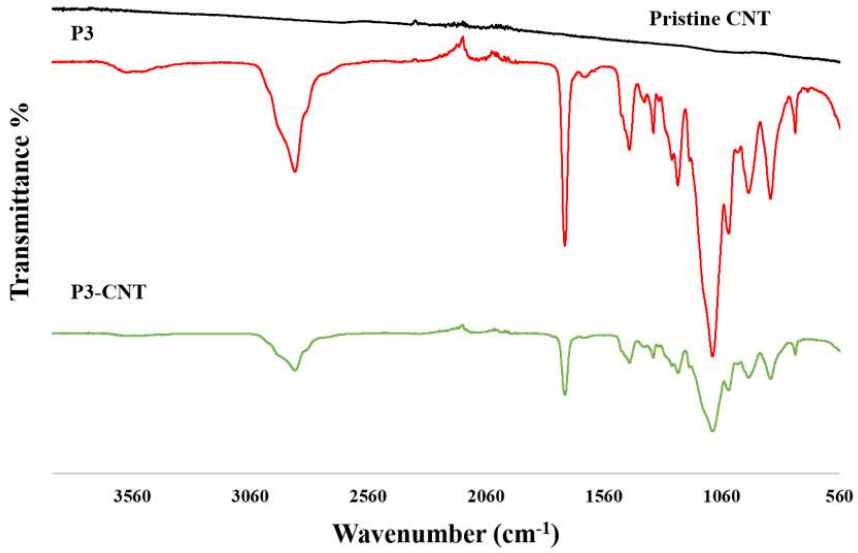

Figure A.21. FTIR spectra of pristine CNT, P3 polymer and P3-polymer coated CNT.

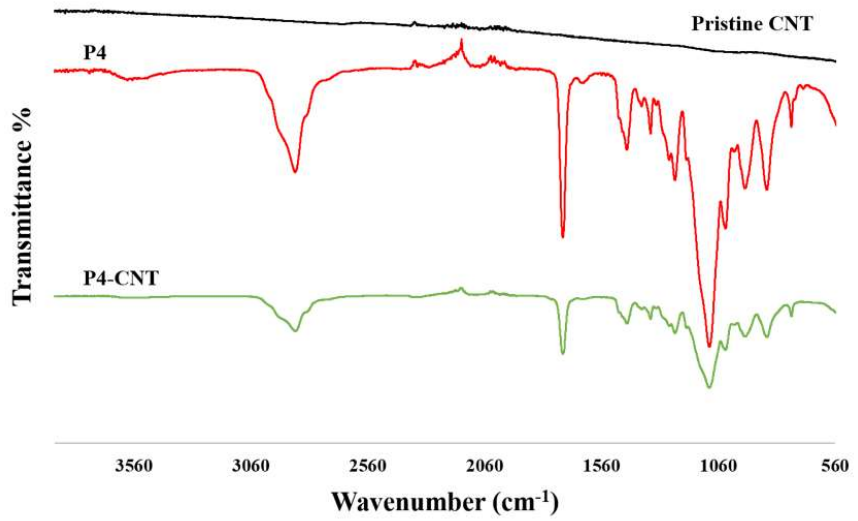

Figure A.22. FTIR spectra of pristine CNT, P4 polymer and P4-polymer coated CNT.



Figure A.23. Streptavidin conjugation to P1-coated CNTs without biotin (scale bar 200 μ).

APPENDIX B: COPYRIGHTS